Proceedings of the I·R·E

SEPTEMBER 1939

VOLUME 27 NUMBER 9

Institute of Radio Engineers

Fourteenth Annual Convention

New York, N. Y., September 20–23, 1939

Rochester Fall Meeting

November 13, 14, and 15, 1939

SECTION MEETINGS

ATLANTA September 15	**DETROIT** September 15	**PHILADELPHIA** September 7
CINCINNATI September 12	**LOS ANGELES** September 19	**PITTSBURGH** September 19
CLEVELAND September 28	**MONTREAL** October 11	**WASHINGTON** September 11

SECTIONS

ATLANTA—Chairman, Ben Akerman; Secretary, J. G. Preston, 125 Vance Cir., Marietta, Ga.

BOSTON—Chairman, H. W. Lamson; Secretary, E. B. Dallin, 64 Oakland Ave., Arlington, Mass.

BUFFALO-NIAGARA—Chairman, H. C. Tittle; Secretary, E. C. Waud, 235 Huntington Ave., Buffalo, N. Y.

CHICAGO—Chairman, V. J. Andrew; Secretary, G. I. Martin, RCA Institutes, 1154 Merchandise Mart, Chicago, Ill.

CINCINNATI—Chairman, H. J. Tyzzer; Secretary, J. M. McDonald, Crosley Radio Corp., 1329 Arlington, Cincinnati, Ohio.

CLEVELAND—Chairman, S. E. Leonard; Secretary, H. C. Williams, Rm. 1932, 750 Huron Rd., Cleveland, Ohio.

CONNECTICUT VALLEY—Chairman, E. R. Sanders; Secretary, W. R. G. Baker, General Electric Co., Bridgeport, Conn.

DETROIT—Chairman, H. D. Seielstad; Secretary, R. J. Schaefer, 9753 N. Martindale, Detroit, Mich.

EMPORIUM—Chairman, R. K. McClintock; Secretary, D. R. Kiser, Hygrade Sylvania Corp., Emporium, Penna.

INDIANAPOLIS—Chairman, I. M. Slater; Secretary, B. V. K. French, P. R. Mallory & Co., E. Washington St., Indianapolis, Ind.

LOS ANGELES—Chairman, F. G. Albin; Secretary, M. T. Smith, General Radio Co., 1000 N. Seward St., Hollywood, Calif.

MONTREAL—Chairman, A. B. Oxley; Secretary, W. A. Nichols, Canadian Broadcasting Corp., 1012 Keefer Bldg., Montreal, Que.

NEW ORLEANS—Chairman, G. H. Peirce; Secretary, D. W. Bowman, 8327 Sycamore St., New Orleans, La.

PHILADELPHIA—Chairman, R. S. Hayes; Secretary, R. L. Snyder, 103 Franklin Rd., Glassboro, N. J.

PITTSBURGH—Chairman, W. P. Place; Secretary, R. E. Stark, 90 Pilgrim Rd., Rosslyn Farms, Carnegie, Penna.

PORTLAND—Chairman, H. C. Singleton; Secretary, E. R. Meissner, United Radio Supply, Inc., 203 S. W. Ninth Ave., Portland, Ore.

ROCHESTER—Chairman, W. F. Cotter; Secretary, H. C. Sheve, Stromberg-Carlson Telephone Manufacturing Co., Rochester, N. Y.

SAN FRANCISCO—Chairman, F. E. Terman; Secretary, L. J. Black, 243-30th St., Oakland, Calif.

SEATTLE—Chairman, R. O. Bach; Secretary, Karl Ellerbeck, Pacific Telephone and Telegraph Co., 612 Northern Life Tower, Seattle, Wash.

TORONTO—Chairman, R. C. Poulter; Secretary, N. Potter, Canadian National Carbon Co., Ltd., 805 Davenport Rd., Toronto, Ont.

WASHINGTON—Chairman, Gerald C. Gross; Secretary, M. H. Biser, 3224-16th St., N. W., Washington, D. C.

Proceedings of the I·R·E

Published Monthly by
The Institute of Radio Engineers, Inc.

VOLUME 27 *September, 1939* NUMBER 9

Entered as second-class matter October 26, 1927, at the post office at Menasha, Wisconsin, under the Act of February 28, 1925, embodied in Paragraph 4, Section 412 of the Postal Laws and Regulations. Publication office, 450 Ahnaip Street, Menasha, Wisconsin. Subscription, $10.00 per year; foreign, $11.00.

THE INSTITUTE

The Institute of Radio Engineers serves those interested in radio and allied electrical-communication fields through the presentation and publication of technical material. In 1913 the first issue of the PROCEEDINGS appeared; it has been published uninterruptedly since then. Over 1500 technical papers have been included in its pages and portray a currently written history of developments in both theory and practice.

STANDARDS

In addition to the publication of submitted papers, many thousands of man-hours have been devoted to the preparation of standards useful to engineers. These comprise the general fields of terminology, graphical and literal symbols, and methods of testing and rating apparatus. Members receive a copy of each report. A list of the current issues of these reports follows:

Standards on Electroacoustics, 1938
Standards on Electronics, 1938
Standards on Radio Receivers, 1938
Standards on Radio Transmitters and Antennas, 1938.

MEETINGS

Meetings at which technical papers are presented are held in the twenty-one cities in the United States and Canada listed on the inside front cover of this issue. A number of special meetings are held annually and include one in Washington, D. C., in co-operation with the American Section of the International Scientific Radio Union (U.R.S.I.) in April, which is devoted to the general problems of wave propagation and measurement technique, the Rochester Fall Meeting in co-operation with the Radio Manufacturers Association in November, which is devoted chiefly to the problems of broadcast-receiver design, and the Annual Convention, the location and date of which are not fixed.

MEMBERSHIP

Membership has grown from a few dozen in 1912 to more than five thousand. Practically every country in the world in which radio engineers may be found is represented in our membership roster. Approximately a quarter of the membership is located outside of the United States. There are several grades of membership, depending on the qualifications of the applicant. Dues range between $3.00 per year for Students and $10.00 per year for Members. PROCEEDINGS are sent to each member without further payment.

PROCEEDINGS

The contents of each paper published in the PROCEEDINGS are the responsibility of the author and are not binding on the Institute or its members. Material appearing in the PROCEEDINGS may be reprinted or abstracted in other publications on the express condition that specific reference shall be made to its original appearance in the PROCEEDINGS. Illustrations of any variety may not be reproduced, however, without specific permission from the Institute.

Papers submitted to the Institute for publication shall be regarded as no longer confidential. They will be examined by the Papers Committee and Board of Editors to determine their suitability for publication. Suggestions on the mechanical form in which manuscripts should be prepared may be obtained from the Secretary.

SUBSCRIPTIONS

Annual subscription rates for the United States of America, its possessions, and Canada, $10.00; to college and public libraries when ordering direct, $5.00. Other countries, $1.00 additional.

The Institute of Radio Engineers, Inc.
Harold P. Westman, Secretary
330 West 42nd Street
New York, N.Y.

A 50-Kilowatt Broadcast Station Utilizing the Doherty Amplifier and Designed for Expansion to 500 Kilowatts*

W. H. DOHERTY,† MEMBER, I.R.E., AND O. W TOWNER‡, MEMBER, I.R.E.

Summary—*Radio station WHAS purchased the first commercial transmitter employing the Doherty high-efficiency amplifier and has installed it in a completely new transmitting plant which is designed for expansion to 500 kilowatts output. The transmitter extends the use of negative feedback for noise suppression and all vacuum-tube filaments are heated with alternating current, completely eliminating rotating equipment except for fans and pumps. Heat for the building is obtained from the water-cooling system, in which porcelain tubes entirely replace rubber hose for the insulating sections. Six-inch concentric transmission line of refined design is used to convey energy from the transmitter to the antenna and for the suppression of harmonics. The novel construction of the feed line to the shunt-excited half-wave antenna makes unnecessary the coupling apparatus ordinarily used between the transmission line and the inclined lead to provide the capacitive reactance required at that point in the circuit.*

The theory and practice followed in the design of the high-efficiency amplifier and other special features are touched upon as the entire plant is described. Performance data of the transmitter and the antenna system are also included.

STATION WHAS at Louisville, Kentucky, has attracted international attention by utilizing the latest and most improved technical methods and equipment in its recent installation. The installation is of interest economically as well as technically because this is the first commercial transmitter employing the Doherty high-efficiency amplifier in the United States.

The new transmitting equipment is located approximately 18 miles east of Louisville, near Eastwood, Kentucky. Situated midway between two civil airways, this site is far enough from them to permit the erection of a half-wave vertical radiator. It is also sufficiently distant from the densely populated areas to prevent their being subject to high field intensities if the ultimate capacity of 500 kilowatts is used. The property has an area of 104 acres and, in addition to the structures required for the transmitting equipment, there are located on it the transmitter engineer's house, an artificial lake from which the water supply is obtained, and the caretaker's cottage.

The transmitter building was especially designed to accommodate a Western Electric 500-kilowatt transmitter. The No. 407A–2 transmitting equipment which it now houses is sufficient only for the present authorized power of 50 kilowatts but is designed to drive a 500-kilowatt amplifier and to permit this expansion to be made with a minimum of added expense.

* Decimal classification: R612.1. Original manuscript received by the Institute, August 11, 1938; abridgment received by the Institute, June 26, 1939. Presented, Thirteenth Annual Convention, New York, N. Y., June 16, 1938.

†Bell Telephone Laboratories, Inc., Whippany, N. J.

‡ The Louisville Times Company, Inc., Louisville, Ky.

The small size of the building necessary to house this equipment is indicative of its over-all economy. Excluding the garage and power platform, it covers an area of approximately 50×68 feet. The front of the units of the 50-kilowatt transmitter, shown stippled in the floor plan of Fig. 1, occupy only 17

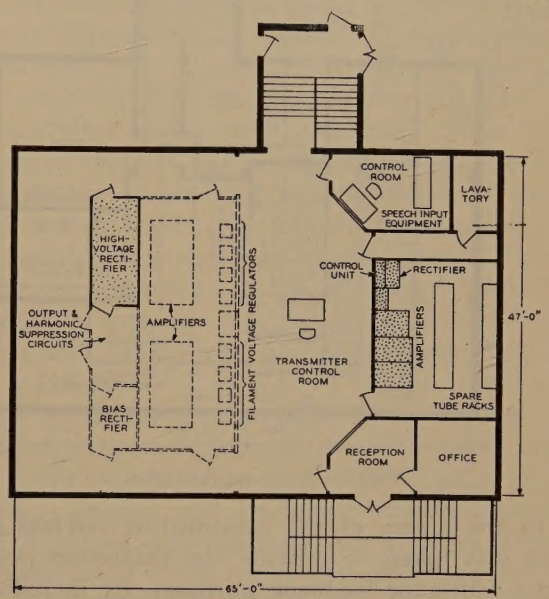

Fig. 1—First-floor plan.

feet of wall space along one side of the transmitter control room, and space is available for those of a 500-kilowatt amplifier on the opposite side, as indicated by the dotted lines. The corridor around the back of the 500-kilowatt amplifier makes possible the observation of that unit and the rectifier. Behind the 50-kilowatt transmitter is a tube and spare-parts room, in which there are no exposed voltages, the transmitter units being completely enclosed. At the front of the building is an office which is accessible from the entrance and the operating room. The steps leading to the basement at the rear connect to the power-platform entrance and an exit.

The basement likewise is laid out for future expansion. Two rooms are available for installation of the 500-kilowatt amplifier grid-input circuits and the associated porcelain pipes of the water-cooling system. In order to co-ordinate the controls, all equipment under gas pressure is fed from a nitrogen control room. Underneath the transmitter units is the 50-kilowatt filter room where the rectifier-filter equipment and the last-stage water piping are in-

stalled. In one corner of the basement a convenient work space is available for use in maintenance. The layout of the basement and outdoor power platform and cooling platform is shown in Fig. 2, existing apparatus again being shown stippled and future additions dotted.

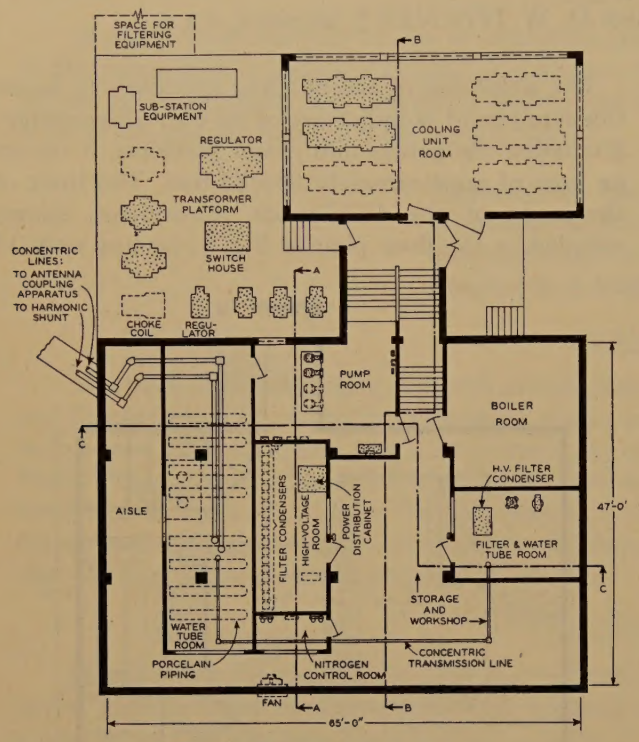

Fig. 2—Basement-floor plan.

In the design of the transmitting circuits great care was taken to provide the maximum possible band width for feedback purposes, by including in the main feedback path only a few stages and by the use of wide-band interstage coupling circuits. The first audio-frequency stage, for example, as shown on the block diagram of Fig. 3, is left outside the feedback loop and is provided with a local feedback of its

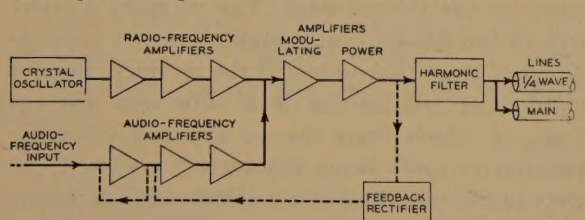

Fig. 3—Block diagram of amplifier circuits.

own to reduce any distortion and noise arising within it. The water-cooled stage preceding the final stage is grid-bias-modulated for maximum band width. As a result of these design considerations, useful feedback is obtained at modulation frequencies even as high as 25 kilocycles. The distortion (Fig. 4), therefore, is low even at the higher audio frequencies where the effective feedback is considerably reduced by the cumulative losses and phase shifts in the various stages.

The feedback at low frequencies is approximately 28 decibels, giving a noise level over 60 decibels down with all tubes heated from alternating current.

The high-efficiency principle used in the final stage has been previously explained.[1] Its operation is based upon a variable load distribution between the tubes, the carrier output being obtained from one tube

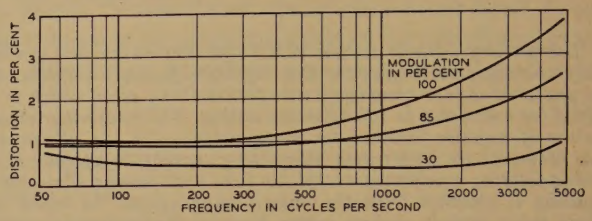

Fig. 4—Distortion measurements at 50 kilowatts.

alone, while at higher instantaneous outputs the load is shared by both tubes. The potentials on the tubes in such a circuit are 90 degrees apart in phase. The essentials of the circuit are shown in Fig. 5. C_1 and C_2 are small variable air condensers for adjusting

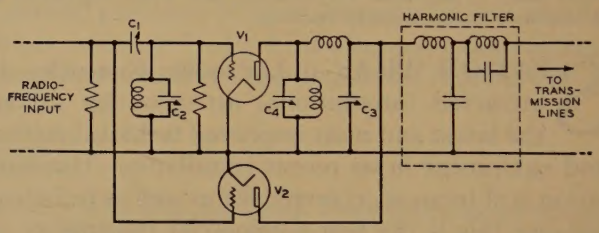

Fig. 5—Essentials of the high-efficiency circuit.

the relative amplitudes and phases of the two grid voltages. Condenser C_3 adjusts the relative phases of the two plate voltages and C_4 tunes the radio-frequency plate voltages of the tubes to the desired 180-degree phase relation to the respective grid voltages. C_3 and C_4 are high-voltage nitrogen-filled variable condensers, which lend themselves admirably to a compact output circuit arrangement.

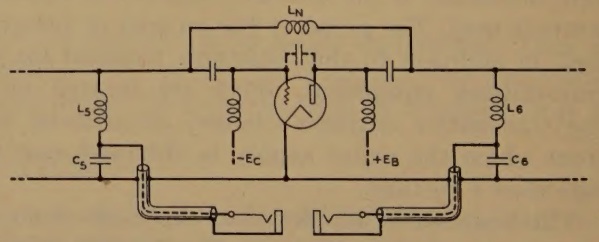

Fig. 6—Method of phase indication and tube neutralization.

The circuit adjustment is an extremely simple matter and is accomplished under power using a cathode-ray oscillograph. Fig. 6 shows the method of obtaining indications of the grid and plate voltages at jacks on the front panel for connection to the oscillograph. By using reactance potentiometers, consisting of high-impedance coils L_5 and L_6, and low-

[1] W. H. Doherty, "A new high efficiency power amplifier for modulated waves," Proc. I.R.E., vol. 24, pp. 1163–1182; September, (1936).

impedance condensers C_5 and C_6, a fraction of the voltage suitable for oscillograph deflections and free of phase shift is obtained across the condensers and conducted to the phase-indicating jacks.

Coil L_N in Fig. 6 is employed to neutralize the tube by antiresonating the grid-plate capacitance at the carrier frequency. This is one of the first methods ever used to neutralize an amplifier.

The 50-kilowatt amplifier is operated at an efficiency of 60 per cent, the plate potential being 18,000 volts and the plate currents in the two tubes being 4.0 and 0.6 amperes, respectively, with no modulation, and 4.0 and 2.9 amperes when the carrier is completely modulated by a single tone. This represents a reduction of nearly one half in the all-day power consumption of the final stage as compared with the power required in the conventional type of linear power amplifier operating at 33 per cent efficiency, and a reduction in plate dissipation to one third of the usual value. At the power rate prevailing at the transmitter location the saving in power cost made possible through the use of this circuit is approximately $6000 a year.

The power supply for the transmitting equipment comes from Louisville over a 66,000-volt transmission line to the substation at the southeast corner of the transmitter grounds. A second transmission line is now being erected to connect the substation through remotely controlled oil circuit breakers to the Dix Dam hydroelectric plant, which is about 50 miles from the transmitter in the opposite direction from Louisville. Stepped down at this substation to 12,000 volts, the power is fed underground approximately 1200 feet to the transmitter building.

In the main switch house are mounted disconnect switches and oil circuit breakers for the regular and spare cables from the substation, for the 100-kilovolt-ampere lighting supply transformer, and for the second 100-kilovolt-ampere transformer operating from an emergency supply. This emergency power line comes to the opposite side of the property from a third direction, going underground approximately 300 feet to the switch house, and is connected to an automatic change-over switch so that in the event of failure of the main power line, there will be no danger of losing the antenna obstruction lights.

Power for the equipment is carried by cable from the main switch house to an oil circuit breaker located in the transmitter switch house. The circuit then branches, one part going to the three auxiliary transformers which step the voltage down to 460 volts for distribution in the transmitter, while the other branch connects to the high-voltage transformers through a second oil circuit breaker, which is electrically tripped and reclosed from the transmitter control panel. Only two plate transformers, operating in open delta, are used. They are rated at 382 kilovolt-amperes each, which is greater than required for 50-kilowatt operation, but with the addition of a third transformer they provide sufficient capacity to supply the requirements of a 500-kilowatt amplifier. At the end of the plate-transformer line-up, provision is made for this third unit. The secondaries of the plate transformers connect through an automatic voltage regulator to the high-voltage rectifier. All connections are made by means of cable, thus making possible a very clean-cut and accessible power platform.

On the inside of the building, immediately adjacent to the power platform, is the 500-kilowatt amplifier room. Here the terminating-end seals of the 500- and 50-kilowatt transmission lines are now connected together. These are so placed in order to provide for switching facilities which will permit the 50-kilowatt transmitter to operate either directly into the antenna, as at present, or to drive the 500-kilowatt amplifier with its output connected to the antenna. Also in this room is the high-voltage rectifier which supplies 18,000 volts to the water-cooled tubes of the transmitter. It uses Western Electric 255B mercury-vapor rectifier tubes for supplying the 50-kilowatt equipment and is capable of rectifying the output required for a high-efficiency 500-kilowatt amplifier by a change of tubes only. An extra rectifier tube is kept heated for quick replacement in case of a tube failure.

In the pump room, two tanks and two pumps are installed, one of each being a spare. The output manifold of the pumps is equipped with a thermometer, pressure gauges, and position indicators on the throttle valves. The cooling-water pipes go through the boiler room to the two water-cooled stages of the transmitter. The return lines terminate at a Venturi manifold, where the rate of flow of the water is measured in each branch and the necessary relays inserted to interlock with those of the plate and filament circuits. The water from the two return lines is then combined and can be routed into the outdoor cooling units or, in cold weather, into units provided in the "boiler room" for heating the building. No other source of heat is required for this purpose.

The filter for the rectifier supplying both water-cooled stages of the 50-kilowatt transmitter is located in a basement room, immediately under the transmitter units, and consists of a 12-microfarad condenser bank and a 5-henry choke coil. Were it not for the large amount of feedback employed in the transmitter, a considerably larger filter condenser would be required to prevent distortion at very low modulation frequencies. The coil is shunted by a Thyrite protector whose inverse voltage-resistance characteristic effectively prevents excessive surge potentials. A charging resistance in series with the filter condensers to limit the starting surge current is automatically short-circuited after a brief period.

On the ceiling of this room, immediately below the

two 100-kilowatt vacuum tubes of the power amplifier, are mounted straight porcelain tubes which convey the distilled water to the anodes. The water for the modulating-amplifier stage is supplied through copper pipes, the insulating porcelain tubes for this stage being incorporated within the amplifier unit itself.

A small room in the basement is provided exclusively for the nitrogen-gas regulators and manifolds for maintaining a 45-pound pressure on the radio-

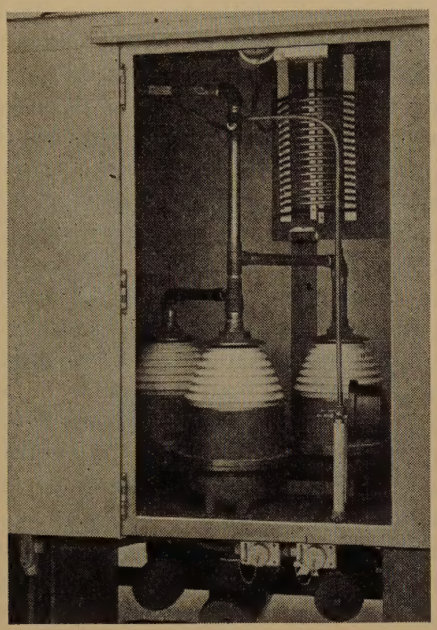

Fig. 7—Interior of coupling house showing transmission-line end seals.

frequency transmission lines and 175 pounds on the two variable condensers of the 50-kilowatt amplifier.

As the entire plot was underlined with limestone at an average depth of from one to two feet, it was necessary to construct the 6-inch transmission line above the ground. The expansion of the line during the seasons and throughout the day requires a support utilizing rollers to permit this movement. By means of specially designed insulators supporting the inner conductor it has been possible to construct the line so that the breakdown voltage is not appreciably decreased by the presence of the insulators.

Two harmonic shunt lines are connected in parallel with the transmission line at the coupling house and connection is made from them through a meter to the antenna feed line. One is a quarter-wave shunt short-circuited at the far end for even-harmonic suppression. The second is a twelfth-wavelength shunt, open at the far end, used for third-harmonic suppression. The only other apparatus required in the coupling house is a coil which parallel resonates with the capacitance of this third-harmonic shunt. Fig. 7 is a view of the interior of the coupling house.

In order to provide the capacitance required to tune the shunt-excited antenna in a form which would withstand the voltage developed by the transmission of 500 kilowatts, a four-conductor feed line was designed by the Bell Telephone Laboratories. The two outside conductors connect to the transmission line and the two inner ones connect to the tower. They are constructed of one-inch copper tubes and the distributed capacitance between them is used to provide a capacitive reactance equal to the inductance reflected by the feed line. The two inner conductors have a flexible joint at the spreader so that the point at which they tap into the tower may be more easily adjusted to terminate the transmission line.

Accurate antenna-power indication at the transmitter is provided by a pickup loop attached to the tower approximately 50 feet above the ground. Current for this loop, conducted by means of a coaxial cable, operates meters on the transmitter panels which have scales marked to correspond with the antenna feed-line meter.

The convenience and practicability of the shunt-excited antenna are very much evident when con-

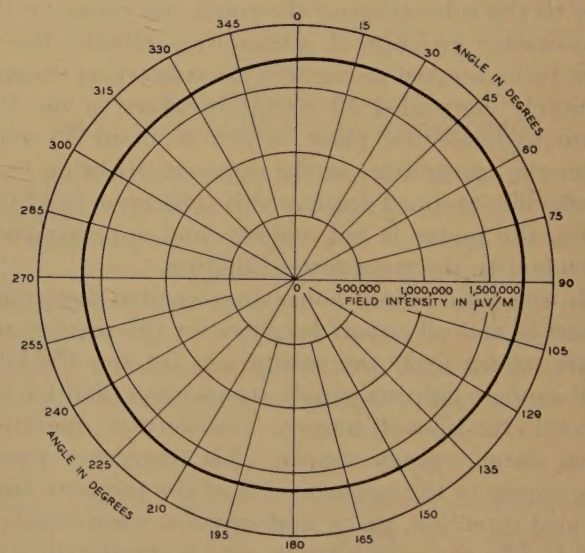

Fig. 8—Field-strength pattern. Station WHAS. 50-kilowatt radio transmitting equipment. 820 kilocycles per second. Attenuated field intensity at one mile. Root-mean-square value = 1,718,000 microvolts per meter.

sideration is given to the tower-lighting system and the inherent protection provided against electrical storms which are frequent in this area.

Every phase of the transmitting equipment has been designed for the highest efficiency, and the last link in the chain, the antenna, is in keeping with this aim, producing an average attenuated signal intensity of 1718 millivolts per meter at a distance of one mile with an antenna input of 50 kilowatts.

Recent Improvements in the Design and Characteristics of the Iconoscope*

R. B. JANES†, ASSOCIATE MEMBER, I.R.E., AND W. H. HICKOK†, ASSOCIATE MEMBER, I.R.E.

Summary—*The sensitivity and picture-signal output of iconoscopes have recently been increased by a factor of two or three times. The spectral response of the newer tubes more closely resembles that of the eye and may be controlled by processing. "Dark spot" has been diminished by the use of a cylindrical envelope.*

The gun design has been changed to give a constant current as the beam is focused, and to prevent secondary electrons from the gun apertures getting into the primary beam. Use of the cylindrical envelope gives a better picture since a good optical window can be employed. Sandblasting of the mosaic improves the picture contrast and quality by minimizing the specular reflection of the mosaic.

More precise methods of measuring signal output, "dark spot," photoemission, and secondary emission of the mosaic, spectral response, and resolution are described.

MANY articles on the operation and characteristics of television pickup tubes of the iconoscope type have been published. In this paper, we will avoid repetition in so far as possible by restricting our attention to some improvements which have recently been incorporated in the iconoscope.

The processing of the mosaic of the iconoscope has been the object of research and development investigations for some time. Although these activities have resulted in considerable improvement in the magnitude and quality of the video-frequency signal generated by the tube; other parts such as the electron gun and the envelope have not been neglected. Their development has progressed along with the improvement of the mosaic.

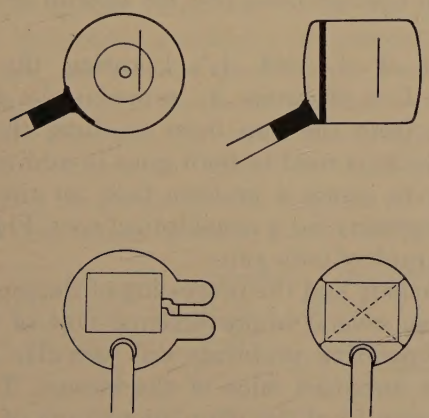

Fig. 1—Schematic drawings of the old and the new envelopes. The old envelope is shown in the drawings on the left, the new in those on the right.

In this paper, the improvements in design of the envelope, gun, and mosaic will be dealt with first. The latter part will cover the changes in characteristics which have resulted from better processing of the mosaic, and the methods of measuring these characteristics.

* Decimal classification: R583×R339. Original manuscript received by the Institute, August 15, 1938. Presented, I.R.E. Convention, New York, N. Y., June 17, 1938.

† RCA Manufacturing Company, Inc., RCA Radiotron Division, Harrison, N. J.

For the new envelope, a cylindrical type of bulb was chosen in preference to the older spherical type. Fig. 1 shows schematic drawings of the old and new design. A high percentage of the spherical bulbs could not be used because of optical defects resulting from the molding operation. The cylindrical envelope offers several advantages from an optical and a constructional standpoint. It is assembled from selected glass parts and comprises a cylindrical section, a gun neck, and two face plates, i.e., front and back. The use of separate face plates is a decided advantage in that it simplifies the problem of obtaining good optical quality. Each optical face plate is a section cut from a large sphere. The use of a face with a small curvature permits the glass to be thinner than if a flat plate were used. The section is ground and polished so that pictures projected through it are not distorted. In assembly, the optical face is attached to one end of the cylinder. Next, the gun neck is sealed onto the lower side of the face at an angle of approximately 30 degrees with respect to the axis of the cylinder. A convenient and strong support is provided for the mosaic assembly by sealing it directly to the walls of the envelope. This procedure serves to simplify the alignment of the mosaic. After the mosaic is mounted, the back of the tube is closed with a plate similar to that used on the front except that no grinding or polishing is necessary. Fig. 2 shows a photograph of the earlier and the present tube.

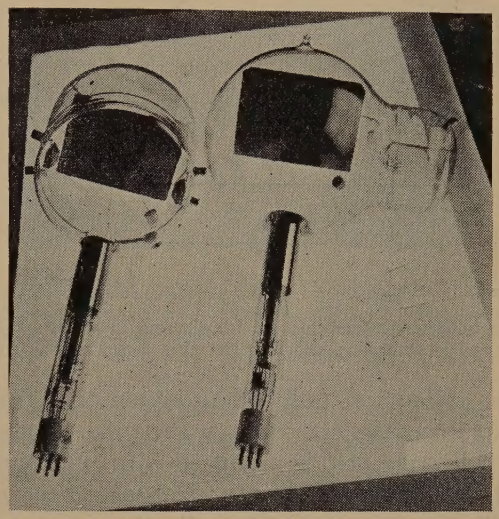

Fig. 2—Photograph of the old and the new tubes.

The use of the cylindrical bulb allows a more advantageous location of the silver evaporators because they can be placed inside of the bulb proper and still produce a deposit of sufficient uniformity upon

the mosaic. With the spherical bulb, the evaporators had to be located in protuberances at the expense of window area. Since care is exercised in assembling the cylindrical bulb to provide a window area at least as large as the mosaic area, a lens of very long focal length can be used, or a motion picture can be projected upon the mosaic from a distance.

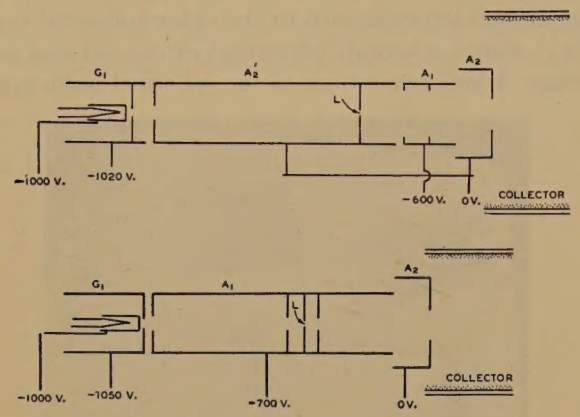

Fig. 3—Schematic drawings of the old and new guns. The older type is shown at the bottom, the newer at the top.

The cylindrical bulb offers advantages from the standpoint of the operation of the tube. A more uniform collecting field is produced with the result that the dark-spot signal is reduced, because the narrow metallic band used for the collection of photo- and secondary-electron emission is symmetrical with respect to the mosaic. By keeping this collector ring narrow, it is possible to hold the capacitance between it and the signal plate of the mosaic to a value of about 5×10^{-12} farads, which is about one half the value for the spherical type.

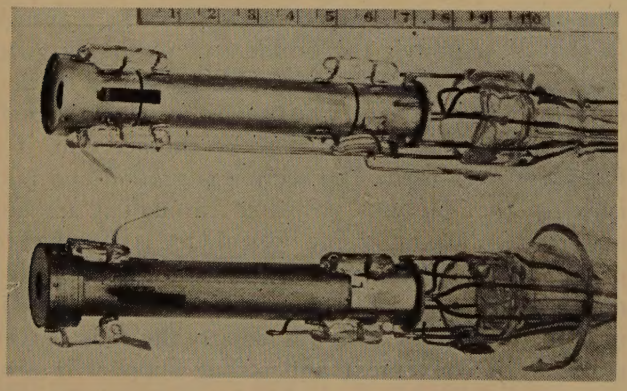

Fig. 4—Photograph of the old and new guns.

Changes in the gun are shown in the schematic drawings of Fig. 3. In the old-type gun, the focusing lens was formed by the potentials on electrodes A_2 and A_1, where A_2 was the more positive. The collector was operated at the same potential as A_2, and the potential of A_1 was varied to focus the beam. Because A_1 also served as an accelerating electrode for the electrons from the cathode, changing its potential in order to focus the beam also changed the beam current. Since the electrodes of this gun were at progressively greater positive voltages, any secondary emission from the apertures (especially the limiting aperture L) was drawn towards the mosaic. The number of electrons reaching the mosaic was greatly reduced by the use of a series of apertures.[1] In the new gun, an additional electrode A_2' is used. It is maintained at a constant potential and provides the accelerating field at the cathode. In order that A_2' and A_2 can be operated at the same potential with respect to the cathode, the aperture of the control grid G_1 is set back to reduce the field of A_2'. This results in a cutoff of the beam current at a grid voltage of about -30 volts with respect to the cathode compared to 50 volts for the older gun. Since the accelerating field is constant, the beam current depends only on the voltage of G_1, and hence focusing the beam by varying the potential of A_1 does not alter the current. The focus potential of A_1 is approximately one third the potential of A_2 and A_2'. Locating the limiting aperture L in electrode A_2' prevents the secondary emission from the gun from reaching the mosaic. Electrode A_2 is used in both guns in addition to the collector to insure a uniform field for the focusing lens, a necessity for a nonelliptical spot. Fig. 4 shows a photograph of both guns.

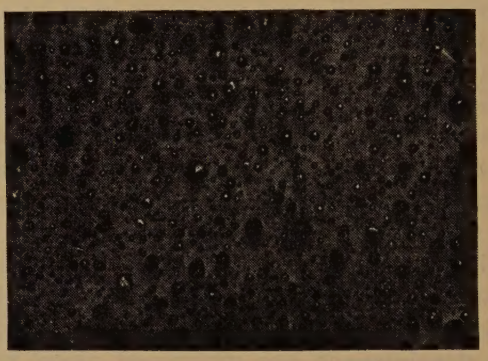

Fig. 5—Photomicrograph of a mosaic section illustrating the specular reflection arising from the uncoated sections of the mica.

The making and the processing of the mosaic have undergone several improvements. One of the most serious operating problems was specular reflection from the uncoated mica of the mosaic. This effect may be seen from the photomicrograph of a mosaic section (see Fig. 5). The curvature of the face plate is such that the reflection is focused back upon a small area of the mosaic. Fig. 6 illustrates this condition. The undesired effect of this condition is eliminated by sandblasting the mica, to break the specular reflection into a diffuse one which is not troublesome. A thin layer of cryolite flashed upon the mica before the silver is deposited tends to prevent leakage between the minute elements of the mosaic in the finished tube and, thus, permits a greater tolerance

[1] Iams and Rose. "Television pickup tubes with cathode-ray beam scanning," Proc. I.R.E., vol. 25, p. 1051; August, (1937).

in the quantity of alkali metal used in sensitizing the mosaic.[2] The cryolite is applied after sandblasting, but before the silver is deposited. The size of the mosaic has been chosen to give an aspect ratio of 4/3 in compliance with the tentative standards of the Radio Manufacturers Association.

In an earlier paper,[2] the authors mentioned a method of processing the mosaic to improve the char-

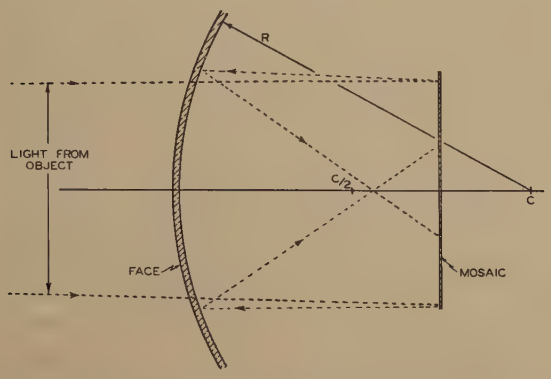

Fig. 6—Illustration of how an image on the mosaic is focused back upon a small area of the mosaic.

acteristics of the iconoscope. This process consisted in evaporating a thin layer of silver over the original sensitive surface which had been applied to the treated mica, and rebaking. Further work on this method has shown that it not only increases the sensitivity and saturated signal output but also improves the spectral response of an iconoscope. Most of this work has been done on tubes of the "new" design so that the comparison given below applies only to the newer type as made with and without the extra sensitization. Since very little has been published on methods of measuring the characteristics of iconoscopes, the method used will be described before a comparison of the characteristics is given.

Probably the most important characteristic of an iconoscope is its current output for various values of illumination on the mosaic. A diagram of the equipment for this measurement is shown in Fig. 7. A slit

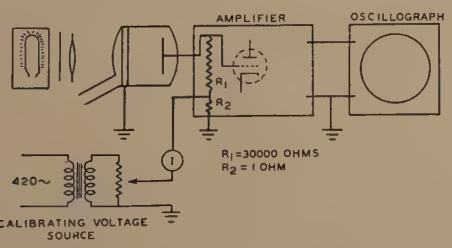

Fig. 7—Diagram of the equipment for measurement of current output of an iconoscope.

of light from a lamp operated at a filament color temperature of 2870 degrees Kelvin is projected upon the mosaic. The intensity of this image is controlled by an iris diaphragm. The illumination in the rectangle of light falling on the mosaic is known for each iris opening in lumens per square centimeter. The current from the iconoscope passes through a resistor (R_1) of 30,000 ohms and in doing so generates a voltage which is amplified by the regular video-frequency amplifier. In order that the amplifier may be calibrated, a known current having a frequency of 420 cycles is passed through the small resistance (R_2). The output of this amplifier at the kinescope grid is applied to an oscillograph synchronized to the horizontal-line frequency. With this arrangement, all of

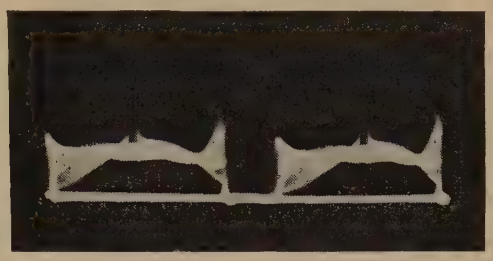

Fig. 8—Photograph of the signal as it appeared on the screen of the oscillograph tube when the oscillograph was synchronized to horizontal-line frequency. The sharp peak is the signal due to a rectangle of light on the iconoscope mosaic.

the horizontal lines should fall into a single straight line. Actually, this does not happen because of the dark-spot signal. However, with a short slit which does not cover too many lines and by proper adjustment of the shading voltages, a good clear signal due to the rectangle of light can be seen. Fig. 8 shows a photograph of such a signal as it appeared on the screen of the oscillograph tube. The shading is adjusted to allow the total signal to be measured. If the amplifier has been properly calibrated, the voltage across the 30,000-ohm resistor can be determined at once by reading the height of the signal on the oscillograph tube. With all shading voltages off, the horizontal dark-spot signal can be measured from the tilt of the horizontal scanning lines as they appear on the oscillograph tube. The tilt will be found to be

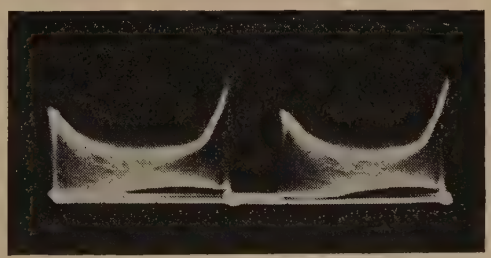

Fig. 9—Photograph of the signal as it appeared on the screen of the oscillograph tube when all shading voltages were off and the oscillograph was synchronized to horizontal-line frequency.

somewhat different for different scanning lines (see Fig. 9). By synchronizing the oscillograph to the vertical speed, it is possible to measure the vertical dark spot in the same way (see Fig. 10). Proper shading appears as shown in Fig. 11.

[2] Iams, Janes, and Hickok. "The brightness of outdoor scenes and its relation to television transmission," Proc. I.R.E., vol. 25, p. 1045; August, (1937).

Fig. 12 shows the signal-output curve for an iconoscope with a beam current of 0.5 microampere before and after the tube has been silver-sensitized. It can be seen that near the origin where the curve is linear the increase is of the order of two or three times. We

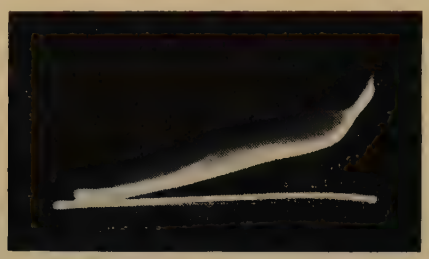

Fig. 10—Photograph of the signal as it appeared on the screen of the oscillograph tube when all shading voltages were off and the oscillograph was synchronized to vertical-frame frequency.

generally refer to the value of this initial slope as the "sensitivity" of the tube. At higher light levels of the order of 10 millilumens per square centimeter, the increase is about 1.5 times. At the same time, the dark-spot signal is not increased so that the ratio of signal output to dark spot is increased for all useful values of illumination. In order not to increase the dark-spot signal, it is essential to take care to evaporate a uniform layer of silver. Small nonuniformity of this layer can give rise to a change in the dark spot before any nonuniformity in the signal output is apparent.

Fig. 13 shows the signal output of a silver-sensitized tube for three different beam currents: 0.1, 0.25, and 0.5 microampere. The signal output, as

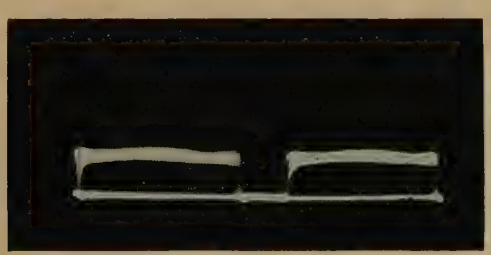

Fig. 11—Photograph of the signal as it appeared on the screen of the oscillograph tube when the shading voltages were correctly adjusted and the oscillograph was synchronized to horizontal-line frequency.

can be seen, increases rapidly with beam current. However, the dark spot increases even more rapidly so that with increasing beam currents the ratio of signal to dark spot falls.

The second important characteristic which is closely connected with the above is the saturated photosensitivity of the mosaic. In this measurement, the light from a small lamp whose filament color temperature is 2870 degrees Kelvin passes through an iris and shutter and falls on the mosaic. The signal plate is connected to ground through the input of an oscillograph while the second anode connects through a 300-volt direct-current source to ground. When a measurement is made, the shutter is kept closed while the second anode and mosaic are brought to ground potential. Then the second anode is connected to the 300-volt supply and the shutter opened for about 1/100 second. The iris opening is such that about 1/30 lumen falls on the mosaic in a spot about an inch in diameter. This flash of light falling on the mosaic gives rise to photoelectrons which are completely collected by the second anode and give a "kick" to the oscillograph. The amount of light is small enough to prevent the mosaic from charging up to 300 volts in 1/100 second. The calibration is

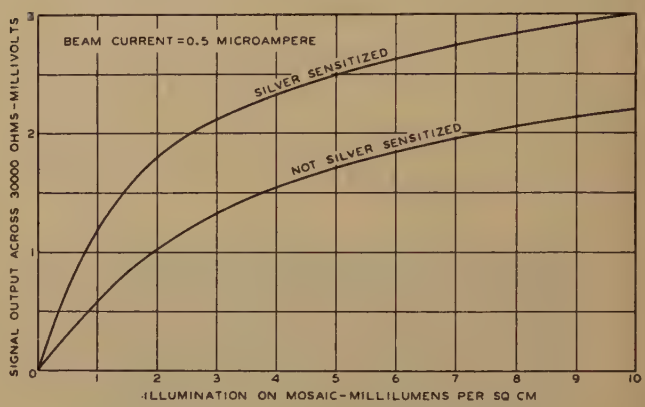

Fig. 12—Signal output for various values of illumination of an iconoscope before and after the tube has been silver-sensitized.

made by means of a known phototube. The sensitivity of the mosaic can thus be determined in microamperes per lumen.

The photosensitivity of the tubes without silver sensitization varied generally from 3 to 6 microamperes per lumen. With silver sensitization, the tubes have a value generally between 9 and 15. Higher values have been registered, but when these occur the infrared sensitivity generally is too great. This point will be taken up later. As would be expected,

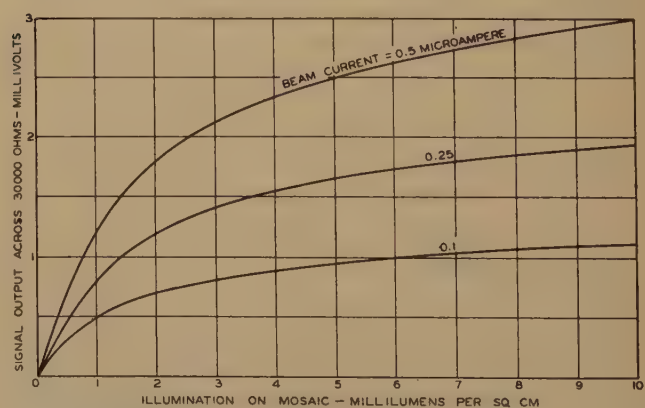

Fig. 13—Signal output for various values of illumination of a silver-sensitized iconoscope for three different beam currents.

the increase in the saturated photoemission is about the same as that in the operating signal output for small values of illumination where sufficient field is present to collect most of the photoelectrons. For

higher light levels where saturation begins, the increase in signal output is not as great.

A third measurement determines the saturated-secondary-electron-emission ratio of the mosaic. The method resembles that for saturated photoemission

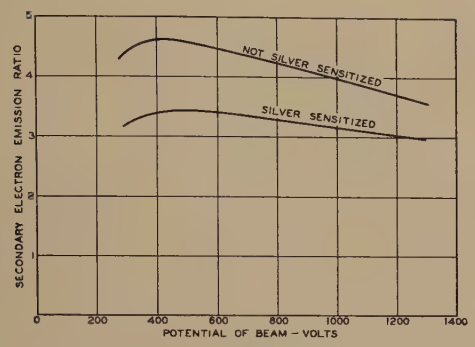

Fig. 14—Saturated-secondary-electron-emission ratio of an iconoscope mosaic before and after the tube has been silver-sensitized as a function of beam voltage.

except that a beam of electrons is used in place of a light beam. The signal plate is connected to ground through the input of an oscillograph. The second anode is arranged so that it can either be grounded or raised to a positive potential. With the second anode grounded, a defocused beam about an inch in diameter is allowed to fall on the mosaic. The second anode is then made positive. If the secondary-emission ratio is greater than unity, a kick occurs on the oscillograph. The density of the beam, of course, must be small enough so that the potential of the mosaic does not rise too rapidly for the "kick" to register. After the potential of the mosaic has risen to the positive potential of the second anode, the second anode is grounded. All of the beam current is now collected by the mosaic, and results in a "kick" on the oscillograph in the opposite direction. The ratio of the first to the second kick plus one gives the saturated-secondary-electron-emission ratio of the

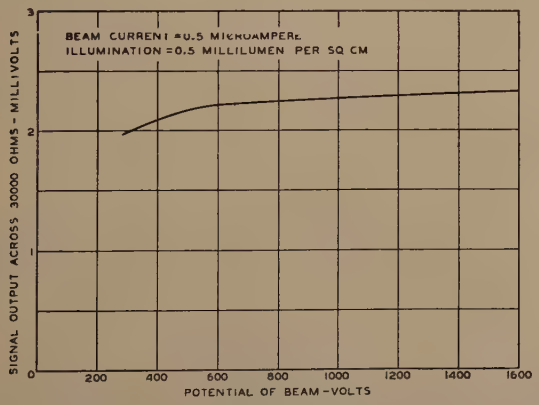

Fig. 15—Signal output of a silver-sensitized iconoscope for different beam voltages.

mosaic. Fig. 14 shows this measured ratio for various values of beam voltage before and after silver sensitization. It is lower for all voltages after sensitization. How this change in the secondary-emission ratio affects the signal output and other characteristics of the tube is difficult to determine because of the changes in photosensitivity and spectral response that occur at the same time. However, as Fig. 14 shows, the secondary-emission ratio changes with beam voltage. In order to determine whether this change affects the signal output, the signal output was measured over the same range of voltages for constant illumination and beam current. The curve of Fig. 15 shows the results of these measurements for a silver-sensitized tube. A comparison of this curve with the lower curve of Fig. 14 shows that there is little correlation between the signal output and the secondary-emission ratio. The signal output increases slowly with increasing beam voltage, while the secondary-emission ratio first increases and then decreases. The small increase in signal output with beam voltage may be due to the improvement in the focus of the beam spot which occurs with increasing

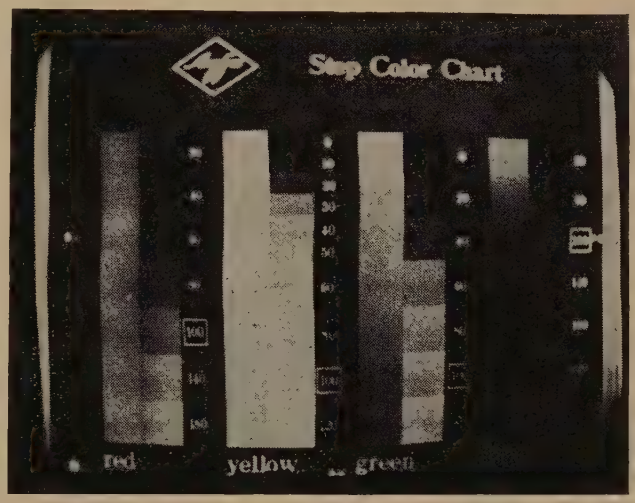

Fig. 16—Photograph of an Agfa color chart as it appears on the screen of a kinescope.

voltage. It can be concluded, however, that the effect of small changes in the secondary-emission ratio on the signal output, for the values of secondary-emission ratio encountered in these tubes, is small.

The fourth measurement is that of spectral sensitivity of the iconoscope. For most of the work, two rough methods of measurement are used. One method employs a series of filters which are used in conjunction with the measurements of saturated photoemission. This method provides a good test of the infrared sensitivity. The other method involves the use of an Agfa color chart, and gives only the response in the visible region. The chart consists of vertical bands of four colors, red, yellow, green, and blue. Parallel to each of these bands is a series of steps going from black through gray to white. An image of this chart is focused on the mosaic and observed on a kinescope. Fig. 16 is a photograph of the chart as it appears on the kinescope. If the mosaic has the same spectral response as the eye, the shade of each of the colored

bands should match the shade of gray marked 100. Before the iconoscope is silver-sensitized, the response to red, yellow, green, and blue is approximately 200, 140, 80, and 60, respectively. After the sensitizing process has been completed, it is about 120, 85, 70, and 100, respectively, values which are acceptable in the light of our present experience. Sometimes after the silver-sensitization bake, the red response is above 120 but below 200. Further evaporation of a small amount of silver (without a subsequent bake) will serve to bring the response down to the correct value. This further evaporation, if done properly, lowers the long-wavelength limit without greatly affecting the total sensitivity (the white-light sensitivity may fall from 15 to 13 microamperes per lumen). Checks with filters during this process are used to make sure that the infrared sensitivity is not too great for good reproduction. The

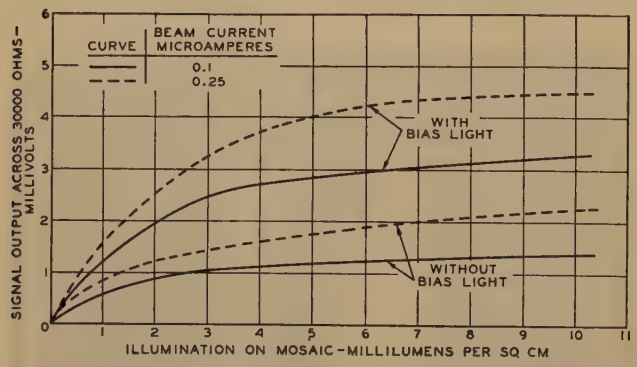

Fig. 17—Signal output for various values of illumination of a "direct pickup" iconoscope with and without "bias lighting."

presence of too much infrared sensitivity causes a graying of certain blacks used in studio work, as well as throwing doubt on the results obtained with the Agfa chart.

The last measurement to be considered is that of the resolution of the iconoscope. A converging-wedge resolution pattern is used. Without the silver-sensitization process, tubes showing unsatisfactory resolution could be improved only by baking. With silver-sensitized tubes, it is found that the resolution improves during the sensitizing process. If the resolution is not sufficient after this sensitization and baking, further evaporation of a small amount of silver generally gives satisfactory improvement. By this process, the final resolution can be made at least as good as for the non-silver-sensitized tubes, and generally better.

So far we have considered the general improvement in the characteristics of iconoscopes when silver sensitization is used. Actual operating experience has led to the development of two types of iconoscopes having silver sensitization. We call these the "movie pickup" and "direct pickup" iconoscopes. The difference between them is in the silver evaporators. In the "movie" type, the silver evaporator is surrounded by a shield which allows silver to be deposited only on the mosaic. In the "direct" type, the evaporator is designed to deposit silver on the walls of the bulb as well as on the mosaic. Deposition of silver on the mosaic only in the "movie" type is necessary to prevent a spurious signal caused by the intermittent and rapidly changing illumination encountered in conventional movie projection when the walls of the tube are photosensitive. A different condition exists in studio use where the illumination is continuous. The photosensitivity of the walls in this case can be used to advantage. A "bias" light so situated as to illuminate the walls, but not the mosaic, increases the sensitivity and signal output of the tube. The advantageous effect of this light was first discovered by engineers of the Electrical and Musical Industries, Ltd., and has been used for some time in their installation for the British Broadcasting Company.[3] The curves of Fig. 17 show the marked improvement in signal output obtained by the use of the "bias" light for two different beam currents. The solid-line curves show the signal output for 0.1 microampere beam current, while the dashed-line curves show it with 0.2 microampere beam current. It is interesting to note that the signal output for a beam current of 0.1 microampere with "bias" light is better than that for a beam current of 0.25 microampere without "bias" light. This increase in signal output is obtained with a decrease in the magnitude of the dark-spot signal, since the latter depends primarily upon the beam current. The explanation of the effect of "bias" lighting is that photoemission from the walls gives rise to a more advantageous field for the collection at the second anode of photoelectrons emitted by the mosaic.

The practical benefits of these recent changes and improvements of the iconoscope are summarized as follows:

1. Greater signal output which results in a better ratio of signal to noise and dark spot.
2. Greater sensitivity which permits the use of less illumination, or a greater depth of focus of the field.
3. Better spectral response which results in better black-and-white reproduction of colors.
4. Elimination of specular reflection.
5. Improved resolution.
6. A constant-current gun.
7. A bulb which provides better optical quality, symmetry of field, smaller size, and a rugged mosaic support.

Acknowledgment

The authors wish to thank the television group of the National Broadcasting Company for assistance in obtaining some of the illustrations, and engineers of Radiotron Research and Engineering Department who contributed helpful advice.

[3] The effect of "bias" lighting is included in this paper by permission of the Electrical and Musical Industries, Ltd., Hayes, Middlesex, England.

The Image Iconoscope*

HARLEY IAMS†, MEMBER, I.R.E., G. A. MORTON‡, ASSOCIATE MEMBER, I.R.E., AND V. K. ZWORYKIN‡, FELLOW, I.R.E.

Summary—An iconoscope having increased sensitivity is to be desired for purposes of improving studio conditions, making possible more universal outdoor work, and permitting greater depths of focus. The new tube described obtains its high sensitivity by making use of an electron image of the scene to be transmitted, projected onto a scanned mosaic. The method permits more efficient and better photocathodes, and also secondary-emission image intensification at the mosaic, resulting in a sensitivity 6 to 10 times greater than that of the standard iconoscope operated under the same conditions. The translucent photocathode is made by evaporating silver on a transparent surface, oxidizing, treating with caesium, and evaporating more silver. The electron image may be focused by either electrostatic or magnetic fields. Several types of mosaics are suitable for receiving and storing the electron picture.

THE iconoscope has been in service as a television pickup tube for some time and its capabilities under a wide variety of conditions are well known.[1,2] Quantitative data on its performance are now sufficiently numerous to be able to state definitely what can be expected from the present standard iconoscope. The conclusion to be drawn from this information is that while the tube is sufficiently sensitive to permit the transmission of an excellent picture from both studio and outdoor scenes, a very real improvement in the quality of the transmitted picture could be had if the sensitivity were increased.

It is found that to obtain an optimum picture with an f/4.5 lens of 7-inch focal length, a surface brightness of from 100 to 200 candles per square foot is desirable. This means, when a reflection coefficient of 0.25 is assumed, that the illumination must be of the order of from 1000 to 2000 foot-candles. Of course, a picture of high entertainment value can be obtained with less than 10 per cent of this light.

In the studio the amount of light available is at the disposal of the operator, and the required 1000 to 2000 foot-candles is always obtainable. Light of this intensity is not harmful and is far from unbearable; however, it is not comfortable and is accompanied by considerable heat. For comparison it may be stated that the illumination in direct sunlight on a summer day is about 9000 foot-candles.

The operating sensitivity of an iconoscope is directly determined by the depth of focus which is needed. In this, the television pickup tube differs from the photographic camera. For either case, only the diameter of the lens determines the distance which an object can be moved toward or away from the lens without the image being blurred a given percentage of its height. Proof of this statement is as follows.

Referring to Fig. 1, the object and image distances

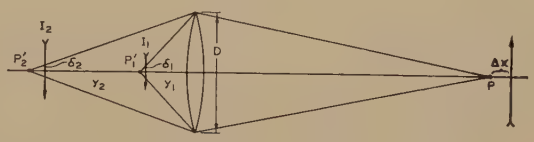

Fig. 1—Depth of focus in the object field.

$$y = \frac{fx}{x - f} \qquad m = \frac{f}{x}$$

$$\frac{dy}{dx} \cong -\frac{f^2}{x^2} \qquad \frac{\delta}{m} = D\frac{\Delta x}{x}$$

$$\delta = \frac{D}{y}\Delta y = D\frac{\Delta x}{x}$$

are x and y, respectively, and the focal length of the lens f. These quantities are related by the equation

$$y = \frac{fx}{x - f}.$$

By differentiation, a change in the object distance Δx is found to produce a change in image distance of

$$\Delta y \cong \frac{-f^2}{x^2}\Delta x.$$

This will produce a circle of diffusion in an image at y of

$$\delta = \frac{D}{y}\Delta y = D\frac{f}{x}\frac{\Delta x}{x}$$

where D is the diameter of the lens, and the object distance is assumed to be large compared with the focal length.

Since the magnification is given by f/x, the quantity to be determined, that is, the circle of diffusion divided by the magnification, can be expressed as follows:

$$\frac{\delta}{m} = D\frac{\Delta x}{x},$$

indicating that the depth of focus at the object is dependent only upon the lens diameter.

Since the blackening on a photographic plate depends upon the light intensity reaching the plate, it is possible to decrease the size of the picture and the focal length of the lens, keeping the numerical aperture constant, thus increasing the depth of focus without loss of sensitivity. In the case of the icono-

* Decimal classification: R583×R330. Original manuscript received by the Institute, August 1, 1938; abridgment received by the Institute, July 12, 1939. Presented, Thirteenth Annual Convention, New York, N. Y., June 17, 1938.

† RCA Manufacturing Company, Inc., Harrison, N. J.
‡ RCA Manufacturing Company, Inc., Camden, N.J.

[1] V. K. Zworykin, "Iconoscopes and kinescopes in television," *RCA Rev.*, vol. 1, pp. 60–84; July, (1936).

[2] V. K. Zworykin, G. A. Morton, and L. E. Flory; "Theory and performance of the iconscope," PROC. I.R.E., vol. 25, pp. 1071–1093; August, (1937).

scope the signal output depends not only upon the intensity of the light falling upon the mosaic, but also the velocity of the scanning spot across the area. Thus, for a given scanning frequency, the picture signal is proportional to the total light flux rather than the intensity. If, then, the mosaic area and lens focal length are decreased, keeping the aperture constant, there is a resultant loss in sensitivity. The conclusion is that the depth of focus can be obtained only by decreasing the lens diameter and increasing the sensitivity of the tube, irrespective of the numerical aperture of the lens. In other words, it may be said that for a given sensitivity of iconoscope the signal output is approximately inversely proportional to the square of the depth of focus in the object field.

The increased sensitivity required for lower light levels and greater depths of focus can be approached from a number of different directions. Perhaps the first to mention is that of improving the performance of the ordinary iconoscope. Important advances

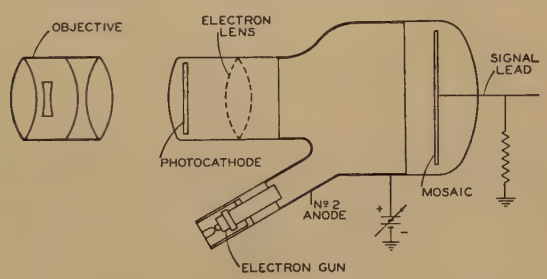

Fig. 2—Schematic diagram of image iconoscope.

have been made along this line in the past few years, by improving the photosensitivity and the operation of the mosaic.[3] Improvements have also been made in the amplifier and coupling circuits which have increased the effective efficiency of the tubes. These advances will undoubtedly continue in the future, but material improvement becomes increasingly difficult.

A second approach is through the use of the secondary-emission multiplier as a means of amplifying the signal. Work is being carried on along this line and shows definite promise.

Another method is by the use of secondary-emission image intensification, that is, an iconoscope in which an electron image of the object being televised, instead of an ordinary light image, is focused onto the mosaic.

It is interesting to note that this general method of increasing iconoscope sensitivity has been proposed by a number of television workers all over the world. To the writers' personal knowledge, by 1934 various phases of the idea had been advocated by A. V. Bedford, H. A. Iams, G. A. Morton, G. N. Ogloblinsky, A. W. Vance, and V. K. Zworykin. On February 12, 1936, British patent 442,666 was issued to H. G. Lubszynsky and S. Rodda. Various experimental results have been published by Knoll and Schröter;[4] Iams and Rose;[5] Zworykin, Morton and Flory;[2] Nagashima, Shinozaki, Udagawa, and Kizurka;[6] and a description of the use of such a tube by British Broadcasting Company appeared in *Wireless World*.[7] This paper is presented for the purpose of giving additional technical information on the subject.

In one practical form the image iconoscope consists of a photoelectric cathode upon which an optical image can be projected, an electron-lens system for focusing the electrons leaving the photocathode onto the mosaic, and an electron gun which scans the mosaic in the ordinary way. This is shown schematically in Fig. 2. The photocathode used in this type of tube is semitransparent so that the light image can be projected on the rear surface while the electrons are emitted from the face. The electron-lens system is so arranged that there is a strong field drawing the electrons away from the photocathode, in order that the photoemission may be completely saturated. The electron-lens system, which will be described in detail later, may make use of magnetic or electrostatic lenses or a combination of the two. When an optical image is projected on the photocathode, electrons are emitted from the latter at a rate per unit area proportional to the light intensity. Thus, close to the photocathode there is a charge reproduction of the light image. The electrons making up this charge image are accelerated toward the mosaic and focused on it by the electron-lens system. Therefore, there is projected on the mosaic an image made up of high-velocity electrons. The mosaic is made in such a way that for every electron which strikes it, several secondary electrons are emitted. In this way areas which are bombarded become positive with respect to the rest of the surface. The electron image striking the mosaic produces, in consequence, a charge image similar to that produced by the photoelectrons from an optical image on a light-sensitive mosaic. When scanned, this charge image gives rise to the picture signal.

The advantages gained by projecting an electron image upon the mosaic are as follows.

First, the photocathode may be improved. By disregarding the shape of the spectral curve it is possible to make semitransparent photocathodes which have a sensitivity between 20 and 50 microamperes per

[3] Some of the results are described in a companion paper, by R. B. Janes and W. H. Hickok, "Recent improvements in the design and characteristics of the iconoscope." Presented, Thirteenth Annual Convention, New York, N. Y., June 17, 1938. Proc. I.R.E., this issue, pp. 535–540.

[4] Knoll and Schröter, "Translation of electron pictures and drawings with insulating and semiconducting layers, *Phys. Zeit.*, vol. 38, pp. 330–333; May 1, (1937).

[5] Iams and Rose, "Television pickup tubes with cathode-ray beam scanning," Proc. I.R.E., vol. 25, p. 544; May, (1937); Proc. I.R.E., vol. 25, pp. 1048–1070; August, (1937).

[6] Nagashima, Shinozaki, Udagawa, and Kizurka, "The 'Tecoscope' C-R television transmitter," *Rep. Rad. Res.* (Japan), vol. 7, pp. 12 and 13; June, (1937).

[7] "Super-Emitron camera," *Wireless World*, vol. 41, pp. 497–498; November 18, (1937).

lumen, and this value will probably become still greater as a result of further research on these emitters. This is to be compared with the present maximum of 15 microamperes per lumen for the standard mosaic. Even more important is the fact that a strong field exists at the photocathode, which saturates the emission. When it is remembered that the efficiency of the mosaic as a photocathode is only 20 to 30 per cent due to the unfavorable field condition in an ordinary iconoscope, the advantage of this method as far as the photoelectric emission is concerned is obvious.

Second, the photoelectrons are focused on the mosaic, which has a high secondary-emission ratio. The actual measured ratios for various types of mosaics have values from 3 to 11. However, since there exists on the mosaics of this type of tube the same unfavorable field conditions found in the case of the ordinary iconoscope, the secondary emission is not saturated. Therefore, only a fraction of the saturated secondary emission is available for producing the charge image. The value of this fraction depends upon the distribution of initial velocities of the substance in question. When there is a large percentage of high-velocity secondary electrons, the fraction of the total secondary-emission ratio available is greater, and for a given ratio both saturated signal output and the sensitivity at low lights is higher. The relation here is very complicated, however, since these same factors influence the behavior of the electrons produced by the beam and, consequently, both

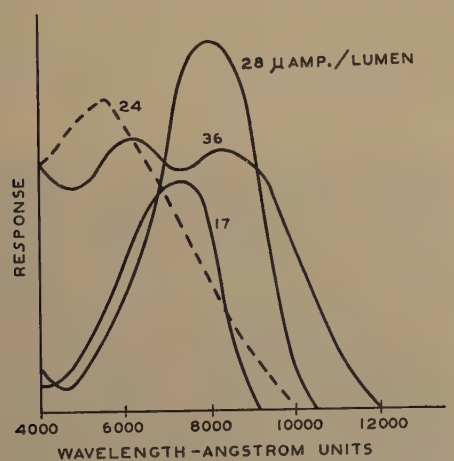

Fig. 3—Spectral response of semitransparent photocathodes.

the electron redistribution and the potential distribution on the mosaic.

Now that the more important general aspects of the image iconoscope have been considered, there are certain details of its construction that should be more completely outlined.

The photoelectric cathode is one of the most important elements of the tube, and perhaps the most difficult to prepare. One convenient form consists of a glass disk, which may be the end of the tube, upon which is evaporated an extremely thin layer of silver. This silver is oxidized by electrically glowing in it an atmosphere of oxygen at low pressure. Caesium is then admitted and the tube is baked. The final sensitization is done by adding another minute layer of silver. The complete preparation and activation is carried out after the tube has been assembled, exhausted, and the thermionic cathode in the gun activated. This procedure requires the mounting of

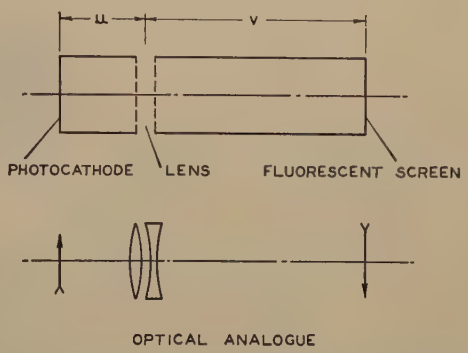

Fig. 4—Diagram of basic electrostatic-lens system.

a source for evaporating silver in the tube in such a way that it does not interfere with the operation of the iconoscope. To meet this requirement the evaporating filament may be mounted in the apertures of the electron lens where it does not interfere with the electron-ray bundle or the field configuration, or it may be made movable so that it can be withdrawn to a position where it does not affect the operation.

The sensitivity of this type of cathode lies between 20 and 50 microamperes per lumen. The value is, in general, somewhat lower when the films are made in such a way as to reduce the ratio of infrared sensitivity to visible response. Even today the technique for making semitransparent films of this type with an emission as high as 50 microamperes per lumen suitable for use in an iconoscope is still being experimentally investigated.

Spectral-sensitivity curves which have been obtained are shown[8] in Fig. 3. To a considerable degree, it is possible to control the shape of the spectral curve by controlling the processes.

The electron-optical system for focusing the electron image from the photocathode on the mosaic may make use of either magnetic or electrostatic lenses.

The electrostatic lens system is based primarily upon the field between two coaxial cylinders.[9,10] It is shown, in its simplest form, in Fig. 4, together with the corresponding optical analogue. In the form ac-

[8] These spectral sensitivity curves were plotted on the automatic spectral sensitivity curve tracer developed by T. B. Perkins, Research and Engineering Department, R.C.A. Manufacturing Company, Inc., Harrison, N.J. A technical description of this instrument is to be published soon.

[9] V. K. Zworykin and G. A. Morton, "Applied electron optics," *Jour. Opt. Soc. Amer.*, vol. 26, pp. 181–189; April, (1936).

[10] G. A. Morton and E. G. Ramberg, "Electron optics of an image tube," *Physics*, vol. 7, pp. 451–459; December, (1936).

tually employed the cathode cylinder is divided into a series of rings which are connected to successive steps of a voltage divider in order to permit electrical focusing of the image. Furthermore, the cathode is curved to reduce curvature of the image-plane distortion and astigmatism. The appearance of a corrected and an uncorrected image produced by this type of system is shown in Fig. 5. The limit of the resolution of a system corrected as described is set by

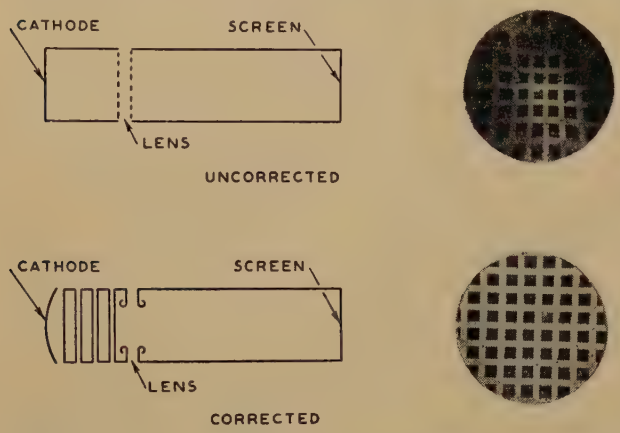

Fig. 5—Corrected and uncorrected electrostatic-lens system.

chromatic aberration, that is, the aberration produced by the distribution of axial initial velocities. Without resorting to very elaborate correcting systems, the only way of raising this resolution limit is to use high over-all potentials, thus reducing the ratio of initial velocity to working velocity.

Experimentally, it is found that with 1000 volts the resolution corresponds to about 400 lines, while at 3000 volts it is 800 lines or better. In the case of the higher voltage, mechanical imperfections of the lens and cathode probably determine the limit. A typical lens structure is shown in Fig. 6.

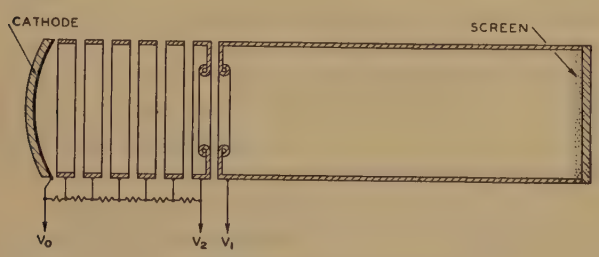

Fig. 6—Electrostatic-image tube.

From a theoretical point of view, the magnetic-lens system is much more complicated than the electrostatic lens. Structurally, however, it is no more difficult.

The simplest magnetic lens is formed by a uniform magnetic field. Such a field will produce an undistorted, erect image whose principal aberration is that due to initial velocities. This form of lens does not readily lend itself to the present image iconoscope. The other extreme is the so-called short-coil lens, which produces an inverted image whose magnification is a function of object-to-coil and coil-to-image distance. Unless this coil can be made large compared with the electron bundle being focused, the aberrations are very severe. Between these two extremes there are a great many possible types of lenses. It is found that if a lens coil is made in such a way that the flux lines close to the cathode approximately coincide with the paths which would be traversed by the electrons in the absence of the magnetic field, the image defects are minimized. To accomplish this, a focusing coil with distributed windings may be used.

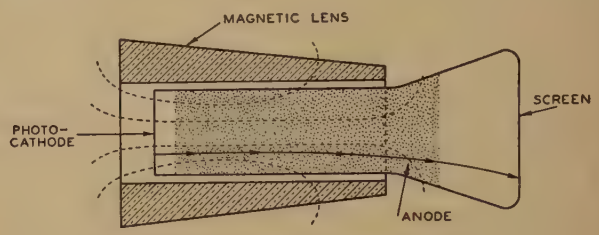

Fig. 7—Magnetic-image tube.

A lens designed on this principle is diagrammed in Fig. 7. This lens produces a real image which is rotated at an angle of about 30 degrees with respect to the object. The electrons do not cross the axis of the system as they do in the case of the electrostatic lens, but execute approximately helical paths about the axis in such a way that their radial distance changes only by an amount equal to the image magnification. Because of this, the variation in convergence for rays originating at different radial distances along the cathode is small, and the curvature of the image plane is much less than in the electrostatic case. The most important image defects in this type of lens are

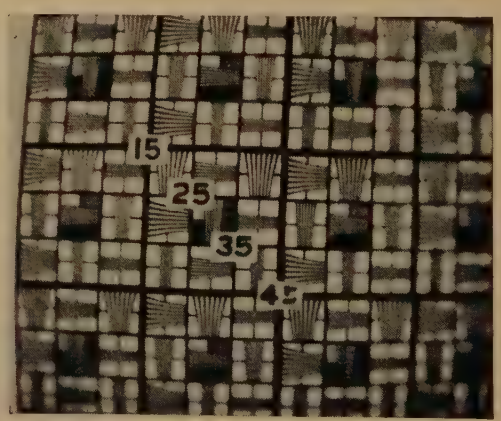

Fig. 8—Resolution pattern by magnetic-image tube.

curvature of the image field, pincushion distortion, and rotational distortion.

The first two are sufficiently small so that it is found unnecessary to curve the cathode to correct for them. By properly choosing the length, position, and distribution of the magnetic coil used as lens, the

rotational distortion can be minimized. Chromatic aberration, similar to that already described, exists in this lens. Its effect can be reduced by using fairly large over-all voltages. Fig. 8 shows an image produced by this type of lens. While the image defects mentioned are observable, they are relatively unimportant.

Considering next the mosaic for the image iconoscope, it is evident that it must meet the following requirements:

(1) Capacitance between the front surface and signal plate of about 100 micromicrofarads per square centimeter. The value used is not at all critical and may be much smaller or larger than this figure, but it should be uniform over the surface of any one mosaic.
(2) The resistance must be high, both through the dielectric and over its surface.
(3) The secondary-emission ratio and initial velocities must be high. These must also be uniform over the surface.

There are many ways of preparing mosaics which are satisfactory for this type of tube. Only three will be considered here.

The first type is prepared in the same way as the mosaic used in the ordinary iconoscope. Before it is mounted in the tube a mica sheet, about 1.5 mils thick and free from flaws, is coated on one side with a conducting film to serve as signal plate, and on the other with a vast number of minute silver elements. After the tube is exhausted the silver is oxidized and caesiated. One thing that recommends this type of mosaic is that it is comparatively easy to produce a surface which is free from blemish and which is uniform.

A second "mosaic," which leads to greater sensitivity and also permits higher resolution, can be made by using mica of the same thickness as given above and having the usual signal plate. Instead of covering the face with silver, the mica is left free. Thus, although the mica serves the purpose of a mosaic, its surface is a continuous insulator. The treatment used to activate the surface is to glow it in oxygen and then expose it to caesium vapor. Both secondary-emission ratio and sensitivity are higher in this case than for the first-described mosaic. It is, however, more difficult to obtain uniformity in the case of a mosaic of this type.

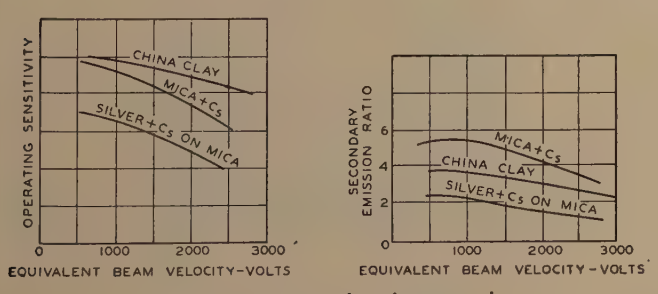

Fig. 9—Properties of various mosaics.

The final form of mosaic to be described differs from those previously mentioned in that it makes use of an insulator in the form of a finely divided powder covering a metallic signal plate. The response for this type of mosaic is considerably higher than for either of the others. With a proper technique excellent mosaics of this type can be obtained, not only in their sensitivity but also in uniformity. When suitably activated this type of mosaic lends itself well to the mode of operation in which use is made of conductivity through the mosaic, a potential being applied between second anode and signal plate. Fig. 9 shows typical secondary-emission[11] and response curves for these mosaics.

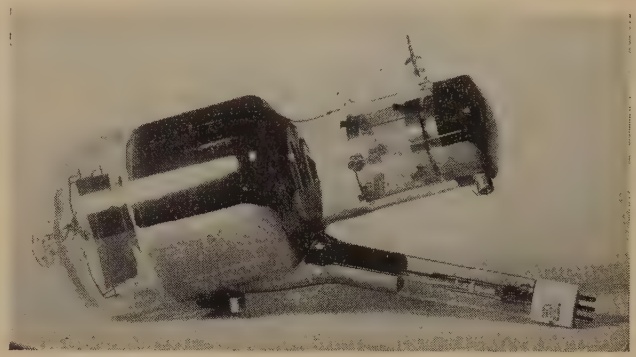

Fig. 10—Photograph of electrostatic-image iconoscope.

The final element, the electron gun, is of conventional design and has been described fully in the literature. The beam voltage used with this type of tube is in the neighborhood of 1000 volts and the current in the scanning beam between 0.1 and 0.2 microampere. In this respect it resembles the ordinary iconoscope.

Several types of image iconoscopes have been developed to a point where they are adequate for practical television transmission. Three of these developmental types are illustrated in Figs. 10, 11, and 12. The first two are electrostatically focused tubes, both embodying the use of a curved cathode. It should be pointed out that the curved cathode presents a rather serious optical problem when used with a large-aperture lens, in that a correcting system must be used to

Fig. 11—Photograph of electrostatic-image iconoscope.

[11] Data supplied by Herbert Nelson and R. B. Janes, Research and Engineering Department, RCA Manufacturing Company, Inc., Harrison, N.J.

fit the light image to the curved surface. The electrostatic tubes are usually operated with the cathode at −2000 to −3000 volts and the second anode at ground potential. The focusing voltage can be supplied from a potential divider between cathode and second anode, which minimizes the filtering required for the voltage source.

Fig. 12 shows a magnetically focused tube, without its lens coil. Since the cathode used in this tube is flat it presents no particular optical problem. The mag-

Fig. 12—Magnetic-image iconoscope.

netic lens has a flux density on the axis of about 50 gauss. No second focusing voltage is required as focusing is done by adjusting the magnetic field.

While the operating conditions of these tubes are in a way similar to those of the ordinary iconoscope, there are some differences which are important and should be considered.

The use of an electron image tube requires that three adjustments be made: the optical image, the electron reproduction, and the beam. In operation, the last two can be adjusted once and for all, and only the optical focus changed to meet the different scenes.

Although, as has already been indicated, the operating sensitivity of the tube decreases as the voltage on the photocathode is increased above 600 to 800 volts, nevertheless the improvement in resolution and crispness of the picture makes it advisable to use from 2000 to 3000 volts, particularly in the case of the electrostatic tube.

Another advantage of using the higher voltages is that it minimizes the interaction between the image and the deflecting field of the scanning beam. Tests indicate that at 2000 volts this interaction is negligible.

The earth's magnetic field constitutes another source of interference. Since in these latitudes the earth's magnetic vector makes an angle of about 70 degrees to the horizontal, its effect is to deflect the electron images to one side and either to shift the image up or down, or to rotate it slightly, depending upon the direction the tube is pointing. In the case of the magnetic tube this may be compensated by letting the axis of the magnetic lens make a slight angle with the axis of the tube. This angle may be adjustable to take care of different directions of the tube. The correction in the case of the electrostatic tube is accomplished by means of three mutually perpendicular sets of coils over the lens end of the tube. Without this compensation, the displacement of the picture on the mosaic may be as much as 5 per cent of its width or the rotation may be as much as 10 degrees.

As is the case with all iconoscopes, a spurious signal (which can easily be compensated) is generated by the scanning action on the mosaic as a consequence of the electron redistribution phenomenon. However, because of the high symmetry of the tube, and the small amount of exposed glass, the spurious signal is very small in these image iconoscopes. This factor is a very important point in their favor.

The sensitivity of the image iconoscopes, which have been described is, under comparable operating conditions, between six and ten times that of the usual form of iconoscope. This sensitivity is in terms of light flux in the optical image rather than in terms of image brightness for reasons explained in the first part of the paper. The lenses used with image iconoscopes are commonly of shorter focal length than those used with iconoscopes. Thus, if the iconoscope uses an $f/4.5$ lens with a 7-inch focal length, the equivalent lens for one of the magnetic image iconoscopes has an f value of 1.6 and a focal length of 2.5 inches, and for one of the electrostatic image iconoscopes, it has an f value of 2.1 and a focal length of 3.25 inches. Such optical systems operate to give equal angles of view, equal depths of focus, and gather the same total light flux.

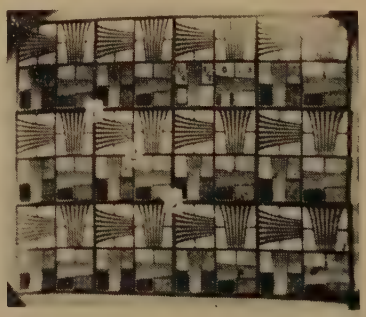

Fig. 13—Resolution pattern reproduced by electrostatic-image iconoscope.

While the sensitivity is important, the quality of the picture is even more important. The resolution in the case of the image iconoscope is about the same as that of the ordinary iconoscope, that is, high enough so that the definition of the picture is limited by electrical circuits rather than the tube. The high saturated signal output gives the tube a somewhat greater contrast range. In order to illustrate the quality of the reproduction by these tubes Figs. 13, 14, and 15 are presented.

The first is a resolution pattern transmitted by an electrostatic tube, the second and third typical scenes by a magnetic and an electrostatic tube, respectively.

Fig. 14—Television image reproduced by a magnetic-image iconoscope.

The pictures just shown clearly indicate that these image iconoscopes are practical working tools, advanced well beyond the laboratory stage. These tubes have been subjected to quite exhaustive tests, both for studio and outdoor pickup, and have been found to have high sensitivity and signal output. The color response can be made high in the visible region, or peaked for infrared radiation.

It is not safe to predict what further increase in sensitivity can be expected from this type of tube; however, work is in progress along the lines of combining secondary-emission signal multiplication with

Fig. 15—Television image reproduced by an electrostatic-image iconoscope.

image intensification, and also of using more than one stage of image multiplication. Both of these investigations should be very fruitful.

Acknowledgment

In closing, the authors wish to express their debt to Mr. G. N. Ogloblinsky, deceased, and their appreciation of the able work of Drs. A. Rose and H. B. DeVore, and Messrs. L. E. Flory and E. A. Massa, which has made these results possible.

Television Pickup Tubes Using Low-Velocity Electron-Beam Scanning*

ALBERT ROSE†, ASSOCIATE MEMBER, I.R.E., AND HARLEY IAMS†, MEMBER, I.R.E.

Summary—*Television pickup tubes which use a low-velocity electron beam for scanning a photosensitive target offer the possibility of avoiding some of the limitations of devices which use a high-velocity beam. Some of the advantages of the low-velocity beam are: (1) low level of spurious signals, (2) high maximum signal output, and (3) high efficiency of conversion of light into signal. The major problems encountered are: (1) ways to keep the beam in focus and (2) ways to obtain undistorted scanning of the photosensitive target.*

One solution to the difficulties of low-velocity-beam scanning involves the use of a uniform axial magnetic field to guide and focus the beam near the target. Because of this magnetic field, the usual type of deflection plates or deflection coils cannot be used to advantage. Two types of scanning which may be used are: (1) the release by a flying light spot of a beam of photoelectrons from successive points on a photocathode already immersed in the magnetic field and (2) the displacement of a beam from a thermionic cathode by a pair of deflection plates or coils operating in conjunction with the axial magnetic field and having an aperture at least as wide as the target to be scanned.

Developmental television pickup tubes using each of these types of scanning with low-velocity electrons were tested and found to give the low spurious signal, high signal output, and high efficiency which had been expected. The second type, which used a thermionic cathode as the source of beam electrons, was preferred because of the greater focused beam current which could be obtained. The measured operating efficiency for one of these tubes was 71 per cent; the resolution of the transmitted picture corresponded to more than 100 lines per inch of target.

* Decimal classification: R583×R330. Original manuscript received by the Institute, September 12, 1938; abridgment received by the Institute, July 10, 1939. Presented, New York, N. Y., June 7, 1939.

† Research and Engineering Department, RCA Manufacturing Company, Inc., Harrison, N. J.

Introduction

MANY different devices have been used to convert an optical image into a sequence of video-frequency signals for television transmission. Of these, some of the most successful have used an electron beam to scan a target electrode upon which is focused the optical image of the scene to be transmitted. The target is usually made in such a way that a photoelectric effect causes a pattern of voltages corresponding to the light and shade of the picture to appear on the surface. When the target is scanned by the electron beam, the pattern of voltages representative of the picture controls the flow of current in the target circuit and so creates the video-frequency signals.

In an earlier paper[1] it was pointed out that in order to originate video-frequency signals the light on the target can be used to (1) control the number of beam electrons which reach the target surface, or (2) cause variations in the secondary-emission ratio

[1] H. Iams and A. Rose, "Television pickup tubes with cathode-ray beam scanning," PROC. I.R.E., vol. 25, pp. 1048–1070; August, (1937).

of different parts of the target, or (3) modulate the escape from the target of an otherwise uniform secondary emission. Of these methods, the third which uses a high-velocity beam to scan the target is exemplified by the well-known iconoscope;[2] the second has previously been discussed and demonstrated.[1,3] At this time, we shall be concerned primarily with the first method, which uses a low-velocity beam to scan the target. A consideration of the subject indicates that, although the use of the third method has resulted in the successful transmission of television pictures, the first method offers possibilities of increase in the efficiency of converting light energy to the video-frequency signal and reduction in the spurious signal. This paper, therefore, will compare the characteristics of high-velocity and low-velocity electron beams and describe several developmental television pickup tubes which use low-velocity-beam scanning.

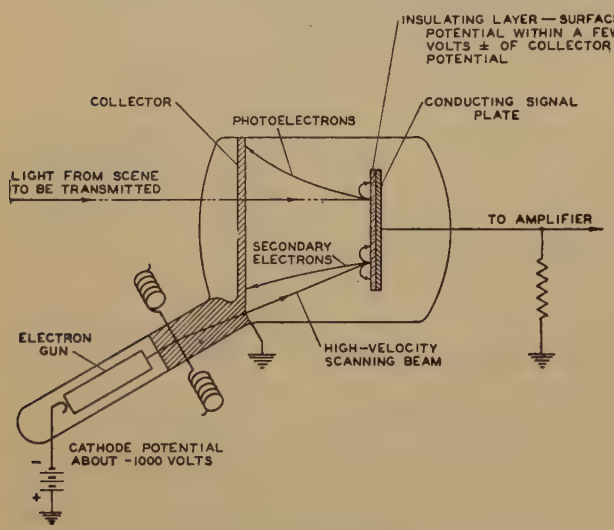

Fig. 1—Pickup tube using high-velocity electron beam for scanning.

A high-velocity electron beam may be defined as one in which the electron velocity is high enough to produce a secondary-emission ratio at the target greater than unity. A low-velocity electron beam may be defined as one in which the electron velocity is not high enough to produce a secondary-emission ratio at the target greater than unity. (The term secondary-emission ratio, in these definitions, is used to denote the ratio of the electron current leaving the target, as the result of bombardment by the electron beam, to the current arriving. The electron current leaving is composed of true secondary electrons and of reflected electrons.) Immediately it is seen that an insulating surface is charged positively when struck by a high-velocity beam, and negatively by a low-velocity beam. Yet, each of these beams may be used to neutralize the positive charges caused by the departure of photoelectrons from an optical image focused on the surface. A low-velocity beam does so by depositing electrons to replace the emitted photoelectrons. A high-velocity beam discharges such a surface by a more complex process which makes use of the redistribution of secondary emission over the target surface. Detailed discussions of this process have already been given in the literature.[1,4,5] From these discussions the following significant facts relative to the scanning of insulated surfaces with high-velocity beams emerge: (see Fig. 1)

(1) Redistribution of the secondary emission over the target surface is an essential part of the discharge process.

(2) The secondary emission produced at the target by the scanning beam, and likewise the photoemission from the target, is unsaturated.

(3) The potential swing of an element of the target is limited. (For targets coated with insulating materials this limitation is significant; for those with semiconducting coatings, it is less so.) Each of these facts may be translated into limitations in the performance of the pickup tube using a high-velocity beam.

(1) The redistribution of secondary electrons is, in general, not uniform over the target surface, and, therefore, gives rise to a spurious signal known as the "dark spot." The "dark spot" or nonuniform shading of the picture limits the usable beam current and the usable amplifier gain.

(2) The lack of saturation of the secondary emission, together with the lack of saturation of the photoemission, combine to reduce the operating efficiency of the pickup tube. In the case of the conventional iconoscope, the efficiency has been estimated to be about five or ten per cent.[4]

(3) The limited potential swing of an element of the target limits the maximum signal that may be obtained. This corresponds to the limited density range of a photographic film.

While high-velocity-beam scanning suffers from these limitations, it has an important virtue which is particularly emphasized when one tries to use a low-velocity beam. This virtue is the ease with which an extended target may be scanned in a rectilinear pattern and in a well-focused state. This virtue is exchanged for relative freedom from the above limitations when one uses a low-velocity beam.

The advantages of a low-velocity beam with respect to "dark spot," operating efficiency, and signal strength may be seen with the aid of Fig. 2. If the beam current is sufficient, the arriving electrons charge the target surface to cathode potential, after

[2] V. K. Zworykin, "The iconoscope—a modern version of the electric eye," Proc. I.R.E., vol. 22, pp. 16–32; January, (1934).

[3] C. E. Burnett, "The monoscope," *RCA Rev.*, vol. 2, pp. 414–420; April, (1938).

[4] V. K. Zworykin, G. A. Morton, and L. E. Flory, "Theory and performance of the iconoscope," Proc. I.R.E., vol. 25, pp. 1071–1092; August, (1937).

[5] H. Iams, G. A. Morton, and V. K. Zworykin, "The image iconoscope," Proc. I.R.E., this issue, pp. 541–547.

which no further electrons can strike the target. The collector potential may be sufficiently high to saturate any electron emission from the target; thus, when an element of the target is lighted a saturated photoemission is drawn to the collector and the element is thereby driven positive during the time when it is not scanned by the beam. When the scanning beam again arrives at the element it deposits enough negative charge to drive the potential back to cathode potential. The charging of the target surface to cathode potential releases a corresponding charge from the signal plate to produce the video-frequency signal. In this schematic form, low-velocity scanning avoids redistribution of electrons over the target surface, since the electrons liberated are all drawn to the highly positive collector. The above remarks, together with Fig. 2, make evident the following advantages of low-velocity scanning: (1) the lack of redistribution prevents the formation of a "dark spot" signal superimposed on the desired signal; (2) the high collecting field saturates both photoemission and secondary emission from the target and, thereby, makes possible one hundred per cent operating efficiency; (3) the potential swing of a target element may be 20 volts[6] or more (that is, up to the potential at which the secondary-emission ratio goes above unity) depending upon the nature of the target surface.

Against these advantages must now be placed the limitations in the use of a low-velocity beam. For example, the simple schematic arrangement of Fig. 2

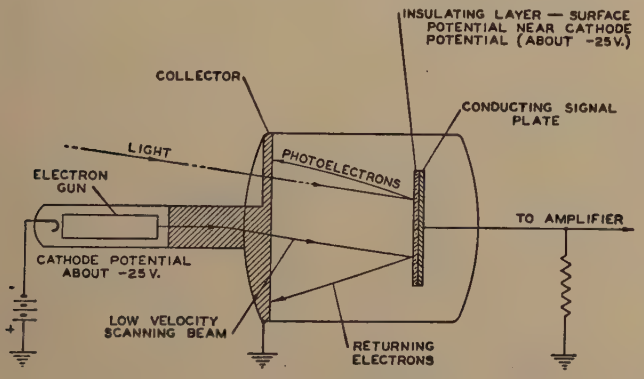

Fig. 2—Pickup tube using low-velocity electron beam for scanning.

is not a practical one, since the beam, as it is slowed down to zero velocity near the target, is very unstable. The operation is markedly affected by wall charges, by small potential differences over the target surface, and by space charge in the beam itself. Also, there is set up, even with no picture on the target, a potential gradient along the target surface due to the varying angle of incidence of the beam. (This will be discussed in more detail below.) In actual tests, using the arrangement in Fig. 2 and a conducting target on whose surface a carbon pattern had been impressed to provide contact-potential differences along the surface, the transmitted picture became badly blurred due to defocusing of the beam, and badly distorted due to wall charges as the beam velocity near the target approached zero. Fig. 3 shows the decreasing resolution that was obtained with decreasing beam velocity in one test of this arrangement.

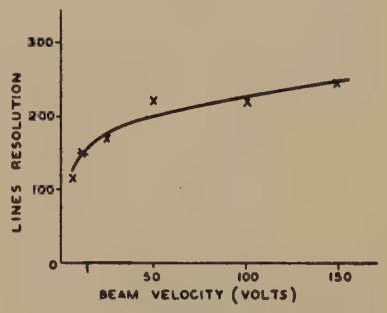

Fig. 3—Curve illustrating tendency of an electron beam to defocus at low velocity.

These introductory remarks have set forth the advantages to be gained from low-velocity scanning and have introduced one important difficulty to be met in devising a low-velocity scanning arrangement. The remainder of the paper will be devoted to the problem of devising and using arrangements for low-velocity scanning. The problem will be considered from the following aspects in order: (1) conditions to be satisfied by low-velocity scanning; (2) means for accomplishing low-velocity scanning; and (3) applications to pickup tubes. Under the last-named heading, the results of tests on pick-up tubes using low-velocity scanning will be presented.

Conditions To Be Satisfied by Low-Velocity Scanning

A satisfactory quantitative discussion of the behavior of a low-velocity beam with respect to resolution, velocity components of the beam at the target, and maximum permissible beam current deserves a more detailed treatment than is consistent with the scope of this paper. Such a treatment will be reserved for a later time. For the present, emphasis will be placed upon setting forth the nature of the problems involved, together with some tested means of solving them.

Resolution

At the outset, the fact that the beam, as the electrons approach the target with velocities near zero, tends to expand by virtue of the mutual repulsion of the electrons in the beam and tends to be distorted from its proper path by small potential differences on the target surface requires that some means be em-

[6] While large potential swings are possible in this formal description of low-velocity scanning, the potential swing in practice is limited to much lower values by the requirement of good resolution. The discussion below on the control of a low-velocity beam near the target will make this point clearer.

ployed to keep the beam in focus and to guide it in its proper path. The means employed for these purposes is a uniform magnetic field normal to the target and immersing the target. The magnetic field causes the electrons to rotate in tight spirals about the axis of the beam. At the same time, the effect of potential differences along the surface of the target, which in the absence of a magnetic field would accelerate the beam along the surface in the direction of the field, now in the presence of a magnetic field causes the beam to drift away from its normal path at right angles to the electric field with a velocity that may be made arbitrarily small by increasing the magnetic field. In brief, a uniform axial magnetic field immersing the target offers a means of keeping

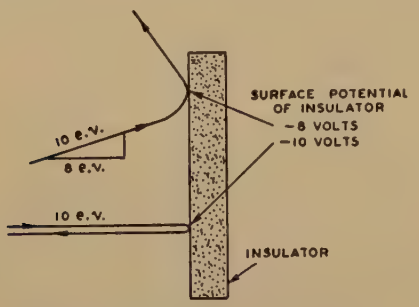

Fig. 4—Electron paths near target.

the beam well focused and substantially in its normal path as it approaches the target.[7]

Velocity Components of the Beam near the Target

It is desirable, though not absolutely essential, to have the electrons in the beam approach the target at all points, not only with low velocity, but also with the same component of velocity normal to the target surface. This is equivalent, if spurious potential gradients along the target surface are to be avoided, to requiring the angle of incidence of the beam to be constant over the target surface. Suppose that the beam does not approach the target at all points with the same component of velocity normal to the target. Then, at those places where this component is the larger, the target surface will be charged more negatively. (A low-velocity electron beam charges an insulator surface negatively until no further beam electrons can reach the surface. This is, of course, a condition of equilibrium.) The result will be a potential gradient along the target surface proportional to the gradient along the surface of the component of electron energy normal to the target.

This situation is illustrated in Fig. 4, which shows a ten-volt electron beam approaching the surface of an insulator at two different angles. At normal incidence the beam charges the surface to minus ten volts before the electrons are reflected. At other angles of incidence the potential assumed by the surface is numerically less than minus ten volts. For example, when, as in Fig. 4, the normal component of velocity corresponds to eight electron volts, the surface is charged to minus eight volts before reflection occurs. The potential gradient set up in this manner, if there is any appreciable conductivity over the target surface, gives rise to a spurious shading signal equivalent in its effect to the "dark spot" that has been cited as a limitation of high-velocity scanning. Other disadvantages will arise from this potential gradient depending on the type of target used. Thus, while the condition of constant angle of incidence is not indispensable to low-velocity scanning, it is favorable to its improved operation.

Beam Current

Relatively high beam currents are desirable in high-velocity scanning since the video-frequency signal strength increases with beam current. But the "dark-spot" signal increases with beam current, and more rapidly than the picture signal. A choice of beam current must often be made which is the best compromise between these two effects. The beam current used in an iconoscope is usually between one-tenth and one-half microampere. The beam current requirement for low-velocity scanning is simpler to state and to understand. The beam current need only be sufficient to discharge the target in one sweep or complete scanning cycle. Increasing the beam current beyond this point does not increase the operating efficiency or signal strength, since already all of the available signal is being generated. Increasing the beam current does, however, increase the light intensity that may be used on the target and, for this reason, the maximum signal that may be obtained. Also since, to discharge the same element of target, a several times larger low-velocity beam current must be used than high-velocity beam current,[8] the beam currents that must be generated for low-velocity scanning will, in general, be higher than those used for high-velocity scanning. The question, then, is, "Can low-velocity beams of the required magnitude (about two microamperes) be generated and controlled?"

There are two limitations to the amount of usable low-velocity-beam current. First, for a given magnetic field and beam velocity, increasing the beam current does tend to increase the beam cross section due to the mutual repulsion of the electrons. For the same beam cross section, increased beam currents require increased magnetic fields. Second, for a beam of given cross section, moving down the axis of a cylinder of given radius and potential, there is an upper limit to the beam current that may be passed.

[7] P. T. Farnsworth has also described the use of an axial magnetic field in other types of television pickup tubes.

[8] The rate of discharge by a low- or high-velocity beam is (secondary-emission ratio -1)$\times$beam current. For a low-velocity beam, the secondary-emission ratio is between zero and unity; for a high-velocity beam, the secondary-emission ratio is more than unity, and it may be as high as ten.

Beam currents in excess of this value are choked off by space charge and do not get through. Also, for beam currents approaching this maximum value, the velocity of the beam is a function of the beam current and surrounding space charges. These limitations may generally be avoided by arranging for the beam to move at a relatively high velocity until it is very near the target where it is slowed down over a short distance to substantially zero velocity.

Means for Accomplishing Low-Velocity Scanning

Up to this point some of the advantages to be gained from low-velocity scanning, and some of the problems involved in controlling the low-velocity beam near the target have been discussed. In this section, our attention moves a little farther away from the target to the problem of how such a low-velocity beam is to be deflected. This is a problem of some concern due to the presence of the previously described magnetic field located in the neighborhood of the target for the purpose of keeping the electron beam in focus. If deflection is accomplished in the usual manner before the beam enters the magnetic field, the pattern will be badly distorted by the fringing of the magnetic field. It is desirable, therefore, to accomplish the deflection within the uniform axial magnetic field. The operation of the several types of deflection, to be described below, is quite different from the operation of those ordinarily used in the absence of an axial magnetic field. Two general types have been tested—photoelectric-beam scanning and thermionic-beam scanning.

Photoelectric-Beam Scanning

The problem of accomplishing scanning in the presence of a uniform, axial, magnetic field is easily solved by letting a moving beam of light scan an extended photocathode already immersed in the magnetic field. Such an arrangement is shown schematically in Fig. 5. The light source in this case

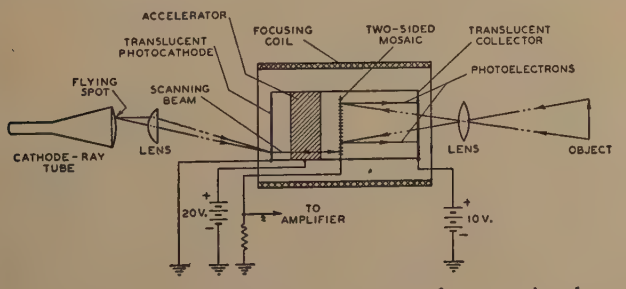

Fig. 5—Pickup tube using photoelectrons for scanning beam.

is the flying spot on the fluorescent screen of a cathode-ray tube located well outside the magnetic field of the pickup tube. The light is focused, by means of a lens, upon the photocathode. As the flying light spot sweeps across the photocathode, a beam of photoelectrons is released from the opposite side to scan the target. When the target is not lighted, the scanning beam charges it to a potential somewhat below that of the photocathode. The beam reverses direction just before striking the target and returns to the photocathode. If an element of the target is made positive by photoemission from

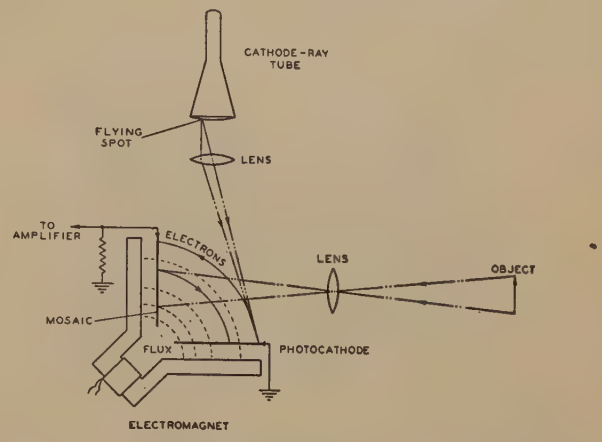

Fig. 6—Schematic diagram of pickup tube with photocathode and mosaic at right angles.

the opposite side, then the photoelectric beam deposits a negative charge on this element until it is driven back to the cathode potential. The amount of charge deposited determines the signal current. Photoelectric beams as high as two microamperes have been generated in this manner. (The objectionable trailing which ordinarily results from using a fluorescent light spot for scanning, for example, scanning film by transmission of the light spot through the film, is considerably reduced in this arrangement. The reason is that, if the photoelectric beam is more than sufficient to discharge an element of the target in one sweep, the photoelectrons arriving at the element during the finite decay time of the fluorescent spot do not land and do not, therefore, contribute an appreciable trailing signal.)

Another form of photoelectric-beam scanning is shown in Fig. 6. This tube has the advantage that an opaque photocathode of higher sensitivity than the translucent photocathode may be used to generate the scanning beam. Also, a one-sided mosaic, which is simpler to construct than a two-sided mosaic, may be used. With magnetic fields of the order of a hundred gausses and beam velocities of about 10 volts, the electrons slide along the magnetic lines almost as beads on a string, and maintain practically all of their energy in velocity along the lines. The condition of the constancy of the component of velocity normal to the target is thus easily satisfied.

Thermionic-Beam Scanning

In the case of photoelectric-beam scanning, the electron gun may be thought of as extending over the entire area of the photocathode, while various elements of it are sequentially actuated by the flying

light spot. The thermionic-beam-scanning method now to be described employs a localized cathode in an electron gun having a final aperture the size of the desired electron-beam cross section. Some separate arrangement must be used to deflect the beam from this localized source over the extended target area, one which preferably does not alter the axial velocity of the beam. Further, the arrangement must operate in conjunction with the uniform, axial,

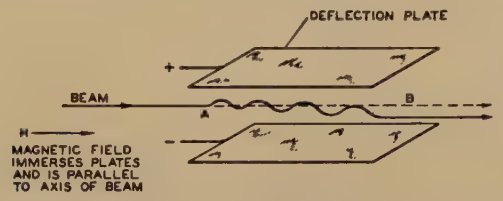

Fig. 7—Path of an electron beam deflected by an electric field in the presence of a magnetic field.

magnetic field used to guide the beam as it approaches the target. The axial magnetic field, rather than imposing an additional difficulty, turns out to be a useful part of the deflection system to be described. Electrostatic deflection in a uniform, axial, magnetic field will be considered first, since it may be used for both horizontal and vertical deflection or for horizontal deflection in conjunction with a pair of magnetic coils for vertical deflection. Deflection by a magnetic field superposed on the axial magnetic field will be considered separately, since the problems it involves are distinct from those of the electrostatic deflection.

The deflection of an electron beam by a varying electrostatic field in the presence of a constant, uniform, axial, magnetic field is illustrated in Fig. 7. When the electrostatic field is zero, the electrons pass between A and B without deviation. When the upper deflection plate is positive, as shown in Fig. 7, the beam is first deflected upward by the electrostatic field; in moving upward, the electrons move across the magnetic field, and the beam is thereby deflected to the side and somewhat downward. This motion continues until the retarding electrostatic field overcomes the downward component of the electron's energy, at which time the cycle is repeated. With each repeated cycle, the beam moves further toward the side of the deflection plates and it finally emerges at C with the electrons moving in a path parallel to their original path, but displaced from it.

If the path taken by the beam as it passes between the deflection plates were projected on a plane perpendicular to the axis, the figure would be a series of cycloids. The time required for one cycloid is a function only of the magnetic field. For best operation, the magnetic field should be so adjusted that the beam performs an integral number of cycloids while it is between the plates (e.g., three cycloids in Fig. 7). The dimensions of the cycloids depend upon both the magnetic and electric fields, and are proportional to the latter. Varying the electric field varies the amplitude of the cycloids, and the displacement of the emerging beam, but not the number of cycloids; reversing the electric field reverses the direction of deflection. From this description it is evident that the direction of scanning is parallel to the plane of a deflection plate, and that the deflection plates must be as wide as the width of the area to be scanned. By way of contrast, the usual electrostatic deflection plates in the absence of a magnetic field are small compared with the target to be scanned and the beam is deflected in a plane perpendicular to the plane of the deflection plates.

In order to make the beam scan a two-dimensional surface, instead of a single line, vertical and horizontal deflection plates may be combined into a rectangular box whose cross section is at least equal to the dimensions of the target to be scanned. Such an arrangement is shown in Fig. 8. The same arguments hold for two-dimensional scanning as for single-line scanning.

To summarize, it is found that the electrostatic deflection plates in a uniform, axial, magnetic field offer a means for moving an electron beam in a direction normal to the axis of the tube without a change of axial velocity of the electrons. The deflection is proportional to the deflecting electric field and to the transit time through the electrostatic plates and inversely proportional to the magnetic field. The width of the deflection plates must be as large as that of the target to be scanned.

The second type of deflection, a magnetic field normal to the axis superposed on the axial magnetic field, is, in the limiting case of low beam velocities, particularly easy to visualize. Fig. 9 shows the combination of these two fields and the electron path for a particular amplitude of deflection. In the limiting case of low beam velocities, the electrons move in a helical path whose axis is a magnetic line and whose

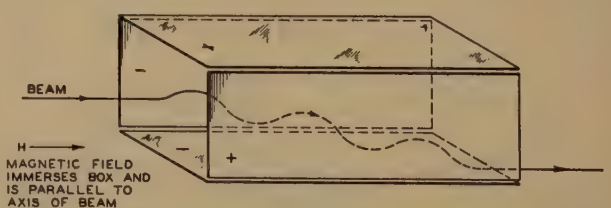

Fig. 8—Path taken by beam passing through rectangular electrostatic box.

diameter is small. The deflecting magnetic field refracts or displaces the axial magnetic field. The electron path is, thereby, displaced from the axis an amount proportional to the deflecting field and on emerging from the deflecting field remains parallel to the axis. The actual displacement, from the geometry of Fig. 9, is $(H_d/H_a)L$, where H_d is the deflecting field, H_a the axial field, and L the length of the deflecting field along the axis. Again, the con-

dition of the conservation of axial velocity is for all practical purposes satisfied for low beam velocities, strong magnetic fields, and large radii of curvature of the magnetic field. An appropriate set of values for these parameters is: beam voltage = 20 volts, magnetic field = 100 gausses, radius of curvature of magnetic field = 10 centimeters.

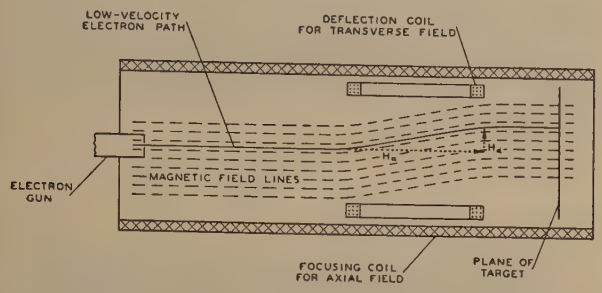

Fig. 9—Schematic diagram showing magnetic deflection of a low-velocity beam in an axial magnetic field.

While the electrostatic deflection can be used with equal convenience for horizontal or vertical deflection, a different result has been observed with magnetic deflection. In view of the large magnetic fields, both in extent and magnitude, that have to be generated by the deflection coils, it is at present more convenient to drive the coils at frame frequency than at line frequency. This leads to the combination of electrostatic horizontal deflection, and magnetic vertical deflection.

To summarize, it is found that magnetic deflection in a uniform, axial, magnetic field offers a means of deflecting a low-velocity electron beam without appreciably affecting the axial velocity of the beam. The amplitude of the deflection is proportional to the magnitude and length of the deflection field and inversely proportional to the axial field. The separation of the deflection coils must be at least as large as the dimensions of the target to be scanned.

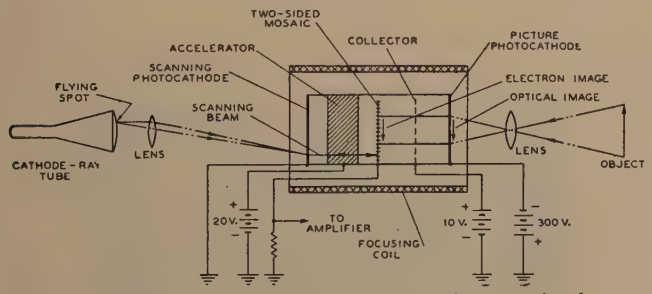

Fig. 10—Pickup tube using photoelectrons for scanning beam.

Applications to Television Pickup Tubes

The several methods of scanning with low-velocity electron beams discussed in the preceding sections have all been tested in television pickup tubes. These tubes, which are still in the developmental stage, were designed primarily for the purpose of testing the characteristics of low-velocity scanning. Nevertheless, the results from even these developmental forms show the advantages to be gained from these types of pickup tubes.

Photoelectric-Beam Scanning

Fig. 10 shows, in schematic form, the operation of a low-velocity photoelectric beam tube with a two-sided mosaic. Fig. 11 is a photograph of the tube itself. The operation is similar to that described above for Fig. 5 with this difference: that instead of projecting the optical picture directly on the two-sided mosaic, the optical picture is focused on a separate photocathode and a high-velocity electron image is projected on the two-sided mosaic. This procedure allows some gain in sensitivity, since each photoelectron knocks out several secondary electrons.

Fig. 11—Photograph of tube illustrated in Fig. 10.

The results obtained from this type of tube were, in general, limited by the amount of focused beam current that could be generated. One tube was able to transmit a picture limited in resolution only by the 65-wires-per-inch two-sided mosaic. Because of the characteristics of the particular cathode-ray tube which was used to produce the flying spot, the resolution decreased as the scanning-beam current was increased to two microamperes. No dark-spot signal attributable to redistribution of the scanning electrons was observed. The conclusions drawn from the operation of these tubes were that, while limitations of the particular developmental setup prevented a final picture of improved quality from being

Fig. 12—Photograph of tube illustrated in Fig. 6.

transmitted, conditions were arranged to demonstrate separately the improvements in signal strength, operating efficiency, and "dark-spot" control to be expected from low-velocity scanning.

A somewhat simpler arrangement for low-velocity photoelectric-beam scanning is shown in Fig. 6 which has been referred to above. Fig. 12 is a photograph of a pickup tube using this arrangement. The operation of the tube is similar to that described above for Fig. 5 except that the photoelectrons released from the mosaic by the optical image are collected by the scanning photocathode, instead of a separate collector electrode. This form of operation is made possible by the fact that the photoelectrons are emitted with appreciable velocity.

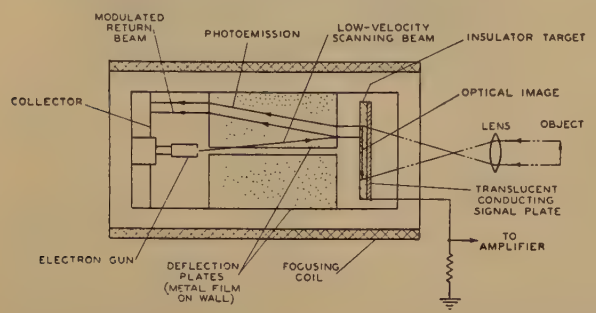

Fig. 13—Diagram showing operation of pickup tube with four electrostatic deflection plates.

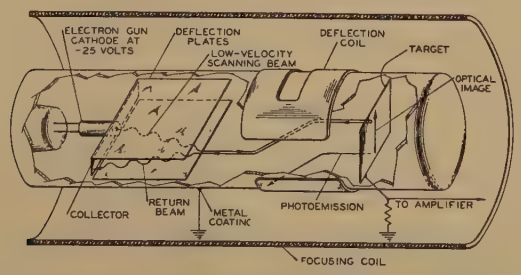

Fig. 14—Diagram showing operation of pickup tube with electrostatic horizontal and magnetic vertical deflection.

The pictures transmitted by this tube were quite free from spurious shading signals. The resolution was limited by the size of the flying spot, which was abnormally large because of the characteristics of the cathode-ray tube used. Because the collecting fields were small, the maximum signal strengths were of the order of those from television pickup devices using high-velocity beams. For the same reason, the operating efficiency was limited by the incomplete collection of photoemission from the optical picture.

Thermionic-Beam Scanning

Two types of tubes using thermionic cathodes have been tested and found to operate. One type used electrostatic horizontal and vertical deflection; the other used electrostatic horizontal and magnetic vertical deflection. These tubes are shown in schematic operation in Figs. 13 and 14 and photographs of the tubes are shown in Figs. 15 and 16.

For the purposes of the tests, a one-sided photosensitive mosaic with translucent signal plate was used, the optical image being projected on the mosaic through the signal plate. Both types of tubes were

Fig. 15—Photograph of tube illustrated in Fig. 13.

Fig. 16—Photograph of tube illustrated in Fig. 14.

able to resolve at least 100 lines per inch on the mosaic. The transmitted picture had very little spurious shading and relatively high signal strength. From the following measurements on one of the tubes, the operating efficiency was computed.

Photosensitivity of mosaic through translucent signal plate—2 microamperes per lumen

Area of mosaic scanned—23 square centimeters

Light intensity of spot on mosaic—6 millilumens per square centimeter.

Coupling resistor between signal plate and first amplifier tube—10,000 ohms

Observed signal across coupling resistor—2 millivolts

Fig. 17—Photograph of television picture transmitted by scanning a light-sensitive mosaic with a beam of low-velocity electrons.

An operating efficiency of 71 per cent was computed in the following manner.

Theoretical signal for 100 per cent operating efficiency

= mosaic area × photosensitivity × light intensity × coupling resistor

$= 23 \times 2 \times 10^{-6} \times 6 \times 10^{-3} \times 1 \times 10^{4} = 2.8$ millivolts.

Operating efficiency $= 2/2.8 = 71$ per cent.

A representative television picture transmitted by the tube of Fig. 14 is shown[9] in Fig. 17.

Conclusions

The experimental results which have been reported support the conclusions reached by a theoretical approach: (1) the use of low-velocity-beam scanning allows the construction of a television pickup tube which produces a negligible spurious signal; (2) the efficiency of conversion of light energy into video-frequency signals may be made higher when low-velocity electrons are used for scanning than when high-velocity electrons are used in the customary manner; and (3) pickup tubes which use low-velocity scanning are capable of large maximum signal outputs.

While many of the developmental problems relating to pickup tubes with these desirable characteristics have been solved, additional work is being done for the purpose of determining optimum designs.

[9] From the subject entitled "The Bandmaster," one of the Krazy Kat series, used by permission of the Columbia Pictures Corporation.

A Phase-Shifting Device for the Rapid Determination of Audio-Frequency Amplifier Characteristics*

KARL SPANGENBERG†, ASSOCIATE MEMBER, I.R.E.,
AND
WINSLOW PALMER†, STUDENT MEMBER, I.R.E.

Summary—*A description is given of a phase-shifting device which can be used with a beat-frequency oscillator and a cathode-ray oscilloscope to determine quickly the essential points on the frequency-response curve of an audio-frequency amplifier. Use is made of the fact that the phase shift through a single-stage amplifier is ±135 degrees when the gain has dropped to 70.7 per cent of the mid-frequency value, if the amplifier coupling circuit has no resonances. By properly introducing a 45-degree phase shift into the cathode-ray oscilloscope circuit from a network equivalent to an ideal cable a straight-line Lissajous figure is obtained at the 70.7 per cent relative-gain frequencies. The method is extended to include the determination of other significant frequencies in the commonest types of single- and multiple-stage audio-frequency amplifiers.*

THERE is a need for a device which will indicate quickly the effective frequency range of an amplifier in the testing of audio-frequency amplifiers. The answer is sought to the question: Over what frequency range is the gain of the amplifier constant within some allowed variation, say three decibels? The phase-shifting device described here gives a visual indication in the form of straight-line Lissajous figures which answers exactly this question. It also locates other significant points on the frequency-response curve.

It has been shown by Terman[1] that in a simple resistance-coupled amplifier the phase of the output voltage shifts 45 degrees from the mid-frequency value of 180 degrees at the high and low frequencies at which the gain is 70.7 per cent (−3 decibels) of the mid-frequency gain. The high and low frequencies at which this occurs will be designated by f_L and f_H, respectively. Hence if an amplifier of the resistance-coupled type is arranged with its output voltage connected to say the vertical plates of a cathode-ray oscilloscope and its input voltage to the horizontal plates, the introduction of a ±45-degree phase shift will result in a straight-line Lissajous figure at the frequencies of ∓45-degree phase shift of the amplifier. This principle provides a simple way of identifying the 70.7 per cent relative-gain frequencies and hence of checking the amplifier response.

A phase shift of 45 degrees independent of frequency may be obtained by using the network equivalent of an ideal cable in series with a very large resistance. An artificial ideal infinite cable is best made up of a cascade connection of symmetrical lattice sections. The form of the lattice sections used in the equivalent cable is shown in Fig. 1. Here the arms of the sections are pure resistances and capacitances. If the arms of a symmetrical lattice section are Z_a and Z_b, respectively, then the characteristic impedance of such a section is given by

$$Z_0 = (Z_a Z_b)^{1/2}. \tag{1}$$

For resistive and capacitive values of Z_a and Z_b this becomes

$$Z_0 = (R/j\omega C)^{1/2} \tag{2a}$$

$$= (R/\omega C)^{1/2} \angle -45°. \tag{2b}$$

From this it is seen that the magnitude of the char-

* Decimal classification: R263. Original manuscript received by the Institute, September 19, 1938; abridgment received by the Institute, July 10, 1939.

† Stanford University, Stanford, California.

[1] F. E. Terman, "Radio Engineering," page 175, McGraw-Hill Book Company, New York, N. Y., (1937).

acteristic impedance varies inversely as the square root of the frequency and that its angle is −45 degrees independent of frequency. To realize these properties it is necessary to terminate the line properly at all frequencies. This is difficult to do without using an infinite number of sections but the same

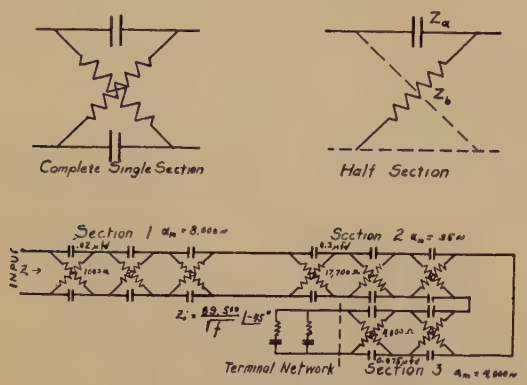

Fig. 1—45-degree network.

effect may be obtained by making the attenuation of the network great enough so that the magnitude of any voltage reflected back to the input terminals is negligible in comparison with the input voltage.

Examination of the attenuation properties of the lattice sections used shows that the attenuation is greatest at the frequency at which the value of the capacitive reactance is equal to the value of resistance. The propagation function γ of a lattice section is related to the impedance elements by the equation

$$\tanh \frac{\gamma}{2} = (Z_a/Z_b)^{1/2}. \qquad (3)$$

From (1) and (3) it is seen that the characteristic impedance depends upon the product of Z_a and Z_b whereas the attenuation depends upon the quotient

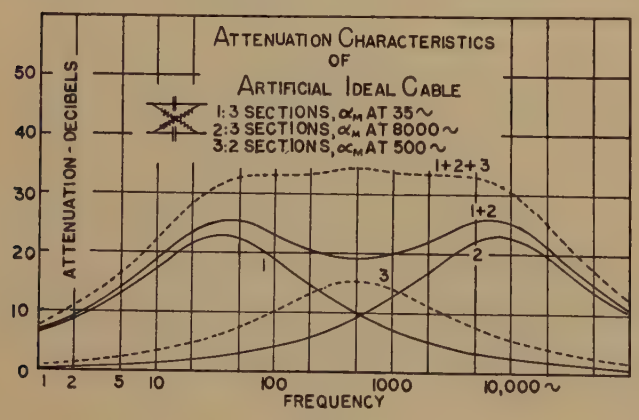

Fig. 2

of these same quantities. This property makes it possible to construct sections with identical characteristic impedances but with different attenuation characteristics. The cable used was made of eight sections with the configuration shown in Fig. 1. Three of the sections were identical and were designed to have a maximum attenuation at 35 cycles, three sections a maximum attenuation at 8000 cycles, and two a maximum attenuation at 500 cycles. All sets of sections have identical characteristic impedances and so match perfectly without reflection from the junction over the entire frequency range. The attenuation characteristic of the entire line is shown in Fig. 2.

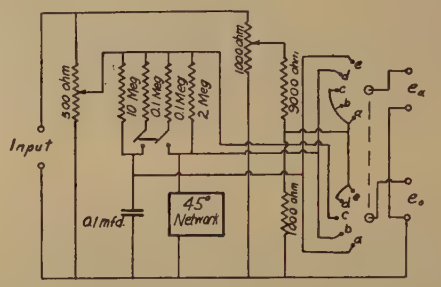

Fig. 3—Wiring diagram of amplifier tester.

The 45-degree network was built into the phase-shifting device shown in Fig. 3. By means of the selector switch incorporated into the phase-shifting device the phase shift between the two output voltages can be made 0, ±45, or ±90 degrees. The 45-degree phase shifts are obtained as indicated above. The 90-degree shifts are obtained by taking the voltage across a condenser in series with a large resistance. A direct connection gives a zero phase shift. Two potential dividers admit of independent adjustment of the magnitude of the output voltages. These potential dividers can be calibrated so that the gain of an amplifier under test can be determined. The voltage to the amplifier leads the voltage to the horizontal oscilloscope plates in phase when the voltage to the oscilloscope is taken directly from the phase-shifter input and the voltage to the amplifier is taken from the condenser or 45-degree network. To

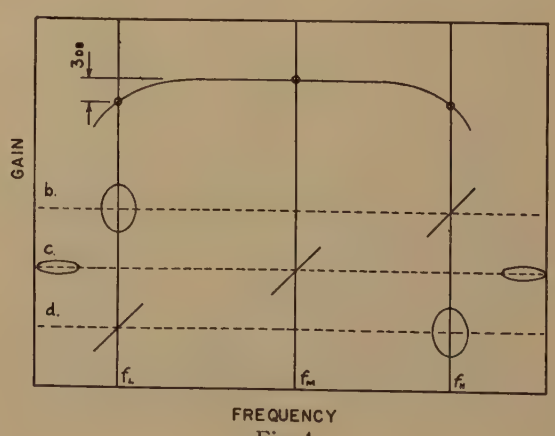

Fig. 4

reverse the sign of the phase shift the sources of these voltages are interchanged.

The interpretation of the results obtained is quite simple. If the amplifier under test is a single-stage resistance-capacitance-coupled amplifier the results

obtained are as shown in Fig. 4. With the selector switch of the phase shifter set on point *c* the two output voltages of the phase shifter are in phase and the oscilloscope registers the Lissajous figures which give directly the phase shift through the amplifier. These are shown on the line *c* of Fig. 4. It is seen that the phase shift is 180 degrees at some mid-frequency and tends to become 270 and 90 degrees at the low and high frequencies, respectively. With the selector switch of the phase shifter in position *b* the voltage to the amplifier lags the voltage to the horizontal plates by 45 degrees and the figures shown on line *b* of Fig. 5 result. It is seen that the oscilloscope figure has become an inclined straight line at f_L and a 90-degree ellipse at f_H. In an actual test the frequency of the beat-frequency oscillator is varied until the Lissajous figure becomes a straight line and this frequency is recorded as being f_L. With the selector switch of the phase shifter in position *d* the figures shown on line *d* of Fig. 4 result. Now the voltage to the amplifier leads the voltage to the horizontal plates by 45 degrees and an inclined straight-line figure is obtained at f_H. Although it has taken considerable time to describe the method of procedure and the interpretation of the results obtained, all of the information indicated above, sufficient for most purposes, can be obtained in less than half a minute once the apparatus is assembled.

The phase relations for a single-stage output-transformer-coupled amplifier with a resistance load are exactly the same as those for the resistance-capacitance-coupled amplifier as described above provided the transformer secondary has no series resonances in the high-frequency range.

For low frequencies the phase relations in a transformer-coupled voltage amplifier are the same as those previously discussed. For high frequencies, however, the phase relations are as shown in Fig. 5. Using the direct connection of the phase shifter, selector switch on *c*, it is seen that there is a resonance condition in the high-frequency range as indicated by a 90-degree ellipse. The frequency at which this occurs will be designated as f_r. At some mid-frequency the phase shift is 180 degrees as with the types previously discussed. Between this mid-frequency and f_r the phase shift passes through the 135-degree value. The frequency at which this occurs will be designated as f_1. Above f_r the phase shift decreases from 90 degrees tending to become 0 degrees at very high frequencies. In doing so the phase shift passes through the 45-degree value. The frequency at which this occurs will be designated as f_2. The frequencies f_1, f_r, and f_2 may be determined by *b*, *a*, and *d*, respectively, and adjusting the oscillator frequency until inclined straight-line figures are obtained on the oscilloscope. From considerations of the equivalent resonant circuit of the transformer at high frequencies it can be shown that the gains relative to the mid-frequency gain at the frequencies f_r, f_1, and f_2 are given by the following relations:

$$\text{relative gain at } f_r = Q = \frac{\sqrt{f_2/f_1}}{f_2/f_1 - 1}$$

$$\text{relative gain at } f_1 = \frac{1}{\sqrt{2}(1 - f_1/f_2)}$$

$$\text{relative gain at } f_2 = \frac{1}{\sqrt{2}(f_2/f_1 - 1)}.$$

Although only the most common types of coupling have been considered here the method can be extended to include any type of coupling. The determination of the response curve of any amplifier is essentially a circuit problem and as such there is always a definite gain associated with a particular value of phase shift. This applies also to amplifier circuits with various frequency-compensating circuits and to amplifiers with feedback.

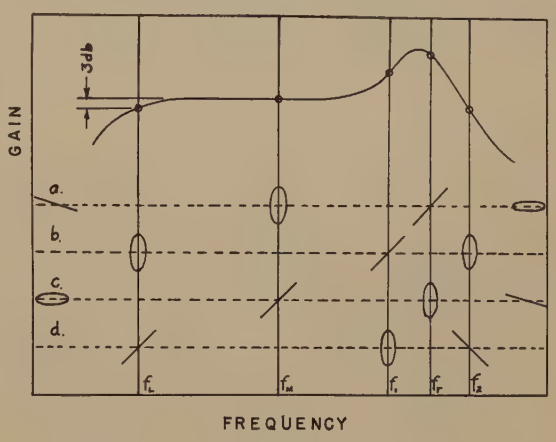

Fig. 5

Multistage amplifiers are subject to the same treatment. If the stages are identical then the phase shift for an *n*-stage amplifier is simply *n* times that of a single stage. Thus in a two-stage resistance-capacitance-coupled amplifier the phase shift corresponding to the frequency of 70.7 per cent relative gain per stage is 90 degrees rather than 45 degrees different from the phase shift at the mid-frequency. Departures in phase of 45 and 135 degrees are readily located giving the frequencies of 92.4, and 38.3 per cent relative gain per stage. The construction of the phase shifter is such that any phase shift which is a multiple of 45 degrees is readily located.

There are a few precautions to be observed in using the phase-shifting device described above. If voltage amplifiers are used on the deflecting plates of the oscilloscope as is usually the case it is necessary that the two amplifiers have identical phase-shift characteristics. If the oscilloscope impedance connected across the amplifier output is not sufficiently high, corrections for its effect upon the amplifier response must be made.

Ease of determination of essential data and sim-

plicity of operation make the above method a great timesaver where much work with audio-frequency amplifiers is done. It is anticipated that the testing method described here would be extremely useful in the routine testing of manufactured amplifiers.

ACKNOWLEDGMENT

The writers wish to thank Professor Terman of Stanford University for valuable suggestions made in the development of the above method.

The Electrostatic Electron Multiplier*

V. K. ZWORYKIN†, FELLOW, I.R.E. AND J. A. RAJCHMAN†, ASSOCIATE MEMBER, I.R.E.

Summary—*This paper describes the design of improved types of electron multipliers in which the electrodes are so shaped and positioned as to provide accurate electrostatic focusing and to minimize space-charge limitations. The first section of the paper describes the general methods available for determining electron trajectories in electrostatic fields. The second section describes the details of design of several experimental self-focusing electron-multiplier tubes.*

INTRODUCTION

THE secondary-emission electron multiplier whose general principles have been described by many authors, is a simple device which is capable of many applications due to its unlimited sensitivity and linear response at all frequencies from direct current to hundreds of megacycles. When photosensitive, it constitutes an ideal pickup for light signals such as are encountered in sound reproduction, facsimile transmission, and many scientific instruments. As an amplifier, the multiplier provided with a thermionic cathode and control elements can also render invaluable services.

In an earlier paper,[1] of which one of the authors is a coauthor, two types of static electron multipliers were described: the magnetically focused multiplier, and the electrostatic multiplier of the types L and T.

The operation of the magnetically focused multiplier requires an external magnet whose field must be carefully adjusted both in intensity and direction. This magnet is a serious practical drawback in most applications and becomes particularly objectionable when the influence of its field is disturbing.

The purely electrostatically focused multipliers of the L and T types, described in the same paper,[1] although operating without the external magnet, also have their drawbacks. They are not able to handle large currents because of space-charge limitations and are difficult to construct and activate.

The present paper describes an electrostatically focused electron multiplier of different design in which the drawbacks of either the magnetic or the L and T types of multiplier are largely overcome.

In principle, a static multiplier consists of a series of secondary-emissive targets maintained at successively higher positive potentials. An initial stream of electrons striking a first target produces secondary electrons which are directed on the next target, giving rise to further secondary electrons. This process is repeated as many times as there are multiplying electrodes. To obtain adequately large secondary currents it is necessary that the primary electrons move against a field gradient in the immediate neighborhood of the secondary emissive target, since such a field is indispensable to saturate the secondary emission. Hence, for satisfactory operation, the shape and potentials of the electrodes must be such as to create a field which is both properly directed at their surface and, in spite of that adverse condition, capable of guiding the electron stream from one stage to another. It will, therefore, be most useful, if not essential to be able to predict the electrostatic field due to a given configuration of electrodes and the motion of an electron in it.

The first part of this paper describes the general methods used in the solution of electron-optical problems, i.e., those regarding electron trajectories in electrostatic fields. These methods, although developed in conjunction with the multiplier, are quite general and constitute a tool of investigation of great value in many electronic problems.

The second part of the paper deals with the exact conditions of good performance of an electron multiplier and describes in some detail several actual designs.

I. ELECTRON TRAJECTORIES IN AN ELECTROSTATIC FIELD

(*A*) *Analytical Considerations*

Let us consider a certain number of electrodes maintained at known constant potentials and the trajectory described by a charged particle under the influence of their electrostatic field alone. In particular, we are not considering the influence of a possible magnetic field, nor that of the electric field produced by other particles, that is, the space charge.

The laws governing the electric field and the motion of a charged particle in it are well known. The potential ϕ at any point will satisfy Laplace's equation

$$\nabla^2\phi = 0 \qquad (1)$$

and be subject to the boundary conditions; that is,

* Decimal classification: 535.38. Original manuscript received by the Institute, August 1, 1938; abridgment received by the Institute, July 12, 1939. Presented, Thirteenth Annual Convention, New York, N.Y., June 17, 1938.

† RCA Manufacturing Company, Inc., RCA Victor Division, Camden, N. J.

[1] V. K. Zworykin, G. A. Morton, and L. Malter, "The secondary emission multiplier—A new electronic device," PROC. I.R.E., vol. 24, pp. 351–375; March, (1936).

must take on the prescribed values at the surface of the given metallic electrodes. Let us consider now a particle of mass m and charge e in that electrostatic field. We shall assume that the particle of subatomic nature, an electron or an ion, behaves like a little charged sphere of vanishingly small radius. This particle, moving under the influence of a conservative system of forces in the potential field ϕ will obey Newton's equation of motion

$$m\frac{d^2\overline{R}}{dt^2} = -e \operatorname{grad}\phi \qquad (2)$$

where $\overline{R}$ is the radius vector of the particle, and will be subject to the initial conditions.

In order to obtain the equation of the trajectory, it suffices in principle to integrate Laplace's equation, (1), introduce the values of the potential thus found in (2), and then eliminate the time. Instead of this, it is sometimes much easier to use the principle of minimum action as it leads to expressions in which the time is eliminated to begin with. This principle states, in our case, that in a conservative system of forces the trajectory between two given points, A and B, is such as to render stationary the integral:

$$S = \int_A^B 2W\,dt \quad \text{or} \quad S = \int_A^B mv\,ds \qquad (3)$$

in which W is the kinetic energy, v the velocity of the particle, ds an element of trajectory, and dt an element of time.

With the proper choice of the origin of the potential ϕ, making the total energy of the particle zero, that is $|e\phi| = |W|$, the integral becomes, neglecting all constant factors,

$$S = \int_A^B \sqrt{\phi}\,ds. \qquad (4)$$

The particle is assumed to move sufficiently slowly to render a relativistic correction negligible. Considering a two-dimensional problem, and referring to a set of Cartesian co-ordinates (x, y), the integral,

$$S = \int_A^B \sqrt{\phi}\sqrt{1 + y'^2}\,dx \qquad (5)$$

where $y' = dy/dx$, becomes stationary if the Euler differential equation is satisfied,

$$\frac{d}{dx}F_{y'} - F_y = 0 \qquad (6)$$

where

$$F(x, y, y') = \sqrt{\phi(x, y)}\sqrt{1 + y'^2}. \qquad (7)$$

This last equation reduces in our case to the so-called ray equation:

$$\frac{d^2y}{dx^2} = \frac{1}{2\phi}\left(\frac{\partial\phi}{\partial y} - \frac{dy}{dx}\frac{\partial\phi}{\partial x}\right)\left(1 + \left(\frac{dy}{dx}\right)^2\right). \qquad (8)$$

From this equation it can be seen that the trajectory of a charged particle in a given electrode arrangement is independent of its mass and charge, and invariant with respect to a proportional change in all electrode potentials. An inspection of the equation of motion (2) in which $\overline{R}$ has been replaced by $\lambda\overline{R}$, shows also that the trajectory in a linearly magnified model is correspondingly amplified. This will be important in the considerations to follow.

The analytical integration of these differential equations giving the potential field and the electron motion is, in general, impossible for most electrode arrangements, even for those which appear to be surprisingly simple. The extremely long and tedious process of numerical integration can be replaced advantageously by experimental methods. Some of these are very expedient and sufficiently accurate for most cases.

(*B*) *Electrolytic Tank and Graphical Methods*

The difficult determination of the potential field from the integration of Laplace's equation can be avoided by the use of the well-known electrolytic-tank method. A scale model of the electrodes under investigation is placed in an electrolyte, and upon it are impressed voltages proportional to those of the corresponding electrodes in the tube. The potential at any point in the electrolyte is then proportional to that at the corresponding point in the investigated field, so that a map of equipotential surfaces is easily obtainable. The potential distribution at the surface of the electrolyte will correspond to that of the plane of symmetry of a structure represented by the submerged portion of the model and its mirror image with respect to that surface. Fortunately, the two types of electrode arrangements which are most frequently used possess such a central plane, and can therefore be investigated by this electrolytic means. These types are those having axial symmetry and those consisting of cylindrical electrodes whose generatrices are normal to a plane. The complete theory and the practical apparatus have been described in many classic textbooks and will not be further discussed here.[2]

The problem of obtaining the electron trajectories on the basis of the map of equipotential lines can be solved by numerical integration, as already indicated. However, it is more expedient to make use of graphical methods which consist substantially in replacing the trajectory by segments of various simple curves such as straight lines, circles, parabolas, etc. One of them, known as the "circle method," is based on a very simple relation between the radius of curvature R of the trajectory at any point P, the potential V at P, and the component of the field E_r, normal to the trajectory at P.

[2] E. Brüche and O. Scherzer, "Geometrische Elektronenoptik," Julius Springer, Berlin, Germany, (1934).

The energy principle for a particle whose initial energy is eV_0, states that

$$\tfrac{1}{2}mv^2 = e(V + V_0). \tag{9}$$

Since the centripetal acceleration of the particle is proportional to the radial force, we can write

$$\frac{mv^2}{R} = eE_R. \tag{10}$$

Eliminating v between (9) and (10), we find that

$$R = 2\frac{V + V_0}{E_R} \tag{11}$$

which is the basis of the graphical construction.

Suppose that the equipotential lines are drawn and the particle has arrived at the point P lying on the equipotential $V-\Delta V$ with the velocity v (Fig. 1). The center C of the circular arc which will approximate the segment of path between the equipotentials $V-\Delta V$ and V will lie on the line PTC normal to the

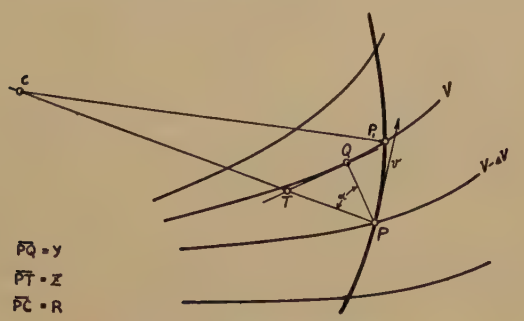

Fig. 1—The circle method.

electron path at P. The distance $y=PQ$ is approximately the shortest distance between the lines V and $V-\Delta V$, so that

$$E = \frac{\Delta V}{y} \tag{12}$$

where E is the value of the field at P within the approximation in which the potential between the equipotentials can be regarded as linear. The component E_r of E along PC is then

$$E_r = E\cos\alpha \tag{13}$$

where $\alpha=QPC$. QT is drawn perpendicular to QP. Noticing that

$$\cos\alpha = \frac{y}{z} \tag{14}$$

where $z=\overline{PT}$, the combination of (11) to (14) leads to

$$R = 2\frac{V + V_0}{\Delta V}z. \tag{15}$$

It suffices now merely to multiply the distance PT by the known coefficient $2(V+V_0)/\Delta V$ to find the position of C. The circular arc PP_1, whose center is at C, is the desired approximate segment of path. By sufficient repetition of this procedure, the entire trajectory is constructed. It is not necessary to draw the velocity v every time since C_1 must lie on P_1C, as the segments of the path must joint without discontinuity of direction. The only elements which have to be determined are the point Q, the tangent QT, and the arc PP_1.

Advantage has been taken of (11) for the development of very ingenious automatic trajectory-plotting machines.[3,4] It has also been used for another method similar to the one described.[5]

(C) *Mechanical Model*

A very convenient experimental method, solving simultaneously potential distribution and trajectory problems, is based on the analogy between the path of a spherical ball rolling on a suitably stretched rubber membrane and that of a charged particle moving in an electrostatic field. Many authors[2,6,7,8] have taken advantage of this analogy, known for a long time, to demonstrate the operation of electron-optical systems. A closer analysis shows that, if properly put into practice, this method is an extremely useful tool in electronic research. It applies to the case of the motion of a charged particle in a plane normal to the generatrices of the electrodes, all of which are assumed to be cylindrical[9] and infinite in extent (or sufficiently long to render the end effects negligible).

The model is constructed by placing on a horizontal board rigid portions of cylinders whose directrices are similar to the electrodes under investigation and whose vertical heights are made proportional to the potential of the corresponding electrodes. If the trajectory of a negatively charged particle, say an electron, is investigated, the most negative electrode will have a correspondingly highest altitude. For a positive ion, the opposite would be true.

A rubber membrane, previously stretched on a solid rectangular or circular frame, is then pressed down on the model and made to be in contact with the whole length of the top edges of the cylinders. This requires means of pressing the rubber downwards against the electrodes at places where the tension is upwards, and where therefore this contact would not be established otherwise.

The horizontal projection of the trajectory of the center of a solid sphere rolling on the surface of this

[3] D. Gabor, "Mechanical tracer for electron trajectories," *Nature*, vol. 139, p. 373; February 27, (1937).
[4] D. B. Langmuir, *Nature*, p. 1066, June 19, 1937.
[5] H. Salinger, "Tracing electron paths in electric fields," *Electronics*, vol. 10, p. 50; October, (1937).
[6] P. H. J. A. Kleynen, "The motion of an electron in a two-dimensional electrostatic field," *Philips Tech. Rev.*, vol. 2, pp. 321–352; November, (1937).
[7] J. R. Pierce, "Electron multiplier design," *Bell Lab. Rec.*, vol. 16, pp. 305–309; September, (1938).
[8] O. H. Schade, "Beam power tubes," Proc. I.R.E., vol. 26, pp. 137–181; February, (1938).
[9] A cylindrical surface is generated by the motion of a straight line (the generatrix) parallel to itself, being guided by a curve (the directrix) in a plane normal to the generatrix.

rubber under the influence of gravitation is similar to the trajectory of a charged particle moving in a corresponding electric configuration, provided the initial conditions are similar in both cases. The justification of this statement can be seen in the following analysis.

Let us consider, to begin with, what will be the shape assumed by the rubber membrane under the conditions described. We will suppose that it has been stretched on its frame so that its tension is uniform and large compared to any additional tension resulting from the deformation due to the cylindrical electrodes. Quantitatively, the problem can be stated as follows: The originally undisturbed plane portion of rubber was raised along some contours to a given height $z(x, y)$ with respect to a horizontal plane carrying the axes, x and y, of a Cartesian co-ordinate system. We will assume that this membrane is an ideal two-dimensional body which presents no resistance to bending, and whose surface potential energy is proportional to its area. The membrane is going to assume such a shape as to minimize that energy, i.e., such as to render the area of its surface minimum. The area of the surface $z(x, y)$ is given by the integral

$$S = \iint_A \sqrt{\quad + \left(\frac{\partial z}{\partial x}\right)^2 + \left(\frac{\partial z}{\partial y}\right)^2}\, dx dy \qquad (16)$$

where A is the horizontal projection of the area within the boundaries. The function $z(x, y)$ sought, minimizing this integral, will satisfy Euler's differential equation,

$$\frac{\partial}{\partial x} F_{z_x} + \frac{\partial}{\partial y} F_{z_y} - F_z = 0 \qquad (17)$$

in which

$$F(x, y, z, z_x, z_y) = \sqrt{1 + \left(\frac{\partial z}{\partial x}\right)^2 + \left(\frac{\partial z}{\partial y}\right)^2}. \qquad (18)$$

This equation becomes

$$\frac{\partial^2 z}{\partial x^2}\left(1 + \left(\frac{\partial z}{\partial y}\right)^2\right) + \frac{\partial^2 z}{\partial y^2}\left(1 + \left(\frac{\partial z}{\partial x}\right)^2\right) - 2\frac{\partial^2 z}{\partial x \partial y}\frac{\partial z}{\partial x}\frac{\partial z}{\partial y} = 0. \qquad (19)$$

If $\partial z/\partial x$ and $\partial z/\partial y$ are small (19) reduces to

$$\frac{\partial^2 z}{\partial x^2} + \frac{\partial^2 z}{\partial y^2} = 0 \qquad (20)$$

which is Laplace's equation, (1), in which ϕ has been replaced by z. In other words, for *small slopes* and similar boundary conditions, the altitude of any point on the membrane is proportional to the electrostatic potential of the corresponding point in the electrical case.

Let us consider now a spherical ball of radius R rolling on this surface $z(x, y)$ under the influence of gravitation. We are bound to admit the existence of some friction, for there would be sliding and no rolling in its complete absence. We will assume, however, that we have to deal with "ideal rolling," where a sufficient static friction assures rolling and yet dynamical frictions, such as torque or sliding frictions, are absent. The ball will thus move in a conservative system of forces, since we choose to neglect the energy dissipated by friction. If the radius of the sphere is sufficiently small compared to the radii of curvature of the membrane, the elementary displacements of the center of the sphere and its point of contact with the surface can be taken as equal. Therefore, if the center undergoes a displacement ds, the sphere will have rotated through an angle $d\alpha$, where

$$d\alpha = \frac{ds}{R}. \qquad (21)$$

Hence, the total kinetic energy W of the ball will be

$$W = \frac{1}{2} mv^2 + \frac{1}{2} I\omega^2 = \frac{1}{2} v^2\left(m + \frac{I}{R^2}\right) \qquad (22)$$

where v is the velocity of the sphere's center, ω its angular velocity, and I its diametral moment of inertia. The principle of least action states that the trajectory between two given points A and B is such as to render the integral S stationary.

$$S = \int_A^B 2W dt = \int_A^B v^2\left(m + \frac{I}{R^2}\right) dt = \int_A^B \left(m + \frac{I}{R^2}\right) v ds. \qquad (23)$$

The kinetic energy being equal to the loss of potential energy, with the proper choice of the origin of the z's we will have,

$$\frac{I}{2} v^2\left(m + \frac{I}{R^2}\right) = |\, mgz\,|. \qquad (24)$$

Substituting this in the integral S and neglecting all constant factors, the integral becomes

$$S = \int_A^B \sqrt{z}\, ds = \int_A^B \sqrt{z}\sqrt{1 + \left(\frac{dy}{dx}\right)^2 + \left(\frac{dz}{dx}\right)^2}\, dx. \qquad (25)$$

The characteristic function under the integral sign,

$$F(x, y, y') = \sqrt{z(x, y)}\sqrt{1 + \left(\frac{dy}{dx}\right)^2 + \left(\frac{dz}{dx}\right)^2}, \qquad (26)$$

can be considered as a function of x, y, and y' only since z is a known function of x and y.

Let us compare now this function (26) with the analogous one (7) established for the motion of a charged particle in a two-dimensional potential field. We have seen by (20) that z can be considered proportional to ϕ, so that (7) and (26) can be regarded as identical as soon as $(dz/dx)^2$ may be neglected which again amounts to assuming *small slopes* of the rubber membrane. The functions F being proportional, the Euler differential equations will be similar and,

Fig. 2—Photograph of mechanical model.

hence, the paths in the electric case and those of its mechanical model will be similar, which proves the statement formulated above. In all these deductions we have tacitly taken advantage of the invariance of the trajectory with respect to a change in mass, charge, proportional changes in potential energy, and its homothety with respect to a change in scale, properties which were established previously.

In the actual model built in our laboratory a steel table, standing on leveling screws, supports a square glass plate (34 inches×34 inches). The cylindrical electrodes are made out of aluminum strips, about 1/16 of an inch thick, which have been cut to various convenient sizes, by steps of 1/2 inch or less. When the aluminum is annealed by baking at 300 to 400 degrees centigrade, it becomes quite soft and can be bent with great facility to any desired shape. These cylinders properly arranged on the glass plate on which the outline of the structure is easily copied, are fastened to it by ordinary "decorators' Scotch tape." The rubber sheet should be smooth, very elastic and yet sufficiently strong to resist puncture by the electrodes and deformation by the weight of the balls. So-called "surgical Latex rubber," gauge 29 or 32, has been found very satisfactory. This membrane is stretched on a wooden frame and fastened to it by thumbtacks. A uniform stretching is secured in practice by drawing on the unstretched rubber a figure similar to that of the frame, but smaller, and then pulling the rubber on all sides until the drawn figure coincides with the frame edges. The membrane is pressed down by auxiliary electrodes maintained by rods having a V-slit at their lower end. These rods are fastened by rectangular clamps to other horizontal rods as is usual in laboratory practice. The "electron" is simply a steel ball from a ball bearing. Tests have shown that balls having any diameter comprised between 1/16 and 1/4 inch are equally satisfactory so that a standard size of 3/16 inch has been adopted. The ball is released by an electromagnet whose current, when interrupted, is allowed to die off in a damped oscillation, so as to suppress all possible residual magnetization which would interfere with a positive release of the ball. The resulting ball paths are simply observed visually. In general, the sole points of interest of the whole trajectory are the starting and striking points which can be easily recorded if proper scales are drawn on the terminal electrodes. These scales can be drawn on the glass plate and then projected on the surface of the rubber by a light source from underneath. (Fig. 2 shows a photograph of the apparatus.)

A permanent record of the complete trajectory can be obtained conveniently by photographic methods.[6] If the model is illuminated by intermittent light flashes as, for instance, by an alternating-current-operated mercury lamp, and a time exposure is taken during the whole period of the ball's motion, the trajectory will reveal itself on the photograph as a dotted line. The spacing between these consecutive images of the ball is a measure of the relative speed of the electron and, consequently, of the potential.

In practice, the idealized conditions assumed for the mathematical deduction are not realized on account of the dissipative friction forces, the deformation of the membrane due to the weight of the ball,

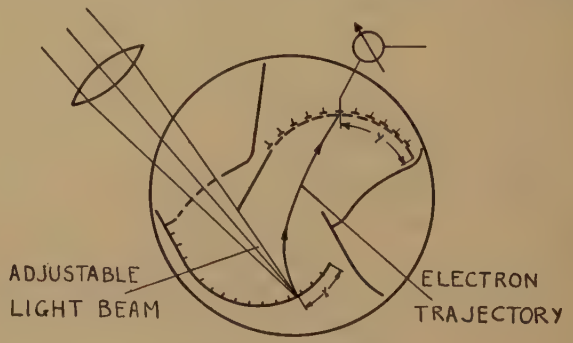

Fig. 3—Test tube.

irregularities in the thickness and roughness of the rubber, because negligible slopes are not practical, etc. Therefore, the applicability of the method has to be tested experimentally. For this purpose, several direct electronic tests were performed. A scale model of the investigated structure was placed in an evacuated envelope. The cathode, i.e., the electrode from which the electrons leave, was made photosensitive so that the starting point of the trajectory was de-

termined by illuminating a point or a line on the cathode with a beam from a small projector. The collector, i.e., the electrode which is to be bombarded by the electrons, was provided with either a single movable probe or a series of fixed probes. The spot of light on the cathode, or the probe on the collector was moved until the probe drew a maximum current. Fig. 3 shows schematically such a tube, made to

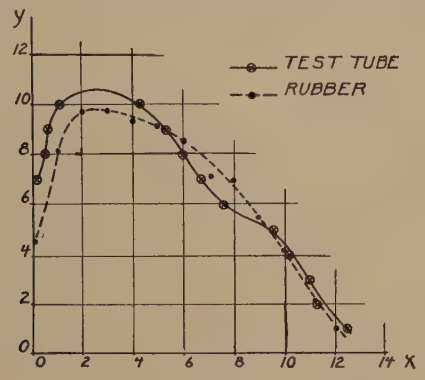

Fig. 4—Comparative focusing curves.

check the operation of one of the designs of the electrostatic multiplier described later.

The curves of Fig. 4 show the landing co-ordinate y as a function of the starting co-ordinate x (as defined in Fig. 7) determined both by the mechanical model and the electronic tests. The agreement between the two methods shown in this case, and found in other cases as well, amply justifies the use of the mechanical model and inspires confidence in its wide applicability.

However, it should be mentioned that the mechanical model cannot be used for structures having axial symmetry nor take into account the effect of the space charge.

II. Electrostatic Photoelectric Electron Multiplier

(*A*) *The Linear Staggered-Type Electrostatic Multiplier*

This type of multiplier comprises two parallel opposite rows of cylindrical electrodes whose genera-

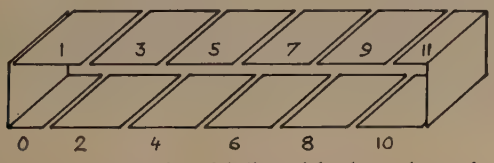

Fig. 5—Staggered multiplier with plane electrodes.

trices are normal to a plane in which their directrices are staggered; i.e., any one faces the interstice between two others in the opposite row. The search for a structure capable of focusing is reduced here to that for the adequate shape and relative position of the directrices. An arrangement of plane electrodes of equal length as shown in Fig. 5 is a simple example thereof. Preliminary calculations on this structure indicated that its focusing properties were entirely inadequate for a satisfactory multiplier. However, they pointed out the possibility of improving the focus by altering the shape of the directrices. Furthermore, with this type of configuration it is possible to establish a strong collecting field over the working portions of the electrodes.

One of the working structures obtained by the general methods outlined, as a result of a gradual evolution starting from the simple plane design, is illus-

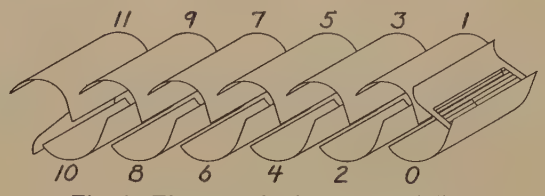

Fig. 6—Electrostatic electron multiplier.

trated by a scale perspective view in Fig. 6. Here the directrices are arcs of circle prolonged on one end by straight tangent segments. The stages numbered in the order of progress of the electron beam are connected to potentials proportional to their ordinal numbers, the voltage step varying between 30 and 300 volts. The first electrode (No. 0) is the photocathode from which the photoelectrons are released by light, the last (No. 11) is the collector carrying away the multiplied current.

The potential field of the structure is not altered if a metallic conductor replaces the equipotential surface, having the potential of one stage, say number n, which extends from it to the opening between stage $n-1$ and $n+1$. Hence, if a structure is terminated by such a conductor, the electron rays at every stage will be identical and the performance of a single stage, or "unit cell," describes that of the multiplier as a whole.

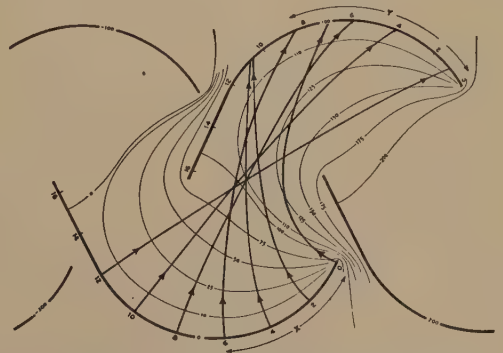

Fig. 7—Electron paths in the electrostatic multiplier.

Fig. 7 represents such a unit cell. An inspection of the map of equipotential lines, obtained in the electrolytic tank, reveals the uniformity, strength, and large effective area of the collecting field. The heavy lines approximate the paths followed by the electrons from one electrode to the next, as found concurrently by several experimental methods.

The excellency of focusing in this structure can be demonstrated with the help of a curve giving the co-ordinate y of the point of incidence of the electron ray on one electrode as a function of the co-ordinate x of its point of origin on the preceding electrode. Referring to such a curve given in Fig. 8, let us follow the progress of the ray through the tube. If the ray originates on an electrode at the abscissa x_1, it will strike the next electrode of the same unit cell at the ordinate y_1, which will in turn be the new starting co-ordinate for the following step. Making use of a line of unity slope through the origin, the abscissa x_2 of point 2 becomes simply that of the point 12, the intersection of this line with a parallel to the x axis through point 1. Thus, the rectangular spiral 1 − 1 2 − 2 − 2 3 − 3 − 3 4 − etc., illustrates the path of the ray in the multiplier. Since the spiral converges on point P for any arbitrary origin, it is clear that the beam can never overflow the area of width d of any electrode, regardless of the number of multiplying steps. The focusing of all structures investigated was

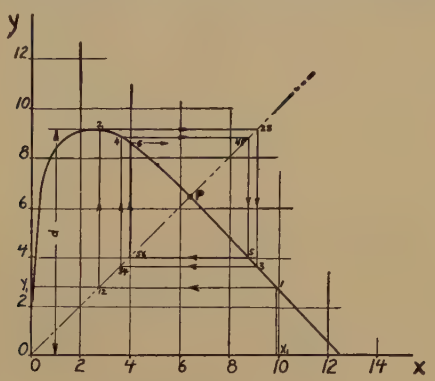

Fig. 8—Focusing curve.

analyzed by such a diagram and its figure of merit was determined by the width of the region from which a ray producing such a convergent spiral could originate.

The necessarily finite length of the cylindrical electrodes has no appreciable effect on the field at their center, if they are at least twice as long as wide, as was shown by measurement with the electrolytic tank. Furthermore, measurements in a tube whose electrodes carried side probes indicated that, due to the strong accelerating fields minimizing the effects of random initial velocities, etc., the side-spreading was scarcely noticeable, as long as the current density remained small. For high current densities the side-spreading, caused by the space charge, resulted in the overflow of the beam with a consequent loss in multiplication. This is a serious drawback, as the linear dependence of the output on the input is of special interest. The sidewise defocusing can be considerably reduced by closing the ends of the electrodes with a conducting strip or sheet, as shown in Fig. 9A and 9B. Side mica mounting plates, visible in Fig. 12, also produce a centering effect, as was observed previously in a magnetic multiplier.[1] When such precautions were taken, measurements limited by safe current densities (densities greater than 7 to 10 milliamperes per square centimeter are destructive to the silver-oxygen-caesium activation) showed no departure from linearity.

The almost perfect focusing capacity of this structure permits the construction of a multiplier having

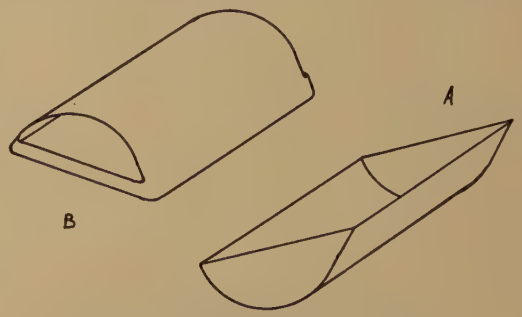

Fig. 9—Terminations of electrode.

as many stages as desired. Tubes having as many as 16 stages have proved to operate satisfactorily, yielding an over-all gain of several billions. Considerable care must be taken in the construction to keep within the tolerances allowed for the electrodes and their relative location. The electrodes are made from a soft sheet metal 0.005 to 0.010 inch thick and should bear stiffening ribs. They can be conveniently stamped out by a steel die which is easily machined because of the simple cylindrical shape. The structure is mounted on insulating supports which can be mica, lavite, or glass, depending on the application of the multiplier. Suitable jigs should be used during the construction to secure the required alignment unless the machining of the supports renders them unnecessary.

The experimental 10-stage multiplier shown in Fig. 10 has a structure consisting of silver-plated

Fig. 10—Photograph of multiplier (glass plate).

nickel electrodes activated with caesium and oxygen in the conventional manner and mounted on glass plates. The photocathode located at the end of the tube away from the press does not bear the perforated terminator as it should according to theory since empirical data indicates that this omission does not affect the operation. The gain, i.e., the ratio of output to input current, of this tube is 30 million when operated at 200 volts per stage.

(B) *Partition-Type Multiplier*

Problems requiring special multipliers are often encountered. The design of such tubes is greatly facilitated by the electron-optical methods described.

A typical example is the partition-type multiplier. This multiplier is constructed in such a way that the photocathode and the multiplying stages can be isolated from one another, thus permitting a different activation schedule on the two types of surfaces. Certain surfaces, such as those activated in the conventional way with alkali metals (silver-oxygen-M, M standing for caesium, rubidium, lithium, sodium, or potassium) yield simultaneously high photoelectric and secondary emission. However, in general, surfaces capable of photoemission are not necessarily good secondary emitters, and conversely, as there is no known direct relation between secondary and photoemission. A multiplier permitting independent activations is therefore desirable.

A design of this type is illustrated in Fig. 11, representing a longitudinal section of the tube. The multi-

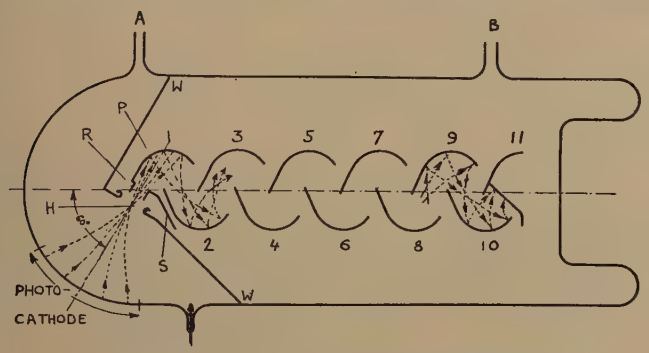

Fig. 11—Partition-type electron multiplier.

plying stages 2, 3, 4 · · · 11 are identical with those described above. The first stage 1 bears a shield S carrying in its center a circular cylinder R whose axis lies in the plane of the figure. The partition P fits tightly in the glass envelope and has in it a circular hole H which is coaxial with R. The tubular glass envelope is terminated by a hemisphere, part of which is internally metallized to form the photocathode. The two parts on each side of the partition can be treated entirely separately, the hole H being closed by a suitable shutter during the process so that active material used on one side (introduced through the side tubes A or B) cannot possibly contaminate the other. After the activation is completed and the tube ready to operate, the hole H is opened. When the electrodes have potentials proportional to their ordinal number, the photocathode hole H and ring R possess a field with axial symmetry capable of focusing photoelectrons through the hole H onto the active part of electrode 1. From there on, the progress of the beam is as previously indicated. The shield S and the ring R separate almost completely the axial and cylindrical fields which are simultaneously present only in a negligibly small region in the vicinity of R. A tube of this kind whose dimensions are 2 inches in diameter and 8 inches long is shown in Fig. 12.

Multipliers of this type behaved satisfactorily in all respects but one. The field at the surface of the photocathode due to the ring R which is largely shielded by the partition P is rather weak so that, with normal operating voltage, the photocurrent is not saturated. However, this lack of saturation does not affect the linearity with respect to light input and

Fig. 12—Photograph of partition-type multiplier.

causes the loss of only 20 per cent of the available photoelectrons when operated at 200 volts per stage.

(C) *Circular-Type Multiplier*

Another special multiplier worthy of mention is one which was developed for the express purpose of economizing in space. This multiplier consists of two rows of cylindrical electrodes whose generatrices are normal to the plane in which their directrices are disposed along two concentric circles. The outline of the electrodes, numbered and energized as before, of a 10-stage multiplier, is represented to scale in Fig. 13. Dotted lines approximate the electron paths. The

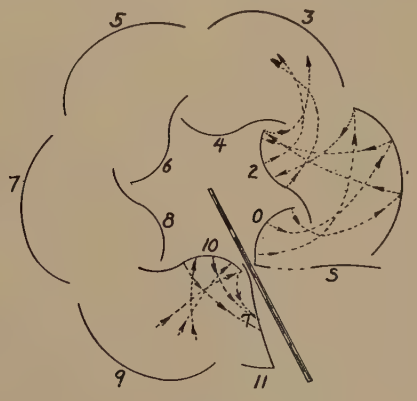

Fig. 13—Circular type.

photocathode (No. 0) which is a member of the inner row of electrodes, carries a screen S through which light can be projected. The terminator T serves as the collector. It should be pointed out that the screen S and the terminator T are shaped so that they preserve the cyclic nature of the field, as explained above.

This structure permits the complete utilization of the available space in a tubular bulb. Ten-stage oper-

ative structures were built to fit in a circular cylinder one inch in diameter and one inch long. Mounting and wiring are particularly simple since the structure may be supported by the leads to the various stages, these leads being sealed directly through the glass of the press.

Conclusion

The elimination of the external magnet and other drawbacks of early multiplier designs represents definite progress. Some problems have yet to be solved[10] to render the photoelectric multiplier foolproof and commercially practical.

The electrostatic multiplier with a thermionic source of electrons and control elements promises to be a development of great importance. Several designs of this sort, with four stages of multiplication, operated quite satisfactorily. However, it is premature to speculate about their future.

Acknowledgment

The authors wish to express their indebtedness to all members of the Electronics Research Laboratory of the RCA Manufacturing Company, in Camden New Jersey, who contributed to this development, and most particularly to Drs. G. A. Morton and E. G. Ramberg, Mr. R. L. Snyder, and Dr. E. W. Pike.

[10] Since this paper was presented for publication Jan Rajchman published "Le courant residuel dans les multplicateurs d'electrons electrostatiques," *Arch. des Sci. Phys. et Naturelles*, 5e periode, vol. 20, September, October, November, and December, 1938. The dark current, i.e., the output current of the multiplier with zero illumination, is an important limiting factor. Its causes are analyzed and means to reduce it are devised.

A Consideration of the Radio-Frequency Voltages Encountered by the Insulating Material of Broadcast Tower Antennas*

GEORGE H. BROWN†, ASSOCIATE MEMBER, I.R.E.

Summary—*A knowledge of the radio-frequency voltages on the insulation of broadcast tower antennas is important to the design engineer, since a too-large factor of safety may add unduly to the tower cost.*

Attention is first given to the base-insulator voltage. The magnitude of this voltage is also of interest in the design of lighting chokes and coupling equipment. Theoretical values are derived and shown in curve form as a function of antenna height. The theoretical curves are supplemented by experimental data taken on self-supporting tapered towers, guyed cantilever towers, guyed uniform-cross-section towers, and guyed tubular steel masts.

A theoretical treatment is then given concerning the role of guy wires from an electrical standpoint. Consideration is given to the currents in the guys, and the voltages on the guy insulators. Measurements are presented of the voltages existing on the guy insulators of two guyed masts of different constructions.

These voltages are found to be so small that there seems little need for elaborate insulation except for the presence of high static or induced lightning voltages. The paper is concluded by some considerations of ways of providing protection against these high instantaneous and random voltages without the use of expensive and elaborate insulation.

I. Introduction

IT IS important to the tower designer to have a knowledge of the radio-frequency voltages encountered by the insulating material of broadcast tower antennas so that adequate insulation may be provided without going to extremes of over-insulation which are very costly. The radio engineer who is responsible for the design of lighting chokes and coupling equipment which is placed at the base of the tower is equally interested in the voltage occurring across the base insulator.

* Decimal classification: R243×R320. Original manuscript received by the Institute, August 1, 1938; abridgment received by the Institute, July 20, 1939. Presented, Thirteenth Annual Convention, New York, N. Y., June 17, 1938.

† RCA Manufacturing Company, Inc., Camden, N. J.

It is the purpose of this paper to present a consideration of the voltages occurring on the base insulator of tower antennas, as well as the voltages on insulators placed in supporting guy wires.

II. Voltage on the Base Insulator of Tower Antennas

The voltage on the base insulator of a tower antenna may be readily calculated, once the resistance and reactance of the antenna are known. The voltage at the base is

$$V = IZ \tag{1}$$

where

I = current at the base of the antenna (amperes)
Z = impedance at the base $\sqrt{R^2+X^2}$ (ohms)
R = antenna resistance (ohms)
X = antenna reactance (ohms).

For a given power, W watts,

$$W = I^2R \tag{2}$$

or

$$I = \sqrt{\frac{W}{R}}. \tag{3}$$

Substituting (3) in (1)

$$V = \sqrt{\frac{W}{R}} \cdot \sqrt{R^2 + X^2}. \tag{4}$$

Thus, for a given resistance, reactance, and power, (4) will yield the base-insulator voltage. The voltage

for one-watt input is

$$V/\sqrt{W} = \frac{\sqrt{R^2 + X^2}}{\sqrt{R}} \text{ (volts for one-watt input)}. \quad (5)$$

It is to be noted that (4) and (5) give the root-mean-square voltage for an unmodulated carrier of W watts. To obtain the peak voltage of the unmodulated carrier, (4) and (5) are multiplied by $\sqrt{2}$. To obtain the peak voltage reached when the carrier is modulated 100 per cent, (4) and (5) are multiplied by $2\sqrt{2}$, or 2.828.

We first examine the theoretical conditions existing on a vertical antenna over a perfectly conducting earth. We assume that the antenna current is distributed sinusoidally along the antenna. The antenna height is a. The resistance at the base of the antenna is[1]

$$R = 15[\{1 - \cot^2 G\}\{C + \log(4G) - Ci(4G)\} + 4\cot^2 G\{C + \log(2G) - Ci(2G)\} + 2\cot G\{Si(4G) - 2Si(2G)\}] \quad (6)$$

where

$G = 2\pi a/\lambda$ radians $= 360 \cdot a/\lambda$ degrees
λ = operating wavelength
C = Euler's constant = 0.5772

and $Ci(x)$ and $Si(x)$ are respectively the integral-cosine and integral-sine functions given by Jahnke and Emde.[2] The antenna resistance as a function of G in degrees is shown by Fig. 1. For values of G less than 50 degrees, the resistance may be obtained from the approximate formula

$$R \doteq 10 \cdot G^2 \quad (7)$$

where G is measured in radians.

The reactance at the base of the antenna is[3]

$$X = 15\left[2\left\{C - \log\frac{G}{(2\pi s/\lambda)^2} + Ci(4G) - 2Ci(2G)\right\}\cot G - \{Si(4G) - 2Si(2G)\}\{\cot^2 G - 1\} + \frac{2Si(2G)}{\sin^2 G}\right] \quad (8)$$

where

s = radius of the antenna conductor.

When G is less than 50 degrees, an approximate relation is

$$X = -60\left\{\log\left(\frac{a}{s}\right) - 1\right\}\cot G. \quad (9)$$

From the analogy with a transmission line, the quantity $60\{\log(a/s) - 1\}$ may be identified as the characteristic impedance of the antenna.

[1] G. H. Brown and Ronold King, "High-frequency models in antenna investigations," PROC. I.R.E., vol. 22, p. 469, equation (2); April, (1934).
[2] E. Jahnke, "Funktionentafeln mit Formeln und Kurven." Published by B. G. Teubner, Leipzig, Germany, (1933).
[3] Footnote reference 1, p. 469, equation (3).

Fig. 2 shows the reactance, computed from (8), as a function of G. The parameter Δ is

$$\Delta = \frac{s(\text{mils})}{\lambda(\text{meters})}. \quad (10)$$

This choice of parameter is chosen for convenience, in preference to keeping s and λ in the same units, as in (8). For example, in the case of a mast whose

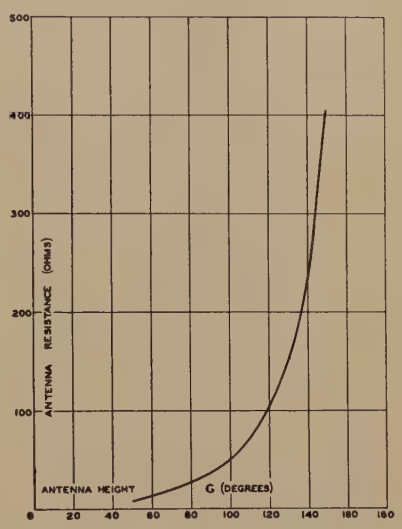

Fig. 1—Theoretical radiation-resistance curve.

radius is three inches, operating at a frequency of 1000 kilocycles ($\lambda = 300$ meters),

$$\frac{s(\text{meters})}{\lambda(\text{meters})} = \frac{0.076}{300} = 0.000253$$

while

$$\Delta = \frac{s(\text{mils})}{\lambda(\text{meters})} = \frac{3000}{300} = 10.0.$$

Both the resistance and reactance expressions given above are useless in the neighborhood of $G = 180$ degrees, since we have assumed a sinusoidal distribution of antenna current, which gives zero current at the base for the half-wave condition, with infinite values of base resistance and reactance. However, for values of G less than 150 degrees, the theoretical values agree rather well with values measured on wire or tubular antennas.

Using the data of Figs. 1 and 2, together with (5), we have computed the base-insulator voltage for one-watt input. The results are shown on Fig. 3 for a number of values of Δ. The abscissa is a/λ, where a is the antenna height and λ is the operating wavelength, both measured in the same units. We see that near the quarter-wave point, the base voltage is about 6.0 volts for one-watt input, and rises rapidly on either side of the quarter-wave point. We see further that as the radius increases, which corresponds to increasing Δ, the reactance lowers thus lowering the base voltage for a given antenna height.

The experimental voltage data to be presented in the following figures were obtained by applying (5) to the resistance and reactance data which were available for a number of antennas. Chamberlain and Lodge[4] have published impedance characteristics which are the average of three self-supporting radiators. From these data, the solid curve of Fig. 4 was computed. On this same figure, the base-voltage curve of KOA, Denver, Colorado, is shown, as well as a single point for the towers of WPEN, Philadelphia, Pennsylvania.

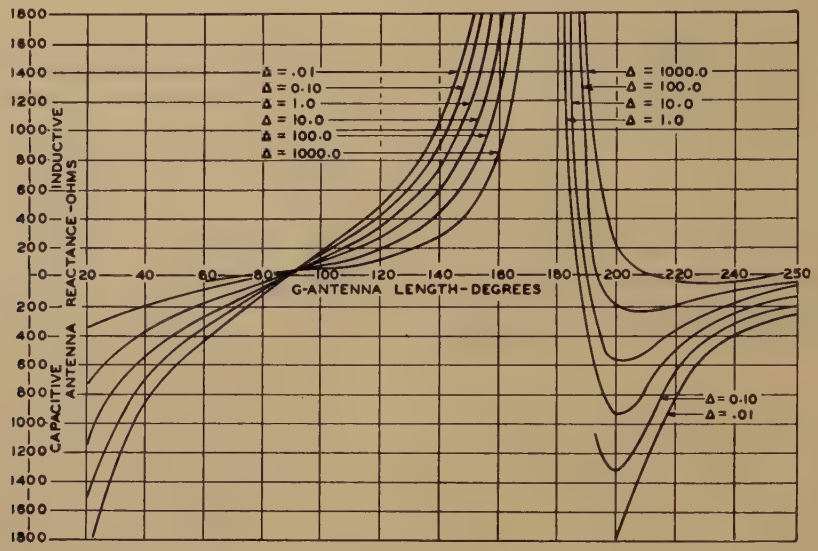

Fig. 2—Reactance of vertical antenna with sinusoidal distribution of antenna current.

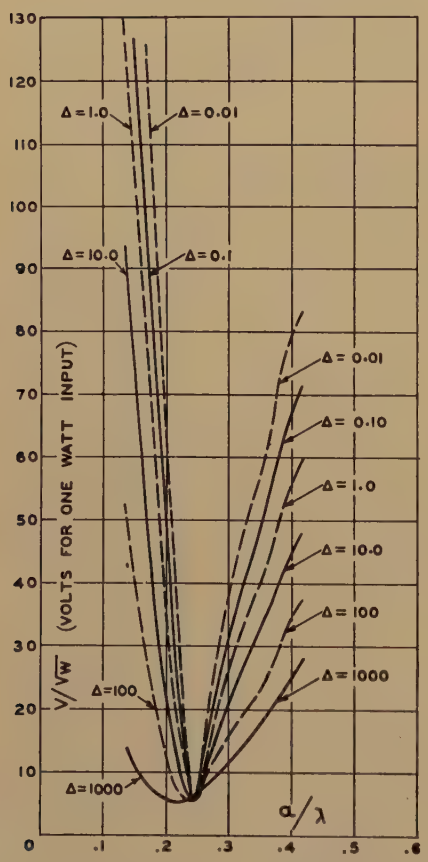

Fig. 3—Voltage on base insulator of sine-wave antenna.

The guyed cantilever type of tower was used for some time. Data on this type of tower have also been published by Chamberlain and Lodge.[4] The solid curve on Fig. 5 has been computed from their data. The broken curve on Fig. 5 shows the base voltage for the guyed cantilever tower in use at Budapest. Single points are shown for the WCAU and WLW towers.

Fig. 6 shows the base-insulator voltage for a number of guyed towers whose cross section is essentially constant from top to bottom. The solid curve of Fig. 6 applies to the WMAQ, Chicago, antenna whose height is 490 feet. This antenna is

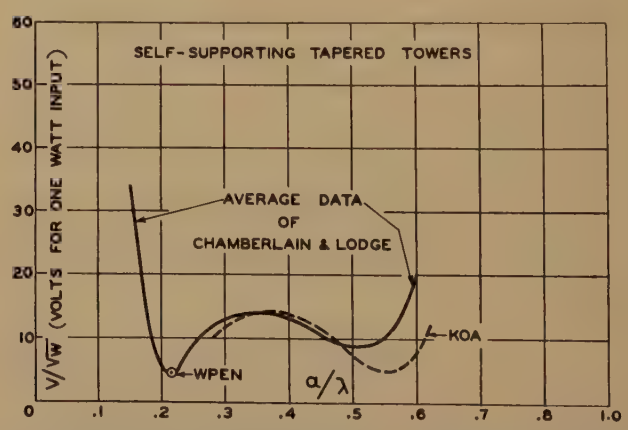

Fig. 4—Voltage on base insulator of self-supporting tapered towers. The tower at KOA, Denver, is 470 feet tall and 30 feet on a side at the base. The WPEN, Philadelphia, towers are 234 feet high, 14 feet on a side at the base, and 14 inches on a side at the top.

capacitance-loaded at the top with a large system of outriggers. The tower is broken at a lower level to allow the insertion of a sectionalizing coil. The curve

[4] A. B. Chamberlain and William B. Lodge, "The broadcast antenna," *Proc. Radio Club Amer.*, vol. 2, pp. 51–59; November, (1934); Proc. I.R.E., vol. 24, pp. 11–35; January, (1936).

of Fig. 6 holds for the condition in which the coil is short-circuited. A curve is shown on Fig. 6 which applies to the WWJ, Detroit, antenna which was computed from data published by Morrison and Smith.[5] This antenna is of constant cross section, 400 feet high. A similar curve is shown for tubular steel masts in use at WTAR, Norfolk, Virginia, and WRTD, Richmond, Virginia. Two of the WTAR masts are 210 feet tall, while the third is 280 feet high. The WRTD mast is 330 feet tall.

On Fig. 6 are also shown points which correspond to the operation of WGR and WKBW, Buffalo, New York. These two stations operate simultaneously on a single 400-foot uniform-cross-section guyed tower.

For purposes of comparison, four points on Fig. 6 show the voltage to ground from the bottom end of the sloping wire of a shunt-excited antenna (essentially the voltage across the series tuning condenser). These values were computed from the data given in Figs. 2 and 6 of the paper by Morrison and Smith.[5] For each height of antenna shown, the slanting wire was in the adjustment which gave 70 ohms of resistance, accompanied by the usual large amount of inductive reactance.

To sum up the results, it seems interesting to tabulate the results for some of the existing stations mentioned in the previous figures. This is done in Table I.

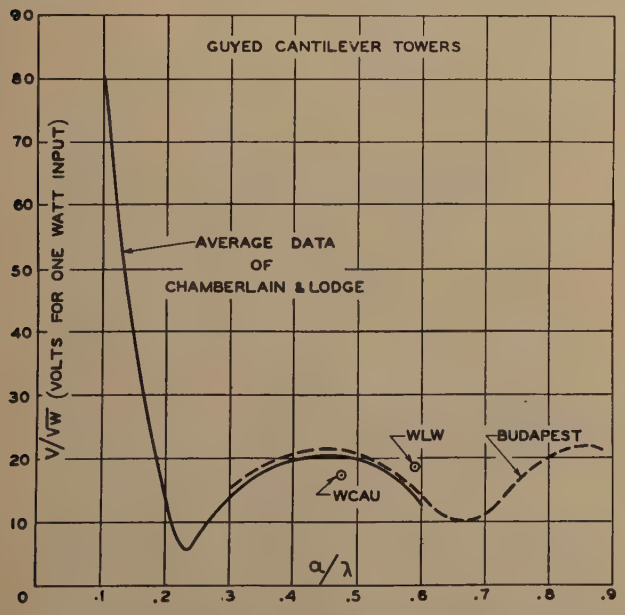

Fig. 5—Voltage on base insulator of guyed cantilever towers. The Budapest antenna is 1000 feet tall while WLW, Cincinnati, is 830 feet in height. The WCAU, Philadelphia, antenna is a guyed cantilever tower, 400 feet tall, and top-loaded with a capacitance-inductance hat.

From Figs. 4, 5, and 6 we see that the voltages on the base insulator of towers above one-quarter wave in height do not rise to excessive values. In fact, the base voltage of half-wave towers is well within the limits of insulation available at present. The base voltage of the tubular steel masts rise to higher values near the half-wave point than do the structural steel masts, because of the much closer approach to the ideal sinusoidal current distribution. These tubular masts are not over twelve inches in diameter at the widest point.

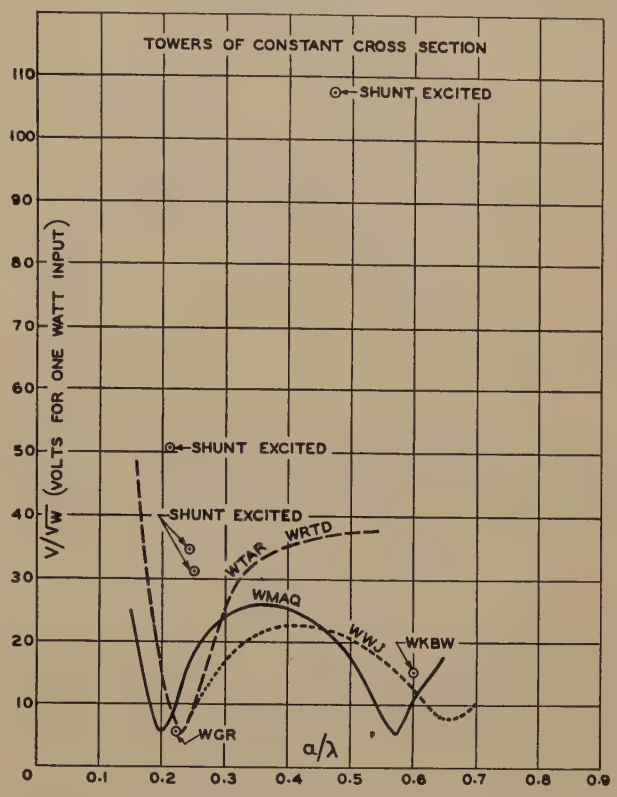

Fig. 6—Voltage on the base insulator of towers of constant cross section.

TABLE I

Station	a/λ	Frequency (kilocycles)	Watts	Volts (root-mean-square)
KOA	0.396	830	50,000	3130
WPEN (non-directional)	0.219	920	500	101
WCAU	0.476	1170	50,000	3810
WLW	0.59	700	500,000	13,100
WRTD	0.5	1500	100	375
WWJ	0.374	920	5000	1560
WKBW	0.6	1480	5000	1070
WGR	0.223	550	5000	390
Shunt-excited	0.47	1150	50,000	24,100

III. Voltage on the Guy Insulators of Tower Antennas

Guyed towers have been in use for many years. The supporting guy wires have been broken up at several points by insulators. This guy insulation has generally been very elaborate and costly, even on antennas which are used for relatively low-power transmission. Practically no information has appeared in the literature concerning the voltages existing on these insulators. Long before an opportunity presented itself to measure the voltage on a

[5] J. F. Morrison and P. H. Smith, "The shunt-excited antenna," Proc. I.R.E., vol. 25, p. 678, Fig. 4; June, (1937).

set of guy insulators, the writer attacked the problem from a theoretical standpoint. A rigorous solution appears to be rather out of the question. An approximate method that appears to be satisfactory for the purpose at hand is presented here.

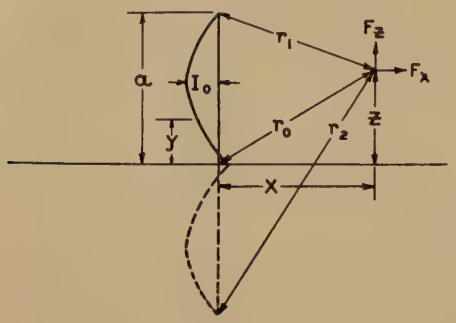

Fig. 7

Let us first examine the field conditions near the antenna shown in Fig. 7. The antenna is of height a and operated at a wavelegth λ. The current is distributed according to the law

$$i_y = I_0 \sin (G - ky) \tag{11}$$

where

i_y = current at a distance y from the earth
I_0 = maximum current on the antenna (one-quarter wavelength from the top)
$k = 2\pi/\lambda$
$G = ka$.

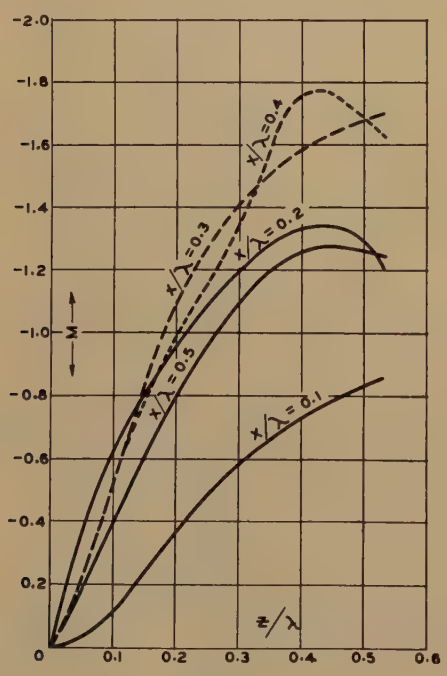

Fig. 8

Then at a point in space a distance z above the earth and x units from the antenna, there exists a horizontal component of electric intensity F_X and a vertical component F_Z. For the antenna in question,

$$F_X = 30I_0[M + jN] \tag{12}$$

and

$$F_Z = 30I_0[S + jT] \tag{13}$$

where[6]

$$M = \frac{z-a}{xr_1}\sin(kr_1) + \frac{z+a}{xr_2}\sin(kr_2) - \frac{2z}{xr_0}\cos(G)\sin(kr_0) \tag{14}$$

$$N = \frac{z-a}{xr_1}\cos(kr_1) + \frac{z+a}{xr_2}\cos(kr_2) - \frac{2z}{xr_0}\cos(G)\cos(kr_0) \tag{15}$$

$$S = \frac{-\sin(kr_1)}{r_1} - \frac{\sin(kr_2)}{r_2} + \frac{2\cos(G)\sin(kr_0)}{r_0} \tag{16}$$

$$T = \frac{-\cos(kr_1)}{r_1} - \frac{\cos(kr_2)}{r_2} + \frac{2\cos(G)\cos(kr_0)}{r_0} \tag{17}$$

$$r_1 = \sqrt{(a-z)^2 + x^2} \tag{18}$$

$$r_2 = \sqrt{(a+z)^2 + x^2} \tag{19}$$

$$r_0 = \sqrt{(z^2 + x^2)}. \tag{20}$$

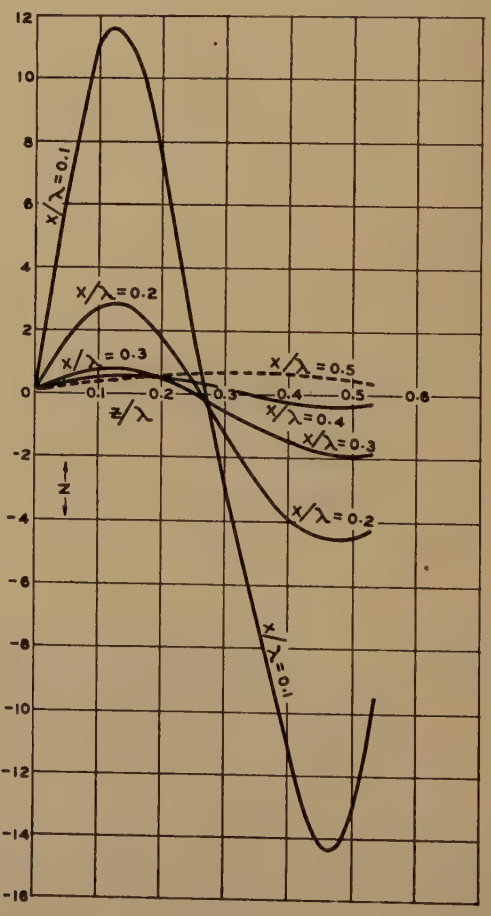

Fig. 9

When the current I_0 is expressed in amperes and all dimensions are measured in centimeters, (12) and (13) yield the electric intensities measured in volts

[6] G. H. Brown, "Directional antennas," Proc. I.R.E. vol. 25, p. 81, equations (5) and (6); January, (1937).

per centimeter. However, if all dimensions are expressed in fractions of a wavelength, the intensities are given in volts per wavelength and perfectly general curves may be plotted.

For a radiated power of W watts,

$$I_0 = \sqrt{\frac{W}{R_r}} \tag{21}$$

where R_r is the radiation resistance of the antenna referred to a current loop or maximum.

The cost of a high-power transmitter is great enough to justify the erection of the best antenna possible. At present, a straight vertical antenna, 0.53λ high ($G=190$ degrees), is believed to be the most desirable. Hence all further considerations will assume this antenna height.

When $G=190$ degrees, $R_r=90.0$ ohms.
Then for a power of one watt,

$$I_0 = \sqrt{\frac{1}{90}} = 0.1053 \text{ ampere.}$$

Thus (12) and (13) become

F_X(root-mean-square volts per wavelength for one watt)

$$= 3.16[M + jN] \tag{22}$$

F_Z(root-mean-square volts per wavelength for one watt)

$$= 3.16[S + jT]. \tag{23}$$

Figs. 8, 9, 10, and 11 show the quantities, M, N, S, and T, respectively, as a function of z, for a number of values of x.

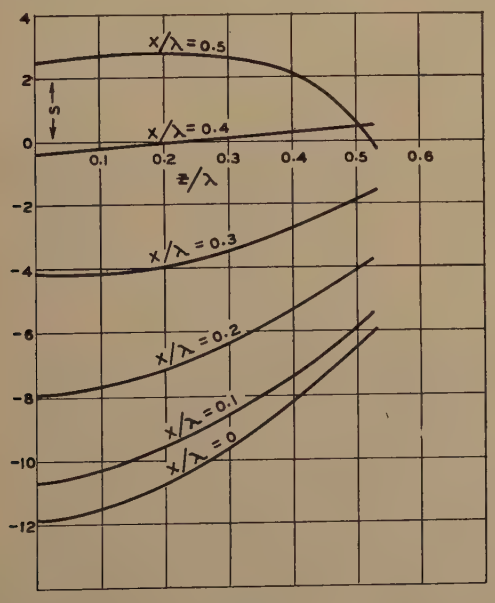

Fig. 10

Before proceeding further with the problem at hand, it is interesting to display the action of the field in a different manner. Since the horizontal and vertical components are not in phase, the direction of the sum of these components will vary with time so that the tip of the electric vector will describe an ellipse in space each time the antenna current goes through a complete cycle.

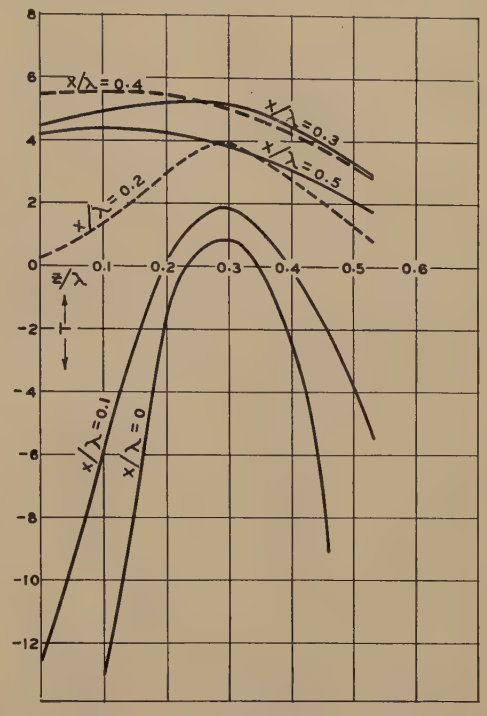

Fig. 11

Let us suppose that the loop current varies with time thus

$$i_o = \sqrt{2}\, I_0 \sin \omega t. \tag{24}$$

Then

$$F_X = 3.16\sqrt{2}\sqrt{M^2 + N^2} \sin(\omega t + \alpha) \tag{25}$$

where

$$\alpha = \tan^{-1}\frac{N}{M}. \tag{26}$$

$$F_Z = 3.16\sqrt{2}\sqrt{S^2 + T^2} \sin(\omega t + \beta) \tag{27}$$

where

$$\beta = \tan^{-1}\frac{T}{S}. \tag{28}$$

At any given instant, the electric vector has a magnitude equal to

$$\sqrt{F_X^2 + F_Z^2} = 3.16\sqrt{2}[(M^2 + N^2)\sin^2(\omega t + \alpha) + (S^2 + T^2)\sin^2(\omega t + \beta)]^{1/2}. \tag{29}$$

At this same moment, the vector makes an angle with the X axis (measured counterclockwise) of $\theta = \tan^{-1}\{\sin(\omega t+\beta)/\sin(\omega t+\alpha)\}\cdot\{\sqrt{S^2+T^2}/\sqrt{M^2+N^2}.\}$

Fig. 12 shows the characteristics of this rotating vector. It is interesting to note that the vectors in the lower left-hand corner of the figure rotate in a clockwise direction, while the remainder of the vectors rotate counterclockwise. As we go to great distances, the ellipses become straight lines which lie normal to radius vectors drawn from the base of the

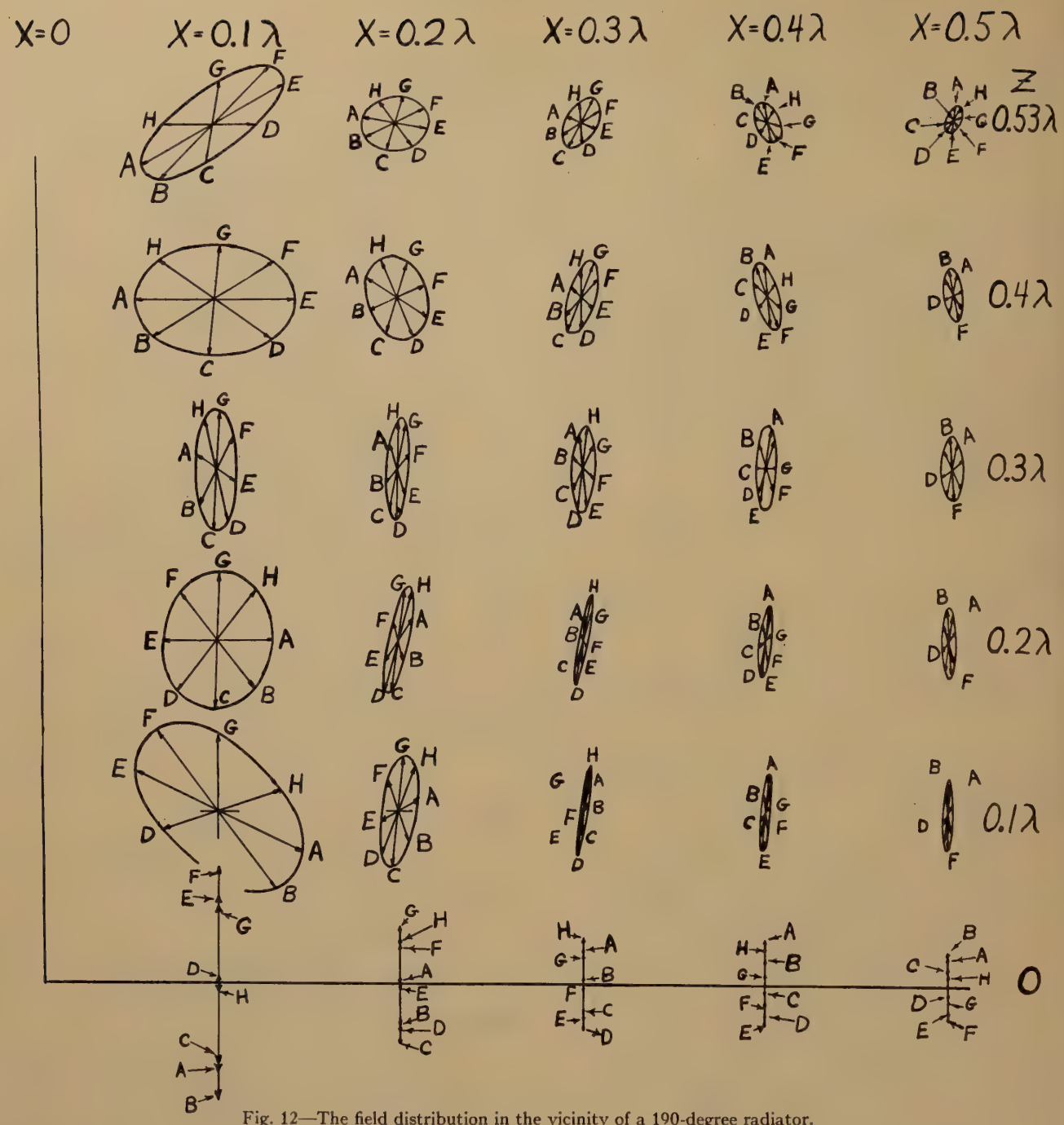

Fig. 12—The field distribution in the vicinity of a 190-degree radiator.

	$\omega t/2\pi$		$\omega t/2\pi$
A	0	*E*	1/2
B	1/8	*F*	5/8
C	1/4	*G*	3/4
D	3/8	*H*	7/8

antenna. At the surface of the earth, the ellipses become vertical straight lines.

Let us now examine the situation of Fig. 13. The guy wire is attached to the tower a distance y from the base of the tower, while the other end is anchored d units from the base. The guy wire then makes an angle ϕ with the surface of the earth. We will measure distance along the guy wire from the point where the guy is anchored at the earth end. Then the electric intensity parallel to the guy wire is $\overline{F}_W$ where

$$\overline{F}_W = \overline{F}_Z \sin \phi - \overline{F}_X \cos \phi. \tag{30}$$

The co-ordinates of the point are found from

$$z = W \sin \phi$$

$$x = d - W \cos \phi.$$

Then to find the electric intensity parallel to any guy wire of a 190-degree tower, we simply use the data of Figs. 8, 9, 10, and 11 to form (22) and (23), and substitute these equations in (30).

Each section of guy wire between any two insulators may be regarded as a transmission line of uniform distributed constants, said transmission line

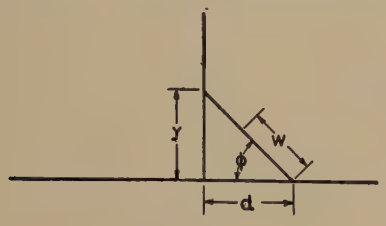

Fig. 13

being terminated at each end by a capacitance represented by the insulator and whatever amount of guy wire appears on the far side of this insulator. The transmission line is excited by the electric-field intensity vector which the tower sets up along the guy cable. Fig. 14 shows the idealized arrangement. Here

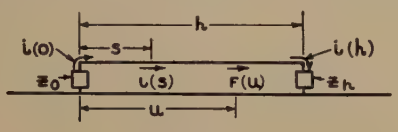

Fig. 14

we have a transmission line with uniform distributed constants, where the total length of the line is h. The line is grounded at either end by the impedances $\overline{Z}_0$ and $\overline{Z}_h$. It is assumed that the dissipative constants of the line, leakage, and ohmic resistance, are negligible. The distribution of electric intensity along the line is known. Then the current in the line at any point a distance s from the impedance Z_0 is

$$
\begin{aligned}
i(s) = \Big\{ & [Z_c^2 + \overline{Z}_h\overline{Z}_0] \int_{u=s}^{u=h} F(u) \cos k(h+s-u)du \\
& + j[Z_c\overline{Z}_h + Z_c\overline{Z}_0] \int_{u=s}^{u=h} F(u) \sin k(h+s-u)du \\
& + [Z_c^2 - \overline{Z}_0\overline{Z}_h] \int_{u=0}^{u=h} F(u) \cos k(h-s-u)du \\
& + j[Z_c\overline{Z}_h - Z_c\overline{Z}_0] \int_{u=0}^{u=h} F(u) \sin k(h-s-u)du \\
& + [Z_c^2 + \overline{Z}_0\overline{Z}_h] \int_{u=0}^{u=s} F(u) \cos k(h-s+u)du \\
& + j[Z_c\overline{Z}_h + Z_c\overline{Z}_0] \int_{u=0}^{u=s} F(u) \sin k(h-s+u)du \Big\} \\
& \div 2jZ_c \sin kh[Z_c^2 + \overline{Z}_0\overline{Z}_h \\
& + (\overline{Z}_0 + \overline{Z}_h)(-jZ_c \cot kh)] \qquad (31)
\end{aligned}
$$

where

$k = 2\pi/\lambda$

λ = operating wavelength

Z_c = characteristic impedance of the transmission line.

For a given distribution of $F(u)$, we may find from (31), the current at any point in the line. The product of $\overline{Z}_0$ and the current at $s=0$ will give the voltage across the terminating impedance $\overline{Z}_0$. Likewise, the

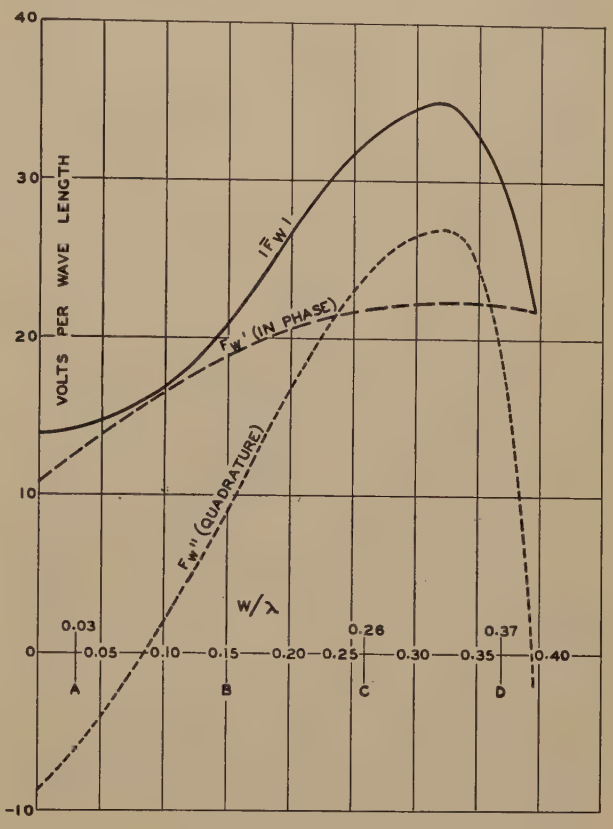

Fig. 15

product of $\overline{Z}_h$ and the current at $s=h$ will yield the voltage across $\overline{Z}_h$. In (31), $F(u)$ is expressed in volts per centimeter when the linear dimensions are measured in centimeters. However, if the linear dimensions are expressed in wavelengths, $F(u)$ is measured in volts per wavelength, and k becomes simply 2π.

We may best illustrate the theory by attacking a specific case. Let us suppose that the guy cable used to support a 190-degree cable is attached to the mast at a point 0.28 λ above the ground. Then y of Fig. 13 is 0.28λ. The angle ϕ is 45 degrees. Then we find $\overline{F}_w$ by means of (22), (23), and (30). It is to be noted that $\overline{F}_w$ has two components, F_w' in phase with the antenna current and F_w'' in time quadrature with the antenna current, so that

$$\overline{F}_w = F_w' + jF_w''. \qquad (32)$$

Fig. 15 shows these two components, as well as $|\overline{F}_w|$, as a function of W, for one watt into the 190-degree antenna. The points A, B, C, and D show the location of the insulators. It should be noted that for this particular situation the total length of guy cable is 0.396λ.

At this point, it might be mentioned that the condition of insulator placement shown on Fig. 15 corresponds closely to the arrangement in use at WCAU,

Philadelphia. Here the operating frequency is 1170 kilocycles, the wavelength 840 feet, and the diameter of each guy cable is 1.5 inches or 0.125 feet. The capacitance of each insulator is about 50 micromicrofarads.

We now examine the conditions in the lower section of the guy which connects the bottom of insulator A to earth. The current at the base of the guy wire is obtained by setting $Z_0=0$ and $s=0$ in (31). This yields

$$i(0) = \left\{ Z_c^2 \int_{u=0}^{u=h} F(u) \cos k(h-u)du + jZ_c\overline{Z}_h \int_{u=0}^{u=h} F(u) \sin k(h-u)du \right\} \qquad (33)$$
$$/jZ_c \sin kh[Z_c^2 - jZ_c\overline{Z}_h \cot kh].$$

At 1170 kilocycles, the 50-micromicrofarad insulator has an impedance of $-j2720$. This impedance in series with the impedance of the guy section A-B forms $\overline{Z}_h$. The guy section A-B may be regarded as an open-ended transmission line, so that its impedance is readily computed. Equation (9) yields a satisfactory expression and gives as a numerical result $-j407$. Thus

$$\overline{Z}_h = -j2720. - j407. = -j3127.$$

Likewise, from (9) where $60\{\log(a/s)-1\}$ was identified as the characteristic impedance, we find that Z_c, the characteristic impedance of the section O-A is 300 ohms.

Then

$$\overline{Z}_h/Z_c = -j3127/300 = -j10.4.$$

Also

$$\sin (kh) = 0.187$$
$$\cot (kh) = 5.25.$$

Before applying these values, (33) may be rewritten as

$$i(0) = \left\{ \int_{u=0}^{u=h} F(u) \cos k(h-u)du + j\frac{\overline{Z}_h}{Z_c} \int_{u=0}^{u=h} F(u) \sin k(h-u)du \right\} \qquad (34)$$
$$/jZ_c \sin kh\left[1 - j\frac{\overline{Z}_h}{Z_c} \cot kh\right].$$

We note from Fig. 15 that $F(u)$ over the length O-A is substantially constant and has the mean value, $F(u)=11.6-j7.5=14.0\angle -33°$ (volts per wavelength for one-watt input to the antenna). Then (34) yields

$$i(0) = 275 \times 10^{-6} \angle +57° \text{ (amperes)}.$$

For a power of 50,000 watts, we multiply by 224 and find the current at the base of the guy wire to be 0.0616 ampere. This is obtained with 23.5 amperes at the current loop of the antenna.

Let us now see what happens to the current at the base of this guy wire when the insulator capacitance becomes so small that the impedance $\overline{Z}_h$ is essentially infinite. Under this condition, (34) becomes[7] (equation for current at base of grounded guy)

$$\boxed{i(0) = \frac{+j}{Z_c \cos kh} \int_{u=0}^{u=h} F(u) \sin k(h-u)du.} \qquad (35)$$

Substituting the mean value for $F(u)$ in (35), we find that

$$i(0) = 134 \times 10^{-6} \angle +57° \text{ (amperes)}.$$

Multiplying by 224 to place on a 50,000-watt basis, we find the current at the base of the lower guy to be 0.03 ampere. Thus the current at the base of the lower guy section is reduced 50 per cent by materially decreasing the insulator capacitance.

Let us now see what happens to this current if the insulator A is short-circuited and the insulator B is infinite in impedance. We make use of (35). The new Z_c is 396 ohms, the mean value of $F(u)$ is 16.0 volts per wavelength, and kh is 54 degrees.

Then

$$\int_{u=0}^{u=h} \sin k(h-u)du = \frac{1-\cos kh}{2\pi} = \frac{0.41}{2\pi} = 0.0652$$

and

$$i(0) = 16 \times 0.0652/396 \times 0.59 = 0.00447 \text{ ampere}$$

for one watt. For 50,000 watts,

$$i(0) = 0.00447 \times 224 = 1.0 \text{ ampere}.$$

Thus, the guy-wire current has multiplied 16 times because of the short circuit on insulator A.

A radio-frequency meter was placed across the insulator A of the WCAU tower, and 50,000 watts supplied to the antenna. To the surprise of the writer, the meter registered 1.2 amperes.

We next turn our attention to the current flowing at the top end of the guy wire O-A. The current at this point is obtained from (31) by letting $Z_0=0$ and $s=h$.

Then

$$i(h) = \frac{Z_c \int_{u=0}^{u=h} F(u) \cos ku\, du}{j \sin (kh)[Z_c^2 - j\overline{Z}_h Z_c \cot kh]}. \qquad (36)$$

Using the values previously established for the guy section O-A, with the 50-micromicrofarad insulator at A, we find

$$i(h) = 143 \times 10^{-6} \angle +57° \text{ (amperes)}.$$

For 50,000 watts, this current becomes 0.032 ampere. This is the current forced through A by virtue of the voltages induced in the grounded guy section O-A. The voltages induced in A-B will also send a current through A which must be added to this first component in order to reckon the total voltage. First, we see what our original component does to the voltage on A. The impedance of A is $-j2720$ ohms. Then, for one-watt input, the lower guy section puts

[7] For the convenience of the reader, all general equations which pertain to voltage and current conditions where the guy insulators are infinite in impedance will be blocked out.

a voltage on A which is

$$e(h) = -j2720 \times 143 \times 10^{-6} \angle +57°$$
$$= 0.368 \angle -33° \text{ (volts)}.$$

This voltage component was thus obtained by forming the product of (36) and the insulator impedance. As this impedance becomes very great, it approaches $\overline{Z}_h$, and $\overline{Z}_h$ approaches infinity. In the limit, the voltage placed on the insulator at the top of the grounded guy section by the grounded guy section is

$$e(h) = \int_{u=0}^{u=h} F(u) \frac{\cos ku}{\cos kh} du. \qquad (37)$$

For this condition of infinite insulator impedance, we find

$$e(h) = 0.428 \angle -33° \text{ (volts)} = 0.36 - j0.232.$$

By reducing the insulator capacitance from 50 micro-microfarads to zero, we have increased the insulator voltage only ten per cent.

If we follow the same general procedure, we obtain the voltage on A due to the fields along A-B. We now assume the length A-B to be the transmission line of Fig. 14. Then the insulator A becomes the impedance $\overline{Z}_0$, and B is the impedance $\overline{Z}_h$. To find the voltage placed on A by the section A-B above A, we multiply (31) by Z_0, and let Z_0 and Z_h approach infinity. Then the voltage on A due to A-B is

$$e(0) = \int_{u=0}^{u=h} F(u) \frac{\sin k(h-u)}{\sin kh} du. \qquad (38)$$

When using Fig. 15 to form (38) to find the voltage A-B places on A, it should be noted that $W/\lambda = u/\lambda + 0.03\lambda$. A sample calculation to show how the voltage is obtained from (38) is given in Table II.

TABLE II

u/λ	W/λ	$(h/\lambda = 0.12)$ $(h-u)/\lambda$	$k(h-u)$ (degrees)	$\sin k(h-u)$	$\frac{\sin k(h-u)}{\sin kh}$	$F(u)$	$F(u)\frac{\sin (hk-u)}{\sin kh}$
0	0.03	0.12	43.2	0.68	1.0	$12.7-j6.1$	$12.7-j6.1$
0.03	0.06	0.09	32.4	0.535	0.787	$14.4-j3.0$	$11.35-j2.36$
0.06	0.09	0.06	21.6	0.367	0.54	$16.0-j0.06$	$8.63+j0.032$
0.09	0.12	0.03	10.8	0.187	0.275	$17.5+j4.6$	$4.81+j1.262$
0.12	0.15	0.00	0	0	0	$18.8+j9.1$	$0+j0$

The integrand formed in Table I is plotted in Fig. 16. The area under the curves of this figure give the voltage of (38), which is the voltage on A due to A-B. This is found to be

$$e(0) = 0.94 - j0.107 = 0.945 \angle -6.5°.$$

Adding to the value found on A due to O-A, we find the total voltage on A to be

$$e_A = 0.94 - j0.107 + 0.36 - j0.232$$
$$= 1.30 - j0.339 = 1.345 \angle -14.75°.$$

To convert this value to a 50,000-watt basis, we multiply by 224, and find

$$e_A = 301.0 \text{ volts}.$$

To find the voltages on the other insulators, we simply work along as before. The voltage on insulator B, due to the guy section A-B below this insulator, is

$$e(h) = \int_{u=0}^{u=h} F(u) \frac{\sin ku}{\sin kh} du. \qquad (39)$$

When we come to the insulator D, we simply find the voltage on D due to the guy section C-D, since the guy wire for this particular case is attached at a point on the tower where no charge occurs. In the case of other points of attachment, doubling the voltage on D due to C-D is satisfactory for design purposes.

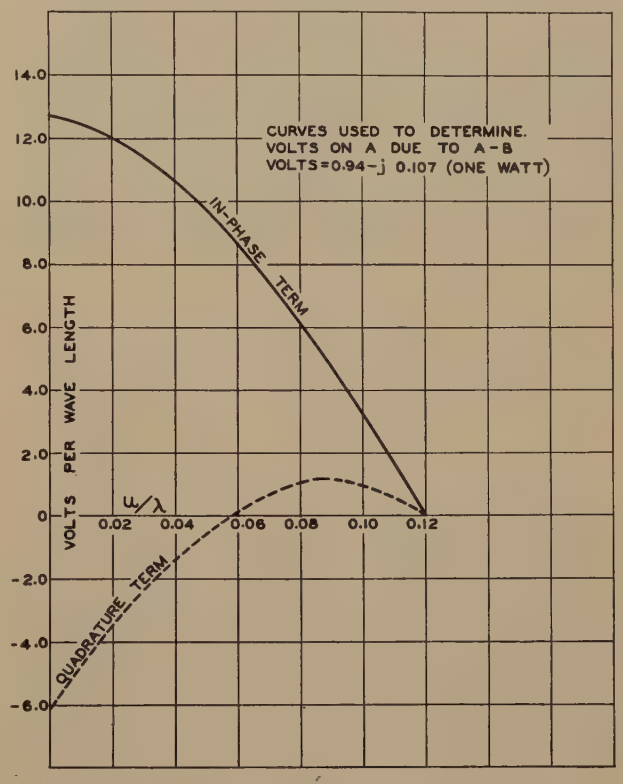

Fig. 16

The series of calculations were continued for the guy situation shown in Fig. 15. These calculations, on a basis of 50,000 watts, are shown in Table II. In this same table, measurements made on the WCAU insulators are given. These measurements were made with a vacuum-tube voltmeter, with the tower operated at a power of less than a watt and converted to 50,000 watts. Further, the measurements on insulator A were checked by operating the tower at full power, placing a 10,000-ohm noninductive resistor across the insulator, and determining the current through this resistor.

The guy insulators in the WCAU tower are huge affairs of the cone type. The insulator D at the point of attachment to the tower is really three of these insulators in series. In Table III, these insulators are indicated by subscripts, where D_1 is the one most re-

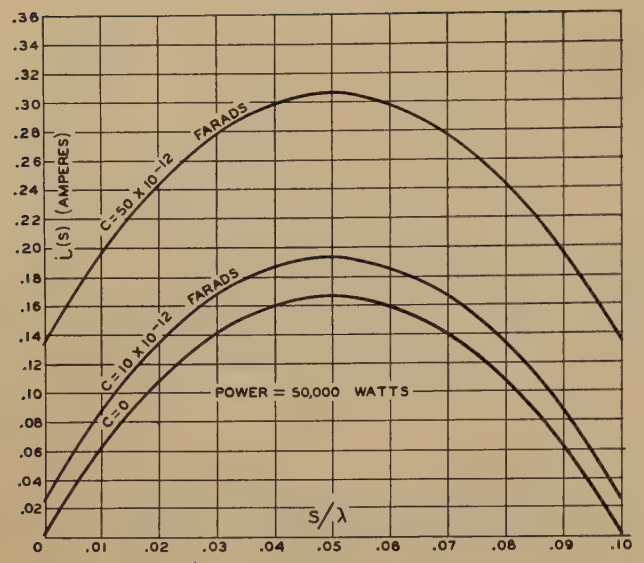

Fig. 17

mote from the tower, D_2 is in the center of the group, and D_3 is closest to the tower.

TABLE III
POWER 50,000 WATTS

Insulator	Volts (Calculated)	Volts (Measured)
A	301.	400.
B	550.	580.
C	795.	630.
D_1		274.
D_2		142.
D_3		158.
$D_1+D_2+D_3$	416.	574.

Before leaving the theoretical considerations, we shall examine the current distribution along an idealized guy-wire section. We assume that we have the transmission line of Fig. 14, where $F(u)$ is taken to be constant in magnitude along the line and has a value of 30.0 volts per wavelength, for one watt into the antenna. This value represents a fair average of the field strength existing near a 190-degree antenna. The line has a characteristic impedance of 330.0 ohms, and a length equal to 0.1λ. Further, the terminating impedances Z_0 and Z_h are capacitors, C farads in value. The system operates at 1170 kilocycles. Equation (31) was used to study the conditions on the wire line. Fig. 17 shows the distribution

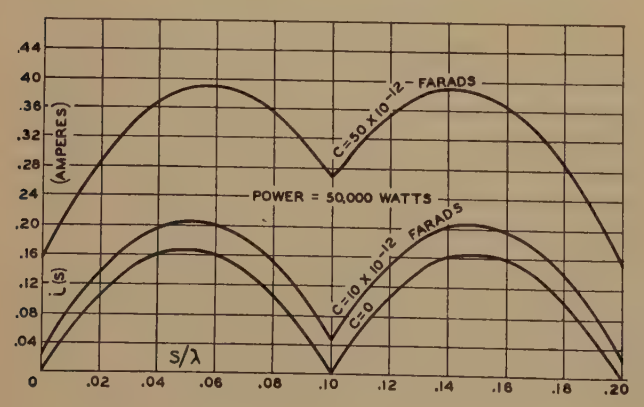

Fig. 18

of current along the line for values of C equal to 50, 10, and zero micromicrofarads. These calculations are based on a power of 50,000 watts. We see that with terminating capacitors which are infinite in impedance the maximum current on the guy is 0.167 ampere. With a capacitance of 10 micromicrofarads, the maximum current is 0.193 ampere, having increased 15 per cent. When the terminating capacitor is 50 micromicrofarads, the maximum current is 0.307 ampere, an increase of 85 per cent over the initial condition.

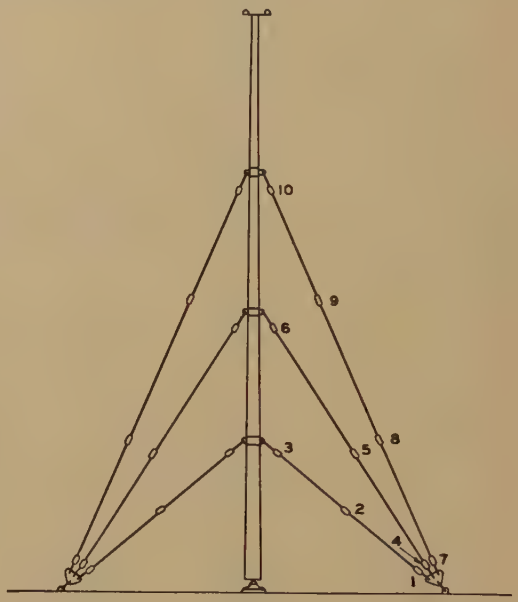

Fig. 19—Guy-insulator distribution for the tubular mast.

The voltage on the capacitors is given below.

C(micromicrofarads)	Volts (50,000 watts)
50	362.
10	351.
0	348.

We now place two of these guy wires in series, separating them by a series condenser which is the same size as the end terminating capacitors. Of course, there are now no capacitors to ground at the point where the two conductors meet. The resulting current distribution is shown on Fig. 18. Likewise, the capacitor voltages are given below.

C(micromicrofarads)	Volts on end *C*	Volts on middle *C*
50.	422.	735.
10	352.	652.
0	348.	692.

The measurements on the WCAU insulators were made in the spring of 1938. As stated previously, calculations were made of the insulator voltages on typical installations long before. In the fall of 1937, the writer was able to make measurements of guy-insulator voltage on a tubular steel guyed mast 150 feet tall. The resistance of the antenna was measured at a number of frequencies so that the power fed to the mast could be determined. A small amount of power was fed to the mast and the voltage across each insulator determined by means of a vacuum-tube voltmeter.

A scale drawing of the mast, with guy-wire and insulator positions shown, is given by Fig. 19. The insulators are numbered for reference purposes. The measured voltages are shown in Tables IV, V, and VI, for three antenna heights.

TABLE IV
ANTENNA HEIGHT 0.1425 WAVELENGTH 51.5 DEGREES
ROOT-MEAN-SQUARE VOLTS ON GUY INSULATORS FOR THE POWERS SHOWN

Insulator	Volts			
	1.0 watt	1000 watts	50,000 watts	500,000 watts
1	1.61	50.8	360.	1138.
2	2.9	91.5	648.	2050.
3	4.25	134.0	950.	3000.
4	2.02	63.6	450.	1420.
5	3.08	97.0	687.	2170.
6	4.12	130.2	925.	2920.
7	1.61	50.8	360.	1138.
8	1.72	54.2	384.	1210.
9	2.60	82.0	580.	1830.
10	5.06	160.0	1130.	3380.

TABLE V
ANTENNA HEIGHT 0.197 WAVELENGTH 71.0 DEGREES
ROOT-MEAN-SQUARE VOLTS ON GUY INSULATORS FOR THE POWERS SHOWN

Insulator	Volts			
	1.0 watt	1000 watts	50,000 watts	500,000 watts
1	0.925	29.2	206.	650.
2	1.395	44.1	312.	985.
3	2.6	82.0	580.	1830.
4	1.12	35.4	250.	790.
5	1.51	47.8	338.	1070.
6	3.28	104.0	735.	2320.
7	0.825	26.0	184.	582.
8	1.02	32.2	228.	720.
9	1.49	47.0	332.	1050.
10	4.15	131.0	925.	2920.

TABLE VI
ANTENNA HEIGHT 0.533 WAVELENGTH 192 DEGREES
ROOT-MEAN-SQUARE VOLTS ON GUY INSULATORS FOR THE POWERS SHOWN

Insulator	Volts			
	1.0 watt	1000 watts	50,000 watts	500,000 watts
1	0.822	26.0	184.	580.
2	1.402	44.3	313.	990.
3	2.06	65.0	460.	1450.
4	1.17	37.0	262.	830.
3	1.402	44.3	313.	990.
6	1.69	53.4	378.	1192.
7	0.838	26.5	187.	590.
8	1.06	33.5	237.	750.
9	1.10	34.8	246.	777.
10	1.48	46.7	330.	1042.

From Fig. 19, we see that the insulators in any one guy of this test mast were equally spaced. This was done so that a picture of the relative fields around the mast would be obtained. Actually, in practice, the insulators are spread unequally so that the voltages are evenly distributed. From the measurements and calculations we see that the voltages on the guy insulators for powers of 50,000 watts or less are not of very great magnitude. In fact, for powers of 500,000 watts, the voltages are not really exciting. By choosing the proper number and spacing of guy insulators it is possible to keep all guy insulator voltages below 1000 volts for powers as high as 500,000 watts. Then very inexpensive insulators may be used. Fig. 20 shows three types that are available. These insulators, including short sections of guy cable, show a measured capacitance of 10 micromicrofarads or less.

The insulators shown in Fig. 20 are marked A, B, and C. The electrical characteristics were obtained in the laboratory. The dry 60-cycle flashover voltages were first determined. After the arc started, the voltage was backed down to determine the voltage at which the arc ceased. eObsrvations were also made of

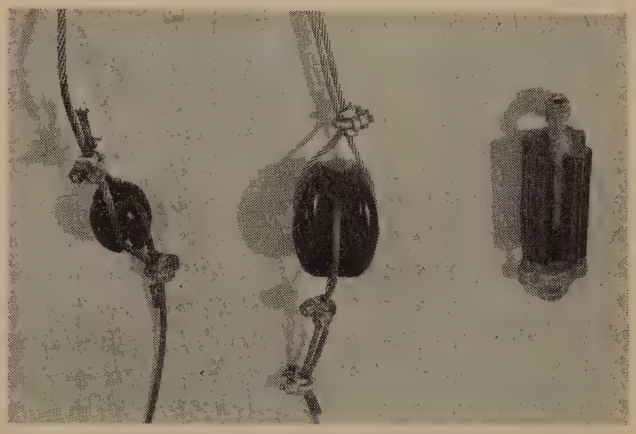

A B C

Fig. 20—Insulators suitable for sectionalizing guy wires.

points at which corona starts. The results of these experiments yield the following table.

TABLE VII

Insulator	60-cycle dry flashover voltage	Voltage at which arc stops	Safe operating voltage at 1000 kilocycles
A	14,000	6,500	1000
B	30,000	7,000–9,000	2000
C	35,000	13,500	4000

In the past two years several antennas have been erected which use the type *A* and *B* insulators. No difficulty has been experienced, either from radio-frequency voltages or from lightning. The writer made measurements on one directional antenna system using three multiguyed towers to obtain a very critical directional pattern. The guys were so broken up that there was no measurable effect upon either the nondirectional characteristics of the individual radiators or upon the directional pattern.

The type-A insulator was placed in parallel with the WCAU guy insulators when the tower was operated at 50,000 watts, with 90 per cent tone modulation. This test was made with the insulator dry, and no opportunity has presented itself to observe the effects when wet. There was no indication of heating, sparking, or corona in the dry condition and none would be expected when wet. The type-A insulator was also placed across the base insulator of the WCAU tower, where under the above conditions of modulation, the peak potential reaches over 10,000 volts. Again, no sign of failure was found.

One possible source of trouble may occur in high-power operation. The lengths of guy cable at times gather a high static charge which finally sparks across the guy insulators to ground. We see from Table VI

that the voltage necessary to maintain the arc or spark is much less than the voltage required to start the arc. If the radio-frequency voltage on the insulator is high, it may at the same time be below the arc-starting voltage but be high enough to maintain the arc once the static charge has broken the gap. Lightning surges may also cause the initial breakdown. The writer knows of only one instance where this difficulty arose, in the case of WLW when operating on a power of 500,000 watts. The difficulty was

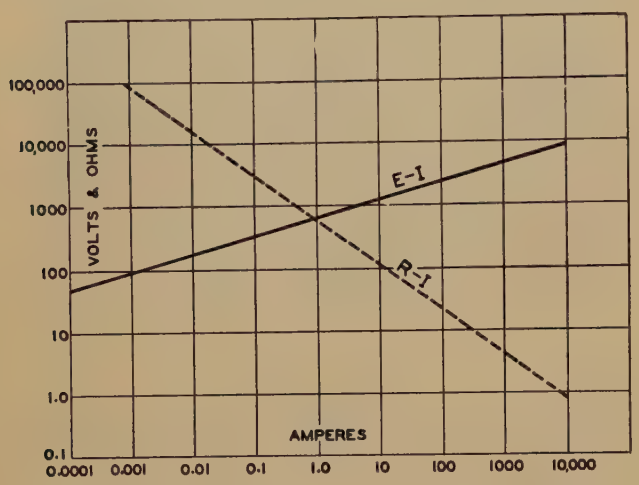

Fig. 21—*E-I* and *R-I* curve for a Thyrite disk six inches in diameter and three quarters of an inch thick, as published by McEachron.

cleared up by placing high-resistance leaks across the guy insulators. In general, resistors placed across the guy insulators will clear up all trouble due to static charges. However, a direct stroke of lightning may take out the leak resistors completely but is not likely to damage the insulator if the insulator glaze is in good condition. In one case within the writer's experience, a guyed mast using type-B insulators was hit with a direct stroke which traveled down one guy wire. A rigger immediately inspected the guy insulators and found no damage.

The type of insulator in use at WCAU has a large capacitance, 50 micromicrofarads. The construction of this insulator is such that it is possible to increase this capacitance somewhat, place an inductance in parallel with the insulator, tune the combination to parallel resonance, and thus secure a very high impedance to the radio-frequency energy and practically a short circuit for most of the components of a steep wave-front lightning stroke. The static drain is also provided by the coil.

However, for real protection a material is available which has been used extensively for lightning arresters in the power transmission field. This material is called Thyrite. It has the property[8] of high resistance at low voltages and currents and exceedingly small resistances at high voltages and currents. Fig. 21 shows the characteristics given by McEachron for a particular Thyrite disk which is six inches in diameter and three quarters of an inch thick. Properly designed disks placed in parallel with the guy insulators of the radio mast would provide practically perfect protection. The Thyrite would have a very high resistance to the radio-frequency voltages and would leak off any static charge which might tend to accumulate. When a wave front of lightning strikes, the resistance drops to low values, passes off the lightning charge, and returns to its normal high-resistance condition. The material has no time lag and returns to its normal condition when current ceases to flow. Since Thyrite can be molded readily, it may be possible to mold the type-A or -B insulator itself from the Thyrite material.

[8] K. B. McEachron, "Thyrite: A new material for lightning arresters," *Gen. Elec. Rev.*, vol. 33, pp. 92–99; February, (1930).

IV. Conclusion

Base-insulator voltages have been considered, and experimental results for several tower types presented in Figs. 4, 5, and 6. These voltages remain within very reasonable limits for towers greater than one-sixth wavelength, for the highest powers now in use.

The study, experimental and theoretical, shows that low guy-insulator voltages and low guy currents exist when the insulator disposition is chosen properly. The importance of low insulator capacitance is demonstrated. Guy-wire currents and guy-insulator voltages decrease very rapidly as guy sections are shortened. Decreasing insulator capacitance decreases guy currents sharply, while no marked effect on the voltage is apparent.

Small and cheap insulators are suitable in even the high-power installations. The currents in the guy wires may easily be held to small values which will not affect the radiation characteristics of the tower itself. In the case of transmitter power of the order of 500,000 watts, means must be provided to quench arcs that may be started by static or lightning discharges. At these powers, the arcs may be sustained by the radio-frequency power. A Thyrite insulator is proposed for this task.

V. Acknowledgment

The writer wishes to express his appreciation for the assistance which made this work possible to Mr. John G. Leitch, WCAU technical supervisor, and Mr. Charles Miller, chief engineer of the transmitting plant of WCAU, for co-operation in the WCAU measurements; to John E. Lingo and Son, Inc., Camden, New Jersey, who made available for measurement the guyed tubular mast; and to Mr. R. F. Lewis and Mr. J. Epstein, of the engineering staff of the RCA Manufacturing Company, who assisted greatly both in the experimental work and in preparing the theoretical data.

Resonant Impedance of Transmission Lines*

L. S. NERGAARD†, MEMBER, I.R.E., AND BERNARD SALZBERG†, MEMBER, I.R.E.

Summary—*The maximum absolute impedance for a tuned circuit which consists of a low-loss radio-frequency transmission line, either short-circuited or open-circuited at its distant end, and shunted at its sending end by a capacitor of negligible resistance is shown theoretically to occur when the line length is practically an integral number of quarter wavelengths and the capacitance is zero. This conclusion disagrees with previous theoretical results, which indicated shorter optimum lengths. It is pointed out that the earlier results are incorrect because of the neglect of the quadrature component of the characteristic impedance. An experimental verification of the theoretical results is provided.*

I. Introduction

THE increasing use of transmission lines as circuit elements in ultra-high-frequency receivers, transmitters, and filters makes it desirable that the engineer have at his disposal an accurate knowledge of the properties of such lines. It is the purpose of this paper to describe a more refined study than has hitherto been available of the impedance of a tuned circuit consisting of a transmission line shunted by a capacitor.

The analysis indicates that the imaginary part of the characteristic impedance cannot be neglected even at the highest frequencies, although it has apparently been common practice to do so. The result of including this quadrature component of the characteristic impedance in the mathematical study of the problem is to reveal that the highest tuned impedance of a low-loss transmission line, either short-circuited or open-circuited at one end and tuned by a variable capacitor of negligible losses at the other end, is obtained when the line is operated at self-resonance; i.e., the line length is practically an integral number of quarter wavelengths. The experimental results confirm this conclusion. This vitiates the theoretical results previously obtained in at least two instances of which we are aware.[1,2]

II. Theory

The theory takes its start with the well-known expression for the sending-end impedance of a uniform line, of length l, which is short-circuited at its distant end.[3]

$$Z = Z_0' \cdot \tanh Pl \tag{1}$$

where $Z_0' = (R_0 + i\omega L_0)^{1/2} \cdot (G_0 + i\omega C_0)^{-1/2}$, the characteristic impedance of the line, and $P = (R_0 + i\omega L_0)^{1/2} (G_0 + i\omega C_0)^{1/2}$, the propagation constant of the line.

In these expressions R_0, L_0, G_0, and C_0 refer to the series resistance, inductance, shunt conductance, and capacitance (all per unit length of line), respectively; ω represents 2π times the operating frequency; and $i = (-1)^{1/2}$.

For the purposes of analysis it is desirable to express each of the quantities Z_0' and P as a sum of a real and an imaginary part.

For the usual radio-frequency line, $G_0 = 0$. Then

$$\begin{aligned} Z_0' &= (L_0/C_0)^{1/2} \cdot [1 - i(R_0/\omega L_0)]^{1/2} \\ &= (L_0/C_0)^{1/2} \cdot \{(1/2)[1 + (R_0/\omega L_0)^2]^{1/2} + (1/2)\}^{1/2} \\ &\quad \cdot [1 - i(R_0/\omega L_0)\{1 + [1 + (R_0/\omega L_0)^2]^{1/2}\}^{-1}] \\ &\equiv Z_0(1 - ik) \end{aligned}$$

and

$$\begin{aligned} P &= \omega(L_0C_0)^{1/2} \cdot [-1 + i(R_0/\omega L_0)]^{1/2} \\ &= \omega(L_0C_0)^{1/2} \cdot \{(1/2)[1 + (R_0/\omega L_0)^2]^{1/2} + (1/2)\}^{1/2} \\ &\quad \cdot [i + (R_0/\omega L_0)\{1 + [1 + (R_0/\omega L_0)^2]^{1/2}\}^{-1}] \\ &\equiv \beta(i + k) \end{aligned}$$

in which

$$Z_0 = (L_0/C_0)^{1/2} \cdot \{(1/2)[1 + (R_0/\omega L_0)^2]^{1/2} + (1/2)\}^{1/2},$$

the characteristic impedance,

$$\beta = \omega(L_0C_0)^{1/2} \cdot \{(1/2)[1 + (R_0/\omega L_0)^2]^{1/2} + (1/2)\}^{1/2},$$

the phase constant,

$$k = (R_0/\omega L_0)\{1 + [1 + (R_0/\omega L_0)^2]^{1/2}\}^{-1},$$

a useful dimensionless parameter. The foregoing expressions involve no approximations whatever and are therefore exact in form. For the special case when $(R_0/\omega L_0)^2 \ll 1$, these quantities may be written as

$$\begin{aligned} Z_0 &\cong (L_0/C_0)^{1/2} \\ \beta &\cong \omega(L_0C_0)^{1/2} \\ k &\cong (R_0/2\omega L_0). \end{aligned}$$

Making use of the foregoing expressions for Z_0' and P we may write (1) as

$$\begin{aligned} Z &= Z_0 \cdot (1 - ik) \tanh (k + i)\beta l \\ &= Z_0(1 - ik) \tanh (k + i)\theta, \end{aligned}$$

in which $\theta = \beta l$, the electrical length of the line.

This may be expanded algebraically in straightforward fashion so as to express the resistive and reactive components of the sending-end impedance of the line. Thus,

$$\begin{aligned} Z &= R + iX \\ &= Z_0 \cdot (\cosh 2k\theta + \cos 2\theta)^{-1} \cdot [(\sinh 2k\theta + k \sin 2\theta) \\ &\quad + i(\sin 2\theta - k \sinh 2k\theta)]. \end{aligned} \tag{2}$$

* Decimal classification: R120×R116. Original manuscript received by the Institute August 11, 1938; revised manuscript received by the Institute, March 23, 1939.

† RCA Manufacturing Company, Inc., RCA Radiotron Division, Harrison, N. J.

[1] Bernard Salzberg, "On the optimum length for transmission lines used as circuit elements," PROC. I.R.E., vol. 25 pp. 1561–1564; December, (1937).

[2] L. A. Leeds, "Concentric narrow-band-elimination filter," PROC. I.R.E., vol. 26, pp. 576–589; May, (1938).

[3] See, for example, W. L. Everitt, "Communication Engineering," McGraw-Hill Book Company, (1932).

If we neglect the quadrature component of the characteristic impedance, which in a low-loss radio-frequency line may be easily made only one thousandth as large as the real component, the sending-end impedance becomes

$$Z \cong Z_0 \cdot (\cosh 2k\theta + \cos 2\theta)^{-1} \cdot [\sinh 2k\theta + i \sin 2\theta]. \quad (3)$$

We shall now show, by means of a simple example, that it is not always permissible to neglect this quadrature component. The limiting sending-end impedance of the line as θ approaches zero should be $Z \sim (R_0 l + i\omega L_0 l)$. According to (3), however, Z behaves for small θ as

$$Z \sim Z_0 \cdot \theta \cdot (k + i) = (R_0 l)/2 + i\omega L_0 l,$$

which is obviously inaccurate with respect to the resistance. If (2) instead of (3) is used Z behaves for small θ as $Z \sim Z_0 \cdot \theta(2k + i) = R_0 l + i\omega L_0 l$, which is the result one must expect.

For lines which are an integral number of quarter wavelengths long, (2) and (3) reduce to the same form. This coincidence does not occur for lines of any other length. The fact that it does occur for lines which are an integral number of quarter wavelengths long may have served in the past to obscure the importance of the quadrature component of the characteristic impedance.

The effect of the quadrature component of the characteristic impedance on the sending-end impedance of the line can be neglected only in a certain range of values of line length. This range is established on one side by the effect of the quadrature component on the real part of Z, and on the other side by its effect on the imaginary part of Z. This may be demonstrated in the following way. In (2) the portion of the real part of Z which is generated by the quadrature component of the characteristic impedance is $k \sin 2\theta$. This is small compared to the other portion of the real part of Z for values of θ which satisfy the inequality

$$\frac{\sinh 2k\theta}{k} \gg |\sin 2\theta|.$$

Also in (2) the portion of the imaginary part of Z which is generated by the quadrature component of the characteristic impedance is $-k \sinh 2k\theta$. This is small compared to the other portion of the imaginary part of Z for values of θ which satisfy the inequality

$$|\sin 2\theta| \gg k \sinh 2k\theta.$$

These two inequalities may be combined to establish a range in which the effect of the quadrature component on the sending-end impedance of the line can be neglected. This range is defined by

$$\frac{\sinh 2k\theta}{k} \gg |\sin 2\theta| \gg k \sinh 2k\theta.$$

It is of interest to note that for θ very large, the sending-end impedance of the line approaches the value for the characteristic impedance; i.e.,

$$Z \sim Z_0(1 - ik).$$

(A). Discussion of the Sending-End Resistance and Reactance

The series combination of resistance and reactance which represents the sending-end impedance of the line is given by (2). For very small values of k, corresponding to low-loss lines, we may write

$$Z = R + iX$$
$$\cong \frac{Z_0 k(2\theta + \sin 2\theta)}{1 + \cos 2\theta + 2k^2\theta^2} + i \cdot \frac{Z_0(\sin 2\theta - 2k^2\theta)}{1 + \cos 2\theta + 2k^2\theta^2}. \quad (4)$$

Examination of R and X indicates that these functions have their maxima near $2\theta = (2n+1)\pi$, where $n = 0, 1, 2, 3 \ldots$. Accordingly, we introduce a new variable $\delta = (2n+1)\pi - 2\theta$ and write (4) as

$$Z \cong \frac{Z_0 k[(2n+1)\pi - \delta + \sin \delta]}{1 - \cos \delta + (1/2)k^2(2n+1)^2\pi^2 - (2n+1)\pi\delta k^2} + i \cdot \frac{Z_0[\sin \delta - k^2\pi(2n+1)]}{1 - \cos \delta + (1/2)k^2(2n+1)^2\pi^2 - (2n+1)\pi\delta k^2}.$$

For small values of δ, we obtain the following approximations:

$$\frac{R}{Z_0} \cong \frac{2(2n+1)\pi k}{\delta^2 + (2n+1)^2\pi^2 k^2 - 2(2n+1)\pi\delta k^2}$$

and

$$\frac{X}{Z_0} \cong \frac{2[\delta - k^2\pi(2n+1)]}{\delta^2 + (2n+1)^2\pi^2 k^2 - 2(2n+1)\pi\delta k^2}.$$

Maximization of these functions indicates that the resistance is a maximum when

$$2\theta \cong (2n+1)(1 - k^2)\pi.$$

For this value of θ, the resistance is

$$R_{\max} \cong 2Z_0/(2n+1)k\pi$$

and the reactance is zero. Also the reactance is a maximum (inductive) or minimum (capacitive) when

$$2\theta \cong (2n+1)(1 \mp k)\pi.$$

For these values of θ, the reactance is

$$X_m \cong \frac{\pm Z_0}{(2n+1)k\pi},$$

and the resistance is

$$R \cong \frac{Z_0}{(2n+1)k\pi}.$$

In passing it may be remarked that the values of θ which make the reactance a maximum or minimum represent the half-energy points; i.e., the reactive energy is equal to the dissipative energy.

It is of interest to note the analogy which exists between the behavior of the sending-end impedance of the transmission line when the line is near self-resonance, and the behavior of the impedance of a parallel-resonant combination of lumped constants. This analogy may be shown in the following way: If the lumped circuit parameters are related to the line parameters as follows,

$$\omega L = Z_0\theta$$
$$\omega C = \theta/Z_0$$
$$R = k\theta Z_0$$

then it may readily be shown that the expressions for the impedances are identical.

$$Z = \frac{Z_0}{k\theta}\cdot\frac{1}{1+i(\Delta\theta/k\theta)} = \frac{L}{CR}\cdot\frac{1}{1+i(\omega\Delta L/R)}.$$

(B). Discussion of the Tuned Circuit

Now that the equivalent series resistance and reactance at the sending-end terminals of a transmission line which is short-circuited at its distant end have been obtained, the elementary tuned circuit consisting of a capacitance shunted by such a line may readily be analyzed. In practice this circuit is tuned to obtain maximum absolute impedance by adjusting either the capacitance or the line length.

The square of the absolute impedance of a circuit consisting of a capacitance C shunted by a series combination of inductive reactance X and resistance R is

$$|z|^2 = \frac{R^2+X^2}{(1-\omega CX)^2+\omega^2C^2R^2}. \qquad (5)$$

Substituting the values of R and X for the line given by (2), and defining $\omega CZ_0=S$, there results

$$\frac{|z|^2}{Z_0^2} = \frac{(1+k^2)\cdot(\cosh 2k\theta-\cos 2\theta)}{(\cosh 2k\theta+\cos 2\theta)-2S(\sin 2\theta-k\sinh 2k\theta)+S^2(1+k^2)\cdot(\cosh 2k\theta-\cos 2\theta)}. \qquad (6)$$

Now if (6) be maximized with respect to S, corresponding to the adjustment of the capacitance with fixed line length, it is found that the condition for the maximum absolute impedance is

$$S = \frac{\sin 2\theta - k\sinh 2k\theta}{(1+k^2)\cdot(\cosh 2k\theta-\cos 2\theta)}. \qquad (7)$$

This adjustment, as in the lumped-circuit case, gives unity power factor. The value of the impedance is given by

$$\frac{r}{Z_0} = (1+k^2)\cdot\frac{\cosh 2k\theta-\cos 2\theta}{\sinh 2k\theta+k\sin 2\theta}. \qquad (8)$$

If, however, (6) be maximized with respect to θ, corresponding to the adjustment of the line length with fixed capacitance, it is found that the maximum absolute impedance occurs when

$$S = \frac{k\sinh 2k\theta\cdot\cos 2\theta+\cosh 2k\theta\cdot\sin 2\theta}{(1+k^2)\cdot(1-\cos 2\theta\cdot\cosh 2k\theta)} \qquad (9)$$

and its value is

$$\frac{r}{Z_0} = (1+k^2)\cdot\frac{1-\cos 2\theta\cdot\cosh 2k\theta}{\sinh 2k\theta+k\sin 2\theta}. \qquad (10)$$

For the low-loss radio-frequency lines under consideration, i.e., $k^2\theta^2\ll 1$, both (7) and (9) may be written as

$$S \cong \cot\theta$$

except in a small range of the order of $k^2\theta$ about $2\theta=(2n+1)\pi$, in which the exact expressions must

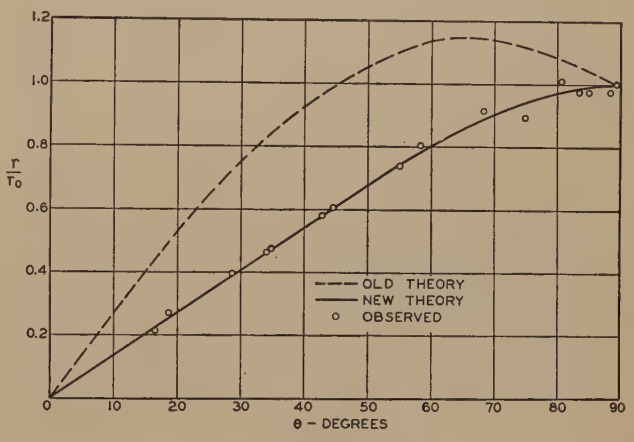

Fig. 1

be used. This indicates that the condition for the maximum absolute impedance is the same whether obtained by adjustment of the capacitance or by adjustment of the line length.

Also, for such lines, both (8) and (10) may be written as

$$\frac{r}{Z_0} \cong \frac{1}{k}\cdot\frac{1-\cos 2\theta}{2\theta+\sin 2\theta}. \qquad (11)$$

This shows that the maximum absolute impedance as a function of line length is the same whether the circuit is tuned by adjustment of the capacitance, with line length fixed, or by adjustment of the line length, with capacitance fixed. The variation of (r/Z_0) with θ as given by (11), is shown in Fig. 1.

Now, as a practical matter, it is desirable to determine the length of line which will result in the maximum obtainable tuned impedance. Maximization of (11) shows that this result is obtained when

$$2\theta = (2n+1)\pi.$$

Maximization of the exact expressions, (8) and (10), yields the same result. However, substitution of this length of line in (7) or (9) gives for the corresponding value of capacitance

$$C = \frac{-k}{\omega Z_0(1+k^2)} \cdot \frac{\sinh (2n+1)\pi k}{1+\cosh (2n+1)\pi k};$$

i.e., the required value of capacitance is negative. The tuned impedance given by both (8) and (10) which corresponds to this value of capacitance is

$$\frac{r}{Z_0} = (1+k^2) \cdot \frac{1+\cosh (2n+1)\pi k}{\sinh (2n+1)\pi k}.$$

For low-loss lines this result can be approximated by

$$\frac{r}{Z_0} \cong (1+k^2) \cdot \frac{4+(2n+1)^2\pi^2 k^2}{2(2n+1)\pi k} \cong \frac{2}{(2n+1)\pi k}.$$

The tuned impedance which is obtained with zero capacitance is, to the same degree of approximation, identical with the above result. The line length which corresponds to zero capacitance (obtained by equating either (7) or (9) to zero, and neglecting terms of degree higher than k^2) is

$$2\theta \cong (2n+1)\pi(1-k^2).$$

In view of the fact that for reasonably low-loss lines $k<10^{-2}$, it would appear impractical to attempt to obtain the vanishingly small increase in impedance which results from an adjustment of the line length within 1 part in at least 10^4.

(C). The Open-Circuited Line

The analysis for the case of a uniform line which is open-circuited at its distant end is similar to the treatment of the short-circuited line, and therefore only the end results will be given. Corresponding to (1) we have

$$Z = Z_0' \cdot \coth Pl. \tag{1a}$$

Making use of the same approximations as before, there results for the sending-end impedance of the line

$$\begin{aligned} Z &= R + iX \\ &= Z_0 (\cosh 2k\theta - \cos 2\theta)^{-1} \cdot [(\sinh 2k\theta - k \sin 2\theta) \\ &\quad - i(\sin 2\theta + k \sinh 2k\theta)]. \end{aligned} \tag{2a}$$

If the quadrature component of the characteristic impedance is again neglected, (2a) becomes

$$Z = Z_0 \cdot (\cosh 2k\theta - \cos 2\theta)^{-1} \cdot [\sinh 2k\theta - i \sin 2\theta]. \tag{3a}$$

The range of θ in which the effect of the quadrature component may be neglected is the same as in the previous case. For very small values of k, corresponding to low-loss lines, we may write (2a) as

$$\begin{aligned} Z &= R + iX \\ &\cong \frac{Z_0 k(2\theta - \sin 2\theta)}{1 - \cos 2\theta + 2k^2\theta^2} - i \cdot \frac{Z_0(\sin 2\theta + 2k^2\theta)}{1 - \cos 2\theta + 2k^2\theta^2}. \end{aligned} \tag{4a}$$

The resistance in this case is a maximum when $\theta \cong n\pi(1-k^2)$, $n=1, 2, \ldots$; the maximum resistance being $R_{max} \cong (Z_0/nk\pi)$, and the reactance zero. The reactance is a maximum or minimum when $\theta \cong n\pi(1 \mp k)$; the maximum or minimum reactance being $X_m \cong \pm(Z_0/2n\pi k)$. For the latter values of θ, the resistance is $R \cong Z_0/2n\pi k$, indicating again that these values of θ represent the half-energy points.

The square of the absolute impedance, obtained by substituting the values of R and X obtained from (2a) in (5), is

$$\frac{|z|^2}{Z_0^2} = \frac{(1+k^2)(\cosh 2k\theta + \cos 2\theta)}{(\cosh 2k\theta - \cos 2\theta) + 2S(\sin 2\theta + k \sinh 2k\theta) + S^2(1+k^2)(\cosh 2k\theta + \cos 2\theta)}. \tag{6a}$$

Maximization of (6a) with respect to S gives, as the condition for a maximum

$$S = -\frac{\sin 2\theta + k \sinh 2k\theta}{(1+k^2)(\cosh 2k\theta + \cos 2\theta)} \tag{7a}$$

and as the corresponding maximum impedance

$$\frac{r}{Z_0} = (1+k^2) \cdot \frac{\cosh 2k\theta + \cos 2\theta}{\sinh 2k\theta - k \sin 2\theta}. \tag{8a}$$

Maximization of (6a) with respect to θ gives, as the condition for a maximum

$$S = -\frac{k \sinh 2k\theta \cdot \cos 2\theta + \cosh 2k\theta \cdot \sin 2\theta}{(1+k^2) \cdot (1 + \cos 2\theta \cosh 2k\theta)} \tag{9a}$$

and as the corresponding maximum impedance

$$\frac{r}{Z_0} = (1+k^2) \cdot \frac{1 + \cos 2\theta \cdot \cosh 2k\theta}{\sinh 2k\theta - k \sin 2\theta}. \tag{10a}$$

For the low-loss radio-frequency lines under consideration both (7a) and (9a) reduce to

$$S \cong -\tan \theta,$$

and (8a) and (10a) reduce to

$$\frac{r}{Z_0} \cong \frac{1}{k} \cdot \frac{1+\cos 2\theta}{2\theta - \sin 2\theta}. \tag{11a}$$

In this case, also, the maximum impedance as a function of line length is the same whether the circuit is tuned by adjustment of the capacitance, with line length fixed, or by adjustment of the line length, with capacitance fixed. The variation of (r/Z_0) with θ, as given by (11a), is included in Fig. 1.

III. Experimental Verification

To verify the foregoing results, particularly with respect to the variation of (r/Z_0) with θ, an experimental check was undertaken. The transmission line on which the measurements were made was of the parallel-conductor type, the center-to-center separation of the conductors being 0.75 inch and their diameter 0.375 inch. The distant end was terminated in a movable short-circuiting bar driven by a micrometer screw. The sending-end was terminated in

a capacitor which consisted of two small parallel plates separated by mica spacers. The capacitance was varied by changing the thickness of the mica between the plates. In order to avoid changes in the capacitance during adjustment of the short-circuit bar, the capacitor plates were firmly bolted together through an insulating bushing.

The impedance of the line was determined by means of the line-length-variation method.[4] This method consists, briefly, in loosely coupling the line to a signal generator; measuring the line length which corresponds to resonance; and then measuring the change in line length required to reduce the voltage across the line to 0.707 times its resonant value. The resonant impedance is then given by

$$\frac{r}{Z_0} = \frac{\sin^2 \theta_r}{\Delta\theta}$$

where

Z_0 = the real part of the characteristic impedance of the line

θ_r = the electrical length of the line at resonance

$\Delta\theta$ = the change in the electrical length of the line required to reduce the voltage to 0.707 of its resonant value.

The line under test was capacitively coupled at its sending end to an auxiliary line excited by a magnetron generator operating at a wavelength of 192 centimeters. To insure that the auxiliary line did not reflect resistance into the test line, the coupling between the two lines was reduced until short-circuiting the sending end of the test line produced only a negligible change in the reading of a voltmeter connected across the auxiliary line. To reduce the possibility of line unbalance the two lines were arranged along a common axis and a common plane. The auxiliary line was shielded so that the coupling between the lines consisted substantially of only the capacitances between the adjacent ends of the two lines. This prevented variation of the coupling with adjustment of the length of the test line during the measurements. Voltages on the test line were read by means of a balanced-diode peak voltmeter, care being taken to arrange the shielded direct-current voltmeter leads in the neutral plane of the line.

Before proceeding to the actual verification, it was necessary to make a number of preliminary measurements. In all of these measurements the conductors of the test line were of copper. The first measurements were required to determine the effective length of the short-circuit bar. This was required because for short lines the effective length of the short-circuit bar may be an appreciable part of the total length. This effective length may be obtained for all practical purposes by measuring the length of free line required for resonance at various wavelengths. The intercept on the length axis of a plot of length versus wavelength obtained in this manner gives directly the effective length of the short-circuit bar. The next measurements were required to determine the voltmeter impedance and the radiation resistance of the line. This was done by measuring, by the method previously described, the joint impedance of the free line and the voltmeter, with the voltmeter first connected at the sending end of the line and then connected near the short-circuit bar where its effect on the line was negligible. These measurements gave the voltmeter impedance as 57,000 ohms, and the line impedance as 167,000 ohms. This value of the voltmeter impedance was taken into account in subsequent measurements of the line impedance. The calculated line impedance, including the calculated radiation resistance, was 192,000 ohms, which checks the measured line impedance within 15 per cent.[5] In view of this agreement between calculated and measured values of line impedance, we assume that our calculation of the radiation resistance effective at the sending-end terminals of the line, 330,000 ohms, is of the right order of magnitude.

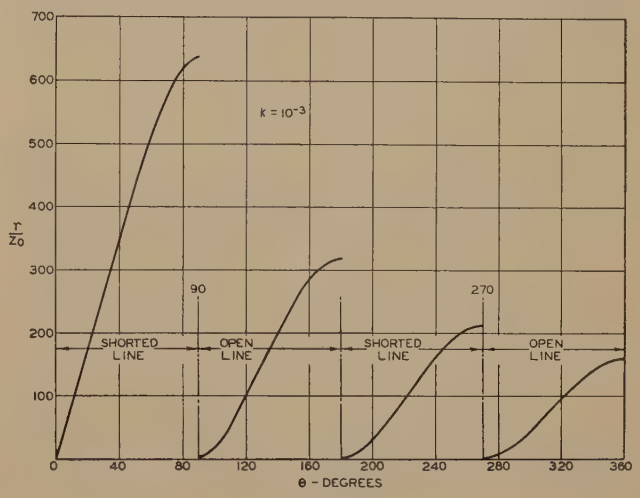

Fig. 2

To make this radiation loss negligible in comparison with the energy lost in the line, and to make the line Q small in comparison with the capacitor Q, the copper conductors were replaced by solid conductors of the same dimensions, made of steel drill rod. This also made the frequency stability requirements of the oscillator less stringent. The sending-end impedance of the quarter-wave drill-rod line was 12,500 ohms.

The experimental verification of the theory was then made on the drill-rod test line. The results are shown in Fig. 2, in which r represents the sending-end impedance of the line, r_0 represents the sending-

[4] L. S. Nergaard, "A survey of ultra-high frequency measurements," *RCA Rev.*, vol. 3, pp. 156–195; October, (1938).

[5] This discrepancy between calculated and measured values may be attributed to experimental difficulty in measuring impedances of this magnitude, uncertainty as to the exact resistivity of the copper conductors, and possibly some residual line unbalance.

end impedance of the quarter-wave line, and θ represents the electrical length of the line. In this figure the solid line is obtained from (11). It will be observed that the experimental points are in close agreement with the theoretical curve, the greatest departure being of the order of 5 per cent. It is interesting to note that there is no indication of the optimum predicted by the previous theoretical results, shown by the dashed line.

We must conclude, therefore, that the short-line calculations based on previous theoretical formulas are in error, and that the theory presented in this paper is adequate for the design of transmission-line circuits.

Currents Induced by Electron Motion*

SIMON RAMO†, ASSOCIATE MEMBER, I.R.E.

Summary—*A method is given for computing the instantaneous current induced in neighboring conductors by a given specified motion of electrons. The method is based on the repeated use of a simple equation giving the current due to a single electron's movement and is believed to be simpler than methods previously described.*

Introduction

IN designing vacuum tubes in which electron transit-time is relatively long, it becomes necessary to discard the low-frequency concept that the instantaneous current taken by any electrode is proportional to the number of electrons received by

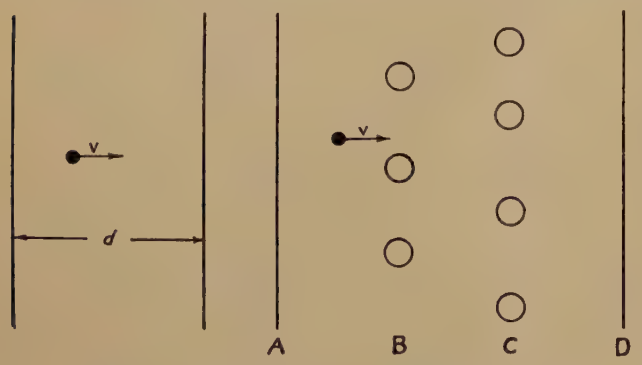

Fig. 1

Fig. 2

it per second. Negative grids, it is known, may carry current even though they collect no electrons and current may be noted in the circuit of a collector during the time the electron is still approaching the collector. A proper concept of current to an electrode must consider the instantaneous change of electrostatic flux lines which end on the electrode and the methods given in the literature for computing induced current due to electron flow are based on this concept.

A method of computing the induced current for a specified electron motion is here explained which is believed to be more direct and simpler than methods previously described. In the more difficult cases, in which flux plots or other tedious field-determination methods must be used, only one field plot is needed by the present method while the usual methods require a large number.

* Decimal classification: R138. Original manuscript received by the Institute, September 16, 1938.

† General Engineering Laboratory, General Electric Company, Schenectady, N. Y.

Method of Computation

The method is based on the following equation, whose derivation is given later:

$$i = E_v e v \tag{1}$$

where i is the instantaneous current received by the given electrode due to a single electron's motion, e is the charge on the electron, v is its instantaneous velocity, and E_v is the component in the direction v of that electric field which would exist at the electron's instantaneous position under the following circumstances: electron removed, given electrode raised to unit potential, all other conductors grounded. The equation involves the usual assumptions that induced currents due to magnetic effects are negligible and that the electrostatic field propagates instantaneously.

Simple Example

A simple example is offered in the computation of the instantaneous current due to an electron's motion between two infinite plates (Fig. 1). (The result is a starting point for the analysis of a diode, for example, when the transit-time is long.)

From (1) we obtain immediately

$$i = evE_v = \frac{ev}{d}.$$

In the literature[1] it is stated that this same result is deduced from image theory. This involves the setting up of an infinite series of image charges on each side of the plates for a given position of the electron and a consideration of the total flux crossing one of the planes due to the series of charges, a method which is lengthy and requires no little familiarity with methods of handling infinite series.

The General Case

Consider a number of electrodes, A, B, C, D, in the presence of a moving electron (Fig. 2) whose path and instantaneous velocity are known. A tedious way to find the current induced in, say, electrode

[1] D. O. North, "Analysis of the effects of space charge on grid impedance," PROC. I.R.E., vol. 24, pp. 108–158; February, (1936).

A is to make a flux plot of the lines of force emanating from the electron, when it is at some point of its path, and note the portion of the total lines which end on A. By making a number of such plots it is possible to observe the change in the number of lines ending on A as the electron moves, and consequently to compute the induced current. The accuracy is dependent upon the number of plots made.

It is much simpler to use (1). One plot is made for the case of A at unit potential, B, C, D grounded, and the electron removed, E_v is then known and

$$i = E_v e v.$$

To minimize the induced current in a negative grid, an important consideration in the design of high-frequency amplifiers and oscillators, it may be that (1) will prove helpful to the designer. The equation states that the electrode configuration should be such as to yield minimum E_v. If the electron's path, for example, is made to coincide with an equipotential of the grid (not an equipotential in the field in which the electron is traveling, of course, but an equipotential in that artificial field due to unit potential on the grid, the electron removed, and all else grounded) the induced current will be zero. It will not be possible to realize this for the complete electronic path, since the electron must start at some equipotential surface, but it may be possible to find practical configurations that will approach this condition over a good share of the path.

Derivation of Equation (1)

Consider the electron, of charge e, in the presence of any number of grounded conductors, for one of which, say A, the induced current is desired. Surround the electron with a tiny equipotential sphere. Then if V is the potential of the electrostatic field, in the region between conductors

$$\nabla^2 V = 0$$

where ∇^2 is the Laplacian operator. Call V_e the potential of the tiny sphere and note that $V=0$ on the conductors and

$$-\int_{\text{sphere's surface}} \frac{\partial V}{\partial n}\, ds = 4\pi e \qquad \text{(Gauss' law)}$$

where $\partial V/\partial n$ indicates differentiation with respect to the outward normal to the surface and the integral is taken over the surface of the sphere.

Now consider the same set of conductors with the electron removed, conductor A raised to unit potential, and the other conductors grounded. Call the potential of the field in this case V', so that $\nabla^2 V' = 0$ in the space between conductors, including the point where the electron was situated before. Call the new potential of this point V_e'.

Now Green's theorem[2] states that

$$\int_{\substack{\text{volume}\\ \text{between}\\ \text{boundaries}}} [V'\nabla^2 V - V\nabla^2 V']\, dv$$

$$= -\int_{\substack{\text{boundary}\\ \text{surfaces}}} \left[V' \frac{\partial V}{\partial n} - V \frac{\partial V'}{\partial n}\right] ds. \qquad (2)$$

Choose the volume to be that bounded by the conductors and the tiny sphere. Then the left-hand side is zero and the right-hand side may be divided into three integrals:

(1) Over the surfaces of all conductors except A. This integral is zero since $V = V' = 0$ on these surfaces.

(2) Over the surface of A. This reduces to $-\int_{\text{surface } A} (\partial V)/(\partial n)\, ds$, for $V' = 1$ and $V = 0$ for conductor A.

(3) Over the surface of the sphere. This becomes

$$-V_e' \int_{\text{sphere's surface}} \frac{\partial V}{\partial n}\, ds + V_e \int_{\text{sphere's surface}} \frac{\partial V'}{\partial n}\, ds.$$

The second of these integrals is zero by Gauss' law since $\int (\partial V')/(\partial n)\, ds$ is the negative of the charge enclosed (which was zero for the second case in which the electron was removed).

Finally, we obtain from (2)

$$0 = -\int_{\text{surface } A} \frac{\partial V}{\partial n}\, ds - V_e' \int_{\text{sphere's surface}} \frac{\partial V}{\partial n}\, ds$$

$$= 4\pi Q_A + 4\pi e V_e'$$

or

$$Q_A = -eV_e'$$

$$i_A = \frac{dQ_A}{dt} = -e\frac{dV_e'}{dt} = -e\left[\frac{\partial V_e'}{\partial x}\frac{dx}{dt}\right]$$

where x is the direction of motion.

Now

$$\frac{dx}{dt} = v \quad \text{and} \quad \frac{\partial V_e'}{\partial x} = -E_v,$$

so

$$i = evE_v. \qquad (1)$$

[2] J. H. Jeans, "Electricity and Magnetism," page 160, Cambridge, London, England, (1927).

Space-Charge Effects in Electron Beams*

ANDREW V. HAEFF†, ASSOCIATE MEMBER, I.R.E.

Summary—*The effects of space charge in long, magnetically focused electron beams directed parallel to positively charged sheath electrodes are determined from a simple analysis. The main effects of space charge are: (a) to introduce departure from the potential distribution of the electrostatic case; (b) to set an upper limit for the beam current; and (c) to introduce instabilities and hysteresis phenomena in the behavior of the tube. It is shown that in a long beam the longitudinal potential gradient is negligible throughout the major portion of the beam length so that the upper limit for beam current is independent of beam length and of potentials of end electrodes, but depends only upon the relative transverse dimensions of the beam and of the surrounding sheath electrode and upon the sheath-electrode potential. The analysis gives expressions for maximum beam current, for space-potential distribution and for the minimum value of the focusing magnetic field, in terms of the beam and sheath-electrode dimensions and the sheath-electrode potential.*

The use of multicellular sheath electrodes to minimize the effects of space charge is discussed. Thin "sheet" beams and "thin-walled" tubular beams are treated separately by a simplified "capacitance" method and expressions for maximum current, space potential, and for minimum-focusing magnetic field are derived.

The effect of space-charge interaction between multiple beams inside a common sheath electrode is considered and a method of control of current in one beam by the current in the adjacent beam is analyzed and also illustrated by experimental data. The effect of modulation of sheath-electrode voltage on the space potential for constant beam current, and the effect of beam-current modulation on the space potential, are discussed.

Application of the theory to the cases of beams focused electrostatically is discussed. The experimentally found characteristics of tubes utilizing long magnetically focused electron beams are presented and compared to those predicted by the theory and a satisfactory agreement is demonstrated.

I. Introduction

ONLY comparatively recently have high-current, low-voltage electron-beam devices received the attention of workers in the field of electronics.[1-4] The unique possibilities offered by beam tubes, such as currentless control and screen grids at positive potentials, currentless positive output electrodes, and many others, are so attractive as to deserve this attention. However, the designer of such tubes is greatly handicapped by the lack of information concerning the formation of beams either by magnetic or electric fields when the space charge is appreciable. Several papers on the effect of space charge on the beam focus in high-voltage cathode-ray tubes have appeared in the literature,[5,6] but the results of these investigations are of a rather limited application in the low-voltage, high-current electron-beam tubes. Although a recent paper[7] deals with high-current, low-voltage electron beams, it does not fully take into account the effect of lowering of space potential by space charge.

It is the purpose of this paper to present the results of a theoretical and experimental analysis of the effects of space charge in long, magnetically focused electron beams. It is hoped that this attempt will stimulate other workers to apply the analytical method to the solution of many important problems involving the space-charge effects in practical tube structures.

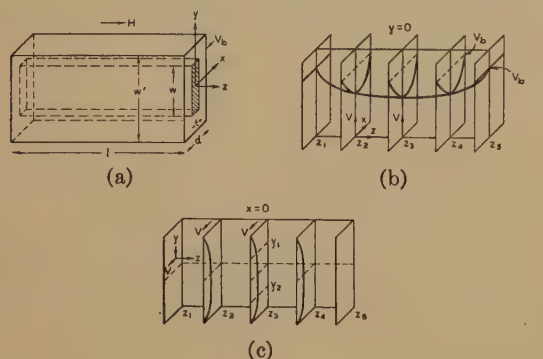

Fig. 1

(a) Electron beam of rectangular cross-section $w \cdot t$, flowing in the direction z inside a rectangular sheath electrode of cross section $w' \cdot d$.
(b) Potential distributions in x, y, and z, y planes for $y=0$.
(c) Potential distribution in x, y planes for $x=0$.

* Decimal classification: R138. Original manuscript received by the Institute, September 6, 1938; abridgement received by the Institute, July 27, 1939.

†RCA Manufacturing Company, Inc., RCA Radiotron Division, Harrison, N. J.

[1] H. C. Thompson, "Electron beams and their applications in low-voltage devices," PROC. I.R.E., vol. 24, pp. 1276–1297; October, (1936).

[2] H. Rothe and W. Kleen, "The importance of electron optics in the technique of amplifying valves," *Zeit. für tech. phys.*, vol. 17, no. 12, pp. 635–542, (1936).

[3] K. Okabe, "A new electron oscillator," *Report of Radio Research in Japan*, vol. 6, pp. 69–74; August, (1936).

[4] T. V. Ionescu, "Short-wave oscillator," *Comptes Rendus*, vol. 204, pp. 1411–1413; May, (1937).

II. Theory of Rectangular Beams

Potential Distribution and Maximum Current in the Beam

Consider a rectangular electron beam of cross section (wt) (see Fig. 1(a)), flowing in the direction z parallel to a focusing magnetic field H inside a long rectangular box of length l, width w', and opening d, held at a potential V_b. Due to space charge, the space potential inside the box is not uniform, but assumes a distribution illustrated in Figs. 1(b) and 1(c). These show that the potential decreases from the sides towards the center of the box. If the length l of the box is large compared to the dimension d, then the electric gradient in the z direction will be practically zero throughout a large portion of the box (between the planes z_2 and z_4) because the sides of the box shield the inside from the effect of potentials on the ends (at planes z_1 and z_5) which, in practice, may be some gridlike structures. Also, if the dimension w is large compared to the dimension d, the electric gradient in the y direction will be very small (say, between the planes y_1 and y_2). Therefore, if we confine our attention to the center portion of the

[5] E. E. Watson, "Dispersion of an electron beam," *Phil. Mag.*, 7th series, vol. 3, pp. 849–853; April, (1927).

[6] M. Cotte, "Calculation of the influence of space charge in electron optics," *Comptes Rendus*, vol. 204, pp. 1933–1935; June 28, (1937).

[7] B. J. Thompson and L. B. Headrick, "Space-charge limitations on the focus of electron beams," Presented, Rochester Fall Meeting, Rochester, N. Y., November 9, 1937.

beam, we can put $\partial V/\partial y = \partial V/\partial z = 0$. Thus, the Poisson equation reduces to the one-dimensional form

$$\frac{d^2V}{dx^2} = -4\pi\rho \tag{1}$$

Fig. 2 illustrates the potential distribution along a line y = constant, z = constant.

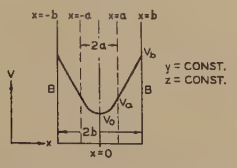

Fig. 2—Potential distribution in x, y plane for z = constant, y = constant.

The potential gradient in the direction x tends to move the electrons towards the sides of the box. We shall assume, however, that the focusing uniform magnetic field H, in the z direction, is so strong that the electrons are constrained to move only in the z direction, or, in other words, the displacement of electrons in the x, y plane is negligible in comparison with the dimension d. We shall also assume that the current density i_0 is uniform throughout the cross section of the beam. This corresponds to the case when the current originates at the cathode and the electrons are accelerated by a uniform field of the control grid. In the following, we also assume that the emission velocities are negligible.

The space-charge density ρ_x at a distance x from the origin can be calculated from the equation of continuity

$$-\rho_x v_x = i_0. \tag{2}$$

The electron velocity v_x is related to the potential of the space as follows:

$$v_x = \sqrt{\frac{2e}{m}}\, V_x^{1/2}. \tag{3}$$

Because the electrons originate from a cathode at zero potential and the electric fields are static, the electrons at x have the velocity corresponding to the potential V_x.

Making use of (2) and (3), we obtain

$$\frac{d^2V_x}{dx^2} = -4\pi\rho_x = 4\pi\frac{i_0}{\sqrt{\frac{2e}{m}}\, V_x^{1/2}}. \tag{4}$$

On making use of the symmetry condition $(dV/dx)_{x=0} = 0$ to determine the constant of integration, we obtain from the first integration of (4)

$$\left(\frac{dV}{dx}\right)^2 = ki_0(V^{1/2} - V_0^{1/2}) \tag{5}$$

where $k = 16\pi(2e/m)^{-1/2}$ and V_0 is the value of the potential minimum. The second integration gives

$$4/3(V^{1/2} - V_0^{1/2})^{1/2}(V^{1/2} + 2V_0^{1/2}) = \pm (ki_0)^{1/2}x. \tag{6}$$

This equation gives the potential V at any point x within the boundaries of the beam.

On letting $V = V_a$ = potential at the edge of the beam ($x = \pm a$), and putting $(V_0/V_a)^{1/2} = p$ = ratio of minimum to maximum electron velocity in the beam, we obtain

$$(1-p)^{1/2}(1+2p) = \pm 3/4(ki_0)^{1/2}V_a^{-3/4}a. \tag{7}$$

In the region $x = a$ to $x = b$ between the edges of the beam and the walls of the box there is no space

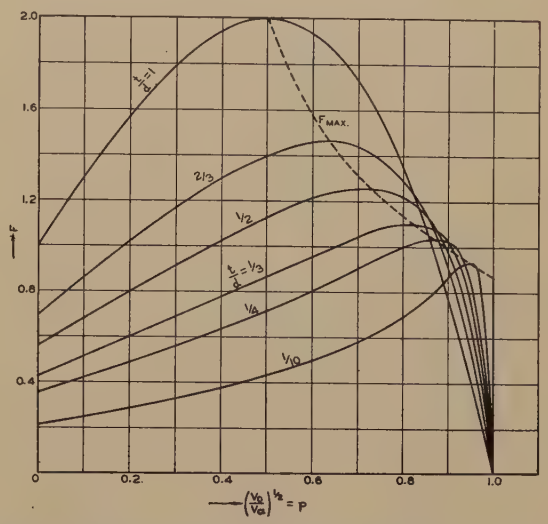

Fig. 3—Variation of function F with the ratio $p = (V_0/V_a)^{1/2}$ for different values of the ratio of beam thickness t to the opening d of the sheath electrode.

charge, so that the potential gradient must remain constant. Furthermore, since at $x = \pm a$ the space-charge density is finite, there is no change in the potential gradient at $x = a$. Therefore,

$$\left(\frac{dV}{dx}\right)^2_{x=a} = ki_0(V_a^{1/2} - V_0^{1/2}) = \left(\frac{V_b - V_a}{b-a}\right)^2. \tag{8}$$

Putting

$d = 2b$ = spacing between the electrodes B-B,
$t = 2a$ = total thickness of the beam, and
$I_0 = ti_0$ = beam current per unit width

we can rewrite (8) and (7) in terms of the known quantities V_b, d, t, and I_0 and of the unknown ratio p as follows:

$$\frac{9}{64}\frac{kI_0}{V_b^{3/2}}d = \frac{d/t(1-p)(1+2p)^2}{\{1+4/3(d/t-1)(1-p)(1+2p)\}^{3/2}} = F(p, t/d) \tag{9}$$

$$\frac{V_b}{V_a} = 1+4/3(d/t-1)(1-p)(1+2p) = G(p, t/d). \tag{10}$$

The functions F and G are plotted against $p = (V_0/V_a)^{1/2}$ for different values of the parameter t/d in Figs. 3 and 4. Starting at $p = 1$, we find that the function F increases rapidly from zero as p decreases,

reaches a maximum, and then decreases slowly on the left-hand side of the diagram. The dotted line in Fig. 3 connects the points of maximum of the function F. The region to the right of this line represents stable conditions: a decrease in potential V_0 corresponds to an increase in beam current. If the current exceeds the maximum value, the conditions in the beam become unstable since a decrease in potential V_0 now corresponds to a decrease in beam current. The potential in the center of the beam must drop to zero suddenly and some electrons must be turned back in the direction of the cathode. Thus, F_{max} corresponds to the maximum current which can be passed between the plates at potential V_b, where the plates are spaced at a distance d, and the beam has a thickness t.

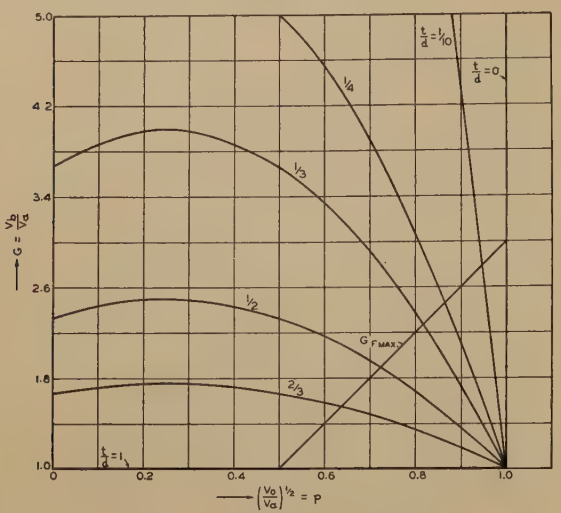

Fig. 4—Variation of function $G=V_b/V_a$ with $p=(V_0/V_a)^{1/2}$ for different values of the parameter t/d.

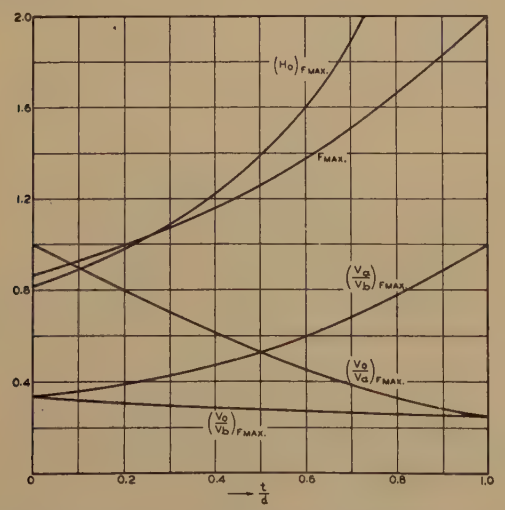

Fig. 5—Variation of the coefficient F_{max} with the ratio t/d (to be used in (15) for calculating maximum current), and of functions H_0, V_a/V_b, V_0/V_b, V_0/V_a for the condition of maximum current.

The value of F_{max} can be found analytically by putting

$$\frac{\partial F}{\partial p}=0. \tag{11}$$

This equation gives a condition for the maximum current

$$\frac{d}{t}-1=\frac{3}{2}\cdot\frac{2p-1}{(1-p)(1+2p)}. \tag{12}$$

Upon substitution of (12) into (9), we find

$$F_{max}=\frac{(1-p)(1+2p)^2+\frac{3}{2}(2p-1)(1+2p)}{(4p-1)^{3/2}} \tag{13}$$

$$(G)_{F_{max}}=4p-1 \tag{14}$$

where p is related to d/t by (12). In Fig. 5 the value of F_{max} is plotted against the ratio t/d, so that if V_b, t, d, and w are known, the maximum current can be easily calculated from the relation

$$I_{max}=9.35\times10^{-6}V_b^{3/2}(w/d)F_{max} \tag{15}$$

where V_b is expressed in volts; $I_{max}=(I_0)_{max}\cdot w=$ total beam current in amperes; and the value of F_{max} is obtained from Fig. 5.

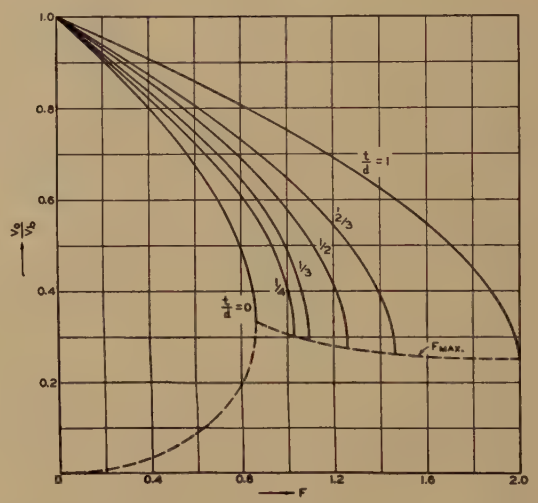

Fig. 6—The variation of the minimum space potential (V_0) with the generalized current F (equation (16)) for different values of t/d.

The value of F_{max} varies between the limits $F_{max}=2$ for $t/d=1$ and $F_{max}=\sqrt{3}/2=0.866$ for $t/d\rightarrow0$. In Fig. 5 there are also shown the values of the ratios $(V_0/V_b)_{F_{max}}$ and $(V_a/V_b)_{F_{max}}$ which permit an easy estimate of the potential distribution in the beam, and the ratio $(V_0/V_a)_{F_{max}}$ which gives the square of the ratio of minimum to maximum electron velocity in the beam.

Since it is also of interest to know the conditions in the beam for currents less than the maximum current, the values of the potential ratios V_0/V_b and V_a/V_b are shown plotted against F for different ratios of (t/d) as parameters in Figs. 6 and 7. When the total beam current I, the sheath electrode voltage V_b, and the dimensions t, d, and w, are known, the value of the function F can be calculated from the relation

$$F = 0.107 \times 10^6 \frac{I}{V_b^{3/2}\left(\frac{w}{d}\right)}. \qquad (16)$$

The potential minimum V_0 and the potential at the edge of the beam V_a can be read then from Figs. 6 and 7.

Calculation of the Minimum Value of the Focusing Magnetic Field

Negligible Initial Transverse Velocity

The foregoing analysis of the space-charge effects in electron beams is strictly correct only under the assumption of a focusing magnetic field of infinite magnitude. In any practical case, however, it is desirable to know what the permissible minimum value of the magnetic field should be so that the results of the above analysis could be utilized as a good approximation to the actual state of affairs. To answer this question we must examine the motions of electrons under the combined actions of the electric and magnetic fields. As a practically convenient term we will define as the minimum focusing magnetic field that field which is just sufficient to prevent any of the electrons in the beam from striking the sheath electrode.

In Fig. 8, it will be seen that those electrons which are on the edge of the beam are subject to the greatest electrical force in the transverse direction. Thus, if these outer electrons are prevented by the magnetic field from reaching the plates B-B no other electrons can do so, and, therefore, no current can flow to the sheath electrode. It has been pointed out by Hull[8] that the value of the critical magnetic field is independent of space-charge conditions and is only a function of electrode potentials, spacing, and initial electron velocities. If we assume that the initial velocity is zero and that the effect of space charge due to electrons performing excursions from the beam towards the sheath electrodes is negligible, then the projection of the electron path on the x, y plane will be a cycloid since the electric field in the region $x=a$ to $x=b$ is assumed uniform. For the condition of zero sheath current, the maximum distance x_m that an electron may travel without striking the plates B-B should be smaller than the clearance between the beam and the electrode; i.e.,

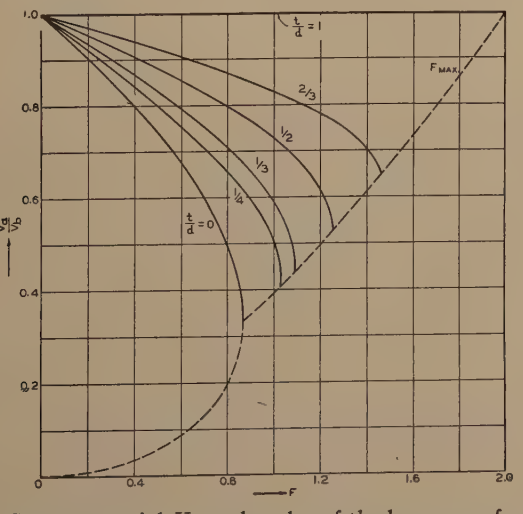

Fig. 7—Space potential V_a at the edge of the beam as a function of generalized current F for different values of t/d.

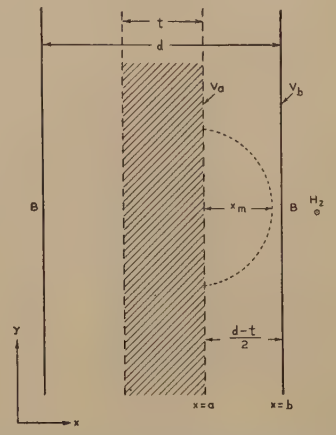

Fig. 8—Projection on x, y plane of the path of the outer electrons moving under the influence of the electric field $E_x=(V_b-V_a)/((d-t)/2)$ and the magnetic field $H=H_z$.

$$x_m < (d-t)/2. \qquad (17)$$

The solution of the equation of motion of an electron in a uniform electric field E_x and a uniform magnetic field H gives the following relations:

$$x = -\frac{E_x}{\omega H}(\cos \omega\tau - 1)$$

$$y = -\frac{E_x}{\omega H}(\sin \omega\tau - \omega\tau) \qquad (18)$$

$$z = v_z \cdot \tau$$

where

$E_x=(V_b-V_a)/\frac{1}{2}(d-t)$ electric field in volts per centimeter

$H=$ focusing field in webers[9] per centimeter square

$\omega=(e/m)H$

$e/m=0.18\times10^{16}$ in coulombs per gram-seventh[10]

$\tau=$ time of electron flight in seconds

$v_z=$ constant electron velocity in the z direction, and

$(v_x)_0=(v_y)_0=0$.

The maximum distance that an electron may travel in the x direction is

$$x_m = 2\frac{E_x}{\omega H} = \frac{4(V_b - V_a)}{(d-t)\frac{e}{m}H^2} < \frac{d-t}{2}. \qquad (19)$$

[8] A. W. Hull, "The effect of a uniform magnetic field on the motion of electrons between coaxial cylinders," *Phys. Rev.*, vol. 18, pp. 31–57; July, (1921).

[9] Webers per centimeter square $=10^8$ gausses.

[10] Gram-seventh $=10^{-7}$ grams.

Hence,

$$H > \frac{2\sqrt{2}}{\sqrt{\frac{e}{m}}} \cdot \frac{V_b^{1/2}}{d} \cdot \frac{\left(1 - \frac{V_a}{V_b}\right)^{1/2}}{\left(1 - \frac{t}{d}\right)} \tag{20}$$

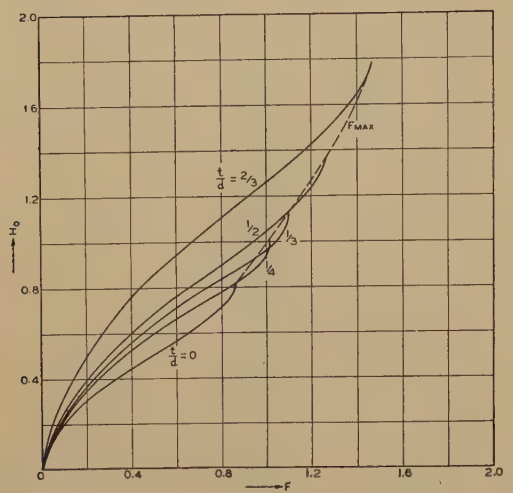

Fig. 9—Variation of the coefficient H_0 (equation (21)) with F (equation (16)) for different values of t/d.

or, in practical units, expressing H in gauss and putting $e/m = 0.18 \times 10^{16}$, we find

$$H > 6.72 \frac{V_b^{1/2}\,(\text{volts})^{1/2}}{d\,(\text{cm})} \cdot \frac{\left(1 - \frac{V_a}{V_b}\right)^{1/2}}{\left(1 - \frac{t}{d}\right)}$$

$$= 6.72 \frac{V_b^{1/2}}{d} \cdot H_0 \tag{21}$$

where

$$H_0 = \frac{\left(1 - \frac{V_a}{V_b}\right)^{1/2}}{1 - \frac{t}{d}}$$

is a dimensionless quantity which depends upon the space-charge conditions (V_a/V_b) in the beam, and upon the beam dimensions (t/d). For convenience in calculating the value of the minimum magnetic focusing field the value of the coefficient H_0 is given in Fig. 5 directly as a function of the ratio t/d, for the condition of maximum current in the beam.

The value of H_0 for currents less than the maximum current has also been calculated and is shown as a function of the dimensionless quantity F in Fig. 9. An increase in beam current (proportional to F) requires an increase in the focusing field. As the clearance between the beam and the sheath electrode becomes small, that is, when the ratio t/d approaches unity, the function H_0 approaches infinity; a very large field is required to prevent the flow of current to the sheath electrode.

Effect of Initial Transverse Velocity

The expression for the minimum focusing field was derived under the assumption that the electrons in the beam entering the sheath electrode move parallel to the field. However, in many practical cases it may happen that because of the nonuniform electric field at the entrance to the sheath electrode, the electrons have an initial transverse velocity. This condition is illustrated in Fig. 10 where the electrons from a cathode are accelerated by two positive slit grids and form a crossover at a point 0. If we denote by γ the half angle of beam divergence, and by v_0

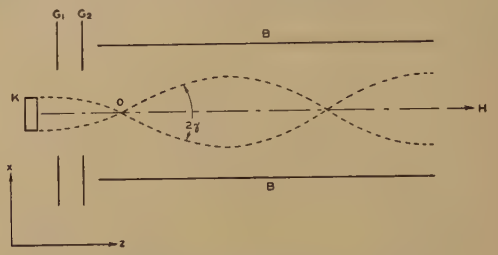

Fig. 10—Diverging beam entering the sheath electrode with a transverse velocity $v_t = v_0 \sin \gamma$.

the total velocity corresponding to the space potential at 0, then the initial transverse velocity can be expressed as

$$v_t = v_0 \sin \gamma. \tag{22}$$

Because of this initial transverse velocity, the electrons approach closer to the plates B-B. Our estimate of the minimum magnetic field was obtained under the assumption that $v_t = 0$. We shall now find how much the field must be increased if the transverse velocity is not negligible.

When the initial velocity is taken into account, the equation of motion of the outer electrons becomes

$$x = \frac{v_t}{\omega} \sin \omega t - \frac{E_x}{\omega H_1} (\cos \omega t - 1) \tag{23}$$

where the notation is similar to that used in (18). Solving for the maximum deflection of electrons and comparing it to the clearance between the beam and the sheath electrode, we obtain the following inequality:

$$x_{\max} = \frac{E_x}{\frac{e}{m} H_1^2} \left\{ 1 + \left[1 + \left(\frac{v_t H_1}{E_x} \right)^2 \right]^{1/2} \right\} < \frac{d - t}{2}. \tag{24}$$

The solution of (24) gives the following value for the minimum magnetic field:

$$H_1 > H \left[1 + \frac{v_t^2}{2E_x \left(\frac{d - t}{2} \right) \frac{e}{m}} \right]^{1/2} \tag{25}$$

where

$$H = \sqrt{\frac{2E_x}{\frac{d - t}{2} \left(\frac{e}{m} \right)}}$$

is the value of the field when $v_t=0$. If we make the following substitutions:

$$v_t = v_0 \sin\gamma = \sqrt{2\frac{e}{m}}\sqrt{V_a}\sin\gamma$$

$$E_x = \frac{V_b - V_a}{\frac{1}{2}(d-t)}$$

we obtain the following simple expression for the correction coefficient H_1/H:

$$\frac{H_1}{H} = \left[1 + \frac{\sin^2\gamma}{\left(\frac{V_b}{V_a} - 1\right)}\right]^{1/2}. \qquad (26)$$

The correction ratio H_1/H is shown in Fig. 11, plotted against the voltage ratio V_a/V_b, for different values of the half angle of beam divergence γ. The correction becomes appreciable for large values of the angle of divergence and for currents smaller than the maximum current, when the ratio V_a/V_b approaches unity.

III. Multicellular Sheath Electrodes

In the design of beam tubes a practical problem of the following sort may arise. If the total cross section of the sheath electrode is given, is it advantageous

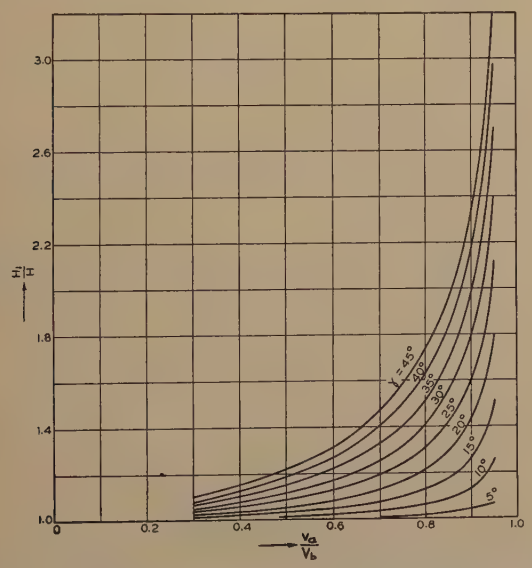

Fig. 11—The value of the correction coefficient H_1/H (equation (26)) for different space-charge condition V_a/V_b and for different values of the angle of divergence (2γ).

to subdivide it into small cells and pass a fraction of the total beam current through each cell? From the standpoint of the total current that can be passed at a given voltage, the answer is affirmative. Indeed, if the cross section is subdivided into n equal cells the maximum current will be

$$I_{max}' = n\cdot 9.35\times10^{-6}\, V_b^{3/2}\frac{w}{\left(\frac{d}{n}\right)} F_{max} = n^2 I_{max}; \qquad (27)$$

i.e., the maximum current is proportional to the square of the number of cells. However, because of the closer spacing between the beam and the sheath electrode the required focusing magnetic field must also be higher; namely,

$$H' = 6.72 V_b^{1/2} H_0 \frac{1}{\left(\frac{d}{n}\right)} = n\cdot H; \qquad (28)$$

i.e., the magnetic field is proportional to the number of cells.

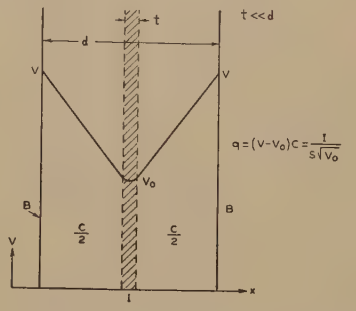

Fig. 12—Potential distribution in x, y plane for the case of a thin beam ($t/d \ll 1$).

If the total current to be passed in the multicellular electrode should be the same as in one large cell, then the required magnetic field must be approximately the same, because

$$\frac{H'}{H} \approx \frac{I}{I_{max}}\cdot\frac{d}{\left(\frac{d}{n}\right)} = \frac{1}{n}\cdot n = 1. \qquad (29)$$

Thus, there is no advantage in using a multicellular electrode in this case; unless it is desirable to minimize the effects of space charge.

IV. Thin Electron Beams

We shall define as a thin electron beam such a beam in which one of the transverse dimensions (the thickness t) is small in comparison with the opening of the sheath electrode (dimension d in Fig. 12). One of the important characteristics of a thin beam is that all electrons in the beam have approximately the same velocity. This is illustrated in Fig. 5 by the curve of V_0/V_a which approaches unity when the beam becomes thin (t/d approaches zero). This characteristic makes possible considerable simplification in the treatment of thin beams.

From the previous analysis it was found that for a limiting case of a thin beam, when t/d approaches zero, the expression for maximum current in the beam becomes

$$(I_{max})_{t/d\to 0} = 9.35\times10^{-6}\, V_b^{3/2} w/d\sqrt{3}/2. \qquad (30)$$

An identical result for this case can be obtained by

the following simple method.[11] The charge contained in one centimeter length of a thin beam is

$$q = \frac{I}{S\sqrt{V_0}} \tag{31}$$

where I is the total current in the beam, and $S\sqrt{V_0}$ is the electron velocity in centimeters per second cor-

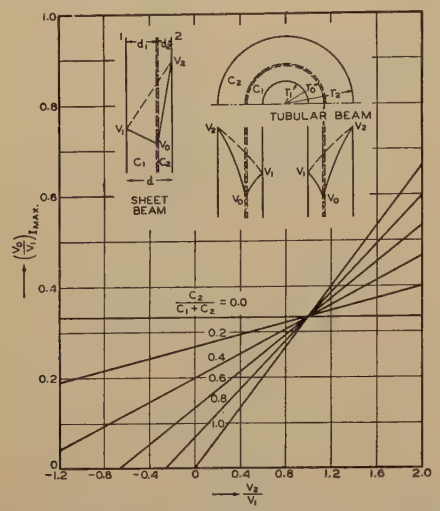

Fig. 13—The value of space potential (V_0) in a thin beam for a condition of maximum current for different values of V_2/V_1 and of the parameter $C_2/(C_1+C_2)$.

responding to the space potential V_0, at the beam. This charge induces an equal charge on the plates B-B, Fig. 12, equal to

$$q = C(V - V_0) \tag{32}$$

where C is the capacitance between the beam and the sheath electrode per centimeter length of the beam and V is the potential of the sheath electrode. Combining (31) and (32), we obtain

$$\frac{I}{SCV^{3/2}} = \left(1 - \frac{V_0}{V}\right)\left(\frac{V_0}{V}\right)^{1/2}. \tag{33}$$

The condition for maximum current, $dI/dV_0 = 0$, gives

$$V_0/V = 1/3. \tag{34}$$

Using this result, and putting into (33) the value of $S = 5.95 \times 10^7$, and the value of the capacitance $C = 4 \times 8.84 \times 10^{-14} w/d$, we obtain

$$I_{\max} = 8.10 \times 10^{-6}\, V^{3/2} w/d. \tag{35}$$

This is the same result as was obtained previously from a more general analysis.

This method for thin beams, which we will call the "capacitance method," gives a sufficiently good approximation in many practical cases. Because of its simplicity, the capacitance method readily yields solutions where a more general treatment of beams of finite thickness becomes too involved. The cases of asymmetrical beams and multiple beams with arbitrary current distribution can, thus, be treated. The capacitance method can be used in all cases where the capacitance between the beam and the sheath electrodes and between the adjacent beams can be calculated, with the limitation that the current distribution along the cross section of the beam must be the same as the surface charge distribution obtained by replacing the beam by a conductor of the same dimensions.

[11] The credit for the first use of this method should be given to Dr. L. S. Nergaard of this laboratory, who employed it in considering possible errors in the measurement of ionization potentials during his research work in 1931 at the University of Minnesota.

Single Thin Beam Between Electrodes Held at Different Potentials

The following analysis is applicable either to the case of a thin "sheet" beam between two infinite planes, or to the case of a "thin-walled" tubular beam between two coaxial cylinders, the sheath electrodes being held at different potentials, one of which can be negative.

Space Potential and Maximum Current

Using the capacitance method, we write that the charge in the beam is equal to the charge induced on the sheath electrodes

$$I/SV_0^{1/2} = C_1(V_1 - V_0) + C_2(V_2 - V_0) \tag{36}$$

where

I = total current in the beam in amperes
$S = 5.95 \times 10^7$
V_0 = space potential in volts at the beam
V_1 and V_2 = voltages, in volts, applied to the sheath electrodes
C_1 and C_2 = capacitances, in farads, of the beam to the sheath electrodes 1 and 2, respectively.

To find the condition for maximum current, we put $dI/dV_0 = 0$, with the result

$$\left(\frac{V_0}{V_1}\right)_{I\max} = \frac{1}{3}\left[1 - \left(1 - \frac{V_2}{V_1}\right)\frac{C_2}{C_1+C_2}\right]. \tag{37}$$

The value of $(V_0/V_1)_{I\max}$ is shown in Fig. 13, and is plotted against the ratio V_2/V_1 for different values of $C_2/(C_1+C_2)$ as a parameter, which become

$$\frac{C_2}{C_1+C_2} = \frac{d}{d_1} \quad \text{for the parallel-plane case, and}$$

$$\frac{C_2}{C_1+C_2} = \frac{\ln \frac{r_0}{r_1}}{\ln \frac{r_2}{r_1}} \quad \text{for the cylindrical case.}$$

The value of maximum current can now be calculated if the value of $(V_0/V_1)_{I\max}$ is substituted in (36), which can be rewritten as follows:

$$\frac{9}{4}\frac{I}{S(C_1+C_2)V_1^{3/2}} = F$$

$$= \frac{9}{4}\left[1 - \frac{C_2}{C_1+C_2}\left(1-\frac{V_2}{V_1}\right) - \frac{V_0}{V_1}\right]\left(\frac{V_0}{V_1}\right)^{1/2}$$

$$= \frac{9}{4}\left[3\left(\frac{V_0}{V_1}\right)_{I_{max}} - \frac{V_0}{V_1}\right]\left(\frac{V_0}{V_1}\right)^{1/2} \quad (38)$$

and, thus, for the condition of maximum current

$$\frac{9}{4}\frac{I_{max}}{S(C_1+C_2)V_1^{3/2}} = F_{max} = \frac{9}{2}\left(\frac{V_0}{V_1}\right)^{3/2}_{I_{max}}. \quad (39)$$

The value of F_{max} is plotted in Fig. 14 against the ratio V_2/V_1 for different values of $C_2/(C_1+C_2)$. The plot extends into the negative region of V_2/V_1 because even when one of the sheath electrodes is at a negative potential the space potential at the beam may be positive and a finite current may flow. Thus the expressions for the maximum current are for the parallel-plane case

$$I_{max} = 2.34\times10^{-6}\frac{w}{d}\left(\frac{d}{d_1}\right)\left(\frac{d}{d_2}\right)V_1^{3/2}\cdot F_{max} \quad (40)$$

and for the cylindrical case

$$I_{max} = 14.7\times10^{-6}\frac{\log\frac{r_2}{r_1}}{\log\frac{r_2}{r_0}\log\frac{r_0}{r_1}}V_1^{3/2}\cdot F_{max}. \quad (41)$$

For the limiting case when one of the sheath electrodes is at infinity, or is not present (in the

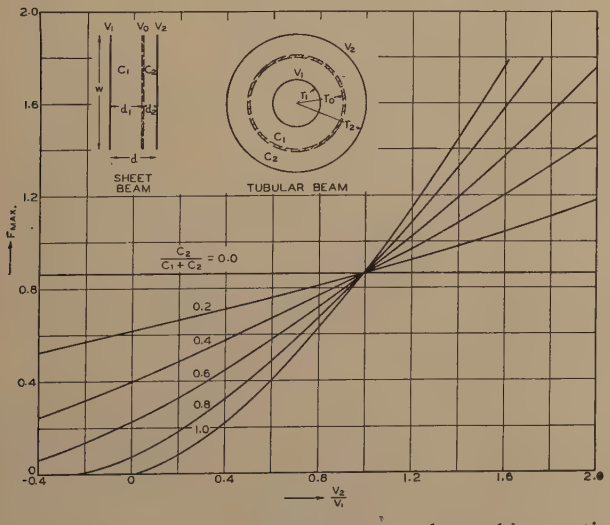

Fig. 14—The value of the coefficient F_{max} to be used in equations (40) and (41) for calculating maximum current.

cylindrical case this is equivalent to either putting $r_2=\infty$, or $r_1=0$), the equations reduce to the following form for parallel planes, when $d_2=\infty$

$$I_{max} = (0.866)2.34\times10^{-6}\frac{w}{d_1}V_1^{3/2} \quad (42)$$

and for the cylindrical case, when $r_2=\infty$

$$I_{max} = (0.866)14.7\times10^{-6}\frac{1}{\log\frac{r_0}{r_1}}V_1^{3/2} \quad (43)$$

and when $r_1=0$

$$I_{max} = (0.866)14.7\times10^{-6}\frac{1}{\log\frac{r_2}{r_0}}V_2^{3/2}. \quad (44)$$

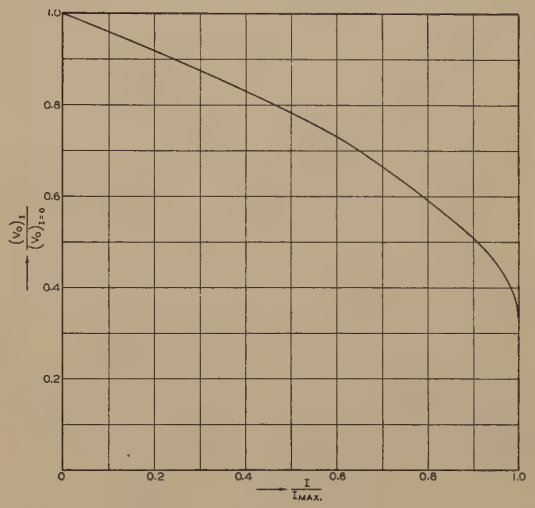

Fig. 15—The variation of space potential at the beam with increase in beam current (for thin beams).

In practical cases it may be of interest to know the value of the space potential in the beam for currents less than the maximum current, for the purpose, say, of calculating electron velocity. This can readily be determined by combining (38) and (39), in the following manner:

$$\frac{I}{I_{max}} = \frac{F}{F_{max}} = \frac{1}{2}\left[3 - \frac{\left(\frac{V_0}{V_1}\right)}{\left(\frac{V_0}{V_1}\right)_{I_{max}}}\right]\left[\frac{\left(\frac{V_0}{V_1}\right)}{\left(\frac{V_0}{V_1}\right)_{I_{max}}}\right]^{1/2}. \quad (45)$$

From this relationship we see that for $I/I_{max}=0$, the ratio V_0/V_1 becomes

$$\left(\frac{V_0}{V_1}\right)_{I_{max}} = \frac{1}{3}\left(\frac{V_0}{V_1}\right)_{I=0}. \quad (46)$$

This is a very interesting result; namely, that when the current in the beam is increased to its maximum value, the space potential at the beam will decrease to one third of its original value (i.e., for the condition when no current flowed). Making use of this generalization, we can write (45) as follows:

$$\frac{I}{I_{max}} = \frac{3\sqrt{3}}{2}\left[1 - \frac{(V_0)_I}{(V_0)_{I=0}}\right]\left[\frac{(V_0)_I}{(V_0)_{I=0}}\right]^{1/2}. \quad (47)$$

This relation is plotted in Fig. 15. If I/I_{max} is known, the space potential can then be found from this fig-

ure, where it is expressed in terms of the space potential at the beam when $I=0$.

Focusing Magnetic Field

Following the same reasoning as used in the discussion of beams of finite thickness, we obtain the following expressions for the minimum magnetic

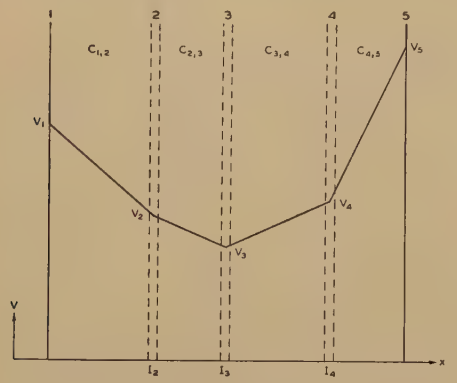

Fig. 16—Potential distribution in case of multiple thin beams.

focusing field,[8] assuming that the initial transverse velocities of electrons are negligible:

(a) For the parallel-plane case,

$$\left.\begin{aligned} H &> 3.36\frac{V_1^{3/2}}{d_1}\left(1-\frac{V_0}{V_1}\right)^{1/2} \\ \text{or} \\ H &> 3.36\frac{V_2^{3/2}}{d_2}\left(1-\frac{V_0}{V_2}\right)^{1/2} \end{aligned}\right\}. \qquad (48)$$

(b) For the cylindrical case,

$$\left.\begin{aligned} H &> 6.72\frac{V_2^{1/2}\left(1-\dfrac{V_0}{V_2}\right)^{1/2}}{r_2\left(1-\dfrac{r_0^2}{r_2^2}\right)} \\ \text{or} \\ H &> 6.72\frac{V_1^{1/2}\left(1-\dfrac{V_0}{V_1}\right)^{1/2}}{r_1\left(\dfrac{r_0^2}{r_1^2}-1\right)} \end{aligned}\right\}. \qquad (49)$$

Two limits are given because electrons may arrive first either at one or the other of the sheath electrodes, depending upon the applied potentials V_1 and V_2, and the relative position of the beam. These expressions show that when the beam is very close to the sheath electrode, a very high magnetic field is required to prevent the current flow to that electrode. So, that even though a close spacing of the beam is desirable to obtain high beam current at low voltages, the magnetic field required for focusing may be prohibitively large.

V. Multiple Thin Beams

We shall indicate here a general method that can be used for solving the case of multiple thin beams. Suppose we have three beams, as shown in Fig. 16, having currents I_2, I_3, I_4, flowing parallel to the electrodes 1 and 5, held at potentials V_1 and V_5, respectively. Using the capacitance method we may write the following relations:

$$\left.\begin{aligned} I_2/SV_2^{1/2} &= C_{1,2}(V_1-V_2)+C_{2,3}(V_3-V_2) \\ I_3/SV_3^{1/2} &= C_{2,3}(V_2-V_3)+C_{3,4}(V_4-V_3) \\ I_4/SV_4^{1/2} &= C_{3,4}(V_3-V_4)+C_{4,5}(V_5-V_4) \end{aligned}\right\}. \qquad (50)$$

For the three unknowns, V_2, V_3, and V_4, the above three equations are sufficient, and thus, the potential distribution could be determined. (This method can be extended to any number of beams.) However, since these equations are cubics, it is necessary to apply special methods for their solution. Because of the complexity, no attempt was made to find the general solutions. For the purpose of demonstrating the usefulness of the capacitance method for multiple thin beams, the solution for two symmetrically spaced thin beams has been obtained and is presented below.

Two Thin Beams in a Common Sheath Electrode

If we denote by I_1 and I_2 the currents in beams 1 and 2, respectively (see Fig. 17), V_1 and V_2 the corresponding space potentials, V the potential of a common sheath electrode, C_1 and C_2 the capacitances of the respective beams to the sheath electrode, and C_{12} the mutual capacitance between the beams, we can write the following equations:

$$\frac{I_1}{SV_1^{1/2}} = C_1(V-V_1)+C_{12}(V_2-V_1) \qquad (51)$$

$$\frac{I_2}{SV_2^{1/2}} = C_2(V-V_2)+C_{12}(V_1-V_2) \qquad (52)$$

or

$$\frac{I_1}{C_1SV^{3/2}} = \left(1-\frac{V_1}{V}\right)\left(\frac{V_1}{V}\right)^{1/2} + \frac{C_{12}}{C_1}\left(\frac{V_2}{V}-\frac{V_1}{V}\right)\left(\frac{V_1}{V}\right)^{1/2} \qquad (53)$$

$$\frac{I_2}{C_2SV^{3/2}} = \left(1-\frac{V_2}{V}\right)\left(\frac{V_1}{V}\right)^{1/2} + \frac{C_{12}}{C_2}\left(\frac{V_1}{V}-\frac{V_2}{V}\right)\left(\frac{V_2}{V}\right)^{1/2}. \qquad (54)$$

For symmetrically placed beams

$$C_1 = C_2 = C.$$

If we make the following substitutions:

$$\alpha_1 = \frac{I_1}{CSV^{3/2}}$$

$$\alpha_2 = \frac{I_2}{CSV^{3/2}}$$

$$\frac{C_{12}}{C_1} = \frac{C_{12}}{C_2} = \frac{C_{12}}{C} = \beta$$

$$\frac{V_1}{V} = \lambda^2$$

$$\frac{V_2}{V} = \mu^2$$

we can rewrite (53) and (54) thus,

$$\alpha_1 = (1 - \lambda^2)\lambda + \beta(\mu^2 - \lambda^2)\lambda \qquad (55)$$

$$\alpha_2 = (1 - \mu^2)\mu + \beta(\lambda^2 - \mu^2)\mu \qquad (56)$$

or

$$\alpha_1 = \lambda - \lambda^3(1 + \beta) + \beta\lambda\mu^2 \qquad (57)$$

$$\alpha_2 = \mu - \mu^3(1 + \beta) + \beta\mu\lambda^2. \qquad (58)$$

The inspection of (57) shows that for λ = constant, the value of α_1 (proportional to I_1) increased directly with μ^2. This property enables one to represent (57) and (58) graphically by means of comparatively few computations. It should be noticed that for λ = constant, μ^2 can vary only within certain limits found

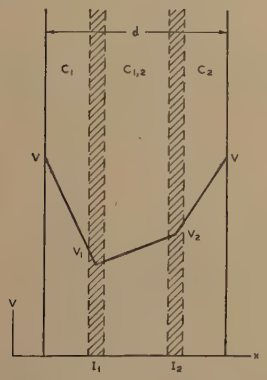

Fig. 17—Potential distribution for the case of two thin beams inside a common sheath electrode at a potential V.

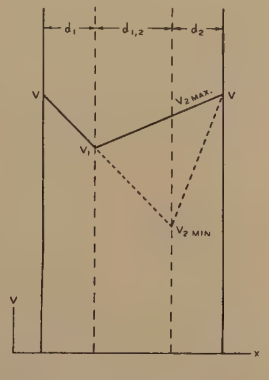

Fig. 18.—Limiting potential distributions for the case $\lambda^2 = V_1/V$ = constant: $(V - V_1 - V)$ for $I_2 = 0$, and $(V - V_1 - V_{2\min} - V)$ for $I_1 = 0$.

from the following considerations (see Fig. 18). When the current $I_2 = 0$, the potential distribution is shown by $V - V_1 - V$ and this determines the value $V_{2\max}$, and hence $\mu_{\max}^2$ for $\alpha_2 = 0$. From the geometry of the figure we find

$$\frac{(V - V_1)}{(V - V_{2\max})} = \frac{d_1 + d_{12}}{d_1} = 1 + \frac{1}{\beta} = \frac{1 - \lambda^2}{1 - \mu_{\max}^2}$$

or

$$\mu_{\max}^2 = \frac{1 + \beta\lambda^2}{1 + \beta}. \qquad (59)$$

Similarly, when $I_1 = 0$, the distribution will be as shown by line $V - V_1 - V_{2\min} - V$, and

$$\frac{V - V_{2\min}}{V - V_1} = \frac{d_1 + d_{12}}{d_1} = 1 + \frac{1}{\beta} = \frac{1 - \mu_{\min}^2}{1 - \lambda^2}$$

or

$$\mu_{\min}^2 = \frac{(1 + \beta)\lambda^2 - 1}{\beta} \qquad (60)$$

for $\alpha_1 = 0$. Since the beams are symmetrical the equations for $\lambda_{\max}^2$ and $\lambda_{\min}^2$ when μ is constant will be given by similar formulas by interchanging the symbols λ and μ.

Thus, the equations for plotting are

$$\alpha_1 = \lambda - \lambda^3(1 + \beta) + \beta\lambda\mu^2 = \beta\lambda(\mu^2 - \mu_{\min}^2) \qquad (61)$$

$$\mu_{\max}^2 = \frac{1 + \beta\lambda^2}{1 + \beta}$$

$$\mu_{\min}^2 = \frac{(1 + \beta)\lambda^2 - 1}{\beta}$$

$$\alpha_2 = \mu - \mu^3(1 + \beta) + \beta\mu\lambda^2 = \beta\mu(\lambda^2 - \lambda_{\min}^2) \qquad (62)$$

$$\lambda_{\max}^2 = \frac{1 + \beta\mu^2}{1 + \beta}$$

$$\lambda_{\min}^2 = \frac{(1 + \beta)\mu^2 - 1}{\beta}.$$

Table I represents the results of calculations for the case of $\beta = 2$.

TABLE I

λ^2	λ	$\mu_{\max}^2$	$\mu_{\min}^2$	$(\mu_{\max}^2 - \mu_{\min}^2)$	$\alpha_{1\max}$	$\beta\lambda$	$1/\beta\lambda$
1.0	1.0	1.0	1.0	0	0	2.0	0.50
0.9	0.948	0.934	0.85	0.084	0.159	1.896	0.527
0.8	0.894	0.867	0.70	0.167	0.298	1.788	0.560
0.7	0.857	0.800	0.55	0.250	0.418	1.67	0.600
0.6	0.774	0.734	0.40	0.334	0.517	1.55	0.645
0.5	0.707	0.666	0.25	0.416	0.588	1.41	0.707
0.4	0.632	0.600	0.10	0.500	0.632	1.26	0.793
0.33	0.577	0.556	0	0.556	0.642	1.15	0.870
0.30	0.548	0.553	−0.05	0.583	0.640	1.097	0.913
0.20	0.447	0.467	−0.20	0.667	0.595	0.894	1.12
0.10	0.316	0.400	−0.35	0.750	0.474	0.632	1.58
0.05	0.223	0.367	−0.425	0.792	0.354	0.446	2.24
0	0	0.333	−0.500	0.833			

The only values needed for plotting the lines of constant current against λ^2 and μ^2 are the values of $1/\beta\lambda$ which give the spacing between the constant-current lines $\alpha_1 = 1$ and $\alpha_1 = 0$. The location of the curve $\alpha_1 = 0$ is given by (60) and is a straight line. The results are presented in Fig. 19, which represents a plot of constant-current lines α_1 = constant and α_2 = constant in steps of 0.1.

To find the condition for maximum current α_1, we put

$$d\alpha_1 = 0 \qquad (63)$$

subject to the condition

$$d\alpha_2 = 0. \qquad (64)$$

Therefore, the conditions for α_1 = max and α_2 = constant coincide with the conditions α_2 = max and α_1 = constant.

On differentiating (61) and (62) we obtain

$$d\alpha_1 = d\lambda[1 - 3\lambda^2(1+\beta) + \beta\mu^2] + 2\beta\lambda\mu d\mu = 0 \quad (65)$$

$$d\alpha_2 = d\mu[1 - 3\mu^2(1+\beta) + \beta\lambda^2] + 2\beta\lambda\mu d\lambda = 0. \quad (66)$$

After combining the two equations, we obtain the following condition for maximum current:

$$[1-3\lambda^2(1+\beta)+\beta\mu^2][1-3\mu^2(1+\beta)+\beta\lambda^2]=4\beta^2\lambda^2\mu^2 \quad (67)$$

The solution of (67) is

$$\lambda^2 = \frac{(m+\beta)+(m^2-3\beta^2)\mu^2}{2m\beta} \pm \sqrt{\left[\frac{(m+\beta)+(m^2-3\beta^2)\mu^2}{2m\beta}\right]^2 - \frac{1+\mu^2(m+\beta)+m\beta\mu^4}{m\beta}} \quad (68)$$

where

$$m = -3(1+\beta).$$

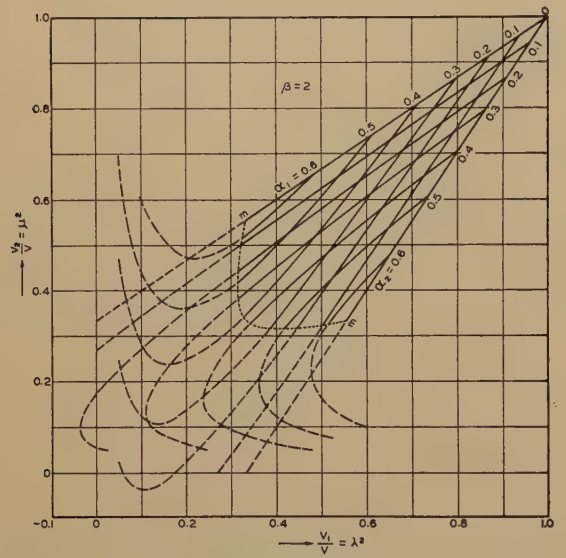

Fig. 19—Graph for determining the potential distribution for the case of two thin beams ($\beta=2$).

Equation (68) represents the condition for maximum current. It has been calculated for the case $\beta=2$, and is shown in Table II and in Fig. 19 as the curve m-m.

TABLE II

μ^2	$\frac{(m+\beta)+(m^2-3\beta^2)\mu^2}{2m\beta}$	$\frac{1+\mu^2(m+\beta)+m\beta\mu^4}{m\beta}$	λ_1^2	λ_2^2
0.333	0.444	0.1853	0.333	0.555
0.400	0.572	0.261	0.315	0.829
0.500	0.763	0.389	0.322	1.204

The constant-current lines are shown dotted below this limiting line of maximum current. This region, although unobservable under static conditions, is useful in predicting whether the virtual cathodes will be formed in both beams, or only in one when the currents are increased. For instance, suppose the generalized current $\alpha_1=0.6$ is kept constant while the current α_2 is increased from zero. The conditions will remain stable until the current α_2 reaches a value $\alpha_2=0.08$, at which point the current α_1 becomes unstable and a virtual cathode will be formed; that is, V_1/V will drop discontinuously to zero. However, even under this condition the current $\alpha_2=0.08$ can be maintained, as is shown by the dotted curve $\alpha_2=0.08$ which intersects the $V_1/V=0$ axis.

However, if we start with $\alpha_1=0.4=$constant, the beams will be stable until $\alpha_2=0.37$ is reached, and then virtual cathodes will be formed in both beams. (The curve $\alpha_2=0.37$ does not intersect the $V_1/V_0=0$ axis.) Thus, the theory indicates a possibility of controlling the current in one beam by varying the current in the other beam in a multiple-beam device, where the space-charge condition in one beam influences the space-charge condition in the other beams. The demonstration of this control is presented in the experimental part of this paper.

VI. Modulation of Electron Beams

Variation of Sheath-Electrode Potential

If a constant current flows through the sheath electrode the potential of which is varied, the effect will be the variation of space potential throughout the cross section of the beam, as illustrated in Fig. 20.

For the symmetrical beam of thickness t the amount of variation dV_0 of the minimum potential V_0 at the beam due to the variation dV_b of the sheath-electrode potential V_b can be calculated as follows:

The expression for current (from equation (9)) is

$$\frac{9}{64} kId = V_b^{3/2}F. \quad (69)$$

Assuming $I=$constant, and differentiating with respect to dV_b, we obtain

$$\frac{dF}{dV_b} = -\frac{3}{2}\frac{F}{V_b}. \quad (70)$$

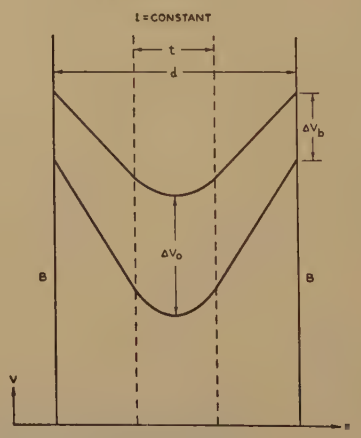

Fig. 20—Variation of space potential ΔV_0 with variation in sheath-electrode potential ΔV_b for constant beam current.

But

$$\frac{dF}{dV_b} = \frac{dF}{d\left(\frac{V_0}{V_b}\right)} \cdot \frac{d\left(\frac{V_0}{V_b}\right)}{dV_b} = \frac{1}{V_b} \cdot \frac{dF}{d\left(\frac{V_0}{V_b}\right)} \left[\frac{dV_0}{dV_b} - \frac{V_0}{V_b}\right]. \quad (71)$$

Combining (71) and (70), we obtain

$$\frac{dV_0}{dV_b} = \frac{V_0}{V_b} - \frac{3}{2}\cdot\frac{F}{\left[\dfrac{dF}{d\left(\dfrac{V_0}{V_b}\right)}\right]}. \qquad (72)$$

The denominator of the last term represents the slope of the curve F versus V_0/V_b represented in Fig. 6. The ratio dV_b/dV_0 is shown plotted against F for different values of the parameter t/d in Fig. 21. Due to space charge the variation in the space potential at the beam is greater than the variation of the potential applied to the sheath electrode. The ratio dV_0/dV_b increases with increasing beam current (F) and, theoretically, approaches infinity when the current approaches its maximum value. However, at this point the beam becomes unstable and, in practice, this condition is difficult to realize.

Effect of Beam-Current Variation on Space Potential

If the sheath-electrode potential is held constant and the beam current is modulated, the space potential inside the sheath will vary with the current. This variation is represented in Figs. 6 and 7 for symmetrical beams of finite thickness, and in Fig. 15 for thin beams. The slope of these curves, taken with a negative sign, gives the value of $(-dV_0/dI)$ which may be called the "characteristic impedance" of the beam by analogy with transmission-line theory. This impedance has a finite value at $I\to 0$ and gradually increases to infinity as the current approaches its maximum value. For thin beams this impedance can

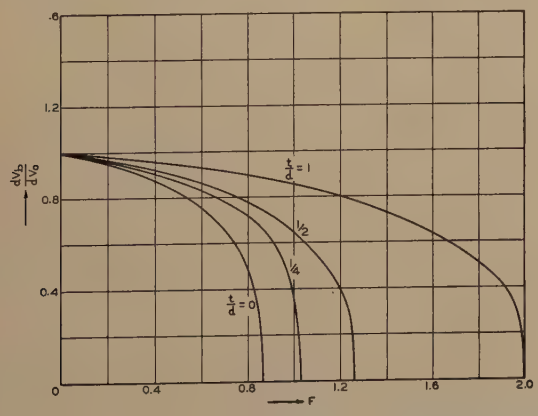

Fig. 21—Ratio of sheath to space-potential modulation (dV_b/dV_0) at constant beam current, as a function of generalized current F, for different values of t/d.

be found using (47) by differentiation of I with respect to V_0 as follows:

$$\frac{dI}{dV_0} = \frac{3\sqrt{3}}{4}\cdot\frac{1-3\dfrac{V_0}{V_{00}}}{\left(\dfrac{V_0}{V_{00}}\right)^{1/2}}\cdot\frac{I_{\max}}{V_{00}} \qquad (73)$$

where V_{00} denotes the value of space potential at the beam for zero current. Substituting the value of $I_{\max}$ from (39) and remembering that $(V_0)_{I\max}=1/3\,V_{00}$, we get

$$-\frac{dI}{dV_0} = -\frac{1-3\dfrac{V_0}{V_{00}}}{2\left(\dfrac{V_0}{V_{00}}\right)^{1/2}}\cdot SV_{00}^{1/2}(C_1+C_2). \qquad (74)$$

For $I=0$, $V_0=V_{00}$, so that

$$\frac{1}{(C_1+C_2)}\left(-\frac{dI}{dV_0}\right)_{I\to 0} = +SV_{00}^{1/2}. \qquad (75)$$

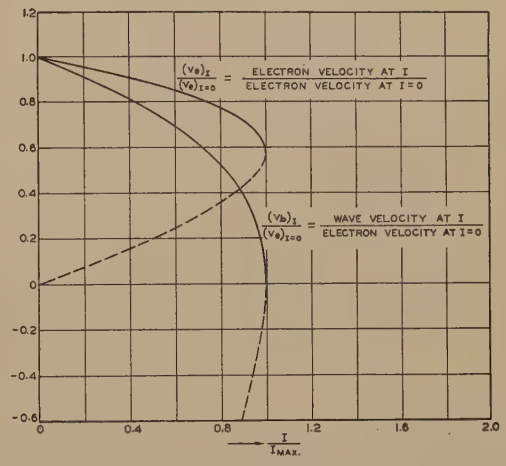

Fig. 22—Electron velocity and "wave velocity" of the beam as a function of beam current in a thin beam. (Velocities expressed in terms of electron velocity at $I=0$.)

But $SV_{00}^{1/2}$ is the electron velocity for $I\to 0$. Hence, at $I\to 0$ the "characteristic beam admittance" $(-dI/dV_0)$ is equal to the electron velocity times the capacitance per unit length of the beam to the sheath electrode. Again by analogy with transmission-line theory we will define as the "wave velocity" v_b of the beam the ratio of beam admittance to the beam capacitance; i.e.,

$$v_b = \left(-\frac{dI}{dV_0}\right)\cdot\frac{1}{(C_1+C_2)}.$$

Using (75) and (74), we obtain

$$\frac{v_b}{SV_{00}^{1/2}} = \left[-\frac{1-3\dfrac{V_0}{V_{00}}}{2\left(\dfrac{V_0}{V_{00}}\right)^{1/2}}\right]. \qquad (76)$$

The ratio of beam velocity for any current I to the electron velocity $(v_e)_{I=0}=SV_{00}^{1/2}$ at $I=0$, is shown in Fig. 22. The curve marked $(v_e)_I/(v_e)_{I=0}$ represents the variation of electron velocity with current I. This diagram shows that as the current is increased the beam velocity v_b becomes smaller than the electron velocity and reaches zero when the current approaches its maximum value while the electron velocity is still finite. At the instant the beam velocity becomes zero the beam becomes unstable and a virtual cathode will be formed. The dotted section

of the curves represent unstable conditions, and show that during the transition from maximum current to virtual cathode the beam velocity becomes negative; i.e., there may be energy reflection even though the electron velocity is still finite and in the forward direction.

The above analysis indicates that it is possible to produce magnetically focused electron beams of

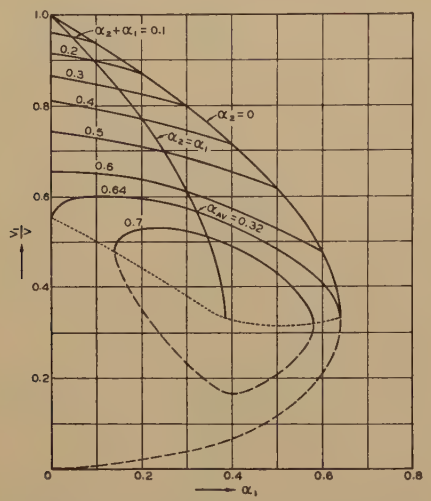

Fig. 23—Variation of space potential with current in the case of two thin beams for in-phase current modulation ($\alpha_1=\alpha_2=\alpha_0$) and for 180-degree out-of-phase modulation ($\alpha_1=\alpha_0-\alpha_2$).

considerable current even at low voltages, provided the sheath electrodes are placed close to the beam. These beams have an interesting property that no potential drop exists along the major portion of a long beam (for steady state) and no leakage of current occurs from the beam to the sheath electrode when the magnetic field is sufficiently high. This property makes it possible to produce nondissipative "electron-beam conductors" of appreciable length, limited only by the degree of vacuum attainable and the availability of an adequate focusing magnetic field.

These "beam conductors" have many other interesting properties in addition to their nondissipative nature. For instance, if a section of the sheath electrode is isolated from the rest of it and is connected to ground through an impedance, it is possible to transfer energy from a modulated electron beam to the external circuit. At low frequencies the coupling between the beam and the sheath electrode is capacitive, so that the coupling admittance increases with frequency. An analysis of the behavior of beam tubes at high frequency is, however, beyond the scope of the present paper.

Current Modulation in Double Beams

An interesting property of double beams is that when the current in one beam is varied 180 degrees out of phase with the variation of current in the other beam, the variation of the space potential in either beam will be smaller than if only one beam was modulated.

To estimate the amount of reduction of space-potential modulation in the case of push-pull beams, we may proceed as follows:

Differentiating (57) and (58), we find

$$\frac{d\alpha_1}{d\lambda^2}=\frac{1}{2\lambda}\left[1-3\lambda^2(1+\beta)+\beta\mu^2\right]+\beta\lambda\frac{d\mu^2}{d\lambda^2} \tag{77}$$

$$\frac{d\alpha_2}{d\lambda^2}=\frac{d\mu^2}{d\lambda^2}\cdot\frac{1}{2\mu}\left[1-3\mu^2(1+\beta)+\beta\lambda^2\right]+\beta\mu. \tag{78}$$

Putting the value of $d\mu^2/d\lambda^2$ from (78) into (77), we obtain

$$\frac{d\alpha_1}{d\lambda^2}=\frac{1}{2\lambda}\left[1-3\lambda^2(1+\beta)+\beta\mu^2\right]+\frac{\dfrac{d\alpha_2}{d\lambda^2}-\beta\mu}{\dfrac{1}{2\beta\lambda\mu}\left[1-3\mu^2(1+\beta)+\beta\lambda^2\right]}. \tag{79}$$

When $\alpha_2=$constant, i.e., $d\alpha_2=0$, we obtain

$$\left(\frac{d\alpha_1}{d\lambda^2}\right)_{d\alpha_2=0}=\frac{1}{2\lambda}\left[1-3\lambda^2(1+\beta)+\beta\mu^2\right]-\frac{2\beta^2\lambda\mu^2}{\left[1-3\mu^2(1+\beta)+\beta\lambda^2\right]}. \tag{80}$$

When $d\alpha_2=-d\alpha_1$ for the push-pull beam

$$\left(\frac{d\alpha_1}{d\lambda^2}\right)_{d\alpha_2=-d\alpha_1}=\left(\frac{d\alpha_1}{d\lambda^2}\right)_{d\alpha_2=0}\cdot\frac{1}{1+\dfrac{2\beta\lambda\mu}{1-3\mu^2(1+\beta)+\beta\lambda^2}}. \tag{81}$$

Thus the reduction in space-potential modulation due to push-pull modulation of the beam is

$$\frac{\left(\dfrac{d\alpha_1}{d\lambda^2}\right)_{d\alpha_2=0}}{\left(\dfrac{d\alpha_1}{d\lambda^2}\right)_{d\alpha_2=-d\alpha_1}}=1+\frac{2\beta\lambda\mu}{1-3\mu(1+\beta)+\beta\lambda^2}. \tag{82}$$

For small currents when λ and μ approach unity, (82) reduces to

$$\rightarrow\frac{1}{1+\beta}=\frac{1}{1+\dfrac{C_{12}}{C}}=\frac{C}{C_{12}+C}. \tag{83}$$

The space potential V_1/V versus current (α_1) has been plotted in Fig. 23 (data taken from the master diagram for $\beta=2$) for the cases of $\alpha_2=0$, $\alpha_1=\alpha_2$, and $\alpha_2=\alpha_0-\alpha_1$, the latter case corresponding to current modulation 180 degrees out of phase. This diagram shows that the push-pull modulation reduces the space-potential modulation; this reduction, on the

average, approaching very nearly the value of $1/(1+\beta)$, even for large currents. Fig. 23 shows that push-pull 100 per cent modulation is possible only when $\alpha_{average} \leqq 0.32$. If $\alpha_{average}$ exceeds this value, complete modulation is impossible because a virtual cathode will be formed in the beam with higher current. The dotted line represents the limiting curve below which any current modulation precipitates the formation of virtual cathodes.

VII. Experimental Verification

Several tubes utilizing magnetically focused electron beams of rectangular cross section were constructed and their performance studied in some detail. In general, a good agreement between theory and experiment was found whenever the assumptions underlying the theory were substantially fulfilled in practice.

General Description of Experimental Tubes

The general electrode arrangement was as shown in Fig. 24. The amount of current drawn from a flat cathode K was controlled by the potential V_1 of the control grid G_1. The entrance and exit electrodes, usually in the form of slot grids G_2 and G_3 were normally held at a potential somewhat higher than the potential of the sheath electrode S. The current was collected by a collector electrode C held at a potential higher than the potential of the sheath electrode V_s in order to collect all current that was passed by the sheath electrode. The magnetic field was produced by solenoids arranged along the tube axis in such a way as to provide a fairly uniform field the whole length of the beam.

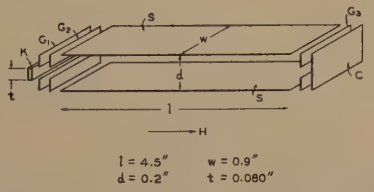

Fig. 24—Electrode arrangement in tubes used for obtaining experimental data on the effects of space charge in long electron beams.

Maximum Current in the Beam

The first point studied was that of finding the maximum beam current. Fig. 25 shows the variation of the collector current with the control-grid voltage V_1 in a long-beam tube, for different values of the sheath-electrode potential. The principal dimensions of the tube are shown in the figure. It is observed that the collector current increases with increase in the control-grid voltage until a maximum value for a given sheath-electrode potential is reached. At this point the virtual cathode is formed and the current drops discontinuously to a smaller value and then continues to decrease with further increase in current injected into the space. With decreasing control-grid potential the curve usually follows the same path, no hysteresis effect being observed, unless the entrance grid is held at a potential considerably higher than the sheath-electrode potential. The latter case is illustrated by the curve labeled $V_s = 50$ volts when $V_{G_2} = 240$ volts. The value of maximum current

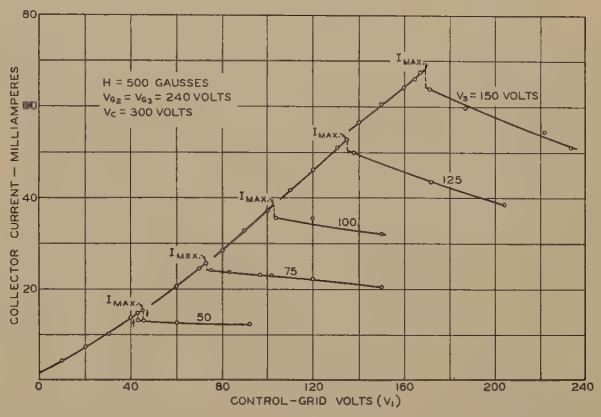

Fig. 25—Variation of the collector current with the control-grid voltage (V_1) in a long-beam tube, for different values of the sheath-electrode potential (V_{sh}). $l = 4.5$ inches; $d = 0.2$ inch; $w = 0.9$ inch; $t = 0.080$ inch; $H = 500$ gausses; $V_{G_1} = V_{G_2} = 240$ volts; $V_c = 300$ volts.

to be expected was calculated from the tube dimensions using formula (15), and the results compared with the experimental values, as shown in Table III.

TABLE III

V_s volts	I_{max} ma calculated for $t/d = 0.4$	I_{max} ma calculated for $t/d = 0.05$	I_{max} ma experimental
50	17.2	13.4	15.2
75	31.7	24.6	25.5
100	48.8	37.9	38.5
125	68.5	53.2	52.8
150	90.0	69.8	68.0

The third column of the table gives the values of current calculated for $t/d = 0.05$ which value gives a better agreement with the experimental values than $t/d = 0.4$. The latter value represents the ratio of the cathode width to the sheath-electrode opening. The reason for this is that, due to the focusing action of the electrostatic fields at the entrance space, the true minimum thickness of the beam t may be smaller than the width of the cathode.

Sheath-Electrode Current

Fig. 26 shows the variation of the sheath-electrode current with control-grid voltage for the same conditions as in Fig. 25. The sheath-electrode current remains quite small until the virtual cathode is formed in the beam; then, the sheath current suddenly increases, and continues to increase with further increase in the potential V_1.

Collector- and Sheath-Electrode Current Versus Sheath Potential

The variation of the collector current with sheath potential for a fixed value of the injected current (V_1 = constant) is illustrated in Fig. 27. The collector

current increases with the increasing sheath-electrode potential V_s as long as the virtual cathode persists in the space. When the potential V_s reaches the value for which the virtual cathode changes into a potential minimum, no further increase in collector current is observed as V_s is still further increased.

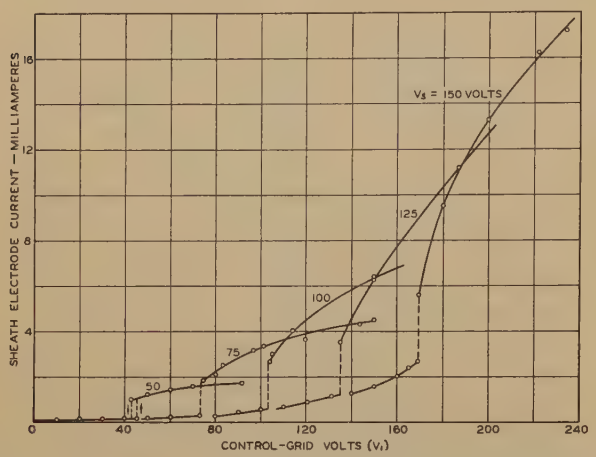

Fig. 26—Variation of the sheath-electrode current with control-grid voltage for the same conditions as in Fig. 25.

The curves of sheath-electrode current versus V_s are shown in Fig. 28. The peculiar shape of these curves can be interpreted as due to the fact that when the magnetic field is not quite uniform the virtual cathode, on disappearing at one point along the beam, may again be formed at another point. Only when the last virtual cathode disappears does the sheath-electrode current drop rapidly to a small value, usually a few per cent of the beam current, if the magnetic field is sufficiently strong.

Effect of Intensity of the Focusing Magnetic Field

The dependence of the collector- and sheath-electrode currents upon the strength of the focusing magnetic field is illustrated in Fig. 29. Two sets of

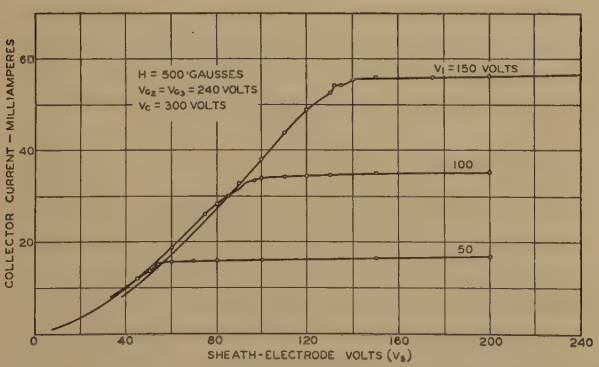

Fig. 27—Collector current versus sheath potential for fixed value of injected current (V_1=constant).

curves are given representing the two conditions: (a) when the injected current is less than the maximum that can be passed, and (b) when the injected current exceeds the maximum. In case (a) the slow increase of the collector current from the point H=170 gausses to the point H=400 gausses, is due to the fact that because of the converging action of the magnetic field more current passes through the entrance grid G_2 with increasing field strength. In case (b), with decreasing H, the collector current increases after the value H=180 gausses is reached, then shows a minor maximum and then again decreases. The explanation of this behavior lies in the fact that with decreasing field strength more and more current is absorbed by the sheath electrode until

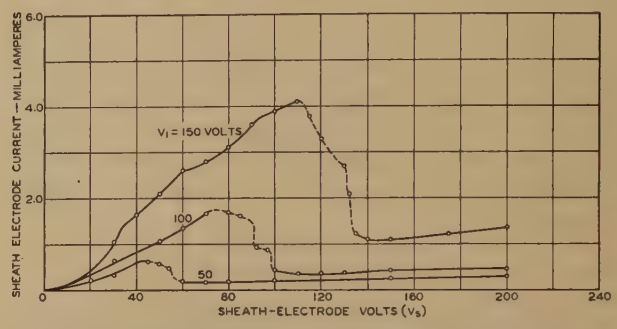

Fig. 28—Sheath-electrode current versus sheath potential for a fixed value of injected current (V_1=constant).

the amount of space charge in the beam becomes too small to maintain the virtual cathode and, thus, more current is permitted to reach the collector. However, with further decrease in the field strength both the collector and sheath-current decrease because less current penetrates through the entrance grid G_2 due to the diminution of the beam convergence with the field.

In a tube of a considerably shorter beam length a very pronounced hysteresis loop in the I_c-versus-H curve can be observed. This is shown in Fig. 30. The

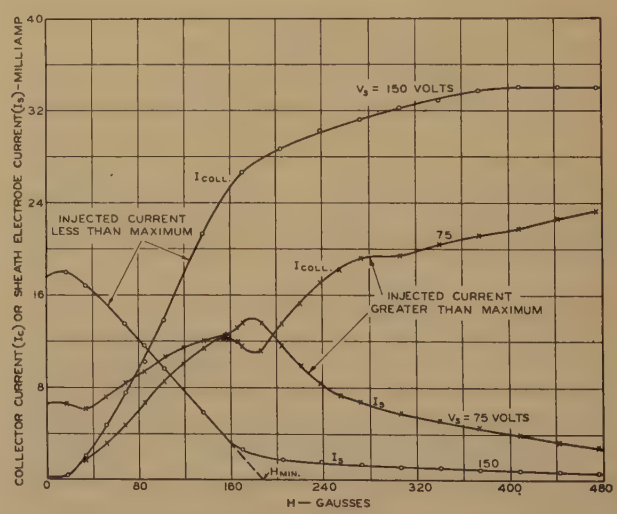

Fig. 29—Collector and sheath currents versus intensity of magnetic field.

collector current increases until the absorption of current by the sheath electrode becomes small and the concentration of the beam becomes sufficient to precipitate the formation of the virtual cathode, at which point the collector current decreases abruptly

to a smaller value. With a decreasing field the virtual cathode persists at smaller values of field strength until the absorption of current by the sheath electrode diminishes the space charge in the beam sufficiently to render the virtual cathode unstable. At

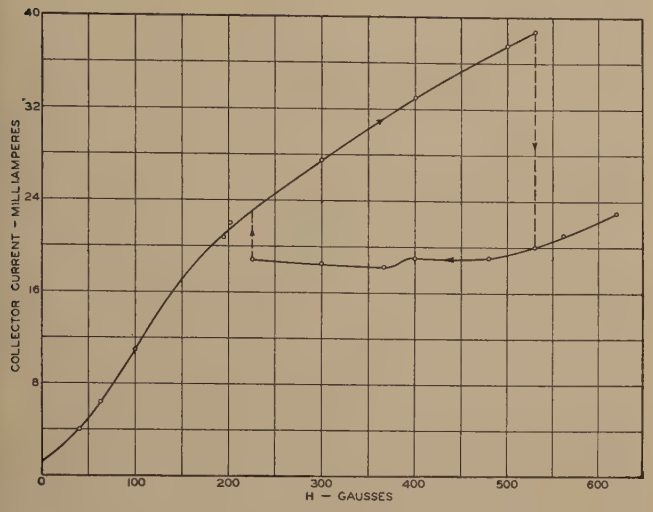

Fig. 30—The curve of collector current versus intensity of magnetic field showing "hysteresis" effect in a short beam.

this point the collector current rises abruptly to the corresponding value on the ascending curve.

The V_1-versus-I_c characteristics of a similar tube, where the hysteresis effect is very pronounced, is shown in Fig. 31. In this tube, the sheath-electrode opening was not sufficiently small compared to the length of the beam, and the voltage applied to the entrance electrode was high compared to the voltage on the sheath electrode. These two factors are apparently responsible for the presence of appreciable hysteresis effects.

The check between the theoretical minimum magnetic field and the field $H_{\min}$, experimentally defined

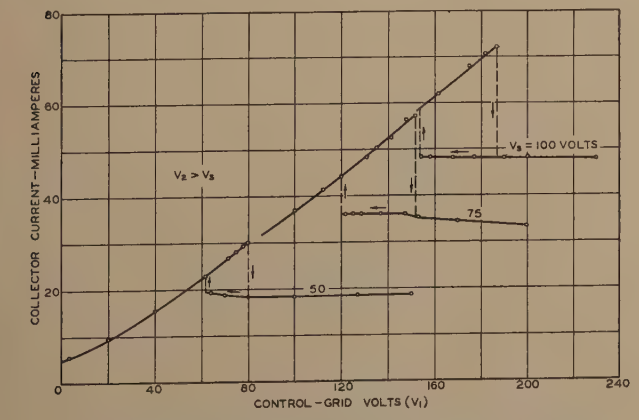

Fig. 31—Hysteresis loops in I_c versus V_1 characteristic (H = constant) of a short-beam tube.

as in Fig. 29, is shown in Fig. 32. A large discrepancy at small values of current is attributable to the initial divergence of the beam, which was not taken into account in calculating the theoretical curve. However, the agreement is very good when the beam divergence is small, a condition which occurs when V_1 is close to V_2.

Effect of Sheath-Electrode Opening

The effect of varying the opening d of the sheath electrode, was also studied and the results are given

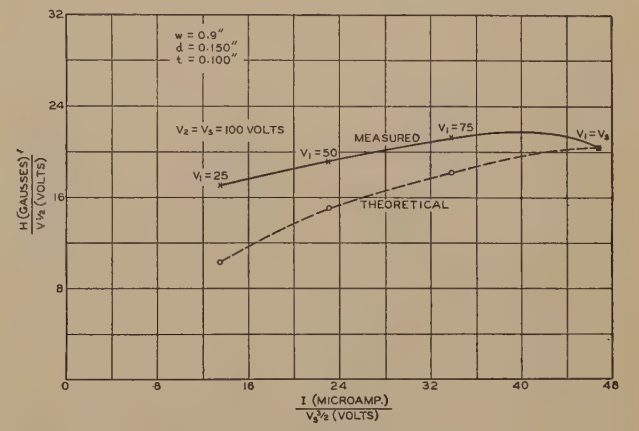

Fig. 32—Comparison between the theoretical and experimentally determined value of the minimum magnetic field.

in Table IV, which shows a good agreement between the observed and calculated values of maximum current for different spacings d and different values of sheath potential.

TABLE IV

V_3	d = 0.4 inch		d = 0.2 inch		d = 0.1 inch	
	Experimental	Calculated	Experimental	Calculated	Experimental	Calculated
50	6.8	6.6	14.3	15.5	34.5	35.7 t = 0.080 in.
75	11.5	12.1	26.1	28.4	70.5	65.5 w = 0.80 in.
100	16.5	18.7	43.5	43.8	102.0	101.0
125	25.7	26.2	63.5	61.3		
150	33.0	34.5				

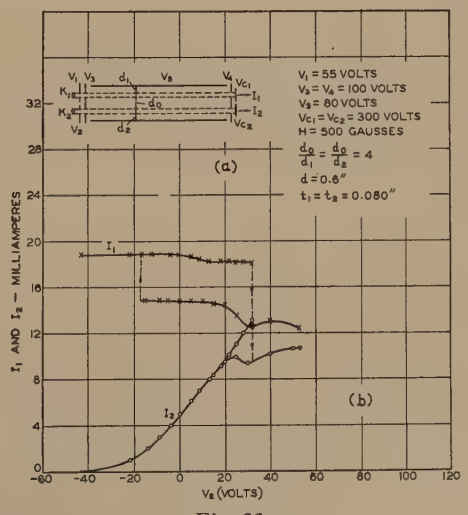

Fig. 33

(a) Electrode arrangement of a two-beam tube.
(b) Illustration of current control of one beam by current in the adjacent beam in a two-beam tube shown in Fig. 33(a).

Control of Current in One Beam by Current in the Adjacent Beam

Fig. 33 is an illustration of the method of control of current in one beam by the current in the adjacent

beam, as was described in section V. As is shown in Fig. 33(a), the rectangular sheath electrode is common to two beams injected into the space parallel to each other. The current in beam No. 1 and the controlling current in beam No. 2, are shown plotted against the No. 2 control-grid voltage, all other voltages and the magnetic field being held constant. The controlling action is discontinuous. The first beam current is not affected by the second current until the space is saturated, at which point the virtual cathodes are formed in both beams, and the No. 1 and No. 2 currents drop discontinuously. With decreasing No. 2 current the virtual cathode first disappears from the second beam, but persists in the No. 1 beam until the controlling current (No. 2) is reduced to a small value. Then the No. 1 current abruptly assumes its original value.

VIII. Application of the Theory to Cases of Beams Focused Electrostatically

The results of the above analysis can be applied in some cases when the focusing of long beams is accomplished not by magnetic but by electrostatic fields, provided the portion of the nearly parallel beam is reasonably long compared to the transverse dimensions of the sheath electrode. A case in which this is approximately true is that of a high-voltage cathode-ray tube. There a long, narrow beam is produced inside a long envelope held at a high positive potential. It is of interest to know how much the space potential is decreased by the presence of the beam. As an illustration, let us assume that the diameter of the beam is $2r_0 = 0.005$ inch; the average diameter of the envelope $2r_2 = 5$ inches; the potential applied to the envelope $V_2 = 10{,}000$ volts; and the beam current is $I = 0.001$ ampere. Using (44) we find that the theoretical maximum current that could be passed provided the focusing field were adequate to maintain the beam diameter is

$$I_{\max} = 0.866 \times 14.7 \times 10^{-6} \frac{1}{\log \frac{5}{0.005}} (10^4)^{3/2}$$

$$= 1.85 \text{ amperes.}$$

The actual current is, however, only 1.0 milliampere, so that the ratio $I/I_{\max} = 0.001/1.85 = 0.00054$. From the curve of Fig. 15, we find that in this case the space potential will be depressed by the presence of the beam only by a very small amount. This result confirms the validity of the assumption of constant longitudinal velocity along the beam made by B. J. Thompson and L. B. Headrick in their recent paper[7] on the effect of space charge on the minimum spot size in television tubes.

It may be added that the formulas developed in the theoretical part of the paper can be used for the design of beam tubes with a fair degree of success. However, if the experimental conditions differ materially from those for the assumed idealized long electron beam in high vacuum—for instance, if the length of the beam is not large compared to the sheath-electrode opening, or the focusing magnetic field is too low, or gas is present in the tube in sufficient quantity to provide an ionized medium[12]—discrepancies will be found between the results predicted by the above simplified theory and those obtained by experiment. Further study of this problem is desirable in order to evaluate the importance of the factors neglected by the theory presented in this paper.

Additional Bibliography

(1) B. Salzberg and A. V. Haeff, "Effects of space charge in the grid-anode region of vacuum tubes," *RCA Rev.*, vol. 2, pp. 336–374; January, (1938).

(2) W. Kleen and H. Rothe, "Space-charge equations for electrons with initial velocity," *Zeit. für Phys.*, vol. 104, pp. 711–723; March 15, (1937).

(3) D. M. Myers, D. R. Hartree, and A. Porter, "The effect of space charge on the secondary current in a triode," *Proc. Roy. Soc.*, series A, vol. 158, pp. 23–37; January 1, (1937).

[12] I. Langmuir and K. T. Compton, "Electrical discharges in gases—Part II, fundamental phenomena in electrical discharges," *Rev. Mod. Phys.*, vol. 3, pp. 255–257; April, (1931).

Characteristics of the Ionosphere at Washington, D. C., July, 1939*

T. R. GILLILAND†, ASSOCIATE MEMBER, I.R.E., S. S. KIRBY†, ASSOCIATE MEMBER, I.R.E. AND N. SMITH†, NONMEMBER, I.R.E.

DATA on the critical frequencies and virtual heights of the ionosphere layers during July are given in Fig. 1. Fig. 2 gives the monthly average values of the maximum usable frequencies for undisturbed days, for radio transmission by way of the regular layers. The F layer ordinarily determines the maximum usable frequencies at night. The effects of the E and F_1 layers are shown by the humps on the graphs during the day. Fig. 3 gives the distribution of hourly values of F and F_2 data about the undisturbed average for the month. Fig. 4 gives the expected values of the maximum usable fre-

TABLE I

IONOSPHERE STORMS (APPROXIMATELY IN ORDER OF SEVERITY)

Date and hour E.S.T.	h_F before sunrise (km)	Minimum f_{F^0} before sunrise (kc)	Noon f^0F_2 (kc)	Magnetic character[1] 00–12 G.M.T.	Magnetic character[1] 12–24 G.M.T.	Ionosphere character[2]
July						
4 (after 1200)	—	—	7500	0.6	1.4	1.0
5	498	<1600	<4700	1.9	1.6	1.8
6 (until 2300)	396	3500	5400	0.7	0.0	1.3
2 (after 0900)	—	—	5400	0.2	0.1	1.0
3	325	3700	<4900	1.1	1.1	1.6
4 (until 0500)	325	3300	—	0.6	1.4	0.4
26	346	diffuse	<4800	1.0	0.8	1.5
27	330	3400	5500	0.4	0.3	0.8
28 (until 0500)	328	3200	—	0.2	0.1	0.5
20 (after 0200)	324	3800	<4800	1.0	1.2	1.3
21 (until 1700)	314	2700	5200	0.9	1.3	1.1
14 (after 0100)	364	3700	5100	1.0	0.8	1.1
15 (until 0500)	320	3600	—	0.3	0.1	0.2
16 (after 1500)	—	—	—	0.3	0.9	0.7
17 (until 0500)	320	3200	—	0.6	0.3	0.2
25 (0100 to 0900)	338	3400	—	0.8	0.1	0.1
For comparison: Average for undisturbed days	300	4500	6920	0.2	0.3	0.0

[1] American magnetic character figure, based on observations of seven observatories.

[2] An estimate of the severity of the ionosphere storm at Washington on an arbitrary scale of 0 to 2, the character 2 representing the most severe disturbance.

TABLE II

SUDDEN IONOSPHERE DISTURBANCES

Date	G.M.T. Beginning	G.M.T. End	Locations of transmitters	Relative intensity at minimum[1]	Other phenomena
July					
2	1623	1648	Ohio Mass. Ont.	0.01	
3	2038	2100	Ohio Mass.	0.01	
15	1835	2000	Ohio Mass. Ont. D.C.	0.0	Ter. mag. pulse 1835–1940
16	1640	1658	Mass. Ont. D.C.	0.0	
22	1910	1940	Ohio Mass. Ont. D.C.	0.0	
31	1700	1738	Ohio Mass. Ont.	0.0	
31	1743	1800	Ohio Mass. Ont.	0.05	
31	1952	2050	Ohio Mass. Ont. D.C.	0.0	

[1] Ratio of received field intensity during fade-out to average field intensity before and after; for station W8XAL, 6060 kilocycles, 650 kilometers distant.

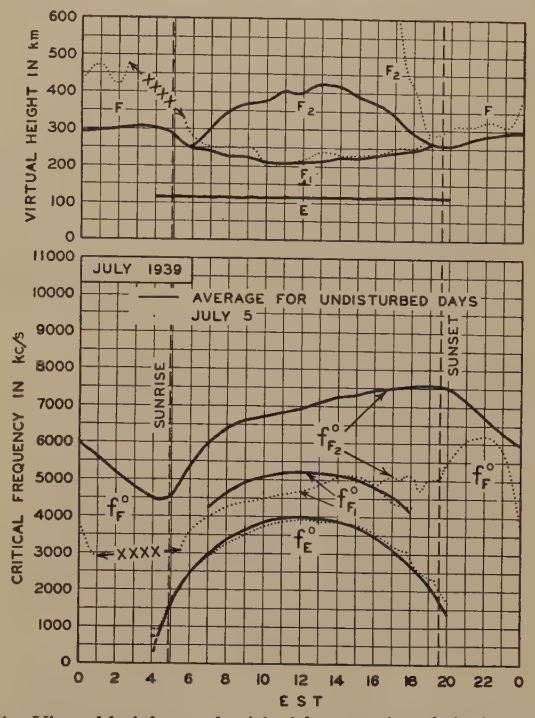

Fig. 1—Virtual heights and critical frequencies of the ionosphere layers, July, 1939. The solid-line graphs are the averages for the undisturbed days; the dotted-line graphs are for the ionosphere storm day of July 5. The crosses represent the times on July 5 when the F-layer reflections were so diffuse that the critical frequencies or virtual heights could not be determined.

It should be noted that all data on critical frequencies are now plotted in terms of the ordinary wave. Previously the F, F_1 and F_2 data were plotted in terms of extraordinary wave; see text.

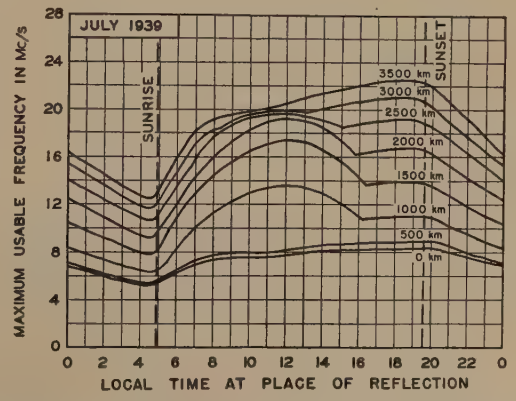

Fig. 2—Maximum usable frequencies for dependable radio transmission via the regular layers. Average for July, 1939, for undisturbed days. The values shown were considerably exceeded during irregular periods by reflections from clouds of sporadic E.

* Decimal classification: R113.61. Oringinal manuscript received by the Institute, August 11, 1939. These reports have appeared monthly in the PROCEEDINGS starting in vol. 25, September, (1937). See also vol. 25, pp. 823-840; July, (1937). Publication approved by the Director of the National Bureau of Standards of the U. S. Department of Commerce.

† National Bureau of Standards, Washington, D. C.

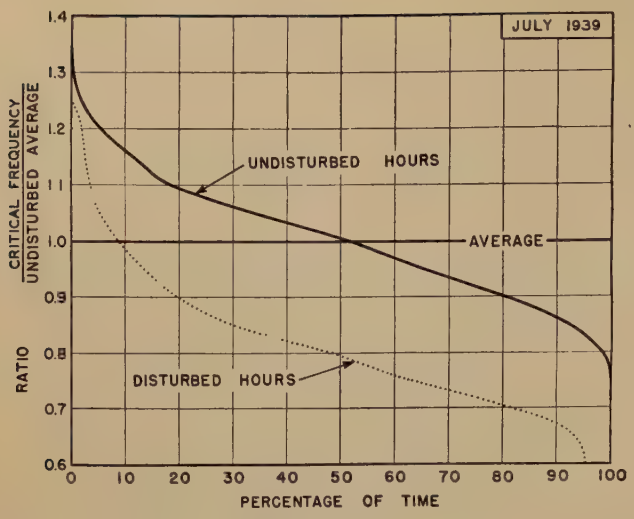

Fig. 3—Distribution of F- and F_2-layer ordinary-wave critical frequencies (and approximately of F- and F_2-layer maximum usable frequencies) about monthly average. Abscissas show percentage of time for which the ratio of the critical frequency to the undisturbed average exceeded the values given by the ordinates. The solid-line graph is for 483 undisturbed hours of observation; the dotted graph is for the 248 disturbed hours of observation listed in Table I.

quencies for radio transmission by way of the regular layers, average for undisturbed days, for

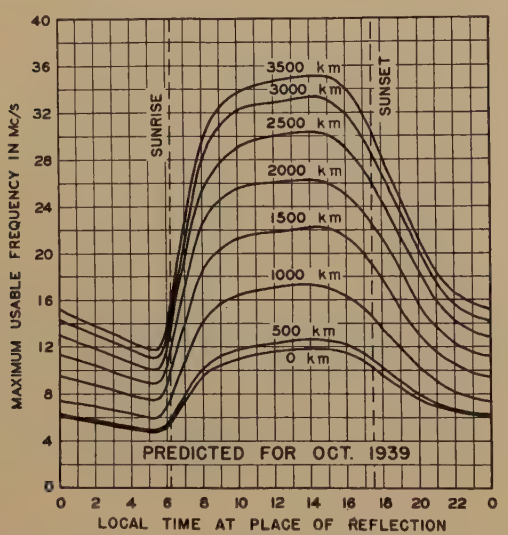

Fig. 4—Predicted maximum usable frequencies for dependable radio transmission via the regular layers, average for undisturbed days, for October, 1939.

TABLE III

APPROXIMATE UPPER LIMIT OF FREQUENCY IN MEGACYCLES OF THE STRONGER SPORADIC-E REFLECTIONS AT VERTICAL INCIDENCE

Date	Midnight to noon											
	Hour											
	00	01	02	03	04	05	06	07	08	09	10	11
July												
4	8	8	8									
7			6	6			6		6		6	4 5
9			4.5	4.5	8	8	8	9	8			
10										6	8	6
12						8	8	10	8			
13									6	8	6	
17									6	8	8	
27	4.5	6	6	4.5	4.5	4.5		6	6	8	4.5	8

Date	Noon to Midnight											
	Hour											
	12	13	14	15	16	17	18	19	20	21	22	23
July												
3		8	8	6						4.5	4.5	6
6		6					6	8				
11								8	8			
13	4.5			4.5		4.5	8	8	8	8		
15											8	8
25							4.5		8		6	8
27		6		8	8			8	8	8	8	6
29					4.5	8	6					8
31									4.5	8	8	8

October. Ionosphere storms and sudden ionosphere disturbances are listed in Tables I and II, respectively. Table III gives the approximate upper limit of frequency of strong sporadic-E reflections at vertical incidence, for the days during which these reflections were most prevalent at Washington.

Attention is called to an important change made this month in the presentation of the critical frequency data. Beginning with this report, all critical frequencies will be given in terms of the ordinary wave. Heretofore the data on the F, F_1, and F_2 layers have been given in terms of the extraordinary wave, for which the critical frequency at Washington is about 800 kilocycles greater than for the ordinary wave. In view of the increasing use of the vertical-incidence critical frequencies to calculate maximum usable frequencies, and of the direct utility of the ordinary-wave values in such calculation, it seems more useful to give the ordinary-wave values hereafter. Extraordinary-wave critical frequencies may be reduced to ordinary-wave critical frequencies by subtracting a constant from the former, and vice versa; for the Washington data the constant is 800 kilocycles.

Institute News and Radio Notes

FOURTEENTH ANNUAL CONVENTION
September 20-23, 1939
New York, N. Y.

A World's Fair inevitably brings to the city in which it is held a large number of conventions. This is easily understood when one considers the great amount of interest which these exhibitions attract both for their educational and entertainment possibilities. However, the holding of two such events simultaneously in a single country, even as large as the United States, is unique in the history of large exhibitions.

When 1939 Institute Conventions were considered it was felt that both San Francisco and New York would be suitable and final agreement resulted in scheduling a national convention in each city.

The June Convention in San Francisco was highly successful and attendance from the Western States and from the rest of the country exceeded all of our estimates. It is, therefore, anticipated that the attendance at our Fourteenth Annual Convention to be held in New York City on September 20–23 will result in a larger gathering of Institute members than has ever occurred previously.

Because of the interest which the New York World's Fair has aroused, arrangements for the Convention do not follow closely our previous convention programs. Four days have been scheduled for the meeting rather than three. Also, no technical sessions or other functions have been arranged for any evening, thus making the maximum amount of time available for visiting the Fair.

There will be eight technical sessions which will be held on the four mornings and afternoons. Twenty-six papers have been scheduled for presentation and will be given practically in full. No duplicate sessions will be held so everyone in attendance can hear every paper in which he is interested.

An informal luncheon will be held on Thursday, September 21, and will take the place of the banquet which normally would be included.

No inspection trips are planned as the industrial and scientific exhibits at the Fair will offer much more return for the time invested than would any trip of the variety normally scheduled for a convention.

Headquarters will be at the Hotel Pennsylvania and trains for the Fair may be boarded at the Pennsylvania station which is directly across the street and may be reached without going out of doors.

The program which follows is substantially complete and any changes will be of a minor nature. All schedules are given in Eastern Daylight Saving Time which is one hour later than Eastern Standard Time.

PROGRAM

Wednesday, September 20

9:00 A.M.

Registration

10:00 A.M.–12:00 NOON

Opening address by R. A. Heising, President of the Institute.

1. "A Single-Sideband Musa Receiving System for Commercial Operation on Transatlantic Radiotelephone Circuits," by F. A. Polkinghorn, Bell Telephone Laboratories, Inc., New York, N. Y.
2. "Medium-Power Marine Radiotelephone Equipment," by J. F. McDonald, Radiomarine Corporation of America, New York, N. Y.

2:00 P.M.–4.00 P.M.

3. "The Corner Reflector," by J. D. Kraus, Ann Arbor, Michigan.
4. "Gaseous Ionization and Surface Corona Discharge Detection at Low and High Frequencies," by H. A. Brown, University of Illinois, Urbana, Ill.
5. "A New Standard Volume Indicator and Reference Level," by H. A. Chinn, Columbia Broadcasting System, New York, N. Y.; D. K. Gannett, Bell Telephone Laboratories, Inc., New York, N. Y.; and R. M. Morris, National Broadcasting Company, New York, N. Y.
6. "Vestigial-Sideband Filters for Use with a Television Transmitter," by G. H. Brown, RCA Manufacturing Company, Inc., Camden, N. J.
7. "A Cathode-Ray Frequency-Modulation Generator," by R. E. Shelby, National Broadcasting Company, New York, N. Y.

Thursday, September 21

10:00 A.M.–12:00 NOON

8. "Solar Cycle and the F_2 Region of the Ionosphere," by W. M. Goodall, Bell Telephone Laboratories, Inc., New York, N. Y.

9. "Attenuation of High Frequencies Over Land at Short Ranges," by John Hessel, Signal Corps Laboratories, Fort Monmouth, N. J.
10. "Demonstration of Aerological Radio Sounding Equipment," by Harry Diamond, F. W. Dunmore, W. S. Hinman, Jr., and E. S. Lapham, National Bureau of Standards, Washington, D. C.

12:30 P.M.–2:00 P.M.

Informal Luncheon: Presentation of the Institute Medal of Honor to Sir George Lee and the Morris Liebmann Memorial Prize to H. T. Friis.

2:30 P.M.–4:30 P.M.

11. "A Parallel-T Circuit for Measuring Impedance at Radio Frequencies," by D. B. Sinclair, General Radio Company, Cambridge, Mass.
12. "High-Speed Multiplex System for Loaded Submarine Cables," by H. H. Haglund and A. W. Breyfogel, Western Union Telegraph Company, New York, N. Y.
13. "Electronic-Wave Theory of Velocity-Modulation Tubes," by Simon Ramo, General Electric Company, Schenectady, N. Y.
14. "On Diffraction and Radiation of Electromagnetic Waves," by S. A. Schelkunoff, Bell Telephone Laboratories, Inc., New York, N. Y.

Friday, September 22

10:00 A.M.–12:00 NOON

15. "Cathode-Ray Tubes in Aircraft Instrumentation," by C. W. Carnahan, Hygrade Sylvania Corporation, Emporium, Penna.

These are three of the fifteen houses which comprise the "Town of Tomorrow."

The sixty-five foot statue of George Washington located on Constitution Mall is silhouetted against the illuminated Perisphere.

16. "A True Qmnidirectional Radio Beacon," by E. N. Dingley, Jr., United States Navy Department, Washington, D. C.
17. "Basic Economic Trends in the Radio Industry," by Julius Weinberger, Radio Corporation of America, New York, N. Y.
18. "Engineering Administration in a Small Manufacturing Company," by C. T. Burke, General Radio Company, Cambridge, Mass.

2:00 P.M.–4:00 P.M.

19. "Aircraft Radio Compasses—Principles and Testing," by R. J. Framme, Aircraft Radio Laboratory, Wright Field, Ohio.
20. "Errors in Closed-Loop Direction Finders Caused by Abnormal Polarization," by R. I. Cole, Signal Corps Laboratories, Fort Monmouth, N. J.

Saturday, September 23

10:00 A.M.–12:30 P.M.

21. "Functions of Electron Bombardment in Television," by I. G. Maloff, RCA Manufacturing Company, Inc., Camden, N. J.
22. "Transient Response in Television," by H. E. Kallmann, formerly of Electrical and Musical Industries, Ltd., in collaboration with R. E. Spencer and S. P Singer, Electrical and Musical Industries, Ltd., Hayes, Middlesex, England.
23. "A Wide-Band Inductive-Output Amplifier," by A. V. Haeff, and L. S. Nergaard, RCA Manufacturing Company, Inc., Harrison, N. J.

2:00 P.M.–4:30 P.M.

24. "Superheterodyne First-Detector Considerations in Television Receivers," by E. W. Herold, RCA Manufacturing Company, Inc., Harrison, N. J.
25. "Development of a 20-Kilowatt Ultra-High-

The mural on the facade of the Hall of Communications is symbolic of both ancient and modern communication methods.

Frequency Tetrode for Television Service." (In three parts.)

Part I. "Electrical Design," by A. V. Haeff, L. S. Nergaard, RCA Manufacturing Company Inc., Harrison, N. J., and W. G. Wagener and P. D. Zottu, formerly of RCA Manufacturing Company, Inc., now, Heintz and Kaufmann, Ltd., and Thermal Engineering Corporation, respectively.

Part II. "Construction," by R. B. Ayer, RCA Manufacturing Company, Harrison, N. J., and P. D. Zottu, formerly RCA Manufacturing Company, Inc., now, Thermal Engineering Corporation.

Part III. "Test Equipment and Results," by R. B. Ayer and H. E. Gihring, RCA Manufacturing Company, Inc., Harrison, N. J. and Camden, N. J., respectively.

26. "Production Alignment Apparatus for Television Receivers," by L. J. Hartley, General Electric Company, Bridgeport, Conn.

TECHNICAL PAPERS

Technical papers will not be preprinted. As the presentation of a paper and its publication in the PROCEEDINGS are considered as being separate and distinct matters, there can be no assurance that any or all of the papers presented will appear in print. No copies of the papers in any form are available from the Institute.

Summaries of all papers are included in this issue. They are arranged alphabetically by the names of the authors. When there are two or more authors, the name of the first author determines the position of the summary. All papers are numbered in the order in which they are presented and these numbers are given with the summaries so the placement of each paper may be readily ascertained.

AWARDS

Our two annual awards will be presented this year by President Heising at the luncheon on Thursday, September 21.

The Institute Medal of Honor will be presented to Sir George Lee, recently retired Engineer-in-Chief of the British Post Office for his accomplishments in promoting international radio services and in fostering advances in the art and science of radio communication.

The Morris Liebmann Memorial Prize will be awarded to Harold Trap Friis for his investigations in radio transmission including the development of methods of measuring signals and noise and the creation of a receiving system for mitigating selective fading and noise interference.

EXHIBITION

Our tenth exhibition will be held as part of the convention and will include displays of radio equipment, components, testing and measuring devices, and manufacturing aids. Its location within a short distance of the meeting room makes the educational features of this exhibition of greatest usefulness. Booths will be in charge of exhibitors who will be competent to discuss the engineering aspects of the products displayed.

WOMEN'S PROGRAM

No formal program has been arranged for the women guests as they will, undoubtedly, want to spend most of their time at the Fair. However, there will be some specific programs recommended and infor-

This "Blue and White Garden" is only one of the various "Gardens on Parade."

Gardens on Parade

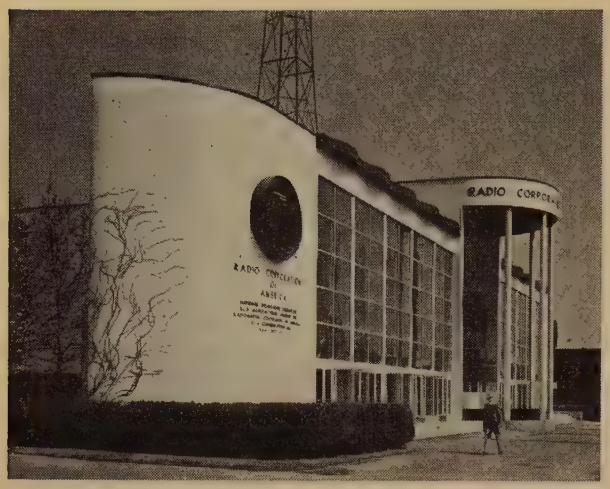

The RCA exhibit portrays that organization's activities in the electrical communications field and includes television demonstrations.

mation and opinions as to what are the most interesting things to be visited at the Fair can be obtained from the Women's Committee.

SUMMARIES OF TECHNICAL PAPERS

6. VESTIGIAL-SIDEBAND FILTER FOR USE WITH A TELEVISION TRANSMITTER

G. H. Brown
(RCA Manufacturing Company, Camden, N. J.)

The television transmission standards adopted by the Radio Manufacturers Association place the carrier of the picture transmitter at a point which is 1.25 megacycles above the lower edge of the 6-megacycle channel, the television receiver characteristic permits reception of the carrier, the upper sideband, and those lower sidebands which lie within 0.75 megacycle of the carrier. Any other lower sidebands which might be transmitted would not be accepted by the receiver and would, therefore, play no part in furnishing picture information. Since these sidebands which are not accepted by the receiver lie outside of the assigned channel, they must be suppressed at the transmitter in order that there may not be any interference caused to other services operating on adjacent channels. This paper describes a filter which has been built for this purpose.

The filter is placed in the transmission line between the power amplifier and the antenna. In order to insure the absence of reflected energy on the transmission line leading to the filter at any frequency generated by the transmitter, the filter is so designed that the input impedance of the filter is practically a constant for both the pass and rejection band while the reactance remains essentially zero.

In order to secure the constant-resistance feature throughout the rejection band, the rejected energy is dissipated in water-cooled resistors of a special type which are of zero reactance and constant resistance throughout the required band.

The equivalent circuit of the filter is shown. Because of the high carrier frequency as well as the extreme selectivity required, the circuit elements are sections of concentric transmission lines. The factors governing the lengths and diameters of these sections are discussed.

The vestigial-sideband filter described here was placed in a practical television installation and has been operating satisfactorily since March, 1939. The tests and observations made at the time of this installation are described.

4. GASEOUS IONIZATION AND SURFACE-CORONA-DISCHARGE DETECTION AT LOW AND HIGH FREQUENCIES

H. A. Brown
(University of Illinois, Urbana, Ill.)

This paper is in part a brief review of past work done on the problem of directly detecting the presence of minute-intensity electrical discharges associated with electrical apparatus or insulating material. The discharges may be either ionization discharges in gaseous voids in insulation or surface corona discharges on insulation or electrical apparatus. Discharge-detection bridges developed for detection of such phenomena at both low or commercial frequencies and for radio frequencies are described. Some data on surface corona on various types of insulation at radio frequencies are presented. Types of electrodes are discussed and a discussion of possible practical application to insulator-support design is outlined. Data of a test on the variation of starting voltage for spacer-insulator surface corona in typical coaxial transmission lines with nitrogen pressure and atmospheric air are given.

18. ENGINEERING ADMINISTRATION IN A SMALL MANUFACTURING COMPANY

C. T. Burke
(General Radio Company, Cambridge, Mass.)

In a company manufacturing measuring instruments, engineering must permeate every company activity. The paper describes the engineering organization and administration of such a company.

Company policies (such as the maintenance of employment stability) affecting the operation of the Engineering Department are outlined and data are given on the relative proportion of engineering and other factors in the total cost of the product.

The method of handling development projects, planning, costs, placing of responsibility, supervision, and engineering are considered.

Engineering relationships with other departments are described with particular attention to the method

of handling production and testing of first lots of a new product.

Since the Sales Department is a division of the Engineering Department, selling methods are also described.

15. CATHODE-RAY TUBES IN AIRCRAFT INSTRUMENTATION

C. W. Carnahan
(Hygrade Sylvania Corporation, Emporium, Penna.)

The present use and future possibilities of cathode-ray tubes as aircraft-instrument indicators are discussed. Emphasis is placed on the advantage of obtaining multiple instrument indications on the screen of one tube. Various circuit means for accomplishing this are outlined.

Improved blind-landing and radio-range systems, making full use of the cathode-ray tube as an indicator, are proposed.

A demonstration will be given.

5. A NEW STANDARD VOLUME INDICATOR AND REFERENCE LEVEL

H. A. Chinn, D. K. Gannett, and R. M. Morris
(Respectively: Columbia Broadcasting System, New York, N. Y.; Bell Telephone Laboratories, Inc., New York, N. Y.; and National Broadcasting Company, New York, N. Y.)

On May 1, 1939, the Bell System, the Columbia Broadcasting System, and the National Broadcasting Company initiated the use of a new standard volume indicator, a new reference volume level, and the term "vu."

Although the new standards directly and immediately affect only the broadcast branch of the communications industry, it is believed that others in the recording, the motion picture, and the general communications field will be interested in and wish to adopt the new volume indicator and new reference level.

The development work which led to the adoption of the new instrument, and its physical and electrical characteristics will be presented together with an explanation of the significance of the new term "vu."

20. ERRORS IN CLOSED-LOOP DIRECTION FINDERS CAUSED BY ABNORMAL POLARIZATION

R. I. Cole
(Signal Corps Laboratories, Fort Monmouth, N. J.)

Bearing errors due to abnormal polarization obtained, using closed-loop direction finders at a frequency of 450 kilocycles, are presented and analyzed. These errors were found not to be directly calculable from theoretical considerations. An empirical formula is presented which permits calculation of bearing errors for any given angle of arrival of the wave front.

10. DEMONSTRATION OF AEROLOGICAL RADIO SOUNDING EQUIPMENT

Harry Diamond, F. W. Dunmore, W. S. Hinman, Jr., and E. G. Lapham
(National Bureau of Standards, Washington, D. C.)

The authors will demonstrate the operation of the radio-sonde equipment in present routine use at some 40 aerological sounding stations of the Weather Bureau, Navy Department, and Coast Guard.

The radio sonde comprises elements for the measurement of barometric pressure, temperature, and humidity, and radio means for remote indication and recording of the values of these factors as the equipment is carried through the troposphere and well into the stratosphere by small rubber balloons.

The information obtained through the routine daily use of a network of radio sounding stations provides data for the more accurate forecasting of weather. The heights reached are from three to four times those possible in upper-air soundings by airplanes, and the regularity of operation and accuracy of measurement are superior. During the first year of operation, some 3500 instruments were used and in the present year the number used will probably total 15,000.

16. A TRUE OMNIDIRECTIONAL RADIO BEACON

E. N. Dingley, Jr.
(Bureau of Engineering, United States Navy Department, Washington, D. C.)

This paper describes a simple apparatus for producing an omnidirectional pattern of radiation in

This is the entrance of the American Telephone and Telegraph Company building, the home of Pedro, the Voder.

which equal amounts of power are radiated simultaneously and continuously in all azimuthal directions but in which the signal radiated on any one aximuth has a characteristic distinguishing it from the signal radiated on all other azimuths. The paper also describes the simple apparatus which may be connected to the audio-frequency output of existing communication receivers and which will continuously indicate the true bearing of the receiver from the omnidirectional beacon. Careful maintenance of antenna tuning or phasing is not required by this system.

19. AIRCRAFT RADIO COMPASSES—PRINCIPLES AND TESTING

R. J. Framme
(Aircraft Radio Laboratory, Wright Field, Ohio)

Standardized methods of testing Army aircraft radio compasses, both in shielded rooms and on aircraft are discussed. A brief introduction describes the

A three-phase million-volt arc plays in Steinmetz Hall at the General Electric exhibit.

application of the radio compass to aircraft and its importance in the Army's instrument landing system. The operation of the left-hand Army aircraft radio compass and the commercial version of the automatic-bearing radio compass is explained. The construction of a transmission line for testing radio compasses is described and formulas for calculating the radio-frequency field strength beneath the line are derived. While these tests are readily adapted to any loop or aural null-type radio compass they are particularly interesting when applied to the antenna-loop radio compass. This equipment requires that two voltages differing in phase by 90 degrees and of different magnitudes be inserted in the loop and antenna. The voltage inserted in the antenna is nondirectional while that inserted in the loop is directional. This is accomplished by the transmission-line test setup and the method has been extensively used for laboratory, factory production, and maintenance tests.

8. SOLAR CYCLE AND THE F_2 REGION OF THE IONOSPHERE

W. M. Goodall
(Bell Telephone Laboratories, Inc., Deal, N. J.)

This paper presents a method of analyzing F_2-region critical-frequency data in a way that shows in a clear-cut manner the correlation that exists between monthly average values of these critical frequencies for undisturbed days and solar activity as measured by the central-zone character figures for calcium flocculi. Curves are presented which show for each month the expected diurnal variation of f^0F_2 for two values of solar activity. Other curves show for a number of different hours the expected values of f^0F_2 at a constant time of day for the same values of solar activity.

23. A WIDE-BAND INDUCTIVE-OUTPUT AMPLIFIER

A. V. Haeff and L. S. Nergaard
(R.C.A. Manufacturing Company, Inc., Harrison, N. J.)

In order to obtain amplification over a wide band of frequencies, a tube having high transconductance and low input and output capacitances is required. A grid-controlled inductive-output tube having these attributes and giving 10 watts output at 500 megacycles is described. A high ratio of transconductance to input capacitance is attained by close cathode-grid spacing and large grid-screen spacing, the latter made possible by use of a very high screen voltage. A low output capacitance is obtained by the use of an inductive output arrangement which requires no power dissipation by the output electrodes. The design of the output circuit for low inherent capacitance is facilitated by the use of magnetic lenses to focus the electron beam. These lenses can be energized by a permanent magnet. Loading caused by secondary electron emission from the current collector is eliminated. The performance of the tube as a wide-band amplifier is described.

25. DEVELOPMENT OF A 20-KILOWATT ULTRA-HIGH FREQUENCY TETRODE FOR TELEVISION SERVICE

A. V. Haeff, L. S. Nergaard, W. G. Wagener, P. D. Zottu, R. B. Ayer, and H. E. Gihring

Part I—Electrical Design

A. V. Haeff, L. S. Nergaard, W. G. Wagener,* and P. D. Zottu†
(RCA Manufacturing Company, Inc., Harrison, N. J.)

The advent of television emphasized the need for a power-amplifier tube capable of delivering kilo-

* Since resigned, now, Heintz and Kaufmann, Ltd., South San Francisco, Calif.

† Since resigned, now, Thermal Engineering Corporation, Atlanta, Georgia.

watts of power into wide-band circuits at carrier frequencies above 40 megacycles. To obtain such power output with wide-band circuits, a low output capacitance and consequently a small anode area are required. The result is high current and high dissipation per unit area. For satisfactory operation at high frequencies, the electron transit-time must be small, necessitating small interelectrode spacings. These requirements are interrelated and in some measure conflicting.

On the basis of an analysis of the above considerations and to meet specific requirements, a tube was designed to deliver 20 kilowatts peak power at 120 megacycles into a circuit of 2 megacycles band width. In order to avoid neutralization difficulties, a cylindrical tetrode design was adopted. To minimize internal coupling and to provide complete isolation of the input and output circuits, the screen was made in the form of a squirrel cage supported at each end of the tube by a radial flange. The two flanges were connected to the external shield. As a result, the screen and shield completely enclose the anode and the tank circuit. The cathode and control grid were supported at opposite ends of the tube to permit independent tuning of grid and cathode circuits. This electrode arrangement makes the tube well suited to operation in a push-pull circuit.

Part II—Construction

R. B. Ayer and P. D. Zottu*
(RCA Manufacturing Company, Inc., Harrison, N. J.)

The mechanical design and construction of the tube to meet the electrical requirements specified in Part I involved problems not usually encountered in power tubes. The high power and high frequency made the elimination of insulating members in the active region imperative. Consequently, the electrodes were supported by the glass work at each end of the tube. The severe thermal conditions required water cooling of the anode, the control-grid support, and the filament leads. The size of the tube ($30\frac{1}{2}$ inches long by $5\frac{1}{2}$ inches in diameter), the close interelectrode spacings, and the necessity of maintaining accurate alignment throughout processing and subsequent use demanded rigid seals, which required the development of special sealing equipment and technique. The exhaust process followed, in general, the usual power-tube procedure.

Part III—Test Equipment and Results

R. B. Ayer and H. E. Gihring
(RCA Manufacturing Company, Inc., Harrison, and Camden, N. J., respectively.)

A push-pull radio-frequency amplifier, designed to operate over a wide range of frequencies beginning at 45 megacycles, was built for testing the tube. Because of the high frequencies involved, special construction of the circuit components was necessary. In order to obtain performance free from parasitics and oscillations at the operating frequency, excellent shielding was found to be imperative.

Since the power output of a television radio-frequency amplifier depends on the transmitted band width (the greater the band width the less the power output will be for a given set of conditions), the tube was tested primarily to determine its suitability as a television amplifier. Because present activity is centered on the lower-frequency television channels, the tests were made at representative frequencies below the one originally contemplated.

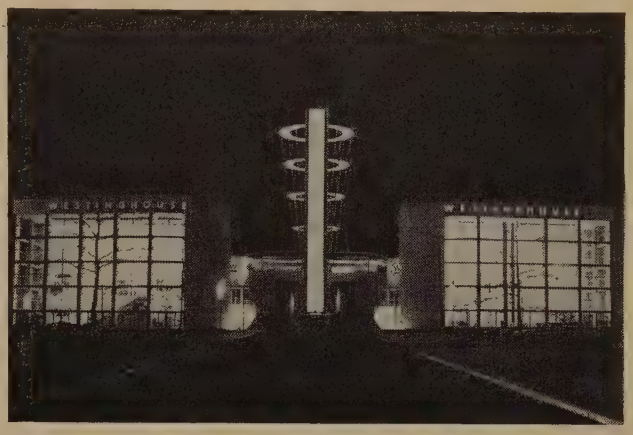

"The Singing Tower of Light" is flanked by the two halves of the Westinghouse structures.

It was found that at 77 megacycles a peak power of 57 kilowatts for two tubes was obtainable for a total band width of approximately 2 megacycles. This value is in agreement with the prescribed output of 40 kilowatts at 120 megacycles. Since the recently standardized channel for television transmission requires a band width greater than 2 megacycles, performance data at 56 megacycles with a band width of approximately 8 megacycles have been taken and a peak power of 40 kilowatts obtained.

12. HIGH-SPEED MULTIPLEX SYSTEM FOR LOADED SUBMARINE CABLES

H. H. Haglund and A. W. Breyfogel
(Western Union Telegraph Company, New York, N. Y.)

This paper describes a high-speed multiplex telegraph system operating over a loaded submarine transatlantic cable, and more particularly the use of the Thyratron as a circuit element. Since the system comprises electronic, mechanical, and electromechanical elements which function in harmony, the paper deals with the signaling system as a whole. Enough multiplex printing-telegraph theory is included to make clear the function of the Thyratron tubes in their circuits.

* Since resigned, now, Thermal Engineering Corporation, Atlanta, Georgia.

In order that the exacting requirements of the Thyratron as a circuit element can be fully appreciated, reference is made to the loaded cable, its attenuation, and time-phase characteristics as compared with those of a nonloaded cable. The problems of signal shaping and signal amplification are described and the Thyratron is shown in its important applications of phase correction, signal selection with signal interpolation, and earth-current correction at the main repeater points.

26. PRODUCTION ALIGNMENT APPARATUS FOR TELEVISION RECEIVERS

L. J. Hartley
(General Electric Company, Bridgeport, Conn.)

The paper deals with apparatus used in the Bridgeport plant of the General Electric Company. A brief outline will be given of the general plan of operation of the apparatus, then the paper will proceed to a more detailed discussion of the unusual features of the installation, including data on the production and utilization of special alignment signals.

24. SUPERHETERODYNE FIRST-DETECTOR CONSIDERATIONS IN TELEVISION RECEIVERS

E. W. Herold
(RCA Manufacturing Company, Inc., Harrison, N. J.)

The process of frequency conversion which is accomplished in the early stages of a superheterodyne receiver is essentially one of small-percentage modulation of a local-oscillator frequency by the incoming signal. There are three methods of operation of vacuum tubes whereby such modulation may be carried out. In the first, signal and oscillator voltages are impressed on the same electrode of the tube and modulation occurs by virtue of curvature of the tube characteristic. In the other two methods, signal and oscillator voltages are placed on different electrodes: these two methods are differentiated by whether the oscillator electrode precedes or follows the signal electrode along the direction of electron flow. Curvature of the tube characteristic is not a requirement for the latter two modes of operation.

Considering three different tubes built around identical cathodes and each designed for one of the three types of modulator operation, it will be shown how they differ in signal-to-noise ratio, gain, input conductance at high frequencies, interaction of oscillator circuit on signal circuit, and ease with which the function of a local oscillator tube can be included in the same mount. For television receivers in which no radio-frequency stage precedes the first detector, the order of importance of these characteristics is approximately as named. For receivers in which an adequate radio-frequency stage is used, however, the order of importance is approximately reversed. At present, most receivers do not fall in the latter class so that this paper is concerned chiefly with evaluating the characteristics of the three types of modulators for use as the first tube in a television receiver. From this point of view, modulators designed for operation with oscillator and signal voltages on the same electrode are advantageous. Practical data will be given showing the signal-to-noise ratios and operating characteristics of available tube types.

Suggestive of milady's powder box is the design of the Coty Building.

9. ATTENUATION OF HIGH FREQUENCIES OVER LAND AT SHORT RANGES

John Hessel
(Signal Corps Laboratories, Fort Monmouth, N. J.)

An investigation was made of the rate of attenuation of frequencies between 1.5 and 80 megacycles at distances up to 10 miles over land. The results indicate increasing attenuation with frequency up to about 4 megacycles and nearly constant attenuation from 4 to 80 megacycles. Greater attentuation is found in daylight than at night on frequencies below 12.5 megacycles. The variation of signal strength with distance may be expressed by an inverse power equation, the signal varying inversely as the nth power of the distance. The value of n is approximately 2.3 for frequencies between 4 and 80 megacycles. Comparison of the data with Sommerfeld's equations shows that the variation of attenuation with frequency may be predicted, but that the measured attentuation is greater than predicted, particularly in the daytime.

22. TRANSIENT RESPONSE IN TELEVISION

H. E. KALLMANN

(Formerly of Electrical and Musical Industries, Ltd., in collaboration with R. E. Spencer and C. P. Singer, Electrical and Musical Industries, Ltd., Hayes, Middlesex, England.)

Transient-response curves, representing the output voltage of amplifiers when an infinitely steep transient of unit height is applied to their input, are taken as criterion for the quality of television amplifiers. Nearly 70 sheets of accurately calculated curves are presented, allowing comparison as well as design of single and cascaded stages of electrical and of ideal networks. Transient response is valued according to (1) transition time Tr from 10 to 90 per cent of the final height, measured in radians of the nominal cut-off frequency; (2) amount (and duration and frequency) of the overswing or recoil in per cent of height. For many cases, amplitude and time-delay response curves are plotted as well to allow correlation of their features.

Part I deals with the transient response of single filters, proceeding from the shunt-peaking coil and the series-peaking coil (as representative of staggered circuits and band-pass systems in carrier amplification) to filters with split capacitances and capacitive-terminated filters without and with m-derived sections. Their relative efficiency $H=C\cdot R/Tr$ and their overswing are given for numerous values of $Q=(1/R)\sqrt{L/C}$, thus supplying design data for many cases. It is shown which, if any, improvements are possible with complicated filters, and that flat time response and steadily dropping amplitude response correspond to the most desirable transient response. The use of low-pass filters as carrier amplifiers is discussed.

Part II describes the deterioration of transients in cascades of equal or different, electrical or ideal, filter systems. The tendency of transients is shown to take on certain ultimate shapes after passage through many stages of phase-true filters. A stretch modulus s is derived which gives the increase in Tr each time the number of stages is double; s is 1.41 for all filters in which the overswing is small and neither rising nor decreasing in repetition; $s<1.41$ for all filters in which the overswing grows; $s>1.41$ when the shape of the transient is progressively rounded. The total gain V_{total} is shown to pass through an early maximum and then to decrease if stages are added but the over-all value of Tr is maintained. The amount of this loss caused by large numbers n of coupling circuits is plotted from $V_{\text{total}}/V_0{}^n=n^{-n/2}$; dodges are described to reduce these considerable losses, e.g., by insertion of "cathode follower" stages or the use of staggered circuits in carrier amplification where they are shown to be superior to band-pass systems.

Part III describes a family of ideal transitions of uniform stretch their even cases corresponding to ideal filters with flat time response and steadily dropping amplitude response and representing the ultimate shapes of transients in filter cascades. These transitions maintain their shape when cascaded and stretch uniformly with a stretch modulus $s=\sqrt[n]{2}$ for the nth case. Their first member, $n=2$, $s=1.41$ is identical with the ERF function which has no overswing, their last member $n=\infty$, $s=1$, is the Si function, known as the transient response of the low-pass filter with infinitely sharp cutoff. Intermediate cases and their combinations supply a ready means to predict s from the steepness of the amplitude response if the time response is assumed to be corrected. The amplitude response of a television channel with which to obtain the most suitable shape of transient response for a given band width is derived; the effect of further band-width trimming is shown.

These twin prows dominate the entrance to the Marine Transportation Building.

In Part IV various procedures are demonstrated to synthetize well-shaped transient-response curves by cascading simple electrical filters and, in more complicated cascades, by manipulating the time-delay curve, e.g., by addition of a phase-correcting stage (a circuit derived from the "cathode follower").

Part V treats the transient response of single-sideband systems. Families of transition curves are plotted for various shapes and cutting slopes of phase-true sideband-suppressing filters. The resulting deformation of the transients is shown to rise with the ratio band width/cut width and with the depth of modulation. The limits for tolerably little distortion are found and the unpromising possibilities of suppressing this type of distortion discussed.

3. THE CORNER REFLECTOR

J. D. KRAUS

Ann Arbor, Mich.

A beam antenna is described which consists essentially of a driven element and a reflector constructed of two flat sheets which meet at an angle

forming a corner. The driven antenna is placed parallel to the corner and equidistant from the flat sheets.

The corner reflector is compared with the parabolic type of reflector. The single, flat, sheet reflector is also discussed and is considered as a special case of the corner reflector.

An analytical method is developed for predicting the performance of various types of corner reflectors. The effect of variations in corner angle, antenna-to-corner spacing, losses, etc., on the power gain and beam width of the antenna are discussed. Curves illustrating these effects, as computed by the above method, are given and are compared with experimental results. Factors involved in the design of both solid-sheet reflectors and those of the grid type are also treated.

20. FUNCTION OF ELECTRON BOMBARDMENT IN TELEVISION

I. G. Maloff

(RCA Manufacturing Company, Inc., Camden, N. J.)

Electron bombardment performs two very important functions in television. In the television transmitter electron bombardment translates variations in brightness into electrical signals. In the television receivers it converts the electrical signals into variations in brightness. The paper outlines and discusses these functions from an engineering angle.

In the pickup tube (iconoscope) electrons fall upon an insulated metal mosaic charged by the incident light. The continuous discharge of the mosaic is accomplished through the medium of secondary emission and is accompanied by several major and minor effects, all affecting the main function of bombardment at the transmitter, the conversion of light into an electrical signal. Among the accompanying effects are redistribution of the secondaries, rate of their collection, charges on the mosaic and glass, saturation of the mosaic, space charge, etc. These factors are treated functionally and also quantitatively and are illustrated by examples taken from specific cases encountered in practice.

In the receiving tube (kinescope) electrons fall upon a luminescent dielectric, exciting its fluorescence and phosphorescence, heating the material and glass, and giving rise to secondaries which are scattered and finally gathered by the collectors. The secondary electron emission determines the potentials and energy losses of the electrons in various stages of their travels. The potentials and energy losses determine the efficiency of the main function of the electron bombardment at the receiver; transformation of electrical energy into light. The above effects are discussed and quantitative as well as functional relations between essential factors are given for specific cases encountered in practice.

2. MEDIUM-POWER MARINE RADIOTELEPHONE EQUIPMENT

J. F. McDonald

(Radiomarine Corporation of America, New York, N. Y.)

Now that radiotelephone harbor stations are in operation along the principal coastal cities of the United States, owners of yachts and commercial ships are equipping their vessels with two-way radiotelephone apparatus to provide ship-to-shore and intership communication.

Many interesting problems are presented in the design of shipboard radiotelephone equipment in order to permit operation by nontechnical personnel.

The equipment described in this paper comprises a 75-watt, 10-frequency transmitter, and a 10-frequency superheterodyne receiver with crystal control for the transmitting and receiving frequencies. Voice-operated relays provide automatic transfer of the circuits to suppress the carrier when receiving and to energize the transmitter when talking. Automatic calling apparatus designed to ring a bell aboard the vessel upon receipt of coded two-tone calls from the harbor stations is also provided.

1. A SINGLE-SIDEBAND MUSA RECEIVING SYSTEM FOR COMMERCIAL OPERATION ON TRANSATLANTIC RADIOTELEPHONE CIRCUITS

F. A. Polkinghorn

(Bell Telephone Laboratories, Inc., New York, N. Y.)

In the operation of short-wave radiotelephone circuits selective fading is observed which is a result of the combination at the receiving antenna of waves which have arrived from the transmitter over paths of different length. The poor quality resulting from this fading may be mitigated by increasing the directivity of the receiving antenna in the vertical plane so as to favor the waves arriving at one angle to the exlcusion of others. Friis and Feldman have described an experimental system designed to accomplish this end which they called a "Musa" receiving system. This system was found under certain transmission conditions to give an improvement in the grade of circuit which could be obtained. A commercial installation of this type has now been constructed for use on the single-sideband circuits of the American Telephone and Telegraph Company to England.

The antenna system consists of a row of 16 rhombic antennas 2 miles long, each antenna connected by a separate transmission line to receivers located near the center of the antennas. In each receiver the signals from the antennas are combined in the proper phase to permit simultaneous reception from 3 adjustable vertical angles. The 3 signals are then added through delay equalizing circuits to obtain diversity reception. A fourth-branch receiver has its

vertical angle of reception continuously varying and is used to set automatically the angles of reception of the 3 diversity branches. The delay equalization is also automatically adjusted. A recorder is provided which continuously registers the relative signal with variation of vertical angle of reception.

Two receivers have been provided in the initial installation for the operation of 2 radiotelephone circuits to England.

13. ELECTRONIC-WAVE THEORY OF VELOCITY-MODULATION TUBES

Simon Ramo
(General Electric Company, Schenectady, N. Y.)

Following a discussion of the Hahn small-signal theory of velocity modulation in which the basic performance of velocity-modulation tubes is explained by means of space-charge waves propagating along the electron beam in its drift tube, the theory is reformulated by means of the retarded scalar electric and magnetic vector potentials. The use of the potential functions is believed to lead to sufficient simplification to merit consideration in choosing the best attack on the theory. The theory is valid for the very high magnetic focusing fields used in practical tubes.

The electronic-wave concept is clarified by a description of the types of space-charge waves which theoretically may propagate along an electron beam. The beam, in its shielding, coaxial, conducting cylinder is seen to serve as a medium in which waves of various types may be excited by the input voltage, after which they will propagate down the drift tube with beneficial change, finally serving to induce an output current in the output circuit. The waves are seen to occur in pairs, one wave of each pair having a velocity somewhat less than that of the beam while its mate travels somewhat faster than the beam. Present methods of starting and utilizing the waves are shown to favor one particular pair of waves of the infinite series that are possible.

It is shown how this pair of space-charge waves is excited by an input voltage across a gap in the shielding drift tube surrounding the beam. The process of conversion from velocity modulation in the waves to conduction-current modulation as the waves propagate away from the input gap is made clear. Numerical results are given for a special case to illustrate the computation of optimum drift-tube length and transconductance by the wave theory.

14. ON DIFFRACTION AND RADIATION OF ELECTROMAGNETIC WAVES

S. A. Schelkunoff
(Bell Telephone Laboratories, Inc., New York, N. Y.)

Inasmuch as it is rarely possible to treat diffraction and radiation of electromagnetic waves exactly, the Kirchhoff formulation of Huygens' principle has been frequently used in approximate calculations. There are cases, however, in which the errors involved in the results are very much in excess of the magnitudes that might have been expected. A critical examination of the Kirchhoff formula shows that under some circumstances there is no way, at least at present, to tell beforehand whether the results obtained with its aid will be fairly satisfactory or grossly inaccurate. The "Equivalence Principle," although from a purely mathematical point of view analogous to the Kirchhoff formula, is free from the above objection and can, therefore, be recommended for the approximate treatment of diffraction and radiation of electromagnetic waves. Another approach to these problems is furnished by the "Induction Theorem."

A further examination of the Kirchhoff formula brings out the fact that contrary to the usual belief the formula is not a mathematical expression of Huygens' principle. It appears that Maxwell's equations do not imply unambiguously any precise form of Huygens' principle and the latter must be framed as a separate postulate.

7. A CATHODE-RAY FREQUENCY-MODULATION GENERATOR

R. E. Shelby
(National Broadcasting Company, New York, N. Y.)

The theory and construction of a new type of electron modulator for frequency modulation is described.

This method of producing frequency modulation is fundamentally sound and appears to possess certain inherent advantages not possessed by other methods.

The fundamental principle involves the use of an electron gun and an anode or target of such configuration that the voltage fluctuations applied to one or more elements of the tube are translated into frequency or phase modulation in the anode circuit.

11. A PARALLEL-T CIRCUIT FOR MEASURING IMPEDANCE AT RADIO FREQUENCIES

D. B. Sinclair
(General Radio Company, Cambridge, Mass.)

The necessary conditions for zero transmission in double-T and bridged-T circuits have already been analyzed and presented.[1] An instrument embodying a special circuit that is particularly well adapted for use as a null method of impedance measurement is described.

In this circuit the driving oscillator, the variable condenser used for reactive balance, the variable condenser used for resistive balance, the unknown

[1] W. N. Tuttle, "Bridged-T and parallel-T null circuits for measurements at radio frequencies," Presented, Thirteenth Annual Convention, June 16, 1938.

impedance to be measured, and the null detector all have one side grounded. Troubles arising in bridges from circuits that are balanced to ground are therefore avoided.

The use of variable air condensers for resistive as well as reactive balances extends the range of accurate resistance measurement to frequencies of the order of 30 megacycles. Careful design of the variable condenser used for the reactive balance results in a reduction in effective inductance of about 16:1 from that of standard models.

The new circuit measures unknown impedances in terms of their parallel components. The dial for the reactive balance is direct reading in micromicrofarads. The dial for the resistive balance is direct reading in micromhos at 1, 3, 10, and 30 megacycles. At other frequencies a simple multiplying factor must be used. The over-all frequency range of the instrument is normally from 500 kilocycles to 30 megacycles.

17. BASIC ECONOMIC TRENDS IN THE RADIO INDUSTRY

JULIUS WEINBERGER

(Radio Corporation of America, New York, N. Y.)

This paper considers the American radio industry from the standpoint of its long-time economic trends, with special reference to the past and probable future public demand for broadcast receivers and vacuum tubes. The history of the annual sales to each of the various markets for these is analyzed, equations are given for their long-time growth trends, and estimates of growth are projected ahead to 1947. Conclusions are stated regarding the probabilities of changes in the nature of the demand for initial and replacement receivers in the form of primary, secondary, automobile, and export receivers, and for vacuum tubes for initial equipment or replacement purposes.

• • • •

Electronics Conference

An informal conference on the advanced problems of ultra-high-frequency electronics, electron optics, and the problems of noise in electronic devices will be held under auspices of the Institute at Stevens Institute of Technology, Hoboken, New Jersey, on October 20 and 21, 1939. Requests for reservations should be addressed to the Secretary.

Membership

The following indicated admissions to membership have been approved by the Admissions Committee. Objections to any of these should reach the Institute office by not later than September 30, 1939.

Admission to Associate (A), Junior (J), and Student (S)

Bailey, R. E., (A) Box 736, Blacksburg, Va.

Bartlett, D. S., (A) R.F.D. 2, Box 723, Edmonds, Wash.

Bateman, A. W., (S) 1373 E. Walnut St., Decatur, Ill.

Brar, S. S., (S) Route 1, Box 64, Clovis, Calif.

Brown, W. N., Jr., (S) 11 Royce Rd., Allston, Mass.

Chopra, H., (A) Wireless Department, Port Commissioners, Rangoon, Burma.

Christensen, A., (S) 2121 N. Harlem Ave., Chicago, Ill.

Cook, W. A., (A) Misiones 48, Buenos Aires, Argentina.

De Fonseka, D. R. H., (A) "Sri Mahal," King St., Kandy, Ceylon.

Eng, W., (S) 409 Harrison St., West Lafayette, Ind.

Ferry, T. R., (S) 616-47th St., Oakland, Calif.

Fortman, K. F., (A) 1573 Waverly, Detroit, Mich.

Foulon, F., (A) 547 N. Sierra Bonita Ave., Los Angeles, Calif.

Grant, F. W., (A) Calle Tacuari 471, 7 Piso, "B," Buenos Aires, Argentina.

Gray, R. O., (S) 611 E. 88th Pl., Chicago, Ill.

Gurrea, A., (A) Cabildo 2505, Buenos Aires, Argentina.

Haley, S. C., (A) 22 Bowers St., Newtonville, Mass.

Hoffman, H. W., (A) 148-20-89th Ave., Jamaica, L. I., N. Y.

Hollmann, H. E., (A) Mittelstrasse 23, Berlin-Lichterfelde, Germany.

Hornby, F. R., (A) 27 Towers Rd., Hatch End, Middx., England.

Hsu, C. P., (S) California Institute of Technology, Pasadena, Calif.

Huckell, N. R., (A) c/o Australia House, The Strand, London W.C. 2, England.

Kamen, I., (A) 710 W. 173rd St., New York, N. Y.

Kurita, M., (A) c/o Nippon Hoso Kyokai Gijutsu Kenkyujo, 440 Kamatacho, Setagaya-Ku, Tokyo, Japan.

Lange, W. W., (A) 6728 N. Campbell Ave., Chicago, Ill.

Logan, M. F., (A) 35 E. Lorain St., Monroe, Mich.

Main, F. S., (A) c/o Box 4588, Johannesburg, South Africa.

Mason, L. D., (A) U. S. Airway Communication Station, Box 497, Great Falls, Mont.

Mehra, R. N., (A) H.M.I. Wireless Station, Mahul, c/o Navy Office, Bombay, India.

Nadosy, A., (A) Florida St. 1065, Buenos Aires, Argentina.

Nichols, N. R., (A) Radio Station KSRO, Santa Rosa, Calif.

Nicoll, F. H., (A) RCA Manufacturing Company, Inc., Camden, N. J.

Orem, E. A., (J) 109 2nd Ave., Brooklyn Park, Baltimore, Md.

Phillipson, N. G., (A) 336 W. 31st St., New York, N. Y.

Pollock, H. S., (A) 471 Earl St., Kingston, Ont., Canada.

Pound, J. P., (A) c/o Barclays Bank Ltd., Budleigh, Salterton, Devonshire, England.

Preiser, G. W., (A) Conesa 840, Buenos Aires, Argentina.

Rado J. A., (A) 147-15 Northern Blvd., Flushing, L. I., N. Y.

Riordan, N. F., (A) 412 S. Kenosha Ave., Tulsa, Okla.

Roberts, W. K., (S) 226½ Florida Ct., Gainesville, Fla.

Ross, C. G., Jr., (A) Pretoria Technical College, Church St., Pretoria, Transvaal.

Rountree, J. G., Jr., (A) 1521 N. Sylvania, Fort Worth, Tex.

Samarawickrama, D. A., (A) 126 Galle Rd., Mount Lavinia, Ceylon.

Seward, G. H., (A) 765 Gower St., Hollywood, Calif.

Stewart, H. E., (A) 714 W. Moreland St., Phoenix, Ariz.

Stuber, R., (A) c/o Brown Brothers Harriman & Company, 59 Wall St., New York, N. Y.

Theisen, J. L., (A) 1462 Van Cortlandt St., Schenectady, N. Y.
Tringham, W. S. L., (A) Administracion General de Correos, Lima, Peru.
Tuli, A., (A) Pasaje El Domador 3159, Buenos Aires, Argentina.
Turitzin, N. M., (S) 217 N. Ingallo, Ann Arbor, Mich.
Weis, C. L., Jr., (A) c/o Bell Telephone Laboratories, Inc., 180 Varick St., New York, N. Y.
Williams, R. H., (A) Snoqualmie, Wash.
Yo, E., (A) Broadcasting Corporation of Japan, 440 Kamata-cho, Setagayaku, Tokyo, Japan.

Books

BBC Handbook 1939

Published by the British Broadcasting Corporation, Broadcasting House, London, W.1., England. 176 pages, $4\frac{3}{4}$ inches by $7\frac{1}{4}$ inches. Price 2 shillings.

This is a yearbook covering the activities of the British Broadcasting Corporation during the year 1938.

About half of the book consists of a very informative "Reference Section." This describes the sources of revenue and nature of expenditures of the Corporation, outlines the work of its engineering, program, and other divisions and gives statistics as to listeners, programs, and various other operating matters.

The other half of the book consists of special articles. Those which are likely to be of particular interest to persons in other countries are the sections entitled: "Broadcasting and the Crisis," "Television in 1938," "Broadcasting Links with the New World," "Broadcasting and Education," and "The Wavelength Problem."

Among the illustrations are pictures of studios and broadcast stations operated by the British Broadcasting Corporation and pictures showing the origin or production of a number of the year's outstanding programs.

L. E. Whittemore
American Telephone and Telegraph Co.
New York, N.Y.

Electrolytic Condensers, by Philip R. Coursey.

John F. Rider, publisher, 404 Fourth Ave., New York, N.Y. 172 pages. $5\frac{1}{2}\times8\frac{1}{2}$ inches. Price $3.00.

This book takes up the properties, design, and practical uses for the electrolytic type of condensers. If the process of manufacturing any item used in the assembly of radio receivers is receiving attention of late it is the electrolytic condenser if anyone can judge by the amount of data appearing about it.

The constructional forms and process, as used in Great Britain, are generally surveyed, and the operating characteristics of various types are taken up quite thoroughly, at least from the viewpoint of the layman. For the condenser expert the technical processes disclosed are of interest, but it is to be regretted that the most recent developments are presented only (to quote from the Preface) "in so far as for commercial reasons it is practicable to reveal them."

However, the book presents many interesting types of construction and condenser applications which are of general interest, not only in the radio fields but as to the many industrial uses to which large capacitors are used.

The book is complete with 112 illustrations of constructional processes and reproductions of characteristic curves of both the wet and semidry forms.

The author has long been an outstanding authority in the condenser field, and is also the author of the book "Electric Condensers." He is the Technical Director of the Dubilier Condenser Co., Ltd., of London.

R. R. Batcher
Hollis, L.I., N.Y.

Ultrasonics and their Scientific and Technical Applications, by Ludwig Bergman. Translated from the German by H. Stafford Hatfield.

Published by John Wiley and Sons, Inc. 440 Fourth Avenue, New York. 264 plus 8 pages. $5\frac{3}{4}\times8\frac{3}{4}$ inches. Illustrated. Price $4.00. Originally published, under the title *Ultraschall*, by VID-Verlag, Berlin.

The extension of the usable frequency range of electromagnetic oscillations to higher and higher frequencies has been rivaled by a similar extension of the range of mechanical vibrations. In fact it is now possible to produce, measure, and utilize mechanical vibrations having frequencies once thought to be high for electrical waves. The applications which have been made of these high-frequency vibrations indicate, by their very diversity, that they have a utility which should not be overlooked by any worker in applied physics. For such workers Dr. Bergman's book will be of great value.

The term "Ultrasonics" has recently been generally adopted as the designation for mechanical vibrations of higher frequency than those which are audible to the human ear. The term "Supersonics," formerly applied to these vibrations by some writers, is now commonly understood to designate mechanical vibrations associated with great energy. At the moment the ultrasonic range extends from 20 kilocycles per second, where it begins by definition, to somewhere in the neighborhood of 500 megacycles per second.

In his book Dr. Bergman, who is Professor of Physics at the University of Breslau, has collected and organized, in a thorough and well-balanced manner, the fundamental information relating to ultrasonics which forms the background for their utilization. Beginning with brief descriptions of the historically important ultrasonic generators, the first chapter deals with the various methods of producing high-frequency mechanical vibrations. These are considered under the headings of mechanical, thermal, magnetostrictive, and piezoelectric generators. This chapter brings out clearly the fact that, although the fundamental relations of mechanically vibrating systems hold without modification throughout the ultrasonic range, the quantitative values which are found at the upper end of the range bring about behaviors which are far from our familiar experience. Displacements are microscopic; velocities are enormous; accelerations are unbelievable.

The second chapter discusses the detection of ultrasonic waves and the measurement of their frequencies and amplitudes. Measuring methods are to be found in each of the major subdivisions of physics; namely, mechanical, thermal, electrical, and optical. This universality suggests the breadth of utility inherent in ultrasonic techniques.

The remainder of the book is devoted to the applications which have already been made of ultrasonic mechanical vibrations. Two chapters are given to its use in the determination of the important physical constants forming the basis of acoustics. The final chapter outlines applications of more utilitarian nature. The list of applications which have already become definitely established is impressive. It includes short-range communication and subaqueous signaling, the stabilization of the frequency of electrical waves, the accurate measurement of time, particularly of short intervals, and the very interesting method of scanning in television reception known as the Scophony system. The use of ultrasonics also opens new fields to both the chemist and the biologist.

Although it is a relatively short book Dr. Bergman's "Ultrasonics" includes all of the fundamental theory necessary for a general survey of the subject. It contains many valuable tables of those physical constants which are particularly significant to this technique. For the student who wishes to investigate more intensively some restricted phase of ultrasonics there is a most complete bibliography, which adds greatly to the value of the book. This bibliography contains 483 references taken from the original German text, and covering publications prior to its appearance in 1937. There are also 92 references to subsequent publications which have been added to the English edition by the translator.

J. Warren Horton
Massachusetts Institute of Technology
Cambridge, Massachusetts

Contributors

GEORGE H. BROWN

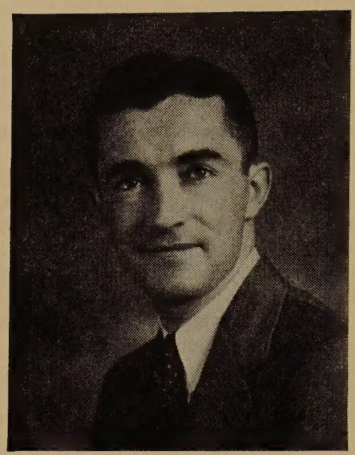

W. H. DOHERTY

ANDREW V. HAEFF

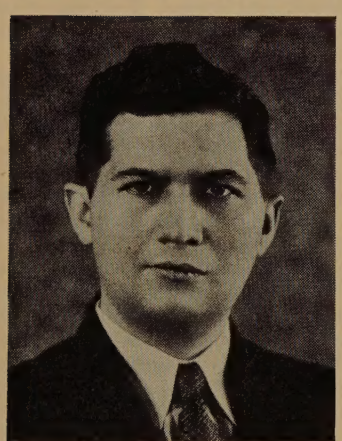

W. H. HICKOK

R. B. JANES

George H. Brown (A'30) was born October 14, 1908, at North Milwaukee, Wisconsin. He received the B.S. degree from the University of Wisconsin in 1930, the M.S. degree in 1931, and the Ph.D. degree in 1933. From 1930 to 1933 Dr. Brown was a Research Fellow in the Electrical Engineering Department of the University of Wisconsin, and since 1933 he has been in the Research Division of the RCA Victor Division of the RCA Manufacturing Company. He is a member of Sigma Xi and the American Association for the Advancement of Science.

❖

W. H. Doherty (A'29–M'36) was born at Cambridge, Massachusetts, on August 21, 1907. He received the S.B. degree in electric communication engineering from Harvard University in 1927 and the S.M. degree in engineering in 1928. Mr. Doherty was a technical employee in the Long Lines Department of the American Telephone and Telegraph Company in 1928; research associate, Radio Section, National Bureau of Standards from 1928 to 1929; and member of the technical staff of Bell Telephone Laboratories, 1929 to date. In 1937 he received the Morris Liebmann Memorial Prize.

❖

Andrew V. Haeff (A'34) received the degree of Electrical and Mechanical Engineer from the Russian Polytechnic Institute at Harbin, China, in 1928. That same year he came to the United States and majored in electrical engineering at the California Institute of Technology where he obtained his M.S. degree in 1929 and his Ph.D. degree in 1932. During 1932–1933, Dr. Haeff was a special Research Fellow in the Electrical Engineering Department of the California Institute of Technology, engaging in research work on ultra-high-frequency problems. In 1934 he joined the RCA Manufacturing Company where he is working in the same field.

❖

W. H. Hickok (A'37) was born on June 21, 1907, at Chenango Forks, New York. He received the B.S. degree from Wesleyan University in 1929. Since 1930 he has been doing research and development work at the RCA Manufacturing Company.

❖

R. B. Janes (A'37–M'39) was born in Burlington, Massachusetts, on February 2, 1909. He received the B.S. degree from Kenyon College in 1928, and from 1928 to 1929 he was a graduate student at Harvard University. From 1929 to 1931 he was an instructor in physics at Colgate University and from 1931 to 1935 he was a research assistant in physics at the University of Wisconsin, where he received his Ph.D. degree in 1935. Since 1935 Dr. Janes has been doing research and development work at the RCA Manufacturing Company.

❖

George A. Morton (A'35) was born on March 24, 1903, at New Hartford, New York. He received the B.S. degree in elec-

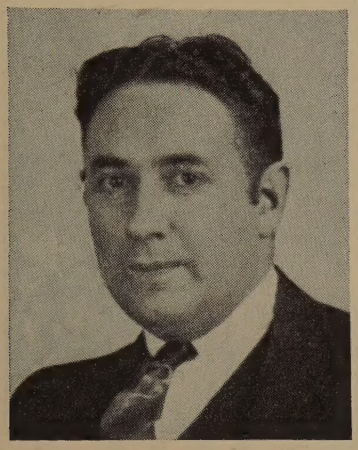

GEORGE A. MORTON

LEON S. NERGAARD

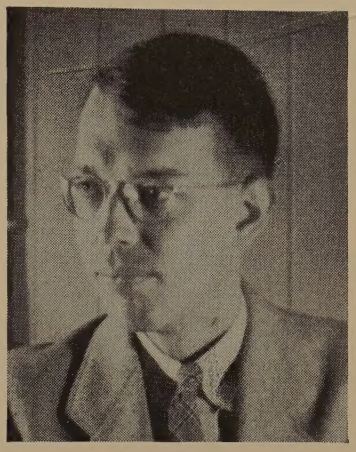

WINSLOW PALMER

trical engineering from the Massachusetts Institute of Technology in 1926, the M.S. degree in 1928, and in 1932 the Ph.D. degree in physics. From 1926 to 1927 Dr. Morton was in the Research Laboratory of the General Electric Company, and from 1927 to 1933 he was a research associate and instructor at the Massachusetts Institute of Technology. Since 1933 he has been in the Electronics Research Laboratory of the RCA Manufacturing Company, RCA Victor Division. He is a member of the American Physical Society.

❖

Leon S. Nergaard (A'29–M'38) was born at Battle Lake, Minnesota, on September 2, 1905. He received the B.S. degree in electrical engineering from the University of Minnesota in 1927, the M.S. degree from Union College in 1930, and the Ph.D. degree from the University of Minnesota in 1935. From 1927 to 1930 Dr. Nergaard was in the Research Laboratory and Vacuum-Tube Engineering Department of the General Electric Company; from 1930 to 1933 he was a teaching assistant in the department of physics at the University of Minnesota, and since 1933 he has been in the Research and Development Laboratory of the RCA Manufacturing Company, RCA Radiotron Division. He is a member of Sigma Xi and the American Physical Society.

❖

Winslow Palmer (S'38) was born on July 8, 1912, at New Brunswick, New Jersey. He received the B.S. degree in physics and mathematics from the University of Hawaii in 1937, and since that time he has been a gradeate student at Stanford University.

❖

Jan A. Rajchman was born in London, England, on August 10, 1911. He received a diploma of electrical engineering in 1934 and the degree of Doctor of Technical Sciences in 1938 from the Swiss Federal Institute of Technology at Zurich, Switzerland. Dr. Rajchman was a student engineer at the RCA Manufacturing Company in 1935 and since 1936 he has been a research engineer.

❖

Simon Ramo (A'38) was born in 1913 at Salt Lake City, Utah. He received the B.S. degree at the University of Utah and a Ph.D. degree at the California Institute of Technology where he held a teaching fellowship. Since graduation he has been employed by the General Electric Company as a supervisor in their advanced course in engineering and in high-frequency research.

❖

Albert Rose (A'36) was born at New York, New York, on March 30, 1910. He received the A.B. degree from Cornell University in 1931 and the Ph.D. degree in physics in 1935. From 1931 to 1934 he was a teaching assistant at Cornell University, and since 1935 he has been a research engineer in the Research and

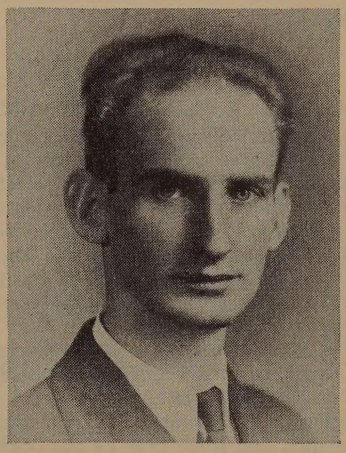

JAN A. RAJCHMAN

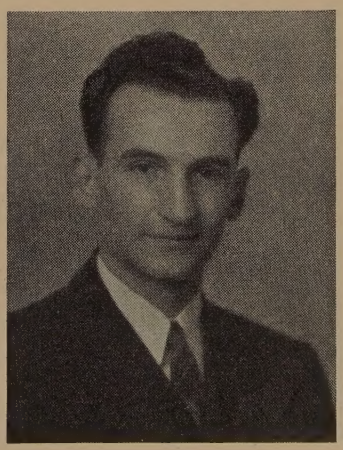

SIMON RAMO

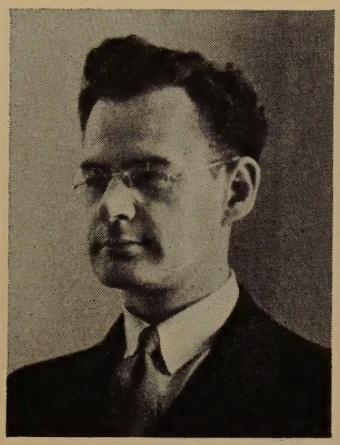

ALBERT ROSE

BERNARD SALZBERG

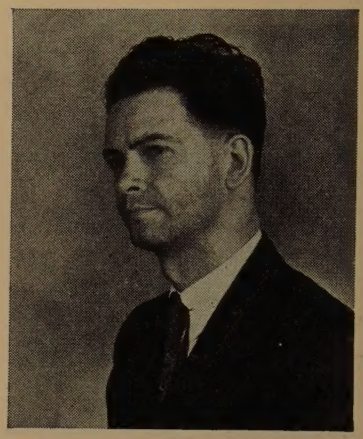

ORRIN W. TOWNER

Engineering Department of the RCA Manufacturing Company, RCA Radiotron Division. Dr. Rose is a member of Sigma Xi.

❖

Vladimir K. Zworykin (M'30–F'38) was born in 1889 in Russia. He received the E.E. degree from the Petrograd Institute of Technology and later studied physics under Professor Boris Rosing and started his first experiments in television. In 1912 Dr. Zworykin entered the laboratory of the College de France in Paris to do X-ray research under Professor P. Langevin. During the World War he served as an officer in the Radio Corps of the Russian Army. From 1920 to 1929 he was in the Research Laboratory of the Westinghouse Electric and Manufacturing Company, and since 1929 he has been in the Research Laboratory of the RCA Manufacturing Company, RCA Victor Division, working on television, electron optics, photoelectric cells, and allied problems. In 1926 he received the Ph.D. degree from the University of Pittsburgh and in 1938 the D.Sc. degree from Brooklyn Polytechnic Institute and the Overseas Premium from the Institution of Electrical Engineers (British). He received the Morris Liebmann Memorial Prize in 1934.

❖

Bernard Salzberg (J'25–A'30–M'38) was born on July 22, 1907. He received the E.E. degree in 1929 and the M.E.E. degree in 1933 from Polytechnic Institute of Brooklyn, Mr. Salzberg was with the Brooklyn Edison Company from 1923 to 1925 and the summers of 1926 and 1927; the Fada Radio Company during the summer of 1928; and RCA Communications from 1929 to 1931. Since 1931 he has been in the Research and Engineering Department of the RCA Manufacturing Company, RCA Radiotron Division.

❖

Orrin W. Towner (A'24–M'29) was born on March 29, 1903, at Peterson, Iowa. He received the B.S. degree in electrical engineering in 1927 and the E.E. degree in 1933 from the University of Kansas. From 1922 to 1925 he was manager and chief engineer of the Towner Radio Manufacturing Company in Kansas City, Missouri; chief operator of WREN in 1927; operator of KFKU in 1927; from 1927 to 1928 he was in the Radio Development Department of the Bell Telephone Laboratories and from 1928 to 1938 in their Radio Installation Department. Since 1938 he has been technical director of WHAS. Mr. Towner is a Member of the American Institute of Electrical Engineers and an Associate member of the Society of Motion Picture Engineers.

❖

For biographical sketches of T. R. Gilliland, S. S. Kirby, and N. Smith, see the PROCEEDINGS for January, 1939; for Harley Iams, see the PROCEEDINGS for February, 1939.

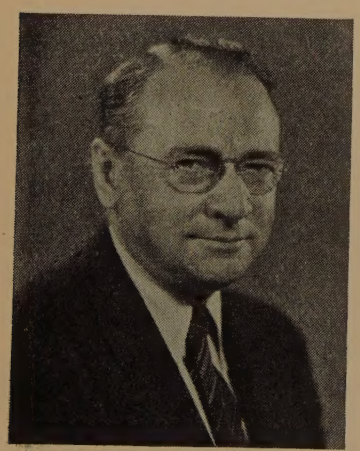

VLADIMIR K. ZWORYKIN

Karl Spangenberg (A'34) was born at Cleveland Ohio, on April 9, 1910. He received the B.S. degree in electrical engineering in 1932 and the M.S. degree in 1933 from the Case School of Applied Science, and the Ph.D. degree in 1937 from Ohio State University. In 1934 he was a radio engineer at WHK, and during 1935 and 1936 he was an instructor in electrical engineering at Rose Polytechnic Institute. Since 1937 Dr. Spangenberg has been an instructor in electrical engineering at Stanford University. He is a member of Sigma Xi and the American Institute of Electrical Engineers.

❖

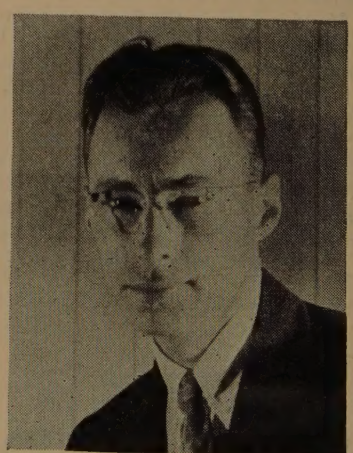

KARL SPANGENBERG